FUNCTIONAL ANALYSIS OF THE MITOCHONDRIAL PROTEOME IN *DROSOPHILA*

by

Daniel Kevin Bricker

A dissertation submitted to the faculty of
The University of Utah
in partial fulfillment of the requirements for the degree of

Doctor of Philosophy

Department of Human Genetics

The University of Utah

May 2014

The University of Utah Graduate School

STATEMENT OF DISSERTATION APPROVAL

The dissertation of **Daniel Kevin Bricker**

has been approved by the following supervisory committee members:

Carl S. Thummel	, Chair	**02/12/2014** Date Approved
Jared Rutter	, Member	**02/12/2014** Date Approved
Gillian M. Stanfield	, Member	**02/12/2014** Date Approved
L. Charles Murtaugh	, Member	**02/12/2014** Date Approved
Shigeru Sakonju	, Member	**02/12/2014** Date Approved

and by **Lynn B. Jorde**, Chair/Dean

of the Department of **Human Genetics**

and by David B. Kieda, Dean of The Graduate School.

ABSTRACT

Mitochondria are complex organelles that have important roles in energy production, intermediary metabolism, signal transduction, and apoptosis. Given these critical cellular functions, major efforts have been made to determine the identity of the mitochondrial proteome. Remarkably, about one fifth of mitochondrial proteins have unknown functions, and many of these are conserved through evolution, suggesting that they play a critical role in mitochondrial biology. We have focused on characterizing a subset of these evolutionarily conserved genes through a collaborative effort in *Drosophila* and yeast model systems. Through this work, we identified novel components of metabolic pathways involved in energy production, represented by the mitochondrial pyruvate carrier (MPC) and two succinate dehydrogenase complex assembly factors (SDHAFs).

The MPC is a multimeric complex comprising the MPC1 and MPC2 proteins. Loss of *MPC1* in yeast, *Drosophila*, and humans results in impaired pyruvate metabolism stemming from a defect in pyruvate import through the inner mitochondrial membrane. A point mutation generated in yeast *MPC1* confers resistance to a known inhibitor of the MPC, thus linking our discovery to classic biochemical analysis of mitochondrial pyruvate transport. Moreover, *Drosophila MPC1* mutants display hallmarks of diabetes, including hyperglycemia, reduced glucose tolerance, and defects in insulin signaling. Taken together, our results demonstrate that the MPC proteins are

required for mitochondrial pyruvate transport and, further, that this function is critical for maintaining carbohydrate homeostasis *in vivo*.

SDHAF3 and SDHAF4 are mitochondrial matrix proteins that are required for maximal SDH activity in yeast, *Drosophila*, and mammalian cells. Both of these proteins interact directly with SDH complex subunits to promote normal assembly of the SDH complex. Moreover, *Drosophila Sdhaf3* and *Sdhaf4* mutants display hallmarks of mitochondrial dysfunction, including muscular and neuronal dysfunction. These studies provide novel candidate causative loci for human diseases characterized by SDH deficiency.

Overall, the work described in this thesis yields key insights into mitochondrial pyruvate transport and succinate dehydrogenase complex assembly, using *Drosophila* to highlight their importance for energy metabolism and animal physiology.

TABLE OF CONTENTS

ABSTRACT……..... iii

LIST OF TABLES……..... vii

ACKNOWLEDGEMENTS……..... viii

CHAPTER

1. INTRODUCTION……..... 1

    Role of the mitochondrion in cellular energy metabolism……..……..... 2
    Mitochondrial dysfunction and disease……..... 8
    The mitochondrial proteome……..... 11
    Mitochondrial pyruvate transport and metabolism……..... 15
    Succinate dehydrogenase complex assembly and function……..... 19
    Drosophila as a model system to study mitochondrial function and the regulation of carbohydrate homeostasis……..... 21
    Thesis outline……..... 27
    References……..... 30

2. A MITOCHONDRIAL PYRUVATE CARRIER REQUIRED FOR PYRUVATE UPTAKE IN YEAST, *DROSOPHILA*, AND HUMANS……..... 45

    Abstract.....……..……..... 46
    References and notes……..... 50
    Acknowledgements……..... 50
    Supplementary materials……..... 51
    Materials and methods……..... 52
    Supplemental references……..... 83

3. *DROSOPHILA MPC1* MUTANTS DISPLAY DEFECTS IN CARBOHYDRATE HOMEOSTASIS AND HALLMARKS OF DIABETES……..... 84

    Summary.....……..……..... 85
    Introduction……..... 85

Experimental procedures……. 91
Results……. 94
Discussion…….105
Future directions…….115
Acknowledgements…….119
References…….119

4. SDHAF4 PROMOTES MITOCHONDRIAL SUCCINATE DEHYDROGENASE ACTIVITY AND PREVENTS NEURODEGENERATION…….125

Summary……..126
Introduction…….126
Experimental procedures…….129
Results…….143
Discussion…….176
Acknowledgements…….184
References…….184

5. TWO LYR ASSEMBLY FACTORS MEDIATE MATURATION OF THE FES SUBUNIT OF SUCCINATE DEHYDROGENASE…….190

Summary……..191
Introduction…….191
Experimental procedures…….196
Results…….208
Discussion…….237
Acknowledgements……. 241
References……. 241

6. CONCLUSIONS…….246

The MPC proteins are required for mitochondrial pyruvate uptake in yeast, *Drosophila*, and humans……247
Drosophila MPC1 mutants display defects in carbohydrate homeostasis and hallmarks of diabetes…….251
The identification of novel succinate dehydrogenase complex assembly factors provides a more comprehensive understanding of SDH assembly…….253
Sdhaf3 and Sdhaf4 are critical for neuronal and muscular function in *Drosophila*…….256
References…….258

LIST OF TABLES

Table Page

S2.1. Primers used for quantitative PCR……..... 70

S2.2 Mpc1 TAP purification……..... 72

S2.3 Mpc2 TAP purification……..... 72

4.1 Yeast strains used in this study…….....137

5.1 Yeast strains used in this study…….....197

5.2 Plasmids used in this study…….....198

ACKNOWLEDGEMENTS

First, I would like to thank my advisor Carl Thummel. Carl has been extremely generous with his time to provide the training that serves as a foundation for a successful career in science. He has always been willing to listen to practice talks, edit writing, or just talk about science. With these attributes and his sense of humor, Carl has fostered a positive lab environment that I have thoroughly enjoyed during my time in graduate school. I would like to thank the members of my thesis committee—Jared Rutter, Gillian Stanfield, Charlie Murtaugh, and Shige Sakonju. They have provided valuable insight that allowed me to focus my efforts on trying to answer good questions. In addition, I would like to thank David Grunwald, David Stillman, and the members of the Genetics Training Grant for providing a fun and informative environment in which to discuss science.

Past and present members of the Thummel lab have always been helpful as they were willing to discuss scientific and nonscientific topics. A special thanks to the former Thummel Lab members Matt Sieber, Anne-Francois Ruaud, Jason Tennessen, Jyoti Misra, and Daniel Seay because they helped me a lot when I was starting my project in the lab. Will Barry, Stefanie Marxreiter, Becky Somer, Roo Wisidagama, Janelle Evans, Mike Horner, Patty Lisiesky, Wendou Yu, and Geanette Lam have also been extremely fun and helpful during my time in Utah. In addition, I would really like

to thank the members of the Rutter lab that I have worked with over the years. This includes Jared Rutter, who initially devised my research project and the many students and postdocs with whom I collaborated, including Thomas Orsak, Yu-Chan Chen, John Schell, Eric Taylor, and Jon Van Vranken.

I am grateful for all of my friends both in and out of science for making the past 6 years really enjoyable. Thanks to my Grandparents, mom, siblings, and in-laws for their support. Most importantly, I would like to thank my wife and best friend Sarah Loughlin for helping me to maintain a positive work/life balance. She always cheers me up if I am having a rough day, and her supportive and loving nature helps me to realize my goals.

CHAPTER 1

INTRODUCTION

Cellular energy production is essential for all forms of life. Mitochondria are central to this process in eukaryotes, as they house the enzymes of the tricarboxylic acid (TCA) cycle and the electron transport chain (ETC) (Alberts et al., 2002). Most major cellular nutrients ultimately feed into the TCA cycle, thus driving the production of high-energy electron donors used for adenosine triphosphate (ATP) synthesis through oxidative phosphorylation (OxPHOS) by the ETC (Berg et al., 2002). ATP generated within the mitochondrion is required for a variety of cellular processes, including metabolic reactions, active transport across membranes, signaling pathways, cell motility, and ribonucleic acid synthesis (Alberts et al., 2002; Berg et al., 2002). Consistent with these broad roles, mitochondrial dysfunction is associated with a variety of human diseases, including type II diabetes, cancer, neurodegenerative disorders, and myopathies (Baysal et al., 2000; Chatterjee et al., 2006; Hanahan and Weinberg, 2011; Lin and Beal, 2006; Mootha et al., 2003; Patti et al., 2003; Petersen et al., 2004; Wallace, 2005; Yan et al., 2009). In addition, mitochondria are critical for other cellular processes, including Ca^{2+} homeostasis, programmed cell death, and iron metabolism (Elmore, 2007; Smaili et al., 2013; Xu et al., 2013).

Role of the mitochondrion in cellular energy metabolism

Carbohydrates, lipids, and amino acids are the major nutrients used to fuel cellular energy production (Berg et al., 2002). The metabolic pathways of these nutrients converge on the mitochondrial TCA cycle, which acts as a central metabolic hub in the cell (Figure 1.1). Complex carbohydrates, glucose, and other sugars are catabolized through the glycolytic pathway in the cytoplasm (Berg et al., 2002). In addition, the metabolic pathways for sugar alcohols, the amino acids serine, alanine, glycine, and cysteine, and the pentose phosphate pathway branch from glycolysis (Lunt and Vander Heiden, 2011). Gluconeogenesis occurs through the reverse reactions of glycolytic enzymes, except for the three rate-limiting steps of glycolysis, hexokinase, phosphofructokinase, and pyruvate kinase, where separate unidirectional enzymes are used for glucose synthesis (Berg et al., 2002). Overall, the glycolytic conversion of one molecule of glucose to two molecules of pyruvate results in the net production of two ATP molecules. Therefore, the full potential energetic yield of glucose (~30 ATP molecules) is dependent on pyruvate oxidation through the TCA cycle in mitochondria (Alberts et al., 2002). Moreover, mitochondrial pyruvate-derived oxaloacetate is a major substrate utilized for gluconeogenesis (Berg et al., 2002). Therefore, mitochondria are critical for the metabolism of carbohydrates, some amino acids, and sugar alcohols through the critical link between mitochondria and glycolysis represented by pyruvate (Figure 1.1).

Phospholipids and triglycerides are the major sources of lipid utilized for cellular energy metabolism (Berg et al., 2002). Fatty acids derived from these molecules are broken down by beta-oxidation to generate the TCA cycle molecules acetyl-CoA and

Figure 1.1. Overview of cellular energy metabolism.
The glycolytic pathway in the cytoplasm and TCA cycle in the mitochondrion are diagrammed. The sites at which the metabolism of amino acids and fatty acids link to glycolysis and the TCA cycle are shown. Amino acids are shown in blue and fatty acids are in red. Several key enzymes discussed in the text are shown in green. DHAP-dihydroxyacetone phosphate; G3P-glyceraldehyde 3 phosphate; LDH-lactate dehydrogenase; ALT-alanine transaminase; MPC-mitochondrial pyruvate carrier; PDH-pyruvate dehydrogenase; PC-pyruvate carboxylase; SDH-succinate dehydrogenase; FH-fumarate hydratase; BCAA-branched chain amino acids; AA-amino acids. (Adapted from Berg et al., 2002; Lunt and Vander Heiden, 2011; Gray et al., 2013).

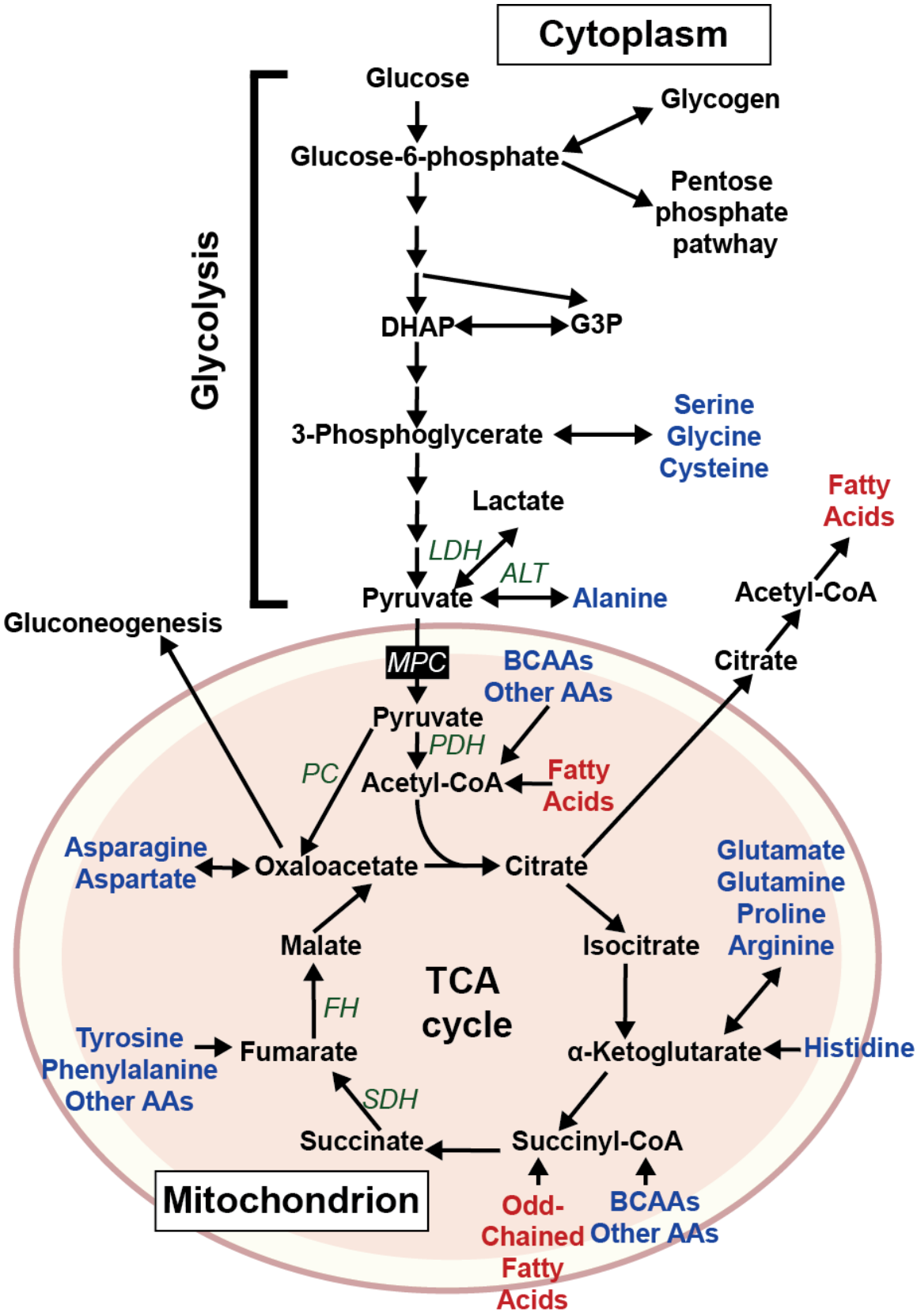
Cytoplasm
Glucose
Glycogen
Glucose-6-phosphate
Pentose phosphate patwhay
Glycolysis
DHAP
G3P
3-Phosphoglycerate
Serine
Glycine
Cysteine
Lactate
LDH
ALT
Pyruvate
Alanine
Fatty Acids
Acetyl-CoA
Gluconeogenesis
MPC
BCAAs
Other AAs
Citrate
Pyruvate
PDH
PC
Acetyl-CoA
Fatty Acids
Asparagine
Aspartate
Oxaloacetate
Citrate
Glutamate
Glutamine
Proline
Arginine
Malate
Isocitrate
TCA cycle
FH
Tyrosine
Phenylalanine
Other AAs
Fumarate
α-Ketoglutarate
Histidine
SDH
Succinate
Succinyl-CoA
Mitochondrion
Odd-Chained Fatty Acids
BCAAs
Other AAs

succinyl-CoA. The oxidation of fatty acids occurs within mitochondria, with the exception of very long chain fatty acids, whose initial oxidation reactions occur within peroxisomes. Moreover, acetyl-CoA derived from the TCA cycle molecule citrate is the major substrate used for fatty acid and sterol biosynthesis (Berg et al., 2002). Thus, mitochondria are central to lipid catabolic and anabolic pathways (Figure 1.1).

Many amino acids can interconvert with glycolytic intermediates, but most amino acid metabolic pathways intersect with TCA cycle (Berg et al., 2002; Lunt and Vander Heiden, 2011). For example, glutamine, glutamate, arginine, and proline can be converted to alpha-ketoglutarate, whereas asparagine and aspartic acid generate oxaloacetate. In addition, the branched chain amino acids valine, leucine, isoleucine, and the sulfur containing amino acid methionine are broken down to yield acetyl-CoA and/or succinyl-CoA (Lunt and Vander Heiden, 2011). Overall, the aforementioned examples demonstrate that the metabolic pathways of most amino acids converge on the TCA cycle directly, or indirectly though the production of pyruvate (Figure 1.1)

The matrix-localized TCA cycle couples the oxidation of incoming metabolites to the reduction of either nicotinamide adenine dinucleotide (NAD) or flavin adenine dinucleotide (FAD) to NADH or $FADH_2$, respectively. Electrons from NADH and $FADH_2$ enter the ETC at complexes I and II, respectively (Figure 1.2A). Once associated with the ETC, electrons are moved via redox transfer reactions through ubiquinone, complex III, cytochrome c, and ultimately to complex IV, where the electrons react with oxygen to form water. This transport of electrons drives the translocation of hydrogen ions (H+) across the inner mitochondrial membrane (IMM) by complexes I, III, and IV to the intermembrane space to generate an electrical membrane potential and H+

Figure 1.2. Diagram of the electron transport chain (ETC), succinate dehydrogenase (SDH), and pyruvate metabolism.
(A) The process of oxidative phosphorylation by the electron transport chain (ETC). Electrons (e-) from NADH generated by the TCA cycle and glycolytic pathway enter the ETC and are transferred to complex I, whereas complex II (SDH) couples the oxidation of succinate to fumarate to the reduction of FAD to $FADH_2$. Complexes I and II (CI and CII) each transfer electrons to ubiquinone (Q), which then passes electrons sequentially to Complex III (CIII), cytochrome c (CytC), and Complex IV (CIV). At Complex IV, electrons react with oxygen to form water. Complexes I, III, and IV pump protons (H+) across the inner mitochondrial membrane (IMM). Protons then move back into the matrix through Complex V (CV; ATP-synthase), thus driving oxidative phosphorylation of ADP to ATP using inorganic phosphate (P_i). The intermembrane space (IMS) is also shown. (B) Mitochondrial pyruvate metabolism. Pyruvate generated during glycolysis is transported through the IMM by the mitochondrial pyruvate carrier (MPC) through a mechanism dependent on the IMM proton gradient. Mitochondrial pyruvate is either converted to oxaloacetate by pyruvate carboxylase (PC), or acetyl-CoA by pyruvate dehydrogenase (PDH). The activity of PDH is regulated by pyruvate dehydrogenase kinase (PDK) and pyruvate dehydrogenase phosphatase (PDP). (C) The succinate dehydrogenase (SDH) complex is shown. The SHDA and SDHB subunits face the mitochondrial matrix and are anchored to the IMM by the SDHC and SDHD subunits. SDHA contains the FAD moiety that is reduced to $FADH_2$ upon the oxidation of succinate to fumarate. SDHB contains three iron sulfur (FeS) clusters, and heme is present at the interface between SDHC and SDHD. (Adapted from Berg et al., 2002; Gottleib and Tomlinson, 2005; Gray et al., 2013).

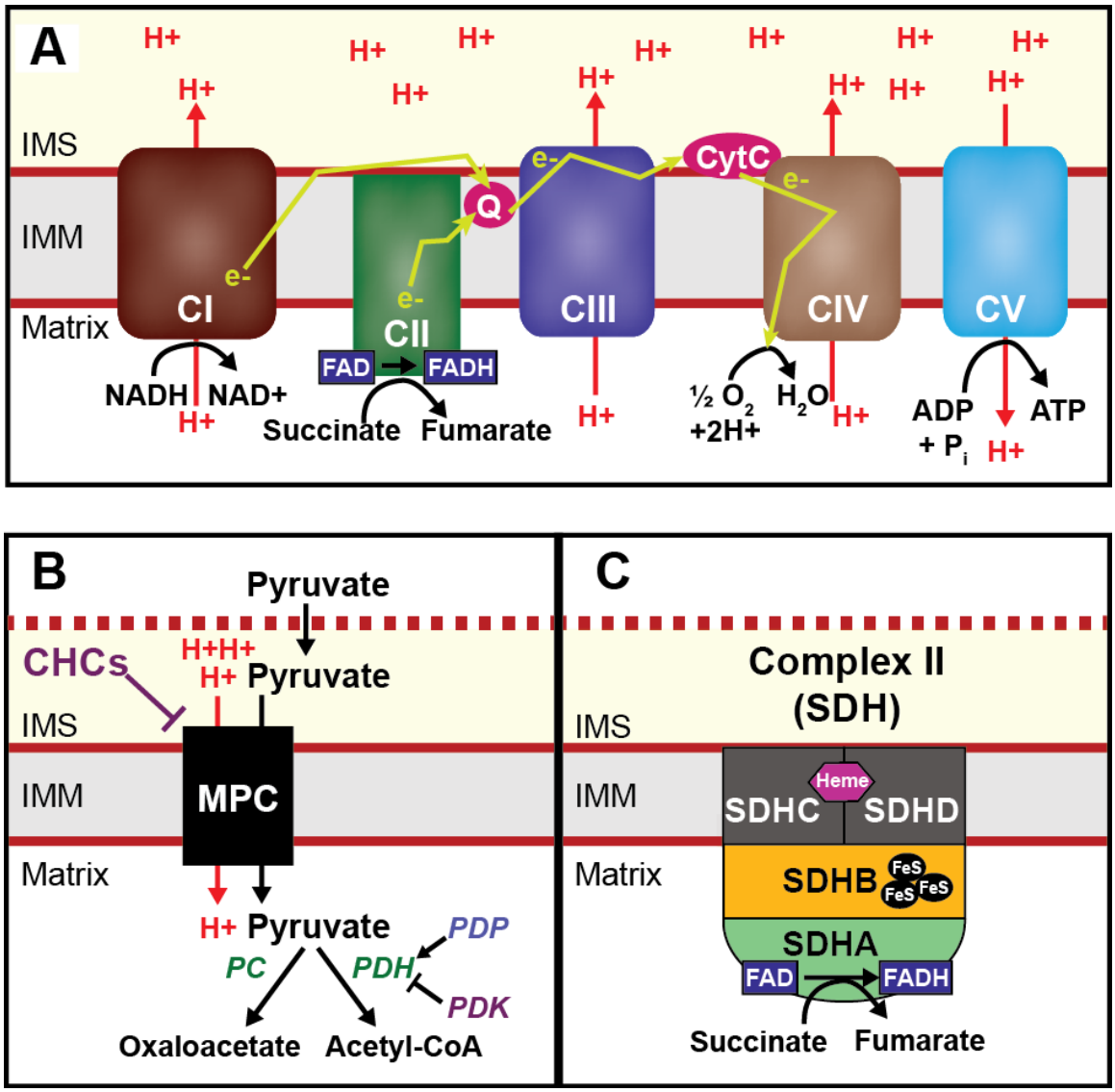
A
IMS
IMM
Matrix
H+
e-
CI
CII
CIII
CIV
CV
Q
CytC
NADH
NAD+
FAD
FADH
Succinate
Fumarate
½ O2
+2H+
H2O
ADP
+ Pi
ATP
B
Pyruvate
CHCs
MPC
PDP
PC
PDH
PDK
Oxaloacetate
Acetyl-CoA
C
Complex II
(SDH)
Heme
SDHC
SDHD
SDHB
FeS
SDHA

concentration gradient. Complex V (ATP-synthase) then couples the movement of H+ ions back into the matrix along the electrochemical gradient to drive oxidative phosphorylation of adenosine diphosphate (ADP) to ATP (Figure 1.2A) (Alberts et al., 2002; Berg et al., 2002).

Mitochondrial dysfunction and disease

ATP is used to fuel almost all aspects of cell biology. As such, defects in mitochondrial function are detrimental to cellular function and, thus, commonly linked to human disease (Wallace, 2005). Hereditary mitochondrial diseases can be caused by mutations in either the mitochondrial genome or in nuclear mitochondrial-protein encoding genes (Schapira, 2006). Although each individual form of mitochondrial disease is rare, taken together they are quite common with an estimated incidence of 1/5,000 to 1/10,000 live births (Schaefer et al., 2004; Skladal et al., 2003). Many forms of mitochondrial disease are caused by loss-of-function mutations in components of the ETC, TCA cycle, or mitochondrial pyruvate metabolic enzymes (Schapira, 2006). These diseases are generally characterized by a broad phenotypic spectrum, with the most severe defects typically manifested in neuronal and/or muscular tissue (Schapira, 2006; Schon and Manfredi, 2003). Work in several genetic model organisms studying mitochondrial diseases is consistent with this observation. For example, mice carrying a mutation in the complex I subunit-encoding gene *Ndufs4* develop age progressive encephalomyopathy, characterized by ataxia, neuronal synaptic transmission defects, and early lethality (Kruse et al., 2008). Muscle-specific genetic inactivation of the cytochrome oxidase assembly gene *cox10* causes severe myopathy and muscle weakness,

while neuron-specific knockout results in behavioral defects and neuronal cell loss in the brain (Diaz et al., 2005; Fukui et al., 2007). Skeletal/cardiac muscle-specific knockout of pyruvate dehydrogenase (PDH) alpha subunit causes cardiomyopathy, while its loss specifically in neurons results in structural defects in the brain (Pliss et al., 2004; Sidhu et al., 2008). Similarly, zebrafish *pdhb* mutants develop retinal degeneration and visual impairment (Maurer et al., 2010). Furthermore, genetic disruption of citrate synthase, cytochrome c oxidase, ATP synthase, or succinate dehydrogenase causes muscular/neuronal defects in *Drosophila* (Celotto et al., 2006; Fergestad et al., 2006a; Liu et al., 2007; Mast et al., 2008; Walker et al., 2006) (Chapter 4, 5). Overall, the similarity between phenotypes observed in human mitochondrial disease and in genetic models of these disorders illustrates the evolutionarily conserved role of mitochondria in maintaining neuronal and muscular function. This susceptibility of neuronal and muscular tissue to mitochondrial dysfunction is thought to be related to their massive bioenergetic and biosynthetic demands and potentially an increased sensitivity of neurons and muscles to reactive oxygen species (ROS) relative to other tissues (Lax and Jaros, 2012; Schon and Manfredi, 2003).

In addition to these specific disorders defined as mitochondrial diseases, mitochondrial dysfunction is also associated with common age-related neurological diseases, such as Alzheimer's disease, Parkinson's disease (PD), and Amyotrophic Lateral Sclerosis (ALS) (Schon and Manfredi, 2003). Neuronal tissue from human patients and mouse models display abnormal mitochondrial morphology, reduced mitochondrial number, reduced energy production, and increased ROS (Hauptmann et al., 2009; Kong and Xu, 1998; Kopeikina et al., 2011; Moreira et al., 2010; Perier et al.,

2007; Schapira et al., 1990; Shi et al., 2010; Winklhofer and Haass, 2010; Wong et al., 1995). However, whether these mitochondrial defects are causative or coincident with the initiation or progression of these complex diseases is controversial (Morais and De Strooper, 2010). Rare familial forms of Parkinson's Disease are caused by mutations in the genes *PARKIN*, *PINK1*, *DJ-1*, *LRRK2*, and *ATP13A2*, all of which have been implicated in mitochondrial quality control and/or dynamics (Bonifati et al., 2003; Gusdon et al., 2012; Kitada et al., 1998; Narendra et al., 2010; Paisan-Ruiz et al., 2004; Ramirez et al., 2006; Winklhofer and Haass, 2010; Zimprich et al., 2004). Similarly, mutations in the mitochondrial ROS scavenging enzyme *Superoxide Dismutase 1* (*SOD1*) cause ALS in humans and ALS-like phenotypes in mouse models (Rosen et al., 1993; Shi et al., 2010). Thus, at least for PD and ALS, there is compelling evidence that is consistent with a causative role for mitochondrial dysfunction in disease etiology.

In addition to degenerative diseases, mitochondrial dysfunction is linked to type 2 diabetes, suggesting that mitochondria play a critical role in regulating systemic metabolic homeostasis (Lowell and Shulman, 2005). For example, skeletal muscle from type 2 diabetics exhibits mitochondrial defects, including abnormal morphology, aberrant size, reduced number, decreased activity of key OxPHOS enzymes, and defects in ATP production (Hojlund et al., 2008; Kelley et al., 2002; Morino et al., 2005; Petersen et al., 2004; Ritov et al., 2005; Sleigh et al., 2011; Szendroedi et al., 2007). One or more of these hallmarks of mitochondrial dysfunction have also been observed in the skeletal muscle, cardiac muscle, liver, pancreatic islets, and adipose tissue of genetic and dietary rodent models of diabetes (Boudina et al., 2007; Cheng et al., 2009; Choo et al., 2006; Koves et al., 2008; Lu et al., 2010; Sparks et al., 2005). Several functional studies have

been performed to assay the role of mitochondria in the pancreatic beta cells and the liver. Mice carrying a mutation in *uncoupling protein 2* (*UCP2*), which encodes a protein expressed in beta cells that uncouples the mitochondrial membrane potential from ATP production, exhibit increased islet ATP production and glucose stimulated insulin secretion (GSIS—see Chapter 3 for a more extensive discussion of this topic) (Zhang et al., 2001). Consistent with these effects, loss of *UCP2* results in an amelioration of defects in insulin release characteristic of dietary models of type 2 diabetes (Joseph et al., 2004; Zhang et al., 2001). Conversely, overexpression of *UCP2* in rat pancreatic beta cells results in defective GSIS (Chan et al., 1999). Taken together, these results underscore the critical nature of mitochondrial ATP production in beta cell function. Furthermore, genetic inactivation of enzymes involved in mitochondrial pyruvate metabolism in hepatocytes or pancreatic beta cells affects processes commonly dysregulated in diabetes, such as insulin secretion, insulin sensitivity, lipogenesis, and gluconeogenesis (discussed in more detail in Chapter 3) (Choi et al., 2010; Kumashiro et al., 2013; Srinivasan et al., 2010). Overall, this evidence suggests that normal mitochondrial function is critical for the maintenance of muscles and neurons and, further, for the regulation of systemic metabolic homeostasis.

The mitochondrial proteome

Given the central role of the mitochondrion in cellular function and the association of mitochondrial dysfunction with disease, it is critical to gain a comprehensive understanding of mitochondrial biology. The identification of all proteins that localize to the mitochondrion, i.e., the mitochondrial proteome, provides an

important resource to address this problem (Calvo and Mootha, 2010). Mass spectrometry-based proteomic approaches were used to identify of all of the proteins associated with mitochondria isolated from a wide variety of species, ranging from protists to humans (Pagliarini et al., 2003; Pagliarini et al., 2008; Reinders et al., 2006; Sickmann et al., 2003; Smith et al., 2007). The number of proteins localized to the organelle varies across species, with ~1200 identifiable proteins localized to mitochondria in mammals and ~850 in yeast (Pagliarini et al., 2008; Reinders et al., 2006). Although the distribution of functions assigned to proteins localized to mitochondria varies from species to species, it is clear that the largest categories include energy metabolism, genome maintenance/transcription, and translation (Figure 1.3) (Lotz et al., 2013; Schmidt et al., 2010). Interestingly, ~20% of mitochondrial proteins in yeast and 11–36% of mitochondrial proteins in humans have unknown functions, thus representing the largest category in the mitochondrial proteome (Figure 1.3) (Pagliarini and Rutter, 2013; Schmidt et al., 2010). Approximately 10% of these uncharacterized proteins are conserved through evolution from yeast to humans, indicating they may play a fundamentally important role in mitochondrial biology (Lotz et al., 2013). Given the prevalence of mitochondrial dysfunction in human disease, we also predicted that new disease genes would be found within this group. Based on this rationale, the Rutter lab began to characterize ~30 proteins of unknown function using budding yeast, *Saccharomyces cerevisiae*, prior to my thesis work (Jared Rutter, personal communication). Yeast is a powerful system for genetic studies of mitochondrial function as respiratory-deficient cells can grow on fermentable media, a characteristic that allows

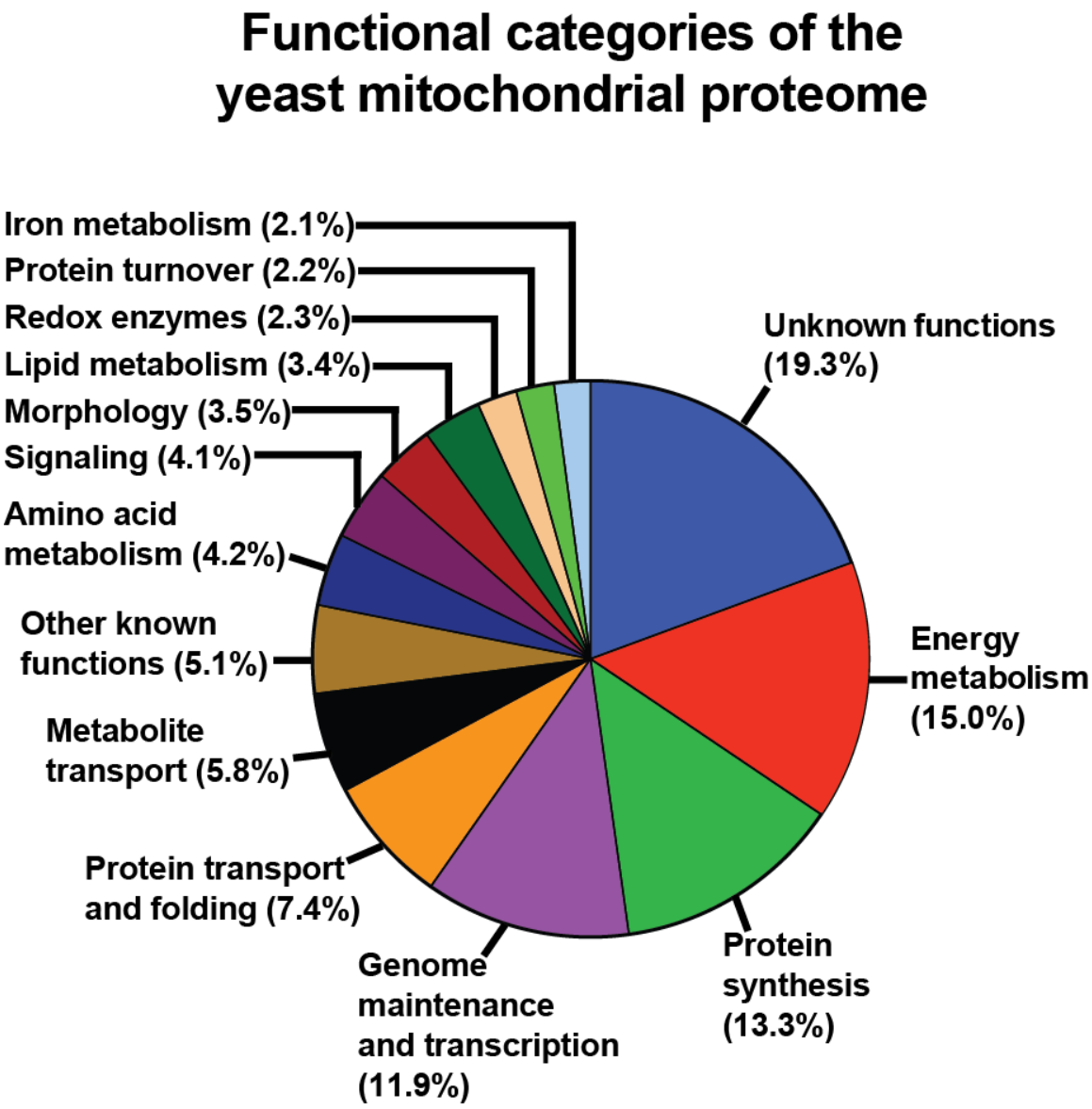

Figure 1.3. Functional classification of the mitochondrial proteome.
The distribution of gene-ontology categories for the ~850 proteins known to localize to yeast mitochondria as of 2010 are shown. (Adapted from Reinders et al., 2006 and Schmidt et al., 2010).

for selective growth screening for mutations that disrupt OxPhos or other mitochondrial processes (Barrientos, 2003). The initial studies from the Rutter lab yielded several important discoveries in aspects of mitochondrial quality control, ETC supercomplex assembly, and SDH complex assembly, as well as the discovery of a novel disease gene (Chen et al., 2012; Hao et al., 2009; Heo et al., 2010). As an extension of this research, I set out to characterize three conserved mitochondrial proteins of unknown function in *Drosophila* in collaboration with the Rutter lab, to complement their work in yeast. As described below, *Drosophila* is a powerful model to understand the physiological role of mitochondria in neuronal and muscular function—and to study the mechanisms underlying the regulation of carbohydrate homeostasis. Thus, through this multisystem approach, we sought to study cellular and biochemical functions of novel mitochondrial proteins in yeast, combined with tissue-specific and physiological functions in *Drosophila*.

To decide which of these ~30 uncharacterized mitochondrial proteins I would study using *Drosophila*, I focused my attention on genes whose deletion in yeast caused a robust growth defect, with the rationale that these would yield a noticeable phenotype when mutated in flies. Yeast *Mitochondrial pyruvate carrier 1* (*Mpc1*) mutants display a growth defect on media lacking leucine, and *Succinate dehydrogenase 7 (Sdh7)* and *Succinate dehydrogenase 8 (Sdh8)* mutants display reduced growth on acetate, suggesting these genes play a role in cellular metabolism. Based on these data, I decided to focus on functionally characterizing the *Drosophila* orthologs of these genes, which we named *dMpc1*, *dSdhaf4*, and *dSdhaf3*. From these studies, we learned that dMpc1 functions in mitochondrial pyruvate transport, whereas dSdhaf3 and dSdhaf4 are involved in SDH

complex assembly. My thesis research thus focused on the mechanisms of mitochondrial pyruvate and succinate metabolism and the physiological roles of these factors, using *Drosophila* as a model system. We also discovered a role for dMpc1 in maintaining carbohydrate homeostasis through the insulin signaling pathway, and thus my introduction ends with a discussion of these pathways in *Drosophila*.

Mitochondrial pyruvate transport and metabolism

Pyruvate occupies a central place in energy metabolism, as its metabolic trajectory can be shifted to produce lactate, alanine, acetyl-CoA, or oxaloacetate, depending on cellular needs (Gray et al., 2013). While the conversion of pyruvate to lactate by lactate dehydrogenase (LDH) and alanine by alanine transaminase (ALT) occurs in the cytoplasm; pyruvate-driven acetyl-CoA and oxaloacetate production takes place in the mitochondrial matrix, catalyzed by pyruvate dehydrogenase (PDH) and pyruvate carboxylase (PC), respectively (Figure 1.2B) (Berg et al., 2002). The PDH enzyme complex is localized to the mitochondrial matrix and comprises three parts: the pyruvate dehydrogenase subunit, the dihydrolipoyl transacetylase subunit, and the dihydrolipoyl dehydrogenase subunit (Patel and Korotchkina, 2006). These components act in succession to couple the dehydrogenation of pyruvate with the production of acetyl-CoA and NADH from CoA and NAD, through a mechanism involving several cofactors, including thiamin pyrophosphate, lipoic acid, and FAD (Patel and Roche, 1990). PDH is central to cellular energy metabolism as it effectively links glycolysis with mitochondrial energy production and fatty acid biosynthesis (Berg et al., 2002). Consistent with this pivotal role, PDH activity is tightly regulated to respond to changes

in cellular metabolic conditions through its repression by phosphorylation of the pyruvate dehydrogenase subunit (Patel and Korotchkina, 2006). This phosphorylation event is controlled antagonistically by pyruvate dehydrogenase kinase (PDK) and pyruvate dehydrogenase phosphatase (PDP) (Figure 1.2B), which are subject to regulation by NAD/NADH, Acetyl-CoA/CoA, and ATP/ADP ratios (Patel and Korotchkina, 2006). This regulation links PDH activity to the cellular bioenergetic state, allowing it to maintain energy homeostasis (Patel and Korotchkina, 2006). PC is a biotinylated mitochondrial matrix enzyme that produces oxaloacetate using pyruvate and Acetyl-CoA as substrates through an ATP-dependent mechanism (Jitrapakdee et al., 2008). Oxaloacetate produced by PC is used for gluconeogenesis in the liver and kidneys through its conversion to phosphoenolpyruvate (PEP) by a rate-limiting enzyme in gluconeogenesis, PEP carboxykinase (PEPCK) (Jitrapakdee et al., 2006). Moreover, PC facilitates the TCA cycle anaplerosis required for lipogenesis in adipose tissue and the synthesis of the neurotransmitter amino acid glutamate in astrocytes (Jitrapakdee et al., 2006). Thus, mitochondrial pyruvate metabolism is critical for cellular energy production and biosynthetic processes across a wide array of cell types. Consistent with these fundamental metabolic roles, alterations in mitochondrial pyruvate metabolism can result in profound physiological effects. For example, mutations in PC, subunits of PDH, or PDP cause diseases characterized by several shared phenotypes, including lactic acidosis, developmental abnormalities and neurological defects (Garcia-Cazorla et al., 2006; Maj et al., 2005; Patel et al., 2012). Conversely, increasing PDH activity by mutating a PDK isoform *PDK4* in mice results in beneficial phenotypes, including protection from insulin resistance, hyperglycemia, and impaired glucose tolerance induced by a high fat diet.

Since pyruvate is produced by the glycolytic pathway in the cytoplasm, it must enter the mitochondrion to be utilized by PDH or PC. Pyruvate passes through the outer mitochondrial membrane (OMM) via diffusion though the nonselective voltage dependent anion channels (VDACs), whereas the mitochondrial pyruvate carrier (MPC) facilitates selective pyruvate transport through the inner mitochondrial membrane (IMM) (Figure 1.2B) (Gray et al., 2013). Prior to our discovery of the genetic nature of the MPC described in chapter 2, *in vitro* studies using mitochondria isolated from plant, yeast, and mammalian cells elegantly defined its biochemical characteristics (Schell and Rutter, 2013). The kinetics and substrate affinities of the MPC were shown to differ from the monocarboxylate transporter (MCT) family of proteins that transport pyruvate and other carboxylic acids across the plasma membrane, indicating that a distinct transporter was indeed present in the IMM (Halestrap, 1975; Papa et al., 1971; Papa and Paradies, 1974). Moreover, the activity of this IMM pyruvate transporter was shown to be pH dependent, suggesting that the MPC may function through a H+/pyruvate symporter (or OH– /pyruvate antiporter) mechanism that could be driven by the IMM H+ concentration gradient generated by the ETC (Figure 1.2B) (Halestrap, 1975; Papa and Paradies, 1974). Building on these observations, the identification of alpha-cyano-4-hydroxycinnamate (CHC) and its derivatives as potent inhibitors of mitochondrial pyruvate transport and the demonstration that MPC activity could be reconstituted in liposomes led to several attempts at isolating the MPC (Halestrap and Denton, 1974; Nalecz et al., 1986). First, a ~15 kDa protein was identified in rat heart and liver mitochondria based on the characteristic that CHC incubation protected it from labeling by radioactive N-phenylmaleimide (Thomas and Halestrap, 1981). Since CHCs also protect the MPC from

this thiol-blocking drug, it was concluded that this 15 kDa protein was the MPC (Thomas and Halestrap, 1981). A later report from the same authors, however, claimed to identify this protein as a subunit of cytochrome oxidase in follow up studies (Hildyard and Halestrap, 2003). Following this work, a mixture of ~6 proteins of various sizes (12, 30, 32, 34, 66, and 74 kDa) purified from castor bean mitochondria were shown to facilitate CHC-sensitive pyruvate transport across a liposomal membrane, suggesting that one or more of them were the MPC (Brailsford et al., 1986). Then, three studies using immobilized CHC to affinity purify and reconstitute the MPC from bovine heart, rat liver, and yeast mitochondria were published (Bolli et al., 1989; Capuano et al., 1990; Nalecz et al., 1986). In each of the mammalian studies, a ~34 kDa protein was isolated that facilitated pyruvate transport *in vitro*, whereas a mix of 26 kDa and 50 kDa proteins were shown to reconstitute pyruvate transport in the yeast paper (Bolli et al., 1989; Capuano et al., 1990; Nalecz et al., 1986). The biochemical characteristics of pyruvate transport facilitated by the ~34 kDa proteins isolated from mammalian tissues, however, differed from that previously described for the MPC and from the pyruvate transporter isolated from yeast mitochondria (Bolli et al., 1989; Capuano et al., 1990; Halestrap, 1975; Nalecz et al., 1986). Moreover, genetic studies were never performed to definitively demonstrate that any of these candidate proteins acted as the MPC *in vivo*. Thus, these reports of MPC isolation lacking a shared definitive candidate MPC molecule were inconclusive. In 2003, a member of the mitochondrial carrier family (MCF) was purported to be the MPC in yeast since its loss abrogated CHC-sensitive mitochondrial pyruvate uptake (Hildyard and Halestrap, 2003). This protein, however, was later shown to be a specific NAD transporter (Todisco et al., 2006). This result indicates that any

effects observed on mitochondrial pyruvate uptake observed by Hildyard and Halestrap in 2003 were indirect and likely caused by defects in the NAD-dependent PDH enzyme reaction (Todisco et al., 2006). Therefore, although over 40 years of elegant *in vitro* studies had defined the biochemical characteristics of the MPC (reviewed extensively in Schell and Rutter, 2013), its genetic identity was still unclear prior to our work described in Chapter 2 of this thesis and a copublished study (Herzig et al., 2012).

Succinate dehydrogenase complex assembly and function

The SDH complex (Complex II) is the only enzyme that acts in both the TCA cycle and the ETC and thus plays a unique role in cellular energy metabolism (Rutter et al., 2010). SDH couples the oxidation of succinate to fumarate with the reduction of FAD to $FADH_2$, which pass electrons through ubiquinone to complex III to drive OxPHOS (Figure 1.2A) (Berg et al., 2002). SDH is a tetrameric protein complex containing two soluble matrix subunits called SDHA and SDHB in animals (Sdh1 and Sdh2 in yeast), and two IMM anchored subunits called SDHC and SDHD in animals (Sdh3 and Sdh4 in yeast) (Figure 1.2C)(Sun et al., 2005). The catalytic core of SDH comprises SDHA/SDHB, where SDHA contains a covalently bound FAD, and SDHB contains three iron sulfur (FeS) clusters. The SDHC/SDHD subunits function to anchor the complex to the IMM and contain a heme at their binding interface (Cecchini, 2003). The configuration of these redox cofactors (FAD, 3FeS cores, and heme) is arranged such that a stable pathway for electron transfer from succinate to ubiquinone is formed (Cecchini, 2003).

Consistent with the central position of SDH in energy metabolism, defects in SDH are linked to human disease. For example, rare mutations in SDH subunit-encoding genes have been shown to cause Leigh's syndrome, infant encephalomyopathy, optic atrophy and Leukodystrophy (Alston et al., 2012; Astuti et al., 2001; Bayley et al., 2005; Bourgeron et al., 1995; Horvath et al., 2006; Parfait et al., 2000). In addition, SDH is a tumor suppressor, as loss-of-function mutations in SDH subunit-encoding genes have been linked to susceptibility to familial paraganglioma, pheochromocytoma, renal cell carcinoma, and gastrointestinal stromal tumors (Bardella et al., 2011; Baysal et al., 2000; Janeway et al., 2011; Niemann and Muller, 2000; Ricketts et al., 2008). Succinate accumulation to supraphysiological levels is thought to drive tumorigenesis associated with SDH deficiency through the inhibition of 2-oxoglutarate-dependent dioxygenases, such as the Jumanji family demethylases and Hypoxia Inducible Factor (HIF) prolyl-hydroxylase (Bardella et al., 2011). The inhibition of these enzymes is purported to contribute to the etiology of SDH deficient tumors, although the exact mechanisms involved remain controversial (Bardella et al., 2011). Thus, SDH function appears to be critical for neuronal and muscular function, as well as maintaining a normal metabolic profile that prevents abnormal signaling or epigenetic events that drive tumorigenesis.

Although it is well established that ETC complexes I and IV assemble through a stepwise process involving ancillary assembly factors, the mechanisms underlying SDH complex assembly have only recently begun to emerge with the discovery of two dedicated SDH assembly factors (SDHAFs) in 2009 (Diaz et al., 2011; Fernandez-Vizarra et al., 2009; Ghezzi et al., 2009; Hao et al., 2009). SDHAF1 (Sdh6 in yeast) was identified through genetic studies of patients with infantile leukoencephalopathy

characterized by loss of the SDH holocomplex (Ghezzi et al., 2009). The exact function of SDHAF1 in SDH complex assembly, however, remained unknown prior to our functional analysis (Chapter 5). SDHAF2 (Sdh5 in yeast) was identified by the Rutter lab through the study of mitochondrial proteins with previously unknown functions described above (Hao et al., 2009). SDHAF2/Sdh5 directly interacts with SDHA/Sdh1 and is required for covalent addition of the FAD to that subunit. Loss of *Sdh5* in yeast and *SDHAF2* in mammalian cells results in a complete loss of the SDH holocomplex and a concomitant elimination of SDH enzymatic activity. Consistent with these observations, mutations in *SDHAF2* were identified that cause a form of familial paraganglioma, linking its activity to human disease (Hao et al., 2009). Taken together, these two studies show that SDH assembly factors are critical for SDH function, and further, demonstrate that mutations in *SDHAF* genes can result in a similar spectrum of diseases to that caused by mutations in core SDH subunit-encoding genes. Building on these discoveries, the identification of two novel SDHAFs, called SDHAF4 and SDHAF3, are detailed in Chapters 4 and 5 of this thesis, respectively.

Drosophila as a model system to study mitochondrial function and the regulation of carbohydrate homeostasis

Drosophila is a powerful genetic model system to study many aspects of biology due largely to a short generation time, inexpensive maintenance in the lab, and the wealth of genetic tools available to the *Drosophila* research community (Pandey and Nichols, 2011). Below, I will describe *Drosophila* studies relevant to my thesis work, mainly

focusing on the role of mitochondria in maintaining neuronal function and architecture and the regulation of carbohydrate homeostasis by the insulin-signaling pathway.

Drosophila as a model to study mitochondrial function

Work in *Drosophila* has yielded valuable insights into many areas of mitochondrial biology, including the role of mitochondria in the regulation of cell cycle checkpoints, mitochondrial fusion/fission mechanisms, and the pathways controlling mitochondrial motility (Guo et al., 2005; Hales and Fuller, 1997; Mandal et al., 2005; Owusu-Ansah et al., 2008; Russo et al., 2009). The field of *Drosophila* mitochondria research most relevant to my thesis, however, is work investigating the role of mitochondria in neuronal and muscular function and maintenance. Similar to humans, defects in neuronal and muscular tissues are hallmarks of mitochondrial dysfunction in *Drosophila*. Viable flies harboring mutations in a nuclear-encoded mitochondrial ribosomal protein *technical knock out (tko),* citrate synthase *knockdown (kdn),* adenine nucleotide translocase, a cytochrome oxidase subunit *levy*, *Superoxide dismutase 2 (SOD2)*, or the mitochondrial genome-encoded ATP-synthase subunit 6 *(mtATP6)*, are all sensitive to mechanical shock-induced paralysis, a phenotype termed bang sensitivity (Celotto et al., 2006; Celotto et al., 2012; Fergestad et al., 2006a; Fergestad et al., 2008; Liu et al., 2007; Zhang et al., 1999). The underlying neuronal mechanism driving bang sensitivity is an increased susceptibility to seizures caused by increased neuronal hyperactivation (Pavlidis and Tanouye, 1995). Consistent with this idea, most bang sensitive mutants display age-progressive neurodegeneration and a reduction in lifespan (Fergestad et al., 2006b; Fergestad et al., 2008). Disruption of ATP production and/or

increased ROS are associated with these behavioral and neurodegenerative phenotypes, although the exact mechanism underlying neuronal cell loss is not known (Celotto et al., 2012; Fergestad et al., 2006a). Mitotic clones lacking *SdhA* display neurodegeneration, thought to be driven by increased ROS production (Mast et al., 2008). Viable *SdhB* hypomorphic mutants are not sensitive to bang-induced seizures but they do exhibit reduced locomotion, aberrant flight muscle mitochondrial morphology, elevated ROS production, and sensitivity to oxidative stress (Walker et al., 2006). *Drosophila* models have also been used to understand the etiology of familial Parkinson's disease. Flies harboring mutations in the familial Parkinson's genes *Pink* and *Parkin* display defects in mitochondrial function and morphology, combined with reduced locomotion, dopaminergic neuron degeneration, and signs of muscular degeneration (Clark et al., 2006; Greene et al., 2003; Park et al., 2006; Yang et al., 2006). The underlying cause of these phenotypes is thought to be a defect in mitochondrial quality control, dynamics, and/or motility (Guo, 2010; Park et al., 2009; Poole et al., 2008). Interestingly, reports using *Drosophila* genetic epistasis experiments to study *Pink* and *Parkin* were the first to show that they function in the same pathway (Clark et al., 2006; Park et al., 2006; Yang et al., 2006)—a result that was later confirmed in mammalian cells (Narendra et al., 2010). Moreover, forward genetic studies of *Pink* and *Parkin* have identified genetic modifiers of these phenotypes, thus revealing potential pathways through which these genes affect mitochondrial quality control and tissue degeneration (Fernandes and Rao, 2011). Taken together, these studies establish *Drosophila* as a powerful model to study the genetic pathways and molecular mechanisms underlying the nervous system and muscular defects caused by mitochondrial dysfunction.

Drosophila as a model to study carbohydrate homeostasis

The insulin signaling pathway is a major regulator of carbohydrate homeostasis in humans (Hers, 1990; Schrayyef and Gerich, 2010). Defects in this pathway lead to diabetes mellitus, a disease characterized by chronic hyperglycemia (Inzucchi, 2012). The insulin signaling pathway is conserved in flies, where it controls growth in larvae and metabolism in both larvae and adults (Teleman, 2010; Grewal, 2009). Here I provide a brief introduction to the insulin signaling pathway as a foundation for my discussion of the role of dMPC1 in regulating carbohydrate homeostasis in Chapter 3.

There are eight *Drosophila* insulin-like peptides (DILPs) in the fly genome (Nassel et al., 2013). Of these, DILP2, DILP3, and DILP5 are produced in the insulin producing cells (IPCs) of the brain, which are functionally analogous to mammalian pancreatic beta cells (Nassel et al., 2013). DILPs are secreted into the circulation in response to feeding, where they bind to the sole insulin receptor (InR) ortholog present in flies in peripheral tissues (Geminard et al., 2009; Kim and Rulifson, 2004; Nassel et al., 2013). Activation of the InR results in its autophosphorylation and the recruitment of Phosphoinositide 3-kinase (PI3K) to the membrane, which ultimately drives the phosphorylation and activation of the kinase Akt (Teleman, 2010). Akt subsequently phosphorylates and inhibits the nuclear translocation of the transcription factor FOXO, thus affecting FOXO target genes (Alic et al., 2011; Hwangbo et al., 2004; Teleman, 2010). DILP signaling likely regulates metabolism through FOXO-dependent and -independent transcriptional changes, as well as nontranscriptional mechanisms (Teleman, 2010). The exact downstream mechanisms by which DILP signaling regulates carbohydrate metabolism, however, remain only partially understood (Teleman, 2010). In

addition, a signaling molecule analogous to mammalian glucagon called adipokinetic hormone (AKH) functions in opposition to the DILP signaling pathway by promoting catabolic metabolism under nutrient deprivation (Bharucha et al., 2008; Van der Horst, 2003). Taken together, the opposing regulation and functions of DILP and AKH signaling maintain a balance of anabolic and catabolic pathways in the animal.

Several studies have demonstrated a role for the DILP signaling pathway in regulating carbohydrate homeostasis. For example, circulating and/or stored carbohydrates were shown to accumulate as a result of disrupting DILP secretion or ablating IPCs (Haselton et al., 2010; Rulifson et al., 2002). Consistent with these results, deletion of *dilp* genes or downstream DILP signaling components, such as *InR* or a PI3K ortholog *dp110*, also leads to an elevation of carbohydrates (Murillo-Maldonado et al., 2011; Shingleton et al., 2005). Conversely, mutants for negative regulators of insulin signaling like the lipocalin *Neural lazarillo (Nlaz)*, *PTEN*, *TORC*, or the ortholog of the insulin-like growth factor binding protein-acid labile subunit *dALS*, display reduced carbohydrate levels (Arquier et al., 2008; Hull-Thompson et al., 2009; Oldham et al., 2002; Wang et al., 2008). These studies provide strong evidence that DILP signaling is central to maintaining carbohydrate homeostasis *in vivo*, analogous to the role of insulin in mammals, and suggest that *Drosophila* may provide a powerful model to study the cellular and molecular mechanisms underlying diabetes pathophysiology. Several lines of experimentation have provided further support for this proposal. For example, although trehalose is the major circulating sugar present in larvae, glucose and trehalose are present at nearly equal levels in adult flies (Figures 3.2A and 3.2B) (Barry et al., manuscript in preparation). Consistent with this observation, disrupting insulin signaling

in adults causes hyperglycemia similar to that observed in humans, as well as hypertrehalosemia, which is specific to insects (Haselton et al., 2010). Moreover, insulin signaling is both necessary and sufficient for the clearance of circulating glucose from hemolymph in adult flies, suggesting DILP signaling promotes glucose uptake *in vivo* (Haselton et al., 2010; Haselton and Fridell, 2010). These results demonstrate that disrupting DILP signaling in flies leads to hyperglycemia and reduced glucose tolerance, which are two defining characteristics of diabetes in the clinic (Inzucchi, 2012).

In addition, a number of recent studies have led to the exciting and important conclusion that *Drosophila* may provide a genetic model to study the mechanisms of glucose stimulated insulin secretion (GSIS). In mammals, GSIS is a process characterized by a series of steps in pancreatic beta cells that link the oxidation of circulating glucose to insulin secretion through ATP production, plasma membrane depolarization, and cellular calcium uptake (Prentki et al., 2013). Although amino acids, but not glucose, were shown to trigger DILP secretion from the IPCs of *Drosophila* larvae, recent evidence from our lab and others indicates that glucose is sufficient to stimulate DILP secretion from adult IPCs, analogous to pancreatic beta cells (Geminard et al., 2009). For example, IPCs isolated from adult flies depolarize and take up Ca^{2+} when incubated with glucose *in vitro* (Fridell et al., 2009; Kreneisz et al., 2010). Moreover, adult IPCs express subunits of the K_{ATP}-dependent channel known to be critical for GSIS in mammals (Fridell et al., 2009; Kreneisz et al., 2010). Consistent with this observation, adult IPCs respond to pharmacological K_{ATP}-dependent channel inhibitors used to promote insulin secretion in patients with diabetes (Fridell et al., 2009; Kreneisz et al., 2010). Finally, glucose

feeding is sufficient to trigger DILP secretion from the IPCs of adult flies (Barry et al., manuscript in preparation).

Interestingly, a *Drosophila* model of diet-induced type 2 diabetes has also been recently reported. A diet containing high sugar levels was shown to cause insulin resistance and hyperglycemia in wild type flies (Musselman et al., 2011). This diet promotes cardiac dysfunction and an increased susceptibility to tumors, similar to complications associated with diabetes (Hirabayashi et al., 2013; Na et al., 2013). Insulin resistance in *Drosophila* promotes changes in fatty acid metabolism and is regulated by the lipocalin *Nlaz* (Musselman et al., 2013; Pasco and Leopold, 2012). In mammals, alterations in lipid homeostasis and lipocalin signaling have been implicated in insulin resistance, suggesting that some mechanisms underlying insulin sensitivity may be conserved from flies to mammals (Law et al., 2010; Samuel and Shulman, 2012). Taken together, these recent findings all suggest that *Drosophila* provides a suitable model to study the molecular mechanisms underlying diabetes etiology.

Thesis outline

The identification and functional analysis of the MPC, SDHAF3, and SDHAF4 is presented in Chapters 2–5. This work, which was done in close collaboration with several other groups, has revealed novel regulators of mitochondrial energy metabolism and new aspects of physiology in *Drosophila*. Moreover, in at least one case, we linked our discovery to the identification of a novel human disease gene.

In Chapter 2, we report the identification and functional characterization of the mitochondrial pyruvate carrier. In this study, we characterized two related proteins called

MPC1 and MPC2 that physically interact with each other to form a oligomeric complex embedded in the mitochondrial inner membrane. *Drosophila MPC1* (*dMPC1*) mutants display phenotypes consistent with altered carbohydrate metabolism, including sensitivity to a sugar-only diet and elevated carbohydrate levels. Loss of *dMPC1* also causes a defect in pyruvate metabolism, as *dMPC1* mutants display elevated pyruvate levels combined with a reduction of TCA cycle intermediates and ATP. Building on these results, we demonstrate that Mpc1 is required for pyruvate uptake in isolated yeast mitochondria. Consistent with these observations in yeast and flies, knockdown of *MPC1* or *MPC1* in human cells causes a defect in pyruvate oxidation. Importantly, our identification of a CHC-resistant point mutation in yeast *Mpc1* suggests that Mpc1 is either the target of the drug, or in close proximity to its target, thus linking our work to previous biochemical studies of the MPC. Interestingly, we found that previously described patients displaying a disease characterized by a defect in mitochondrial pyruvate uptake carry loss-of-function mutations in *MPC1*. Overall, this chapter demonstrates that the conserved MPC complex is, or is a component of, the previously uncharacterized mitochondrial pyruvate carrier. As a co-first author of this work, I performed all of the *Drosophila* experiments presented in this chapter.

Chapter 3 represents an extension of our analysis of the defects in carbohydrate homeostasis observed in *dMPC1* mutants. This work demonstrates that *dMPC1* mutants display hallmarks of diabetes, including toxicity associated with increased dietary sugar, hyperglycemia, elevated fasting glucose levels, and impaired glucose tolerance. Moreover, we show that defects in peripheral insulin signaling accompany these phenotypes. Preliminary results suggest that the reduction in peripheral insulin signaling

may be caused by a defect in DILP secretion from the IPCs. Future directions aimed at determining the mechanisms by which the MPC promotes glucose homeostasis and insulin signaling activity in *Drosophila* are also described.

Chapters 4 and 5 are complementary studies in which we identified two novel SDH assembly factors, called SDHAF4 (Chapter 4) and SDHAF3 (Chapter 5), and performed a mechanistic characterization of the previously discovered protein SDHAF1 (Chapter 5). Loss of SDHAF3 or SDHAF4 results in reduced assembly and activity of SDH in yeast, flies, and human cells. Accompanying this defect, flies or yeast cells mutant for either *SDHAF3* or *SDHAF4* accumulate succinate and display reduced levels of fumarate and malate. Further, we show that *Drosophila SDHAF4* mutants display a reduced lifespan, seizure susceptibility, neurodegeneration, and sensitivity to oxidative stress. Similar, but weaker, phenotypes are present in *dSDHAF3* mutants. All of these assembly factors appear to affect redox homeostasis through protein-protein interactions with SDH subunits to promote SDH complex assembly. SDHAF3 and SDHAF1 physically interact with the SDHB subunit to protect FeS clusters from ROS, whereas SDHAF4 physically interacts with the flavinated SDHA subunit to prevent auto-oxidation. Together, these studies provide new insights into the mechanisms of SDH complex assembly and reveal novel candidate causative genes for diseases characterized by SDH deficiency. As a co-first author on chapter 4, I performed all *Drosophila* experiments in this study. My contribution to chapter 6 is smaller, however, as I generated the *dSDHAF3* mutants and transgenic flies carrying the *UAS-dSDHAF4* construct, both of which were subsequently characterized by Wendou Yu. All other experiments in Chapters 4 and 5 were performed by other co-authors.

References

Alberts, B., Johnson, A., Lewis, J., Raff, M., Roberts, K., and Walter, P. (2002). Molecular Biology of the Cell, 4th edition. (New York: Garland Science). Accessed online at http://www.ncbi.nlm.nih.gov/books/NBK21054.

Alic, N., Andrews, T.D., Giannakou, M.E., Papatheodorou, I., Slack, C., Hoddinott, M.P., Cocheme, H.M., Schuster, E.F., Thornton, J.M., and Partridge, L. (2011). Genome-wide dFOXO targets and topology of the transcriptomic response to stress and insulin signalling. Mol. Syst. Biol. *7*, 502.

Alston, C.L., Davison, J.E., Meloni, F., van der Westhuizen, F.H., He, L., Hornig-Do, H.T., Peet, A.C., Gissen, P., Goffrini, P., Ferrero, I., et al. (2012). Recessive germline SDHA and SDHB mutations causing leukodystrophy and isolated mitochondrial complex II deficiency. J. Med. Genet. *49*, 569–577.

Arquier, N., Geminard, C., Bourouis, M., Jarretou, G., Honegger, B., Paix, A., and Leopold, P. (2008). Drosophila ALS regulates growth and metabolism through functional interaction with insulin-like peptides. Cell Metab. *7*, 333–338.

Astuti, D., Latif, F., Dallol, A., Dahia, P.L., Douglas, F., George, E., Skoldberg, F., Husebye, E.S., Eng, C., and Maher, E.R. (2001). Gene mutations in the succinate dehydrogenase subunit SDHB cause susceptibility to familial pheochromocytoma and to familial paraganglioma. Am. J. Hum. Genet. *69*, 49–54.

Bardella, C., Pollard, P.J., and Tomlinson, I. (2011). SDH mutations in cancer. Biochim. Biophys. Acta *1807*, 1432–1443.

Barrientos, A. (2003). Yeast models of human mitochondrial diseases. IUBMB Life *55*, 83–95.

Bayley, J.P., Devilee, P., and Taschner, P.E. (2005). The SDH mutation database: an online resource for succinate dehydrogenase sequence variants involved in pheochromocytoma, paraganglioma and mitochondrial complex II deficiency. BMC Med. Genet. *6*, 39.

Baysal, B.E., Ferrell, R.E., Willett-Brozick, J.E., Lawrence, E.C., Myssiorek, D., Bosch, A., van der Mey, A., Taschner, P.E., Rubinstein, W.S., Myers, E.N., et al. (2000). Mutations in SDHD, a mitochondrial complex II gene, in hereditary paraganglioma. Science *287*, 848–851.

Berg, J.M., Tymoczko, J.L., and Stryer, L. (2002). Biochemistry. 5th Edition. (New York: W. H. Freeman). Accessed online at http://www.ncbi.nlm.nih.gov/books/NBK21154.

Bharucha, K.N., Tarr, P., and Zipursky, S.L. (2008). A glucagon-like endocrine pathway in *Drosophila* modulates both lipid and carbohydrate homeostasis. J. Exp. Biol. *211*, 3103–3110.

Bolli, R., Nalecz, K.A., and Azzi, A. (1989). Monocarboxylate and alpha-ketoglutarate carriers from bovine heart mitochondria. Purification by affinity chromatography on immobilized 2-cyano-4-hydroxycinnamate. J. Biol. Chem. *264*, 18024–18030.

Bonifati, V., Rizzu, P., van Baren, M.J., Schaap, O., Breedveld, G.J., Krieger, E., Dekker, M.C., Squitieri, F., Ibanez, P., Joosse, M., et al. (2003). Mutations in the DJ-1 gene associated with autosomal recessive early-onset parkinsonism. Science *299*, 256–259.

Boudina, S., Sena, S., Theobald, H., Sheng, X., Wright, J.J., Hu, X.X., Aziz, S., Johnson, J.I., Bugger, H., Zaha, V.G., et al. (2007). Mitochondrial energetics in the heart in obesity-related diabetes: direct evidence for increased uncoupled respiration and activation of uncoupling proteins. Diabetes *56*, 2457–2466.

Bourgeron, T., Rustin, P., Chretien, D., Birch-Machin, M., Bourgeois, M., Viegas-Pequignot, E., Munnich, A., and Rotig, A. (1995). Mutation of a nuclear succinate dehydrogenase gene results in mitochondrial respiratory chain deficiency. Nat. Genet. *11*, 144–149.

Brailsford, M.A., Thompson, A.G., Kaderbhai, N., and Beechey, R.B. (1986). The extraction and reconstitution of the alpha-cyanocinnamate-sensitive pyruvate transporter from castor bean mitochondria. Biochem. Biophys. Res. Commun. *140*, 1036–1042.

Calvo, S.E., and Mootha, V.K. (2010). The mitochondrial proteome and human disease. Annu. Rev. Genomics. Hum. Genet. *11*, 25–44.

Capuano, F., Di Paola, M., Azzi, A., and Papa, S. (1990). The monocarboxylate carrier from rat liver mitochondria. Purification and kinetic characterization in a reconstituted system. FEBS Lett. *261*, 39–42.

Cecchini, G. (2003). Function and structure of complex II of the respiratory chain. Annu. Rev. Biochem. *72*, 77–109.

Celotto, A.M., Frank, A.C., McGrath, S.W., Fergestad, T., Van Voorhies, W.A., Buttle, K.F., Mannella, C.A., and Palladino, M.J. (2006). Mitochondrial encephalomyopathy in *Drosophila*. J. Neurosci. *26*, 810–820.

Celotto, A.M., Liu, Z., Vandemark, A.P., and Palladino, M.J. (2012). A novel *Drosophila* SOD2 mutant demonstrates a role for mitochondrial ROS in neurodevelopment and disease. Brain Behav. *2*, 424–434.

Chan, C.B., MacDonald, P.E., Saleh, M.C., Johns, D.C., Marban, E., and Wheeler, M.B. (1999). Overexpression of uncoupling protein 2 inhibits glucose-stimulated insulin secretion from rat islets. Diabetes *48*, 1482–1486.

Chatterjee, A., Mambo, E., and Sidransky, D. (2006). Mitochondrial DNA mutations in human cancer. Oncogene *25*, 4663–4674.

Chen, Y.C., Taylor, E.B., Dephoure, N., Heo, J.M., Tonhato, A., Papandreou, I., Nath, N., Denko, N.C., Gygi, S.P., and Rutter, J. (2012). Identification of a protein mediating respiratory supercomplex stability. Cell Metab. *15*, 348–360.

Cheng, Z., Guo, S., Copps, K., Dong, X., Kollipara, R., Rodgers, J.T., Depinho, R.A., Puigserver, P., and White, M.F. (2009). Foxo1 integrates insulin signaling with mitochondrial function in the liver. Nat. Med. *15*, 1307–1311.

Choi, C.S., Ghoshal, P., Srinivasan, M., Kim, S., Cline, G., and Patel, M.S. (2010). Liver-specific pyruvate dehydrogenase complex deficiency upregulates lipogenesis in adipose tissue and improves peripheral insulin sensitivity. Lipids *45*, 987–995.

Choo, H.J., Kim, J.H., Kwon, O.B., Lee, C.S., Mun, J.Y., Han, S.S., Yoon, Y.S., Yoon, G., Choi, K.M., and Ko, Y.G. (2006). Mitochondria are impaired in the adipocytes of type 2 diabetic mice. Diabetologia *49*, 784–791.

Clark, I.E., Dodson, M.W., Jiang, C., Cao, J.H., Huh, J.R., Seol, J.H., Yoo, S.J., Hay, B.A., and Guo, M. (2006). *Drosophila* pink1 is required for mitochondrial function and interacts genetically with parkin. Nature *441*, 1162–1166.

Diaz, F., Kotarsky, H., Fellman, V., and Moraes, C.T. (2011). Mitochondrial disorders caused by mutations in respiratory chain assembly factors. Semin. Fetal Neonatal Med. *16*, 197–204.

Diaz, F., Thomas, C.K., Garcia, S., Hernandez, D., and Moraes, C.T. (2005). Mice lacking COX10 in skeletal muscle recapitulate the phenotype of progressive mitochondrial myopathies associated with cytochrome c oxidase deficiency. Hum. Mol. Genet. *14*, 2737–2748.

Elmore, S. (2007). Apoptosis: a review of programmed cell death. Toxicol. Pathol. *35*, 495–516.

Feichtinger, R.G., Zimmermann, F., Mayr, J.A., Neureiter, D., Hauser-Kronberger, C., Schilling, F.H., Jones, N., Sperl, W., and Kofler, B. (2010). Low aerobic mitochondrial energy metabolism in poorly- or undifferentiated neuroblastoma. BMC Cancer *10*, 149.

Fergestad, T., Bostwick, B., and Ganetzky, B. (2006a). Metabolic disruption in *Drosophila* bang-sensitive seizure mutants. Genetics *173*, 1357–1364.

Fergestad, T., Ganetzky, B., and Palladino, M.J. (2006b). Neuropathology in *Drosophila* membrane excitability mutants. Genetics *172*, 1031–1042.

Fergestad, T., Olson, L., Patel, K.P., Miller, R., Palladino, M.J., and Ganetzky, B. (2008). Neuropathology in *Drosophila* mutants with increased seizure susceptibility. Genetics *178*, 947–956.

Fernandes, C., and Rao, Y. (2011). Genome-wide screen for modifiers of Parkinson's disease genes in *Drosophila*. Mol. Brain *4*, 17.

Fernandez-Vizarra, E., Tiranti, V., and Zeviani, M. (2009). Assembly of the oxidative phosphorylation system in humans: what we have learned by studying its defects. Biochim. Biophys. Acta *1793*, 200–211.

Fridell, Y.W., Hoh, M., Kreneisz, O., Hosier, S., Chang, C., Scantling, D., Mulkey, D.K., and Helfand, S.L. (2009). Increased uncoupling protein (UCP) activity in *Drosophila* insulin-producing neurons attenuates insulin signaling and extends lifespan. Aging *1*, 699–713.

Fukui, H., Diaz, F., Garcia, S., and Moraes, C.T. (2007). Cytochrome c oxidase deficiency in neurons decreases both oxidative stress and amyloid formation in a mouse model of Alzheimer's disease. Proc. Natl. Acad. Sci. USA *104*, 14163–14168.

Garcia-Cazorla, A., Rabier, D., Touati, G., Chadefaux-Vekemans, B., Marsac, C., de Lonlay, P., and Saudubray, J.M. (2006). Pyruvate carboxylase deficiency: metabolic characteristics and new neurological aspects. Ann. Neurol. *59*, 121–127.

Geminard, C., Rulifson, E.J., and Leopold, P. (2009). Remote control of insulin secretion by fat cells in *Drosophila*. Cell Metab. *10*, 199–207.

Ghezzi, D., Goffrini, P., Uziel, G., Horvath, R., Klopstock, T., Lochmuller, H., D'Adamo, P., Gasparini, P., Strom, T.M., Prokisch, H., et al. (2009). SDHAF1, encoding a LYR complex-II specific assembly factor, is mutated in SDH-defective infantile leukoencephalopathy. Nat. Genet. *41*, 654–656.

Gray, L.R., Tompkins, S.C., and Taylor, E.B. (2013). Regulation of pyruvate metabolism and human disease. Cell. Mol. Life Sci. Advanced online publication. PMID: 24363178.

Greene, J.C., Whitworth, A.J., Kuo, I., Andrews, L.A., Feany, M.B., and Pallanck, L.J. (2003). Mitochondrial pathology and apoptotic muscle degeneration in *Drosophila* parkin mutants. Proc. Natl. Acad. Sci. USA *100*, 4078–4083.

Grewal, S.S. (2009). Insulin/TOR signaling in growth and homeostasis: a view from the fly world. Int. J. Biochem. Cell. Biol. *41*, 1006–1010.

Guo, M. (2010). What have we learned from *Drosophila* models of Parkinson's disease? Prog. Brain Res. *184*, 3–16.

Guo, X., Macleod, G.T., Wellington, A., Hu, F., Panchumarthi, S., Schoenfield, M., Marin, L., Charlton, M.P., Atwood, H.L., and Zinsmaier, K.E. (2005). The GTPase dMiro is required for axonal transport of mitochondria to *Drosophila* synapses. Neuron *47*, 379–393.

Gusdon, A.M., Zhu, J., Van Houten, B., and Chu, C.T. (2012). ATP13A2 regulates mitochondrial bioenergetics through macroautophagy. Neurobiol. Dis. *45*, 962–972

Hales, K.G., and Fuller, M.T. (1997). Developmentally regulated mitochondrial fusion mediated by a conserved, novel, predicted GTPase. Cell *90*, 121–129.

Halestrap, A.P. (1975). The mitochondrial pyruvate carrier. Kinetics and specificity for substrates and inhibitors. Biochem. J. *148*, 85–96.

Halestrap, A.P., and Denton, R.M. (1974). Specific inhibition of pyruvate transport in rat liver mitochondria and human erythrocytes by alpha-cyano-4-hydroxycinnamate. Biochem. J. *138*, 313–316.

Hanahan, D., and Weinberg, R.A. (2011). Hallmarks of cancer: the next generation. Cell *144*, 646–674.

Hao, H.X., Khalimonchuk, O., Schraders, M., Dephoure, N., Bayley, J.P., Kunst, H., Devilee, P., Cremers, C.W., Schiffman, J.D., Bentz, B.G., et al. (2009). SDH5, a gene required for flavination of succinate dehydrogenase, is mutated in paraganglioma. Science *325*, 1139–1142.

Haselton, A., Sharmin, E., Schrader, J., Sah, M., Poon, P., and Fridell, Y.W. (2010). Partial ablation of adult *Drosophila* insulin-producing neurons modulates glucose homeostasis and extends life span without insulin resistance. Cell Cycle *9*, 3063–3071.

Haselton, A.T., and Fridell, Y.W. (2010). Adult *Drosophila melanogaster* as a model for the study of glucose homeostasis. Aging *2*, 523–526.

Hauptmann, S., Scherping, I., Drose, S., Brandt, U., Schulz, K.L., Jendrach, M., Leuner, K., Eckert, A., and Muller, W.E. (2009). Mitochondrial dysfunction: an early event in Alzheimer pathology accumulates with age in AD transgenic mice. Neurobiol. Aging *30*, 1574–1586.

Heo, J.M., Livnat-Levanon, N., Taylor, E.B., Jones, K.T., Dephoure, N., Ring, J., Xie, J., Brodsky, J.L., Madeo, F., Gygi, S.P., et al. (2010). A stress-responsive system for mitochondrial protein degradation. Mol. Cell *40*, 465–480.

Hers, H.G. (1990). Mechanisms of blood glucose homeostasis. J. Inherit. Metab. Dis. *13*, 395–410.

Herzig, S., Raemy, E., Montessuit, S., Veuthey, J.L., Zamboni, N., Westermann, B., Kunji, E.R., and Martinou, J.C. (2012). Identification and functional expression of the mitochondrial pyruvate carrier. Science *337*, 93–96.

Hildyard, J.C., and Halestrap, A.P. (2003). Identification of the mitochondrial pyruvate carrier in *Saccharomyces cerevisiae*. Biochem. J. *374*, 607–611.

Hirabayashi, S., Baranski, T.J., and Cagan, R.L. (2013). Transformed *Drosophila* cells evade diet-mediated insulin resistance through wingless signaling. Cell *154*, 664–675.

Hojlund, K., Mogensen, M., Sahlin, K., and Beck-Nielsen, H. (2008). Mitochondrial dysfunction in type 2 diabetes and obesity. Endocrinol. Metab. Clin. North Am. *37*, 713–731.

Horvath, R., Abicht, A., Holinski-Feder, E., Laner, A., Gempel, K., Prokisch, H., Lochmuller, H., Klopstock, T., and Jaksch, M. (2006). Leigh syndrome caused by mutations in the flavoprotein (Fp) subunit of succinate dehydrogenase (SDHA). J. Neurol. Neurosurg. Psychiatry *77*, 74–76.

Hull-Thompson, J., Muffat, J., Sanchez, D., Walker, D.W., Benzer, S., Ganfornina, M.D., and Jasper, H. (2009). Control of metabolic homeostasis by stress signaling is mediated by the lipocalin NLaz. PLoS Genet. *5*, e1000460.

Hwangbo, D.S., Gershman, B., Tu, M.P., Palmer, M., and Tatar, M. (2004). *Drosophila* dFOXO controls lifespan and regulates insulin signalling in brain and fat body. Nature *429*, 562–566.

Inzucchi, S.E. (2012). Clinical practice. Diagnosis of diabetes. N. Engl. J. Med. *367*, 542–550.

Janeway, K.A., Kim, S.Y., Lodish, M., Nose, V., Rustin, P., Gaal, J., Dahia, P.L., Liegl, B., Ball, E.R., Raygada, M., et al. (2011). Defects in succinate dehydrogenase in gastrointestinal stromal tumors lacking KIT and PDGFRA mutations. Proc. Natl. Acad. Sci. USA *108*, 314–318.

Jeoung, N.H., and Harris, R.A. (2008). Pyruvate dehydrogenase kinase-4 deficiency lowers blood glucose and improves glucose tolerance in diet-induced obese mice. Am. J. Physiol. Endocrinol. Metab. *295*, E46–54.

Jitrapakdee, S., St Maurice, M., Rayment, I., Cleland, W.W., Wallace, J.C., and Attwood, P.V. (2008). Structure, mechanism and regulation of pyruvate carboxylase. Biochem. J. *413*, 369–2387.

Jitrapakdee, S., Vidal-Puig, A., and Wallace, J.C. (2006). Anaplerotic roles of pyruvate carboxylase in mammalian tissues. Cell. Mol. Life Sci. *63*, 843–854.

Joseph, J.W., Koshkin, V., Saleh, M.C., Sivitz, W.I., Zhang, C.Y., Lowell, B.B., Chan, C.B., and Wheeler, M.B. (2004). Free fatty acid-induced beta-cell defects are dependent on uncoupling protein 2 expression. J. Biol. Chem. *279*, 51049–51056.

Kelley, D.E., He, J., Menshikova, E.V., and Ritov, V.B. (2002). Dysfunction of mitochondria in human skeletal muscle in type 2 diabetes. Diabetes *51*, 2944–2950.

Kim, S.K., and Rulifson, E.J. (2004). Conserved mechanisms of glucose sensing and regulation by *Drosophila* corpora cardiaca cells. Nature *431*, 316–320.

Kitada, T., Asakawa, S., Hattori, N., Matsumine, H., Yamamura, Y., Minoshima, S., Yokochi, M., Mizuno, Y., and Shimizu, N. (1998). Mutations in the parkin gene cause autosomal recessive juvenile parkinsonism. Nature *392*, 605–608.

Kong, J., and Xu, Z. (1998). Massive mitochondrial degeneration in motor neurons triggers the onset of amyotrophic lateral sclerosis in mice expressing a mutant SOD1. J. Neurosci. *18*, 3241–3250.

Kopeikina, K.J., Carlson, G.A., Pitstick, R., Ludvigson, A.E., Peters, A., Luebke, J.I., Koffie, R.M., Frosch, M.P., Hyman, B.T., and Spires-Jones, T.L. (2011). Tau accumulation causes mitochondrial distribution deficits in neurons in a mouse model of tauopathy and in human Alzheimer's disease brain. Am. J. Path. *179*, 2071–2082.

Koves, T.R., Ussher, J.R., Noland, R.C., Slentz, D., Mosedale, M., Ilkayeva, O., Bain, J., Stevens, R., Dyck, J.R., Newgard, C.B., et al. (2008). Mitochondrial overload and incomplete fatty acid oxidation contribute to skeletal muscle insulin resistance. Cell Metab. *7*, 45–56.

Kreneisz, O., Chen, X., Fridell, Y.W., and Mulkey, D.K. (2010). Glucose increases activity and Ca2+ in insulin-producing cells of adult *Drosophila*. Neuroreport *21*, 1116–1120.

Kruse, S.E., Watt, W.C., Marcinek, D.J., Kapur, R.P., Schenkman, K.A., and Palmiter, R.D. (2008). Mice with mitochondrial complex I deficiency develop a fatal encephalomyopathy. Cell Metab. *7*, 312–320.

Kumashiro, N., Beddow, S.A., Vatner, D.F., Majumdar, S.K., Cantley, J.L., Guebre-Egziabher, F., Fat, I., Guigni, B., Jurczak, M.J., Birkenfeld, A.L., et al. (2013). Targeting pyruvate carboxylase reduces gluconeogenesis and adiposity and improves insulin resistance. Diabetes *62*, 2183–2194.

Law, I.K., Xu, A., Lam, K.S., Berger, T., Mak, T.W., Vanhoutte, P.M., Liu, J.T., Sweeney, G., Zhou, M., Yang, B., et al. (2010). Lipocalin-2 deficiency attenuates insulin resistance associated with aging and obesity. Diabetes *59*, 872–882.

Lax, N., and Jaros, E. (2012). Neurodegeneration in primary mitochondrial disorders. In Mitochondrial Dysfunction in Neurodegenerative Disorders. A.K. Reeve, K.J. Krishnan, M.R. Duchen, and D.M. Turnbull, *Eds*., pp. 21–41.

Lin, M.T., and Beal, M.F. (2006). Mitochondrial dysfunction and oxidative stress in neurodegenerative diseases. Nature *443*, 787–795.

Liu, W., Gnanasambandam, R., Benjamin, J., Kaur, G., Getman, P.B., Siegel, A.J., Shortridge, R.D., and Singh, S. (2007). Mutations in cytochrome c oxidase subunit VIa cause neurodegeneration and motor dysfunction in *Drosophila*. Genetics *176*, 937–946.

Lotz, C., Lin, A.J., Black, C.M., Zhang, J., Lau, E., Deng, N., Wang, Y., Zong, N.C., Choi, J.H., Xu, T., et al. (2013). Characterization, Design, and Function of the Mitochondrial Proteome: From Organs to Organisms. J. Proteome Res. Advanced online publication. PMID: 24070373.

Lowell, B.B., and Shulman, G.I. (2005). Mitochondrial dysfunction and type 2 diabetes. Science *307*, 384–387.

Lu, H., Koshkin, V., Allister, E.M., Gyulkhandanyan, A.V., and Wheeler, M.B. (2010). Molecular and metabolic evidence for mitochondrial defects associated with beta-cell dysfunction in a mouse model of type 2 diabetes. Diabetes *59*, 448–459.

Lunt, S.Y., and Vander Heiden, M.G. (2011). Aerobic glycolysis: meeting the metabolic requirements of cell proliferation. Ann. Rev. Cell. Dev. Biol. *27*, 441–464.

Maj, M.C., MacKay, N., Levandovskiy, V., Addis, J., Baumgartner, E.R., Baumgartner, M.R., Robinson, B.H., and Cameron, J.M. (2005). Pyruvate dehydrogenase phosphatase deficiency: identification of the first mutation in two brothers and restoration of activity by protein complementation. J. Clin. Endocrinol. Metab. *90*, 4101–4107.

Mandal, S., Guptan, P., Owusu-Ansah, E., and Banerjee, U. (2005). Mitochondrial regulation of cell cycle progression during development as revealed by the tenured mutation in *Drosophila*. Dev. Cell *9*, 843–854.

Mast, J.D., Tomalty, K.M., Vogel, H., and Clandinin, T.R. (2008). Reactive oxygen species act remotely to cause synapse loss in a *Drosophila* model of developmental mitochondrial encephalopathy. Development *135*, 2669–2679.

Maurer, C.M., Schonthaler, H.B., Mueller, K.P., and Neuhauss, S.C. (2010). Distinct retinal deficits in a zebrafish pyruvate dehydrogenase-deficient mutant. J. Neurosci. *30*, 11962–11972.

McFate, T., Mohyeldin, A., Lu, H., Thakar, J., Henriques, J., Halim, N.D., Wu, H., Schell, M.J., Tsang, T.M., Teahan, O., et al. (2008). Pyruvate dehydrogenase complex activity controls metabolic and malignant phenotype in cancer cells. J. Biol. Chem. *283*, 22700–22708.

Mootha, V.K., Lindgren, C.M., Eriksson, K.F., Subramanian, A., Sihag, S., Lehar, J., Puigserver, P., Carlsson, E., Ridderstrale, M., Laurila, E., et al. (2003). PGC-1alpha-responsive genes involved in oxidative phosphorylation are coordinately downregulated in human diabetes. Nat. Genet. *34*, 267–273.

Morais, V.A., and De Strooper, B. (2010). Mitochondria dysfunction and neurodegenerative disorders: cause or consequence. J. Alzheimers Dis. *20 Suppl 2*, S255–263.

Moreira, P.I., Carvalho, C., Zhu, X., Smith, M.A., and Perry, G. (2010). Mitochondrial dysfunction is a trigger of Alzheimer's disease pathophysiology. Biochim. Biophys. Acta *1802*, 2–10.

Morino, K., Petersen, K.F., Dufour, S., Befroy, D., Frattini, J., Shatzkes, N., Neschen, S., White, M.F., Bilz, S., Sono, S., et al. (2005). Reduced mitochondrial density and increased IRS-1 serine phosphorylation in muscle of insulin-resistant offspring of type 2 diabetic parents. J. Clin. Invest. *115*, 3587–3593.

Murillo-Maldonado, J.M., Sanchez-Chavez, G., Salgado, L.M., Salceda, R., and Riesgo-Escovar, J.R. (2011). Drosophila insulin pathway mutants affect visual physiology and brain function besides growth, lipid, and carbohydrate metabolism. Diabetes *60*, 1632–1636.

Musselman, L.P., Fink, J.L., Narzinski, K., Ramachandran, P.V., Hathiramani, S.S., Cagan, R.L., and Baranski, T.J. (2011). A high-sugar diet produces obesity and insulin resistance in wild-type *Drosophila*. Dis. Model. Mech. *4*, 842–849.

Musselman, L.P., Fink, J.L., Ramachandran, P.V., Patterson, B.W., Okunade, A.L., Maier, E., Brent, M.R., Turk, J., and Baranski, T.J. (2013). Role of fat body lipogenesis in protection against the effects of caloric overload in Drosophila. J. Biol. Chem. *288*, 8028–8042.

Na, J., Musselman, L.P., Pendse, J., Baranski, T.J., Bodmer, R., Ocorr, K., and Cagan, R. (2013). A *Drosophila* model of high sugar diet-induced cardiomyopathy. PLoS Genet. *9*, e1003175.

Nalecz, M.J., Nalecz, K.A., Broger, C., Bolli, R., Wojtczak, L., and Azzi, A. (1986). Extraction, partial purification and functional reconstitution of two mitochondrial carriers transporting keto acids: 2-oxoglutarate and pyruvate. FEBS Lett. *196*, 331–336.

Narendra, D.P., Jin, S.M., Tanaka, A., Suen, D.F., Gautier, C.A., Shen, J., Cookson, M.R., and Youle, R.J. (2010). PINK1 is selectively stabilized on impaired mitochondria to activate Parkin. PLoS Biol. *8*, e1000298.

Nassel, D.R., Kubrak, O.I., Liu, Y., Luo, J., and Lushchak, O.V. (2013). Factors that regulate insulin producing cells and their output in *Drosophila*. Front. Physiol. *4*, 252.

Niemann, S., and Muller, U. (2000). Mutations in SDHC cause autosomal dominant paraganglioma, type 3. Nat. Genet. *26*, 268–270.

Oldham, S., Stocker, H., Laffargue, M., Wittwer, F., Wymann, M., and Hafen, E. (2002). The Drosophila insulin/IGF receptor controls growth and size by modulating PtdInsP(3) levels. Development *129*, 4103–4109.

Owusu-Ansah, E., Yavari, A., Mandal, S., and Banerjee, U. (2008). Distinct mitochondrial retrograde signals control the G1-S cell cycle checkpoint. Nat. Genet. *40*, 356–361.

Pagliarini, D.J., Calvo, S.E., Chang, B., Sheth, S.A., Vafai, S.B., Ong, S.E., Walford, G.A., Sugiana, C., Boneh, A., Chen, W.K., et al. (2008). A mitochondrial protein compendium elucidates complex I disease biology. Cell *134*, 112–123.

Pagliarini, D.J., and Rutter, J. (2013). Hallmarks of a new era in mitochondrial biochemistry. Genes Dev. *27*, 2615–2627.

Paisan-Ruiz, C., Jain, S., Evans, E.W., Gilks, W.P., Simon, J., van der Brug, M., Lopez de Munain, A., Aparicio, S., Gil, A.M., Khan, N., et al. (2004). Cloning of the gene containing mutations that cause PARK8-linked Parkinson's disease. Neuron *44*, 595–600.

Pandey, U.B., and Nichols, C.D. (2011). Human disease models in *Drosophila melanogaster* and the role of the fly in therapeutic drug discovery. Pharmacol. Rev. *63*, 411–436.

Papa, S., Francavilla, A., Paradies, G., and Meduri, B. (1971). The transport of pyruvate in rat liver mitochondria. FEBS Lett. *12*, 285–288.

Papa, S., and Paradies, G. (1974). On the mechanism of translocation of pyruvate and other monocarboxylic acids in rat-liver mitochondria. FEBS J. *49*, 265–274.

Parfait, B., Chretien, D., Rotig, A., Marsac, C., Munnich, A., and Rustin, P. (2000). Compound heterozygous mutations in the flavoprotein gene of the respiratory chain complex II in a patient with Leigh syndrome. Hum. Genet. *106*, 236–243.

Park, J., Kim, Y., and Chung, J. (2009). Mitochondrial dysfunction and Parkinson's disease genes: insights from *Drosophila*. Dis. Model. Mech. *2*, 336–340.

Park, J., Lee, S.B., Lee, S., Kim, Y., Song, S., Kim, S., Bae, E., Kim, J., Shong, M., Kim, J.M., et al. (2006). Mitochondrial dysfunction in *Drosophila* PINK1 mutants is complemented by parkin. Nature *441*, 1157–1161.

Pasco, M.Y., and Leopold, P. (2012). High sugar-induced insulin resistance in *Drosophila* relies on the lipocalin Neural Lazarillo. PloS One *7*, e36583.

Patel, K.P., O'Brien, T.W., Subramony, S.H., Shuster, J., and Stacpoole, P.W. (2012). The spectrum of pyruvate dehydrogenase complex deficiency: clinical, biochemical and genetic features in 371 patients. Mol. Genet. Metab. *106*, 385–394.

Patel, M.S., and Korotchkina, L.G. (2006). Regulation of the pyruvate dehydrogenase complex. Biochem. Soc. Trans. *34*, 217–222.

Patel, M.S., and Roche, T.E. (1990). Molecular biology and biochemistry of pyruvate dehydrogenase complexes. FASEB J. *4*, 3224–3233.

Patti, M.E., Butte, A.J., Crunkhorn, S., Cusi, K., Berria, R., Kashyap, S., Miyazaki, Y., Kohane, I., Costello, M., Saccone, R., et al. (2003). Coordinated reduction of genes of oxidative metabolism in humans with insulin resistance and diabetes: Potential role of PGC1 and NRF1. Proc. Natl. Acad. Sci. USA *100*, 8466–8471.

Pavlidis, P., and Tanouye, M.A. (1995). Seizures and failures in the giant fiber pathway of *Drosophila* bang-sensitive paralytic mutants. J. Neurosci. *15*, 5810–5819.

Perier, C., Bove, J., Wu, D.C., Dehay, B., Choi, D.K., Jackson-Lewis, V., Rathke-Hartlieb, S., Bouillet, P., Strasser, A., Schulz, J.B., et al. (2007). Two molecular pathways initiate mitochondria-dependent dopaminergic neurodegeneration in experimental Parkinson's Disease. Proc. Natl. Acad. Sci. USA *104*, 8161–8166.

Petersen, K.F., Dufour, S., Befroy, D., Garcia, R., and Shulman, G.I. (2004). Impaired mitochondrial activity in the insulin-resistant offspring of patients with type 2 diabetes. N. Engl. J. Med. *350*, 664–671.

Pliss, L., Pentney, R.J., Johnson, M.T., and Patel, M.S. (2004). Biochemical and structural brain alterations in female mice with cerebral pyruvate dehydrogenase deficiency. J. Neurochem. *91*, 1082–1091.

Poole, A.C., Thomas, R.E., Andrews, L.A., McBride, H.M., Whitworth, A.J., and Pallanck, L.J. (2008). The PINK1/Parkin pathway regulates mitochondrial morphology. Proc. Natl. Acad. Sci. USA *105*, 1638–1643.

Prentki, M., Matschinsky, F.M., and Madiraju, S.R. (2013). Metabolic signaling in fuel-induced insulin secretion. Cell Metab. *18*, 162–185.

Ramirez, A., Heimbach, A., Grundemann, J., Stiller, B., Hampshire, D., Cid, L.P., Goebel, I., Mubaidin, A.F., Wriekat, A.L., Roeper, J., et al. (2006). Hereditary parkinsonism with dementia is caused by mutations in ATP13A2, encoding a lysosomal type 5 P-type ATPase. Nat. Genet. *38*, 1184–1191.

Reinders, J., Zahedi, R.P., Pfanner, N., Meisinger, C., and Sickmann, A. (2006). Toward the complete yeast mitochondrial proteome: multidimensional separation techniques for mitochondrial proteomics. J. Proteome Res. *5*, 1543–1554.

Ricketts, C., Woodward, E.R., Killick, P., Morris, M.R., Astuti, D., Latif, F., and Maher, E.R. (2008). Germline SDHB mutations and familial renal cell carcinoma. J. Natl. Cancer Inst. *100*, 1260–1262.

Ritov, V.B., Menshikova, E.V., He, J., Ferrell, R.E., Goodpaster, B.H., and Kelley, D.E. (2005). Deficiency of subsarcolemmal mitochondria in obesity and type 2 diabetes. Diabetes *54*, 8–14.

Rosen, D.R., Siddique, T., Patterson, D., Figlewicz, D.A., Sapp, P., Hentati, A., Donaldson, D., Goto, J., O'Regan, J.P., Deng, H.X., et al. (1993). Mutations in Cu/Zn superoxide dismutase gene are associated with familial amyotrophic lateral sclerosis. Nature *362*, 59–62.

Rulifson, E.J., Kim, S.K., and Nusse, R. (2002). Ablation of insulin-producing neurons in flies: growth and diabetic phenotypes. Science *296*, 1118–1120.

Russo, G.J., Louie, K., Wellington, A., Macleod, G.T., Hu, F., Panchumarthi, S., and Zinsmaier, K.E. (2009). *Drosophila* Miro is required for both anterograde and retrograde axonal mitochondrial transport. J. Neurosci. *29*, 5443–5455.

Rutter, J., Winge, D.R., and Schiffman, J.D. (2010). Succinate dehydrogenase - Assembly, regulation and role in human disease. Mitochondrion *10*, 393–401.

Samuel, V.T., and Shulman, G.I. (2012). Mechanisms for insulin resistance: common threads and missing links. Cell *148*, 852–871.

Schaefer, A.M., Taylor, R.W., Turnbull, D.M., and Chinnery, P.F. (2004). The epidemiology of mitochondrial disorders—past, present and future. Biochim. Biophys. Acta *1659*, 115–120.

Schapira, A.H. (2006). Mitochondrial disease. Lancet *368*, 70–82.

Schapira, A.H., Cooper, J.M., Dexter, D., Clark, J.B., Jenner, P., and Marsden, C.D. (1990). Mitochondrial complex I deficiency in Parkinson's disease. J. Neurochem. *54*, 823–827.

Schell, J.C., and Rutter, J. (2013). The long and winding road to the mitochondrial pyruvate carrier. Cancer Metab. *1*, 6.

Schmidt, O., Pfanner, N., and Meisinger, C. (2010). Mitochondrial protein import: from proteomics to functional mechanisms. Nat. Rev. Cell. Mol. Biol. *11*, 655–667.

Schon, E.A., and Manfredi, G. (2003). Neuronal degeneration and mitochondrial dysfunction. J. Clin. Inv. *111*, 303–312.

Schrayyef, M.Z., and Gerich, J.E. (2010). Normal Glucose Homeostasis. Principles of Diabetes Mellitus. 16th Edition. (New York, NY: Springer Publishing). L. Poretsky (ed.) pp. 19–34.

Shi, P., Gal, J., Kwinter, D.M., Liu, X., and Zhu, H. (2010). Mitochondrial dysfunction in amyotrophic lateral sclerosis. Biochim. Biophys. Acta *1802*, 45–51.

Shingleton, A.W., Das, J., Vinicius, L., and Stern, D.L. (2005). The temporal requirements for insulin signaling during development in *Drosophila*. PLoS Biol. *3*, e289.

Sickmann, A., Reinders, J., Wagner, Y., Joppich, C., Zahedi, R., Meyer, H.E., Schonfisch, B., Perschil, I., Chacinska, A., Guiard, B., et al. (2003). The proteome of *Saccharomyces cerevisiae* mitochondria. Proc. Natl. Acad. Sci. USA *100*, 13207–13212.

Sidhu, S., Gangasani, A., Korotchkina, L.G., Suzuki, G., Fallavollita, J.A., Canty, J.M., Jr., and Patel, M.S. (2008). Tissue-specific pyruvate dehydrogenase complex deficiency causes cardiac hypertrophy and sudden death of weaned male mice. Am. J. Physiol. Heart Circ. Physiol. *295*, H946–H952.

Skladal, D., Halliday, J., and Thorburn, D.R. (2003). Minimum birth prevalence of mitochondrial respiratory chain disorders in children. Brain *126*, 1905–1912.

Sleigh, A., Raymond-Barker, P., Thackray, K., Porter, D., Hatunic, M., Vottero, A., Burren, C., Mitchell, C., McIntyre, M., Brage, S., et al. (2011). Mitochondrial dysfunction in patients with primary congenital insulin resistance. J. Clin. Inv. *121*, 2457–2461.

Smaili, S.S., Pereira, G.J., Costa, M.M., Rocha, K.K., Rodrigues, L., do Carmo, L.G., Hirata, H., and Hsu, Y.T. (2013). The role of calcium stores in apoptosis and autophagy. Curr. Mol. Med. *13*, 252–265.

Smith, D.G., Gawryluk, R.M., Spencer, D.F., Pearlman, R.E., Siu, K.W., and Gray, M.W. (2007). Exploring the mitochondrial proteome of the ciliate protozoon Tetrahymena thermophila: direct analysis by tandem mass spectrometry. J. Mol. Biol. *374*, 837–863.

Sparks, L.M., Xie, H., Koza, R.A., Mynatt, R., Hulver, M.W., Bray, G.A., and Smith, S.R. (2005). A high-fat diet coordinately downregulates genes required for mitochondrial oxidative phosphorylation in skeletal muscle. Diabetes *54*, 1926–1933.

Srinivasan, M., Choi, C.S., Ghoshal, P., Pliss, L., Pandya, J.D., Hill, D., Cline, G., and Patel, M.S. (2010). Beta-cell-specific pyruvate dehydrogenase deficiency impairs glucose-stimulated insulin secretion. Am. J. Physiol. Endocrinol. Metab. *299*, E910–917.

Sun, F., Huo, X., Zhai, Y., Wang, A., Xu, J., Su, D., Bartlam, M., and Rao, Z. (2005). Crystal structure of mitochondrial respiratory membrane protein complex II. Cell *121*, 1043–1057.

Szendroedi, J., Schmid, A.I., Chmelik, M., Toth, C., Brehm, A., Krssak, M., Nowotny, P., Wolzt, M., Waldhausl, W., and Roden, M. (2007). Muscle mitochondrial ATP synthesis and glucose transport/phosphorylation in type 2 diabetes. PLoS Med. *4*, e154.

Teleman, A.A. (2010). Molecular mechanisms of metabolic regulation by insulin in *Drosophila*. Biochem. J. *425*, 13–26.

Thomas, A.P., and Halestrap, A.P. (1981). Identification of the protein responsible for pyruvate transport into rat liver and heart mitochondria by specific labelling with [3H]N-phenylmaleimide. Biochem. J. *196*, 471–479.

Todisco, S., Agrimi, G., Castegna, A., and Palmieri, F. (2006). Identification of the mitochondrial NAD+ transporter in *Saccharomyces cerevisiae*. J. Biol. Chem. *281*, 1524–1531.

Van der Horst, D.J. (2003). Insect adipokinetic hormones: release and integration of flight energy metabolism. Comp. Biochem. Physiol. B Biochem. Mol. Biol. *136*, 217–226.

Walker, D.W., Hajek, P., Muffat, J., Knoepfle, D., Cornelison, S., Attardi, G., and Benzer, S. (2006). Hypersensitivity to oxygen and shortened lifespan in a *Drosophila* mitochondrial complex II mutant. Proc. Natl. Acad. Sci. USA *103*, 16382–16387.

Wallace, D.C. (2005). A mitochondrial paradigm of metabolic and degenerative diseases, aging, and cancer: a dawn for evolutionary medicine. Ann. Rev. Genet. *39*, 359–407.

Wang, B., Goode, J., Best, J., Meltzer, J., Schilman, P.E., Chen, J., Garza, D., Thomas, J.B., and Montminy, M. (2008). The insulin-regulated CREB coactivator TORC promotes stress resistance in *Drosophila*. Cell Metab. *7*, 434–444.

Winklhofer, K.F., and Haass, C. (2010). Mitochondrial dysfunction in Parkinson's disease. Biochim. Biophys. Acta *1802*, 29-44.

Wong, P.C., Pardo, C.A., Borchelt, D.R., Lee, M.K., Copeland, N.G., Jenkins, N.A., Sisodia, S.S., Cleveland, D.W., and Price, D.L. (1995). An adverse property of a familial ALS-linked SOD1 mutation causes motor neuron disease characterized by vacuolar degeneration of mitochondria. Neuron *14*, 1105–1116.

Xu, W., Barrientos, T., and Andrews, N.C. (2013). Iron and copper in mitochondrial diseases. Cell Metab. *17*, 319–328.

Yan, H., Parsons, D.W., Jin, G., McLendon, R., Rasheed, B.A., Yuan, W., Kos, I., Batinic-Haberle, I., Jones, S., Riggins, G.J., et al. (2009). IDH1 and IDH2 mutations in gliomas. N. Engl. J. Med. *360*, 765–773.

Yang, Y., Gehrke, S., Imai, Y., Huang, Z., Ouyang, Y., Wang, J.W., Yang, L., Beal, M.F., Vogel, H., and Lu, B. (2006). Mitochondrial pathology and muscle and dopaminergic neuron degeneration caused by inactivation of *Drosophila* Pink1 is rescued by Parkin. Proc. Natl. Acad. Sci. USA *103*, 10793–10798.

Zhang, C.Y., Baffy, G., Perret, P., Krauss, S., Peroni, O., Grujic, D., Hagen, T., Vidal-Puig, A.J., Boss, O., Kim, Y.B., et al. (2001). Uncoupling protein-2 negatively regulates insulin secretion and is a major link between obesity, beta cell dysfunction, and type 2 diabetes. Cell *105*, 745–755.

Zhang, H., Liu, J., Li, C.R., Momen, B., Kohanski, R.A., and Pick, L. (2009). Deletion of *Drosophila* insulin-like peptides causes growth defects and metabolic abnormalities. Proc. Natl. Acad. Sci. USA *106*, 19617–19622.

Zhang, Y.Q., Roote, J., Brogna, S., Davis, A.W., Barbash, D.A., Nash, D., and Ashburner, M. (1999). Stress sensitive B encodes an adenine nucleotide translocase in *Drosophila melanogaster*. Genetics *153*, 891–903.

Zimprich, A., Biskup, S., Leitner, P., Lichtner, P., Farrer, M., Lincoln, S., Kachergus, J., Hulihan, M., Uitti, R.J., Calne, D.B., et al. (2004). Mutations in LRRK2 cause autosomal-dominant parkinsonism with pleomorphic pathology. Neuron *44*, 601–607.

CHAPTER 2

A MITOCHONDRIAL PYRUVATE CARRIER REQUIRED FOR PYRUVATE UPTAKE IN YEAST, *DROSOPHILA*, AND HUMANS

Originally published as–Bricker, D.K., Taylor, E.B., Schell, J.C., Orsak, T., Boutron, A., Chen, Y.C., Cox, J.E., Cardon, C.M., Van Vranken, J.G., Dephoure, N., et al. (2012). A mitochondrial pyruvate carrier required for pyruvate uptake in yeast, Drosophila, and humans. Science *337*, 96-100.

*E.B. Taylor, J.C. Schell, T. Orsak and myself are co-first authors on this article.

PDH activity was almost normal in *mpc1*Δ cells grown in rich medium [when the E2 subunit was lipoylated (Fig. 2C)]. Thus, the MPC proteins appeared to act upstream of PDH and may function in the transport of pyruvate into mitochondria. We therefore measured uptake of ^{14}C pyruvate in mitochondria isolated from WT, *mpc1*Δ, *mpc2*Δ, *mpc3*Δ, and *mpc2*Δ*mpc3*Δ cells grown in lactate medium (Fig. 3A). The specificity of uptake was assessed by the use of UK5099, an inhibitor of the mitochondrial pyruvate carrier (*14*). Uptake of pyruvate in WT mitochondria was sensitive to the proton ionophore carbonyl cyanide m-chloro phenyl hydrazone (CCCP) (Fig. 3B). Mitochondria from *mpc1*Δ and *mpc2*Δ*mpc3*Δ cells showed decreased pyruvate uptake (Fig. 3, A and B), despite a normal mitochondrial membrane potential (fig. S5). Surprisingly, deletion of *MPC3* alone impaired pyruvate uptake in mitochondria, whereas mitochondria from the *mpc2*Δ mutant transported pyruvate normally. Because this result did not correlate with the phenotypes of *mpc2*Δ and *mpc3*Δ single mutants grown in SD, we investigated the expression of Mpc2 and Mpc3 in SD and lactate media. In SD, yeast expressed mainly Mpc2, whereas in lactate medium, they mainly expressed Mpc3 (Fig. 3C). This expression pattern could be explained, at least in part, by the presence of binding sites for Gcn4 (a transcription factor activated by amino acid starvation) upstream of *MPC2* (*15*). This raises the possibility that under certain growth conditions, these two proteins might have specific, nonredundant functions.

We next assessed whether mouse MPC1 (mMPC1) and MPC2 (mMPC2) could restore growth of yeast cells lacking a functional pyruvate transporter (Fig. 4, A and B). mMPC1 alone restored growth of *mpc1*Δ cells, but mMPC2 failed to restore growth of the double-deletion strain of its orthologous genes *MPC2* and *MPC3*. However, growth of the triple-deletion strain *mpc1*Δ*mpc2*Δ*mpc3*Δ or of *mpc2*Δ*mpc3*Δ cells was restored by coexpression of both mMPC1 and mMPC2 (Fig. 4A). Thus, mMPC1 and mMPC2 together functionally complement the absence of pyruvate transport. We next expressed mMPC1 and mMPC2, alone and in combination, in the bacterium *Lactococcus lactis* (Fig. 4C), which has been successfully used to express and characterize mitochondrial transporters (*16*). No pyruvate uptake was observed in bacteria expressing either protein alone compared with the empty vector control. However, a fourfold increase in pyruvate uptake was detected when mMPC1 and mMPC2 were coexpressed (Fig. 4, D and E). This uptake was sensitive to the mitochondrial pyruvate carrier inhibitor UK5099 and to 2-deoxyglucose, which collapses the proton electrochemical gradient (Fig. 4E) (*17*). Moreover, artificially increasing the membrane potential by lowering the pH in the import buffer from 7.2 to 6.2 significantly increased pyruvate uptake (two-tailed *t* test, $P < 0.05$) (Fig. 4E). Thus, coexpression of mMPC1 and mMPC2 in bacteria is sufficient to allow import of pyruvate with similar properties to the mitochondrial pyruvate carrier (*3*). We therefore conclude that the mitochondrial pyruvate carrier is composed of Mpc1 and either Mpc2 or Mpc3 in yeast and of MPC1 and MPC2 in mammals.

References and Notes

1. J. K. Hiltunen, Z. Chen, A. M. Haapalainen, R. K. Wierenga, A. J. Kastaniotis, *Prog. Lipid Res.* **49**, 27 (2010).
2. L. J. Reed, *J. Biol. Chem.* **276**, 38329 (2001).
3. A. P. Halestrap, *Biochem. J.* **148**, 85 (1975).
4. S. Da Cruz *et al.*, *J. Biol. Chem.* **278**, 41566 (2003).
5. D. K. Bricker *et al.*, *Science* **337**, 96 (2012).
6. J. R. Dickinson, I. W. Dawes, *J. Gen. Microbiol.* **138**, 2029 (1992).
7. J. R. Dickinson, D. J. Roy, I. W. Dawes, *Mol. Gen. Genet.* **204**, 103 (1986).
8. R. A. Harris, M. Joshi, N. H. Jeoung, M. Obayashi, *J. Nutr.* **135** (suppl.), 1527S (2005).
9. M. S. Schonauer, A. J. Kastaniotis, V. A. Kursu, J. K. Hiltunen, C. L. Dieckmann, *J. Biol. Chem.* **284**, 23234 (2009).
10. J. E. Lawson, R. H. Behal, L. J. Reed, *Biochemistry* **30**, 2834 (1991).
11. K. M. Humphries, L. I. Szweda, *Biochemistry* **37**, 15835 (1998).
12. H. Wada, D. Shintani, J. Ohlrogge, *Proc. Natl. Acad. Sci. U.S.A.* **94**, 1591 (1997).
13. U. Hoja *et al.*, *J. Biol. Chem.* **279**, 21779 (2004).
14. A. P. Halestrap, R. M. Denton, *Biochem. J.* **148**, 97 (1975).
15. K. D. MacIsaac *et al.*, *BMC Bioinformatics* **7**, 113 (2006).
16. E. R. Kunji, D. J. Slotboom, B. Poolman, *Biochim. Biophys. Acta* **1610**, 97 (2003).
17. E. R. Kunji, E. J. Smid, R. Plapp, B. Poolman, W. N. Konings, *J. Bacteriol.* **175**, 2052 (1993).

Acknowledgments: We are grateful to R. Loewith and F. Stutz for strains and technical help, L. Szweda for antibodies, A. Kastaniotis for technical help on lipoic acid determination, Y. Que for erythromycin resistance cassette, and H. Riezman, A. Jourdain, and the Martinou lab for fruitful discussions. This work was supported by Novartis Science Foundation (S.H.), the Swiss National Science Foundation (subsidy 31003A-141068/1 to J.-C.M.), and the state of Geneva.

Supplementary Materials

www.sciencemag.org/cgi/content/full/science.1218530/DC1
Materials and Methods
Supplementary Text
Figs. S1 to S5
Table S1
References (*18*–*23*)

29 December 2011; accepted 11 May 2012
Published online 24 May 2012;
10.1126/science.1218530

A Mitochondrial Pyruvate Carrier Required for Pyruvate Uptake in Yeast, *Drosophila*, and Humans

Daniel K. Bricker,[1]* Eric B. Taylor,[2]* John C. Schell,[2]* Thomas Orsak,[2]* Audrey Boutron,[3] Yu-Chan Chen,[2] James E. Cox,[4] Caleb M. Cardon,[2] Jonathan G. Van Vranken,[2] Noah Dephoure,[5] Claire Redin,[6] Sihem Boudina,[7] Steven P. Gygi,[5] Michèle Brivet,[3] Carl S. Thummel,[1] Jared Rutter[2]†

Pyruvate constitutes a critical branch point in cellular carbon metabolism. We have identified two proteins, Mpc1 and Mpc2, as essential for mitochondrial pyruvate transport in yeast, *Drosophila*, and humans. Mpc1 and Mpc2 associate to form an ~150-kilodalton complex in the inner mitochondrial membrane. Yeast and *Drosophila* mutants lacking *MPC1* display impaired pyruvate metabolism, with an accumulation of upstream metabolites and a depletion of tricarboxylic acid cycle intermediates. Loss of yeast Mpc1 results in defective mitochondrial pyruvate uptake, and silencing of *MPC1* or *MPC2* in mammalian cells impairs pyruvate oxidation. A point mutation in *MPC1* provides resistance to a known inhibitor of the mitochondrial pyruvate carrier. Human genetic studies of three families with children suffering from lactic acidosis and hyperpyruvatemia revealed a causal locus that mapped to *MPC1*, changing single amino acids that are conserved throughout eukaryotes. These data demonstrate that Mpc1 and Mpc2 form an essential part of the mitochondrial pyruvate carrier.

Pyruvate occupies a pivotal node in the regulation of carbon metabolism as it is the end product of glycolysis and a major substrate for the tricarboxylic acid (TCA) cycle in mitochondria. Pyruvate lies at the intersection of these catabolic pathways with anabolic pathways for lipid synthesis, amino acid biosynthesis, and gluconeogenesis. As a result, the failure to correctly partition carbon between these fates lies at the heart of the altered metabolism evident in diabetes, obesity, and cancer (*1*, *2*). Owing to the fundamental importance of pyruvate, the mitochondrial pyruvate carrier (MPC) has been studied extensively (*3*, *4*). This included the discovery that α-cyanocinnamate analogs, such as UK-5099, act as specific and potent inhibitors of carrier activity (*5*). In spite of this characterization, however, the gene or genes that encode the mitochondrial pyruvate carrier remain unknown (*6*, *7*).

As part of an ongoing effort to characterize mitochondrial proteins that are conserved through evolution, we initiated studies of the MPC protein family (originally designated BRP44 and BRP44L

in humans) (*8*). This family contains three members in *Saccharomyces cerevisiae*, encoded by *YGL080W*, *YHR162W*, and *YGR243W*, hereafter referred to as *MPC1*, *MPC2*, and *MPC3*, respectively. Mpc2 and Mpc3 are 79% identical in amino acid sequence and appear to be the product of a recent gene duplication event. Mpc1, Mpc2, and Mpc3 colocalize with mitochondria (Fig. 1A and fig. S2A), consistent with published mitochondrial proteomic studies (*9*, *10*). The mitochondrial localization of Mpc1 and Mpc2 was confirmed by biochemical fractionation (Fig. 1B). Mpc1, Mpc2, and Mpc3 were enriched in mitochondrial membranes (fig. S2B), consistent with the presence of predicted transmembrane domains in their sequences (fig. S1). Mpc1 and Mpc2 were resistant to protease treatment unless the mitochondrial outer membrane was ruptured (Fig. 1B and fig. S2C), implying that they are embedded in the mitochondrial inner membrane. Chromatographic purification of tagged variants of Mpc1 and Mpc2, followed by mass spectrometry, revealed that Mpc2 and Mpc3 were among the major interacting proteins of Mpc1, and Mpc1 and Mpc3 were among the major interacting proteins of Mpc2 (table S1). Consistent with this, immunoprecipitation of tagged Mpc1 copurified Mpc2 and vice versa (Fig. 1C, lanes 3 and 4). In addition, Mpc2 can interact with itself (Fig. 1C, lane 8), whereas an Mpc1 homotypic interaction was not detected (Fig. 1C, lane 7). Blue native–polyacrylamide gel electrophoresis showed that both Mpc1 and Mpc2 migrated as part of an ~150-kD complex (fig. S2D). Loss of Mpc2 prevented Mpc1 from migrating in this complex, whereas an *mpc1*Δ strain showed elevated Mpc2 complex formation (fig. S2E). We conclude that Mpc1 and Mpc2 form a multimeric complex embedded in the mitochondrial inner membrane, with Mpc2 likely being the major structural subunit.

Mutant yeast strains were subjected to a variety of growth conditions. The *mpc1*Δ and *mpc2*Δ cells displayed mild growth defects on nonfermentable carbon sources like glycerol, with greater effects on glucose medium (fig. S3) and a strong growth defect in the absence of leucine (Fig. 1D). In contrast, *mpc3*Δ mutant displayed no apparent growth phenotypes. Yeast, *Drosophila*, or human *MPC1* orthologs, but not human *MPC2*, could rescue the *mpc1*Δ growth phenotype (Fig. 1E), indicating that Mpc1 function is conserved through evolution.

To analyze the physiological function of MPCs in a multicellular animal, we extended our studies to the *Drosophila* ortholog of MPC1 (dMPC1; encoded by *CG14290*), which also localized to mitochondria (fig. S4). Analogous to yeast *mpc1*Δ mutants, *dMPC1* mutants (fig. S5) were viable on standard food, but sensitive to a carbohydrate-only diet, with rapid lethality after transfer to a sucrose medium (Fig. 2A). Whereas the amount of adenosine 5′-triphosphate (ATP) was reduced in *dMPC1* mutants (Fig. 2C), along with triacylglycerol (TAG) and protein (fig. S6, B and C), the amounts of carbohydrates were elevated, including the circulating sugar trehalose (Fig. 2D), glucose (Fig. 2E), fructose, and glycogen (fig. S6, A and D). These results suggest that *dMPC1* mutants are defective in carbohydrate metabolism and may consume stored fat and protein for energy. Consistent with this, the lethality of *dMPC1* mutants on the sugar diet was rescued by expression of the wild-type gene in tissues that depend heavily on glucose metabolism: the fat body, muscle, and neurons (Fig. 2B).

Metabolomic analyses revealed that the concentration of pyruvate was highly elevated, whereas TCA cycle intermediates were significantly

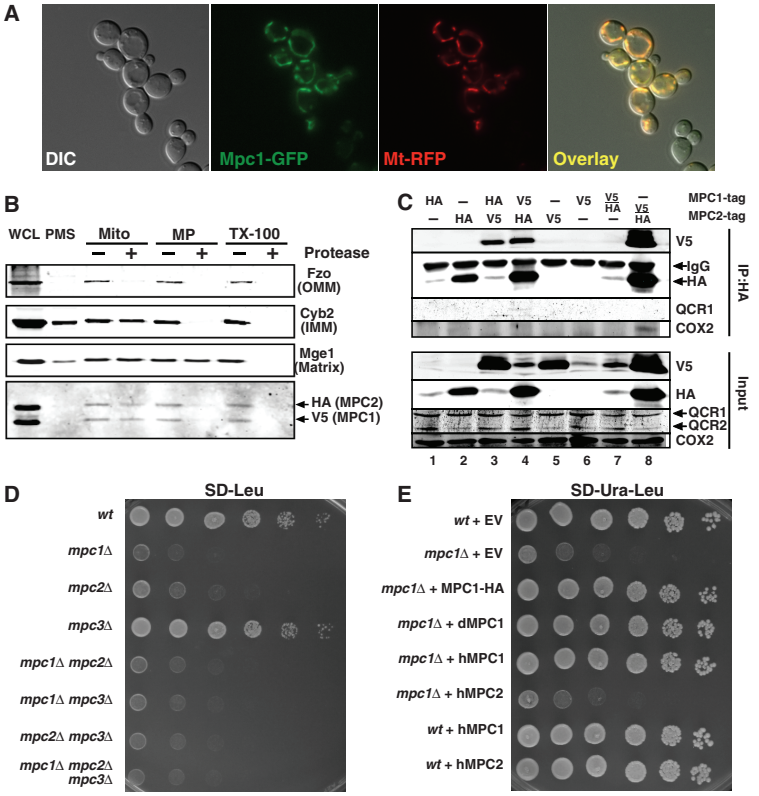

Fig. 1. Mpc1 and Mpc2 are evolutionarily conserved mitochondrial inner-membrane proteins. (**A**) Mpc1 labeled with green fluorescent protein (Mpc1-GFP) and mitochondrial targeted red fluorescent protein (MtRFP) coexpressed in yeast cells. DIC, differential interference contrast. (**B**) Intact mitochondria, hypotonic-swollen mitoplasts, and TritonX-100–solubilized mitochondria from a strain expressing Mpc1-V5 and Mpc2-His_6/HA_2 with (+) or without (–) proteinase K incubation. An immunoblot of extracts using the indicated antibodies with the whole-cell lysate (WCL) and postmitochondrial supernatant (PMS) is shown. Mge1, Cyb2, and Fzo1 are matrix, intermembrane space, and outer-membrane proteins, respectively. (**C**) Immunoprecipitations from mitochondrial extracts from *mpc1*Δ *mpc2*Δ cells expressing Mpc1 and Mpc2 tagged as indicated. Immunoblot of either immunoprecipitate (IP:HA) or input is shown (HA, hemagglutinin). QCR1 and 2 (ubiquinol–cytochrome c reductase complex core protein 1 and 2) along with Cox II (cytochrome c oxidase subunit 2) are controls for the specificity of the immunoprecipitation. (**D**) Serial dilutions of the indicated yeast strains spotted on synthetic media lacking leucine and grown at 30°C for 24 hours. (**E**) Serial dilutions of indicated strains spotted on synthetic media lacking leucine and grown at 30°C for 48 hours. *wt*, wild type; EV, empty vector.

[1]Department of Human Genetics, University of Utah School of Medicine, Salt Lake City, UT 84112, USA. [2]Department of Biochemistry, University of Utah School of Medicine, Salt Lake City, UT 84112, USA. [3]Laboratoire de Biochimie, AP-HP Hôpital de Bicêtre, Le Kremlin Bicêtre, France. [4]Metabolomics Core Research Facility, University of Utah School of Medicine, Salt Lake City, UT 84112, USA. [5]Department of Cell Biology, Harvard Medical School, Boston, MA 02115, USA. [6]Institut de Genetique et de Biologie Moleculaire et Cellulaire (IGBMC), Strasbourg, France. [7]Department of Medicine, University of Utah School of Medicine, Salt Lake City, UT 84112, USA.

*These authors contributed equally to this work.
†To whom correspondence should be addressed. E-mail: rutter@biochem.utah.edu

depleted in *dMPC1* mutants on the sugar diet (Fig. 2F). Similarly, the amounts of glycine and serine, which can interconvert with glycolytic intermediates, were elevated in the mutants on the sugar diet (fig. S6E), whereas glutamate, aspartate, and proline, which can interconvert with TCA cycle intermediates, were depleted under these conditions (fig. S6F). Consistent with this, metabolomic analysis of *mpc1*Δ and *mpc2*Δ yeast mutants revealed elevated pyruvate concentrations (Fig. 3A), depletion of malate (fig. S7), depleted acetyl–coenzyme A (CoA), and elevated CoA concentrations (Fig. 3B). Taken together, these results suggest that *MPC1* mutants are unable to efficiently convert cytosolic pyruvate to mitochondrial acetyl-CoA to drive the TCA cycle and ATP production.

These phenotypes could arise from either a defect in mitochondrial pyruvate uptake or the conversion of mitochondrial pyruvate into acetyl-CoA by the pyruvate dehydrogenase (PDH) complex. Yeast lacking Mpc1, however, had nearly wild-type PDH activity, unlike the strong decrease seen in *pda1*Δ mutants (Fig. 3C), which lack PDH function (*11*). A decrease in PDH activity also does not explain the growth defect of *mpc1*Δ mutants, which is more severe than that of the *pda1*Δ mutant (fig. S8). However, combining the *mpc1*Δ allele with a deletion for *mae1*, which encodes a malic enzyme that converts malate to pyruvate in the mitochondrial matrix (*12*), revealed a profound growth defect on glucose medium that was completely rescued by plasmid expression of either *MAE1* or *MPC1* (Fig. 3D). Notably, mitochondria from the *mpc1*Δ mutant displayed almost no uptake of ^{14}C-pyruvate, which could be fully rescued by plasmid expression of wild-type *MPC1* (Fig. 3E). Moreover, Mpc1 appears to be a key target for UK-5099, which is an inhibitor of the mitochondrial pyruvate carrier (*5*). The *mae1*Δ *mpc1*Δ double mutant displayed reduced growth on glucose medium lacking leucine, and this phenotype could be effectively rescued by transgenic expression of wild-type *MPC1* in the absence, but not the presence, of UK-5099 (Fig. 3F). By screening for *MPC1* mutants that could grow in the presence of UK-5099, we recovered an Asp^{118}→Gly (D118G) substitution in Mpc1 that conferred UK-5099 resistance (Fig. 3F). Moreover, whereas ^{14}C-pyruvate uptake into mitochondria expressing wild-type *MPC1* was almost completely inhibited by UK-5099, efficient pyruvate uptake that is resistant to UK-5099 was recovered upon expression of *MPC1-D118G* (Fig. 3G). We conclude that Mpc1 is a key component of the mitochondrial pyruvate carrier that corresponds to the activity studied for decades by Halestrap and others (*5*, *13*).

Depletion of *MPC1* in mouse embryonic fibroblasts (fig. S9A) caused a modest decrease in pyruvate-driven oxygen consumption under basal conditions, and a stronger reduction in the presence of carbonyl cyanide-*p*-trifluoromethoxyphenylhydrazone (FCCP), which stimulates maximal respiration (Fig. 4A). Similar results were also seen upon silencing *MPC2* (Fig. 4B and fig. S9A). This suppression of pyruvate oxidation, which occurred without affecting components of the oxidative phosphorylation machinery (fig. S9, B and C), suggests that mammalian Mpc1 and Mpc2 mediate mitochondrial pyruvate uptake in a manner similar to that seen in yeast and *Drosophila*.

We have previously described a French-Algerian family with two offspring that exhibited a devastating defect in mitochondrial pyruvate oxidation (*14*) (Fig. 4C, family 1). We subsequently discovered two additional families, each with one affected child who displayed a similar, but less severe, phenotype (Fig. 4C, families 2 and 3). Linkage analysis and homozygosity mapping allowed us to focus on one candidate region on chromosome 6 (163,607,637 to 166,842,083, GRCh37/hg19). This interval contained 10 potential candidate genes: *PACRG*, *QKI*, *C6orf118*, *PDE10A*, *SDIM1*, *T*, *PRR18*, *SFT2D1*, *RPS6KA2*, and *BRP44L*, which is the human *MPC1*. DNA sequencing of the exons and intron/exon boundaries of the *MPC1* gene in fibroblasts from the affected patients in families 2 and 3 revealed the same molecular lesion, c.236T→A, causing a predicted p.Leu^{79}→His (L79H) alteration (Fig. 4D). Analysis of DNA from family 1 revealed a distinct sequence change, c.289C→T, which resulted in a predicted p.Arg^{97}→Trp (R97W) mutation (Fig. 4D). Both of the affected residues are conserved through evolution between *MPC1* orthologs, and Arg^{97} is conserved among both *MPC1* and *MPC2* orthologs (fig. S1).

Cells from the affected individuals in families 1 and 2 exhibited impaired basal and FCCP-stimulated pyruvate oxidation (Fig. 4E), whereas glutamine-driven oxygen consumption was normal or elevated, demonstrating that they have not acquired a generalized impairment of mitochondrial respiration (Fig. 4E). As expected, expression of wild-type human *MPC1* in the cells from family 2 (Fig. 4F) or family 1 (Fig. 4G) either completely or partially rescued the defect in FCCP-induced pyruvate oxidation. Moreover, expression of the *MPC1-Leu79His* allele was less effective at suppressing the yeast *mpc1*Δ growth defect relative to wild-type human *MPC1* (Fig. 4H), and the stronger *MPC1-Arg97Trp* allele was

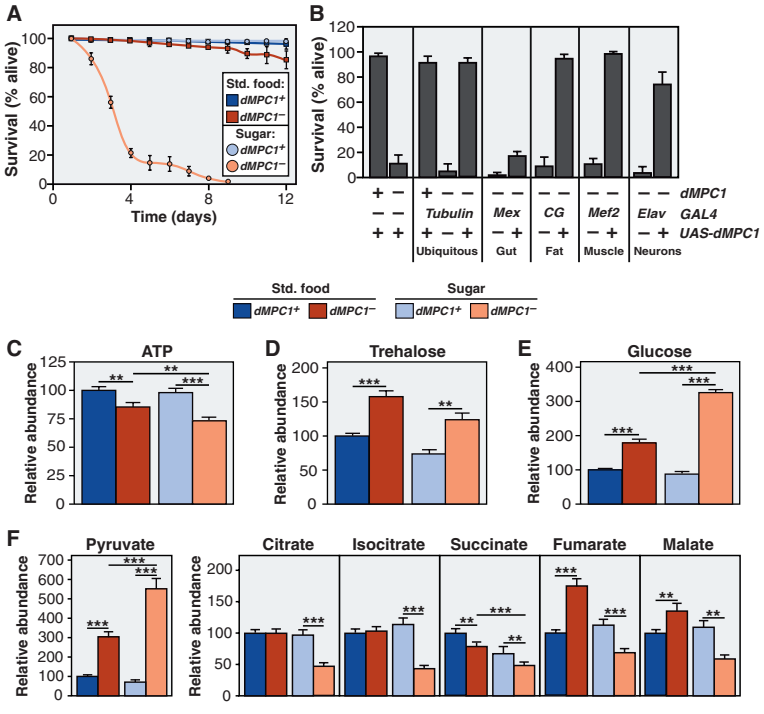

Fig. 2. *dMPC1* is required for pyruvate metabolism in *Drosophila*. (**A**) Percentage of living control (*dMPC1*$^+$) or *dMPC1* mutant (*dMPC*$^-$) flies after transfer to standard laboratory medium (std. food) or to media containing only sugar. (**B**) Percentage of living *dMPC1*$^+$ or *dMPC*$^-$ flies carrying the indicated GAL4 and UAS transgenes on sugar media after 8 days. (**C** to **E**) Relative concentration of ATP (C), trehalose (D), and glucose (E) in extracts from *dMPC1*$^+$ or *dMPC*$^-$ flies on the indicated diet after either 2 days (D and E) or 3 days (C). (**F**) Relative abundance of pyruvate and TCA cycle intermediates in *dMPC1*$^+$ or *dMPC*$^-$ flies after 2 days on the indicated diet as measured by gas chromatography–mass spectrometry. **P* < 0.05, ***P* < 0.01, and ****P* < 0.001 (Student's *t* test). Data are shown as mean ± SEM.

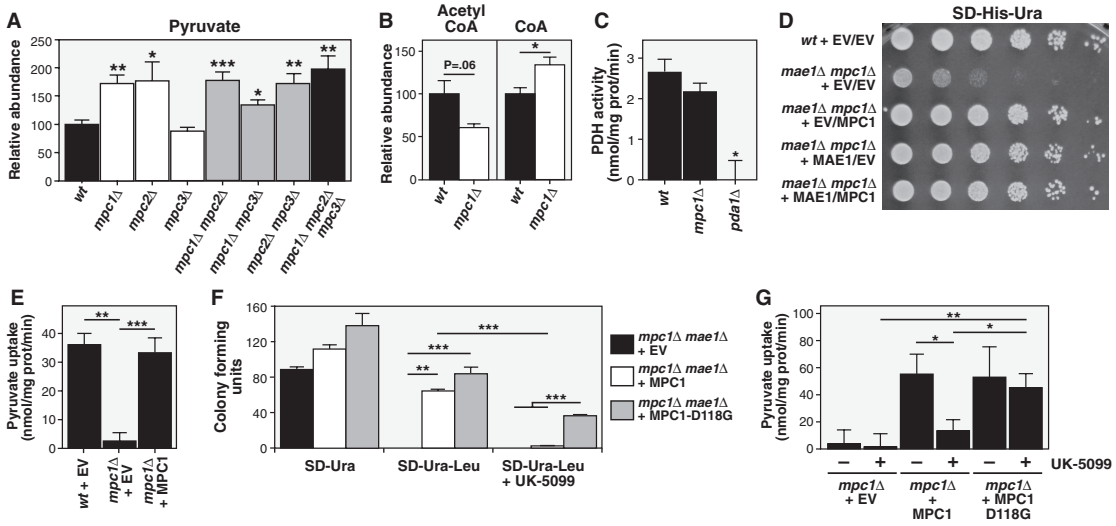

Fig. 3. *MPC1* is required for mitochondrial pyruvate uptake. (**A**) Relative abundance of pyruvate in the indicated strains. *P* values relative to *wt*. (**B**) Relative abundance of acetyl-CoA and CoA in the indicated strains. (**C**) Mitochondrial pyruvate dehydrogenase activity in the indicated strains. *P* value relative to *wt* and *mpc1*Δ. (**D**) Serial dilutions of the indicated strain on glucose medium grown at 30°C for 48 hours. (**E**) Uptake of ^{14}C-pyruvate into mitochondria purified from either *wt* or *mpc1*Δ cells containing the indicated plasmid. *P* value relative to *wt* + *EV* and *mpc1*Δ + *MPC1*. (**F**) *Mae1*Δ *mpc1*Δ cells transformed with the indicated plasmid and plated on media containing or lacking combinations of leucine or UK-5099. (**G**) Uptake of ^{14}C-pyruvate into mitochondria isolated from the *mpc1*Δ strain containing the indicated plasmid in the presence or absence of UK-5099. ***$P < 0.001$, **$P < 0.01$, *$P < 0.05$; NS, not significant (Student's *t* test). Data are shown as mean ± SEM.

Fig. 4. Mammalian *MPC1* and *MPC2* are required for normal pyruvate metabolism. (**A** and **B**) Pyruvate-driven respiration in mouse embryonic fibroblasts under basal and FCCP-stimulated conditions in cells transfected with either control (Cont) small interfering RNAs (siRNAs) or three different siRNAs (si 1–3) targeted to either *MPC1* (A) or *MPC2* (B). *P* values relative to control. (**C**) Pedigrees of families 1, 2, and 3. Circles indicate females; squares, males; and diamonds, unknown sex. Black indicates deceased and white, living. Arrows mark individuals from whom fibroblasts were obtained. (**D**) The protein region of MPC1 containing the predicted amino acid substitutions from all three families aligned by ClustalW. Single-letter abbreviations for the amino acid residues are as follows: A, Ala; C, Cys; D, Asp; E, Glu; F, Phe; G, Gly; H, His; I, Ile; K, Lys; L, Leu; M, Met; N, Asn; P, Pro; Q, Gln; R, Arg; S, Ser; T, Thr; V, Val; W, Trp; and Y, Tyr. *Saccharomyces cerevisiae, Drosophila melanogaster, Homo sapiens, Caenorhabditis elegans, Danio rerio, Arabidopsis thaliana*. (**E**) Pyruvate- (left) and glutamine- (right) supported respiration of fibroblasts harboring either L79H or R97W *MPC1* mutations. (**F**) Pyruvate-supported respiration of either a control or an L79H patient cell line after transduction with the indicated vector. (**G**) Pyruvate-supported respiration of either a control or an R97W patient cell line after transduction with the indicated vector. (**H**) Serial dilutions of *wt* or *mae1*Δ *mpc1*Δ yeast strains carrying the indicated plasmid grown on medium lacking uracil for plasmid selection at 30°C for 40 hours. Both long (L) and short (S) forms of R97W were used (with or without exon 4). ***$P < 0.001$, **$P < 0.01$, *$P < 0.05$, $^{\dagger}P < 0.10$; NS, not significant (Student's *t* test). Data are shown as mean ± SEM.

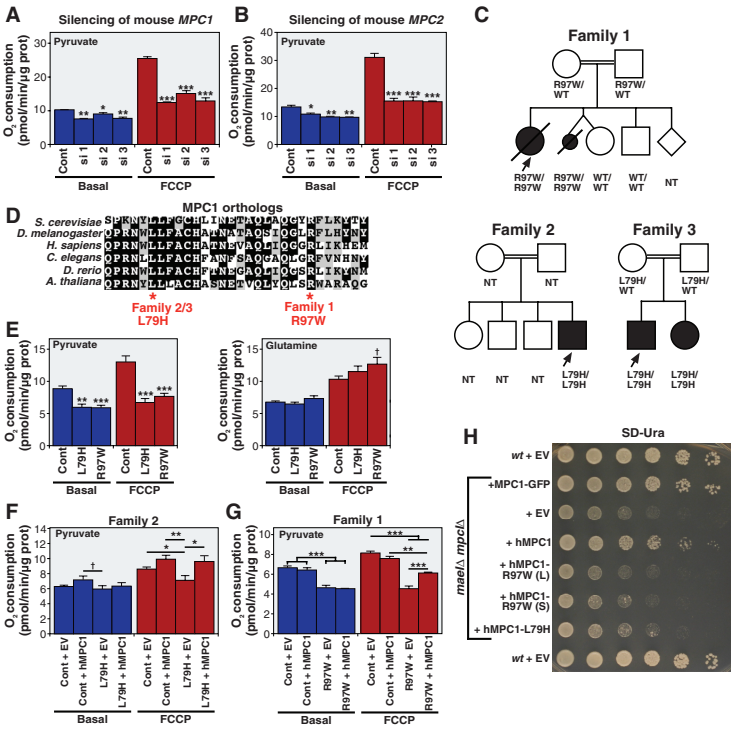

essentially inactive (Fig. 4H), suggesting that *MPC1* function is evolutionarily conserved from yeast to humans.

The data presented here demonstrate that the Mpc1-Mpc2 complex is an essential component of the mitochondrial pyruvate carrier in yeast, flies, and mammals. This is consistent with experiments performed in rat liver, heart, and castor beans, which implicated proteins of 12 to 15 kD in mitochondrial pyruvate uptake (*15*)—similar to the molecular masses of Mpc1 (15 kD), Mpc2 (14 kD), and Mpc3 (16 kD). Although these individual sizes are relatively small, Mpc1 and Mpc2 form a complex of ~150 kD, suggesting that an oligomeric structure mediates pyruvate transport. The demonstration that Mpc1 and Mpc2 are sufficient to promote pyruvate uptake in a heterologous system provides further evidence that they constitute an essential pyruvate transporter (*16*). Finally, the degree to which carbohydrates are imported into mitochondria and converted into acetyl-CoA is a critical step in normal glucose oxidation as well as the onset of diabetes, obesity, and cancer. Thus, like PDH, which is controlled by allostery and posttranslational modification (*17*), the mitochondrial import of pyruvate is likely to be precisely regulated (*18*, *19*). The identification of Mpc1 and Mpc2 as critical for mitochondrial pyruvate transport provides a new framework for understanding this level of metabolic control, as well as new directions for potential therapeutic intervention.

References and Notes

1. D. Hanahan, R. A. Weinberg, *Cell* **144**, 646 (2011).
2. S. E. Kahn, R. L. Hull, K. M. Utzschneider, *Nature* **444**, 840 (2006).
3. A. P. Halestrap, R. M. Denton, *Biochem. J.* **138**, 313 (1974).
4. A. P. Halestrap, *Biochem. J.* **172**, 377 (1978).
5. A. P. Halestrap, *Biochem. J.* **148**, 85 (1975).
6. S. Todisco, G. Agrimi, A. Castegna, F. Palmieri, *J. Biol. Chem.* **281**, 1524 (2006).
7. J. C. Hildyard, A. P. Halestrap, *Biochem. J.* **374**, 607 (2003).
8. M. Jiang *et al.*, *Mol. Biol. Rep.* **36**, 215 (2009).
9. D. J. Pagliarini *et al.*, *Cell* **134**, 112 (2008).
10. A. Sickmann *et al.*, *Proc. Natl. Acad. Sci. U.S.A.* **100**, 13207 (2003).
11. H. Y. Steensma, L. Holterman, I. Dekker, C. A. van Sluis, T. J. Wenzel, *Eur. J. Biochem.* **191**, 769 (1990).
12. E. Boles, P. de Jong-Gubbels, J. T. Pronk, *J. Bacteriol.* **180**, 2875 (1998).
13. S. Papa, G. Paradies, *Eur. J. Biochem.* **49**, 265 (1974).
14. M. Brivet *et al.*, *Mol. Genet. Metab.* **78**, 186 (2003).
15. A. P. Thomas, A. P. Halestrap, *Biochem. J.* **196**, 471 (1981).
16. S. Herzig *et al.*, *Science* **337**, 93 (2012).
17. R. A. Harris, M. M. Bowker-Kinley, B. Huang, P. Wu, *Adv. Enzyme Regul.* **42**, 249 (2002).
18. F. M. Zwiebel, U. Schwabe, M. S. Olson, R. Scholz, *Biochemistry* **21**, 346 (1982).
19. R. Rognstad, *Int. J. Biochem.* **15**, 1417 (1983).
20. Materials and methods are available as supplementary materials on *Science* Online.

Acknowledgments: We thank members of the Rutter, Thummel, Winge, Stillman, Shaw, and Metzstein laboratories for helpful discussions. We thank the Shaw and Winge labs for the antibodies against Fzo1, Cyb2, and Mge1 and for the mito-RFP constructs. We thank J. M. Saudubray, L. Burglen, and H. Tevissen for referring patients and C. Thibault and J. L. Mandel (IGBMC, Strasbourg, France) for assistance in single-nucleotide polymorphism array hybridization. This research was supported by NIH grants R01GM083746 (J.R.), RC1DK086426 (C.S.T.), and R24DK092784 (J.R. and C.S.T.) and a pilot grant from P30DK072437 (J.R.). D.K.B. and C.M.C. were supported by the NIH Genetics Predoctoral Training Grant T32GM007464. E.B.T. was supported by NIH Pathway to Independence award K99AR059190. D.K.B., T.O., C.S.T., and J.R. are inventors on a patent application by the University of Utah covering the discovery of the MPC complex.

Supplementary Materials

www.sciencemag.org/cgi/content/full/science.1218099/DC1
Materials and Methods
Figs. S1 to S10
Table S1
References

19 December 2011; accepted 9 May 2012
Published online 24 May 2012;
10.1126/science.1218099

An Abundance of Rare Functional Variants in 202 Drug Target Genes Sequenced in 14,002 People

Matthew R. Nelson,[1]*† Daniel Wegmann,[2]* Margaret G. Ehm,[1] Darren Kessner,[2] Pamela St. Jean,[1] Claudio Verzilli,[3] Judong Shen,[1] Zhengzheng Tang,[4] Silviu-Alin Bacanu,[1] Dana Fraser,[1] Liling Warren,[1] Jennifer Aponte,[1] Matthew Zawistowski,[5] Xiao Liu,[6] Hao Zhang,[6] Yong Zhang,[6] Jun Li,[7] Yun Li,[4] Li Li,[1] Peter Woollard,[3] Simon Topp,[3] Matthew D. Hall,[3] Keith Nangle,[1] Jun Wang,[6,8] Gonçalo Abecasis,[5] Lon R. Cardon,[9] Sebastian Zöllner,[5,10] John C. Whittaker,[3] Stephanie L. Chissoe,[1] John Novembre,[2]†‡ Vincent Mooser[9]‡

Rare genetic variants contribute to complex disease risk; however, the abundance of rare variants in human populations remains unknown. We explored this spectrum of variation by sequencing 202 genes encoding drug targets in 14,002 individuals. We find rare variants are abundant (1 every 17 bases) and geographically localized, so that even with large sample sizes, rare variant catalogs will be largely incomplete. We used the observed patterns of variation to estimate population growth parameters, the proportion of variants in a given frequency class that are putatively deleterious, and mutation rates for each gene. We conclude that because of rapid population growth and weak purifying selection, human populations harbor an abundance of rare variants, many of which are deleterious and have relevance to understanding disease risk.

Understanding the genetic contribution to human disease requires knowledge of the abundance and distribution of functional genetic diversity within and among populations. The "common-disease rare-variant" hypothesis posits that variants affecting health are under purifying selection and thus should be found only at low frequencies in human populations (*1*–*3*). This hypothesis has become increasingly credible because very large genome-wide association studies of common variants have explained only a fraction of the known heritability of most traits (*4*, *5*). Investigating the role of rare variants for complex trait mapping has led to tests that aggregate rare variants (*6*) and determine the abundance, distribution, and phenotypic effects of rare variants in human populations (*7*, *8*).

Population genetic models predict that mutation rates, the strength of selection, and demography affect the abundance of rare variants, although the relative importance of each is a long-standing question (*9*–*11*). To understand rare variant diversity in humans, we sequenced 202 genes in a sample of 14,002 well-phenotyped individuals (table S1). These genes represent approximately 1% of the coding genome and approximately 7% of genes considered current or potential drug targets (*12*) and are enriched for cell-signaling proteins and membrane-bound transporters (table S2). A total of 864 kb were targeted, including 351 kb of coding and 323 kb of untranslated (UTR) exon regions (database S1). More than 93% of target bases were successfully

[1]Department of Quantitative Sciences, GlaxoSmithKline (GSK), Research Triangle Park, NC 27709, USA. [2]Department of Ecology and Evolutionary Biology, University of California–Los Angeles, Los Angeles, CA 90095, USA. [3]Department of Quantitative Sciences, GSK, Stevenage SG1 2NY, UK. [4]Department of Genetics and Biostatistics, University of North Carolina–Chapel Hill, Chapel Hill, NC 27599, USA. [5]Department of Biostatistics, University of Michigan–Ann Arbor, Ann Arbor, MI 48109, USA. [6]BGI, Shenzhen 518083, China. [7]Department of Human Genetics, University of Michigan–Ann Arbor, Ann Arbor, MI 48109, USA. [8]Department of Biology, Novo Nordisk Foundation Center for Basic Metabolic Research, University of Copenhagen, Copenhagen 3393 9524, Denmark. [9]Department of Quantitative Sciences, GSK, Upper Merion, PA 19406, USA. [10]Department of Psychiatry, University of Michigan–Ann Arbor, Ann Arbor, MI 48109, USA.

*These authors contributed equally to this work.
†To whom correspondence should be addressed. E-mail: matthew.r.nelson@gsk.com (M.R.N); jnovembre@ucla.edu (J.N.)
‡These authors contributed equally to this work.

Supplementary Materials for:

The Mitochondrial Pyruvate Carrier is required for mitochondrial pyruvate uptake in yeast, *Drosophila*, and humans

Daniel K. Bricker, Eric B. Taylor , John C. Schell, Thomas Orsak, Audrey Boutron, Yu-Chan Chen, James E. Cox, Caleb M. Cardon, Jonathan G. Van Vranken, Noah Dephoure, Claire Redin, Sihem Boudina, Steven P. Gygi, Michèle Brivet, Carl S. Thummel, and Jared Rutter

Correspondence to rutter@biochem.utah.edu

Materials and methods

Yeast strains

Saccharomyces cerevisiae haploid strain BY4741 (*MATa his3 leu2 met15 ura3*) was used as the parental wild-type strain in the *mae1*Δ *mpc1*Δ spot tests and JRY472 (W303a *MATa his3 leu2 met15 trp1 ura3*) was used as the strain for all other experiments. Single deletion mutations were created in diploid strains by the standard PCR-based homologous recombination method using KanMX4 (kanamycin resistance), NatMX4 (nourseothricin resistance), or HphMX4 (hygromycin B resistance) cassettes to replace the entire gene, followed by sporulation and tetrad dissection to isolate the desired haploid knockout. Double and triple deletion mutants were created by standard crosses. Deletion strains were verified by PCR.

Yeast plasmids

Nontagged and tagged yeast DNA fragments with the promoter, coding, and terminator sequences were inserted into low-copy centromeric expression vectors or high-copy 2μ expression vectors to enable endogenous level or overexpression expression. Coding sequences were tagged at the 3' end with coding sequences for either Green Fluorescent Protein (GFP), a tandem affinity purification-tag that consist of a His_6 tag and either two HA tags, or a single V5 tag. The human *BRP44* and *BRP44L* and *Drosophila CG14290* genes were inserted into pRS416 (*URA3*) with a GPD promoter to create a constitutively transcribed construct. For expression of the patient-derived mutants, cDNA was used as a template to insert the patient sequences into pRS416 (*URA3*) with the native promoter for yeast *MPC1*.

Assessment of yeast MPC1 sub-mitochondrial localization

This experiment was done following a protocol adapted from Boldogh and Pon (Boldogh and Pon, 2007). Mitochondria harvested from the indicated strain expressing Rcf1-His_6/HA_3 were washed once with SH buffer (0.6 M sorbitol and 20 mM Hepes-KOH, pH 7.4) to remove protease inhibitors. Fifty micrograms of mitochondria were incubated in the isotonic SH buffer or hypertonic H buffer (20mM Hepes-KOH) with and without 1% Triton X-100. To initiate protease digestion, 1μg of Protease K was added and incubated on ice for 20–30 minutes. One microliter of 200 mM PMSF was added into the reaction mixtures to stop protease activity, and lysate was denatured in Laemmli buffer and resolved on a 12% SDS-PAGE, followed by immunoblot. To assess the solubility of MPC proteins, soluble and membrane fractions of the intact mitochondria homogenized by sonication were separated by centrifugation and precipitated in 15% TCA.

Blue-native polyacrylamide gel electrophoresis (BN-PAGE)

BN-PAGE was done as described previously (Wittig et al., 2006). Seventy-five μg of mitochondria harvested from the strain indicated was resuspended in lysis buffer (50 mM NaCl, 5 mM 6-aminocaproic acid, 50 mM imidazole, 1 mM AEBSF, and protease inhibitor cocktail) and solubilized in 1% digitonin. The lysate was resolved on a 8–18% gradient native PAGE gel using a PROTEAN® II xi Cell gel running system (Bio-rad). Immunoblot was performed by soaking the gel in transfer buffer (192 mM glycine, 25 mM Tris-base, 5% methanol, and 0.1% SDS) for 1 hour and transferring it onto a

PVDF membrane in a Trans-Blot® transfer cell (Bio-rad). Membrane was blocked in 5% nonfat milk/TBST and probed with antibodies as indicated.

Drosophila stocks

The transposable P-element insertion *P(XP)CG14290*$^{[d00809]}$ was used to generate *dMPC1* mutant alleles by imprecise excision. Two deletion alleles *(dMPC1*^{1} *and dMPC1*^{2}*)* and a precise excision were isolated and verified by PCR and sequencing. For all experiments, *dMPC1*$^{-}$ denotes *dMPC1*^{1}/*dMPC1*^{2} transheterozygotes and *dMPC1*$^{+}$ denotes animals that are homozygous for the precise excision allele and thus wild-type for *dMPC1* function. To generate the *UAS-dMPC1* construct, the *dMPC1* cDNA (BDGP Gold GH10244) was sequenced, excised by digestion with *XhoI* and *EcoRI,* and cloned into the *pUAST* vector. To generate the *UAS-MPC1*-eGFP construct, *eGFP* was amplified from *pPelican* using the primers 5'-CTCGAGGTGAGCAAGGGCGAGG-3' and 5'-GGTACCTTACTTGTACAGCTCGTCCATG-3', cut with *XhoI* and *KpnI* and cloned into *pUAST* to create *pUAST-eGFP*. The *dMPC1* cDNA was then amplified by PCR to exclude the stop codon using primers 5'-CGGAATTCAACTTTCGGAGTG ACAACACG-3' and 5'-CGCTCGAGGGCTGCCGCCTGCTGCTCCTTAGAC-3', cut with *XhoI* and *EcoRI* and cloned into *pUAST-eGFP*. All vectors used for generating transgenic lines were verified by restriction digestion and DNA sequencing. Transgenic lines were generated using standard P-element mediated transformation. All *GAL4* lines were obtained from the Bloomington Stock Center. *Mex-GAL4, CG-GAL4* and *Elav-GAL4* transgenes on the second chromosome were crossed into the *dMPC1*^{1} and mutant background using balanced crossing schemes. *Tubulin-GAL4, Mef2-GAL4,* and *UAS-*

dMPC1 on the third chromosome were recombined onto either the $dMPC1^{1}$ or $dMPC1^{2}$ chromosome. The presence of *dMPC1* deletion alleles in the transgenic lines was verified by PCR.

Assessment of *Drosophila* MPC1 mitochondrial localization

Fat body from adult *Tubulin-GAL4/+; UAS-dMPC1-eGFP/+* animals was dissected in PBS and incubated for 30 minutes in 100 nM Mitotracker Orange CMTMROS (Invitrogen M7510). Following several washes, tissue was mounted in PBS. Imaging was performed using a Leica TCS SP2 confocal microscope using an excitation wavelength of 488 nm for eGFP and 543 nm for Mitotracker Orange CMTMROS. Emission spectra analyzed were 500–550 nm for eGFP and 550–620 nm for Mitotracker Orange CMTMROS. A Z-stack of 25 slices was imaged for each setting sequentially. The maximum intensity projection was generated in Image-J and used to generate an overlay. A 400 x 400 pixel region was enlarged and shown to focus on subcellular features.

Drosophila dietary treatments

Flies were maintained on standard Bloomington stock center medium at 25˚C in a 12:12 light:dark cycle. For diet switching experiments, animals were allowed to eclose for 4 days and were then transferred to standard media supplemented with yeast paste and allowed to mature for 5 days. Males were collected and transferred in groups of 10–20 to vials containing the same food, or to vials containing 10% sucrose, 1% agar in PBS. Lethality was assayed by counting immobile flies that were not responsive to touch. For

survival assays, at least 40 flies of each genotype/dietary condition were assayed per experiment and each experiment was repeated two to three times. Representative data are shown.

Drosophila metabolic assays

For ATP measurements, adult male flies were homogenized in extraction buffer (6 M guanidine-HCL, 100mM Tris, 4 mM EDTA) and boiled for 5 minutes. Homogenates were spun down and diluted 1:750 in ATP assay buffer (25mM Tris, 100uM EDTA) without GuCl essentially as described (Park et al., 2006), and ATP was measured using a luminescence-based assay (ATP Determination Kit, Invitrogen). ATP was measured 3 days after transfer to either standard food or the sugar diet as indicated. To measure glycogen, glucose, TAG, and protein, male adult flies were homogenized in cold PBS, and metabolites were measured essentially as described (Palanker et al., 2009), except that lysates used for glycogen, glucose, and TAG determination were heat treated at 70˚C for 10 minutes immediately after homogenization. Amyloglucosidase (Sigma) and a glucose assay kit (GO kit, Sigma) were used for glycogen and glucose determination. TAG was measured using Triglyceride Reagent and Free Glycerol Reagent (Sigma). Protein was measured using Bradford's reagent (Bio-Rad). For trehalose determination, male adult flies were homogenized in trehalase buffer and trehalose levels were measured as previously described (Tennessen et al., 2011) using a porcine trehalase and a glucose assay kit (GO kit, Sigma). TAG, trehalose, glucose, glycogen, and protein levels were measured 2 days after transfer to either the standard food or sugar diet as indicated. In all experiments, five flies were pooled per biological

replicate and 5–6 biological replicates were assayed per condition/genotype. Combined results from at least three independent experiments are shown.

Drosophila metabolomics sample preparation

For GC/MS analysis, male adult flies were transferred to either standard food or the sugar diet for 2 days, after which, they were washed multiple times in PBS and snap frozen in liquid nitrogen. Frozen flies were transferred to tubes containing 1.4 mm ceramic beads, and 500 uL of cold (-20˚C) 90% MeOH was added and the flies pulverized using a MP Bio FastPrep 24 bead mill. The tubes were quickly transferred to -20˚C and incubated for 1 hour. Following this cell debris was removed by centrifugation. A second extraction step was performed on the pellet using cold (-20˚C) 60% MeOH. The supernatants were combined and dried *en vacuou*. Samples were then analyzed by GC/MS as described below. For each experiment, 15 flies were pooled per biological replicate and 5–6 biological replicates were assayed per condition/genotype. Combined results from three independent experiments are shown.

Yeast metabolomics sample preparation

Starter cultures were inoculated with a single colony into either YPD for glycolytic conditions or YPE for respirative conditions and grown overnight. These cultures were used to inoculate 80 mL of SD media containing the nutrients needed to supplement the auxotrophies. The initial inoculation was OD_{600} of 0.01 for YPD and 0.1 for YPE. 10 mL of this culture was transferred into eight 25 x 150 mm culture tubes containing three 3 mm glass beads. Eight biological replicates of each strain were used per experiment. The

cultures were grown to an OD_{600} of 1 and harvested using the method of Canelas (Canelas et al., 2009). Briefly, 5 mL of culture was added to 20 mL of -40˚C MeOH followed by centrifugation at 5000 x g for 3 minutes at -20˚C. The supernatant was removed and the pellet gently washed with 2 mL of -40˚C 80% MeOH (aq) and centrifuged. The wash was removed and 5 mL of boiling 75% EtOH (aq) was immediately added, vortexed then incubated at 90˚C for 5 minutes. Cell debris was removed by centrifugation at 5000 x g for 3 minutes. The supernatant was removed to new tubes and dried under vacuum. A total of six biological replicates per group were prepared for GC/MS analysis and four biological replicates per group were prepared for LC/MS analysis.

GC/MS analysis

All GC/MS analysis was performed with a Waters GCT Premier mass spectrometer fitted with an Agilent 6890 gas chromatograph and a Gerstel MPS2 autosampler. Dried samples were suspended in 40µL of a 40 mg/mL O-methoxylamine hydrochloride in pyridine and incubated for 1 hour at 30˚C. 20µL of this solution with MSTFA was added to autosampler vials and incubated for 30 minutes at 37˚C while shaking. 1µL of sample was injected to the inlet which was held at 250˚C. The gas chromatograph was set to an initial temperature of 95˚C for 1 minute followed by a 40˚C/min ramp to 110˚C and a hold time of 2 minutes. This was followed by a second 5˚C/min ramp to 250˚C, then a third ramp to 350˚C, and a final hold time of 3 minutes. A 30 m Restek Rxi-5 MS column with a 5-m long guard column was employed for analysis. Data were collected by MassLynx 4.1. Data analysis for known metabolites was performed using QuanLynx. To find possible unknown metabolites MarkerLynx was used for peak picking, and these

data were exported to SIMCA-P ver. 12.0.1 where PCA and PLS-DA analysis was performed. All data were saved to an Excel spread sheet for further analysis.

LC/MS analysis

Samples were analyzed using a Phenomenex (Torrence, CA) 3.0 mm x 150 mm Gemini-NX C_{18} (5µm) column with a Phenomenex Security Guard column filled with the same packing material. The chromatographic system consisted of an integrated Shimadzu HPLC system consisting of two LC-10AD pumps, column oven and a CBM-20A 82 controller. A PE200 autosampler with a cooling unit set to 4˚C was used for sample handling. A PE Sciex API 365 mass spectrometer modified with an Ionics EP 10+ source was used for analyte detection. A mobile phase consisting of solvent A (water with 15 mM ammonium formate/6.5 mM N-dibutylamine) and solvent B (methanol/6.5 mM N-dibutylamine) was used for elution of samples. The initial condition was 5% B with an initial hold time of 3 minutes followed by a ramp to 73% B over 21 min. A second ramp to 90% B was employed over the next minute with a 1 minute hold. The column was brought back to 5% B over 2 minutes and reequilibrated for 9 minutes. The flow rate was 0.3 mL/min at 24˚C. Mass spectrometer transition optimization was performed using a syringe pump. For each metabolite optimized it was dissolved in buffer A as a 1 mg/mL solution. Infusion was performed at 20µL/min while 10% B/90% A buffer was coinfused using the HPLC at 0.3 mL/min. Samples were prepared as follows: to prevent the exogenous oxidation of GSH it was derivatized using 2-vinyl pyridine. To each sample was added 48µL of 10 mM K_2PO_4 pH 7 and 2µL of 2-VP. A brief sonication using a water bath was performed to fully elute each sample. After 30 minutes of incubation at

room temperature 50μL of buffer A was added followed by 10 minutes of centrifugation at 20000 x g. 90μL of this was transferred to an autosampler vial and immediately transferred to the autosampler, which was held at 4˚C until analysis. After analysis each metabolites peak height was recorded in Excel.

Mitochondrial isolation

Yeast mitochondria were isolated using a simplified version of the method described by Boldogh and Pon (2007). Briefly, yeast were grown in synthetic 2% raffinose media to an A_{600}~3.0 and collected. The cells were pelleted, washed with sterile water, re-pelleted, and then frozen at -80˚C. Mitochondrial isolation began by thawing the cells on ice, digesting the cell wall with lyticase (Sigma) for 1 hour to generate spheroplasts. Following 40 minutes in regeneration buffer, spheroplasts were lysed using a Dounce homogenizer. The mitochondria were further purified through several high and low speed centrifugation steps.

Pyruvate uptake

Mitochondria used for pyruvate uptake experiments were extracted from live cells, kept on ice, and used within 5 hours of harvest without freezing. An estimate of mitochondrial concentration was calculated using A_{280}. Samples were then diluted to yield equal mitochondrial mass and centrifuged at 10000 rpm for 10 minutes to pellet mitochondria. The supernatant was then removed, and the mitochondrial pellet was resuspended in respiratory buffer (120 mM KCl, 5 mM KH_2PO_4, 1 mM EGTA, and 3 mM HEPES pH 7.4) and placed on ice. To initiate pyruvate uptake, 50 μL of

mitochondria was added to 100 μL of room temperature respiratory buffer at pH 6.8 in a microcentrifuge tube. The final concentration of the reaction mixture included 0.05 mM unlabeled malate along with 0.1 mM labeled pyruvic acid mixture (0.01 mM ^{14}C-pyruvate and 0.09 mM unlabeled pyruvate). The reaction was carried out at room temperature with constant stirring using a micro stir bar. Immediately following the addition of mitochondria to the reaction buffer the timer was started and 50 μL samples were taken and spotted onto binderless glass fiber filters (0.5 to 0.7 μm pore size) at 1, 2, or 3 min timepoints. The filter was then rinsed with 3 mL of ice cold TBS using an aspirator to draw the wash buffer through the filter and dry it. The filter was then placed in a scintillation vial containing Ultima Gold MV for liquid scintillation counting. Blank samples in which the 50 μL of mitochondria was replaced with the buffer used to resuspend the mitochondria were taken at corresponding timepoints, and these blank values were subtracted from the experimental data. Five biological replicates were analyzed per group.

Drug inhibitor studies

Pyruvate uptake was carried out as above with the following modifications. Prior to initiating the reaction, individual mitochondrial samples were incubated in 0.2 mM UK-5099 or DMSO (vehicle) for 2 min at room temperature with constant stirring. Following incubation, 100 μL of buffer containing radiolabeled pyruvate was added and the timer was started, and samples were collected as described above. Results shown are combined from four independent experiments, and a total of 17–21 biological replicates per group.

Screen for UK-5099-resistant mutants

A plasmid library harboring *MPC1* mutants was generated by PCR mutagenesis using methods previously described (Cadwell and Joyce, 1994). *mpc1Δ mpc3Δ mae1Δ* triple mutant yeast cells were transformed with the *MPC1* mutant library and plated onto SD-Ura-Leu supplemented 500 uM UK-5099. Plates were incubated at 30˚C for 72 hours, and mutant plasmids were isolated from viable colonies, amplified in *E. coli*, and then transformed into naive *mpc1Δ mpc3Δ mae1Δ* triple mutant yeast cells to confirm the conferral of resistance to UK-5099. An *MPC1* mutant containing a D118G substitution was recovered from this screen. To quantify UK-5099 resistance conferred by the D118G substitution, uniform suspensions of *mpc1Δ mpc3Δ mae1Δ* triple mutant yeast cells were transformed with 2 μg empty vector, plasmid harboring wild-type *MPC1*, or plasmid harboring *MPC1* D118G, and then plated onto either SD-Ura, SD-Ura-Leu, or SD-Ura-Leu plus 500 uM UK-5099.

Immunoprecipitation

JRY472 *mpc1*Δ *mpc*2Δ was transformed with plasmids expressing tagged proteins (MPC1-HA, MPC1-V5, MPC2-HA, and MPC2-V5) or untagged MPC1 or MPC2 as controls. These strains were then grown to log phase in selective synthetic media containing 2% raffinose. Following harvest, mitochondria were isolated as above and stored at -80˚C. For immunoprecipitation, 2 mg of total mitochondria was solubilized in 500 μL XWA buffer containing 150 mM NaCl, 0.8% digitonin, and protease and phosphatase inhibitors for 1 hour at 4˚C with gentle agitation. The debris was then pelleted and the supernatant was saved, one aliquot for input and the remainder being

used for the IP. 20 μL/10 mg of HA-Agarose beads were rinsed and incubated with the supernatant from above at 4˚C with gentle agitation for 2 hours. The HA-agarose beads were then washed 5 times with buffer as above with 0.1% digitonin. Following the final wash the supernatant was aspirated and the beads resuspended in 1X SDS loading buffer and incubated at 95˚C for 10 minutes. 60 uL was then loaded to a 15% SDS polyacrylamide gel and separated by electrophoresis. Following transfer to a nitrocellulose membrane, anti-HA and anti-V5 primary antibody were used in combination with fluorescent anti-mouse and anti-rabbit secondary antibodies respectively. Protein bands were visualized using an Odyssey imager (Licor Biosciences).

Pyruvate dehydrogenase activity assay

The indicated strains were grown to stationary phase at 30˚C in selective media containing 2% raffinose. Once in stationary growth phase the strains were harvested and pelleted at 3000 g for 5 minutes and washed once with sterile water. Following resuspension, concentration was determined by A_{600} and used to dilute to an OD of 1.0 in 1 liter of synthetic media containing 2% glucose. After 3 hours of growth the strains were harvested and mitochondria were isolated as described above. Mitochondria were diluted to 4 mg/mL and sonicated on ice at an amplitude of 1.0, 3 seconds on and 9 seconds off for a total sonication time of 60 seconds. Debris was pelleted by centrifugation at 10,000 rpm for 1 minute. Sonicated mitochondrial samples were then subjected to a coupled enzymatic assay with a spectrometric readout modified from the assay explained by Hinman and Blass (Hinman and Blass, 1981). Briefly, purified sonicated mitochondria was used to start the pyruvate dehydrogenase reaction in 50mM potassium phosphate

buffer pH 7.8, 0.2mM thiamine diphosphate, 2.5mM NAD+, 0.1mM CoA, 1mM $MgCl_2$, 0.3mM dithiothreitol, 5mM pyruvate, with coupling molecules 0.6mM 2(p-iodophenyl)-3-p-nitrophenyl-5-phenyl-tetrazolium chloride and 6.5µM phenazine methosulfate. The reaction proceeded with intermittent shaking at 25˚C and absorbance readings at 495 nm are taken every 30 seconds over 30 minutes. Rates are determined by calculating the change in absorbance in the linear range per unit of time. Pyruvate dehydrogenase activity is calculated by subtracting the rate of absorbance change in samples supplied with 5 mM pyruvate from identical samples lacking pyruvate. The molar absorption of INT (12.4 mM^{-1} $cm^{-1)}$ (Hinman and Blass, 1981) was used to calculate the amount of NADH in nanomoles per milligram of protein per minute. Three biological replicates were analyzed per group.

Fluorescence colocalization

The indicated strains were transformed with a vector for expression of a C-terminally GFP-tagged Mcp1, Mcp2, or Mcp3 shown to rescue the relevant phenotype along with a Mito-RFP plasmid. These cells were grown in selective synthetic media with 2% glucose to an A_{600} = 1.0. The cells were then observed using a Zeiss Axioplan 2 Imaging microscope (Carl Zeiss).

Mammalian cell culture

Mouse embryonic fibroblasts (MEFs) were isolated on day-13 post coitum. MEFs were transformed by viral transduction with SV40 Large-T antigen (pLNX SV-40) and selection with hygromycin (200 ug/ml). Transformed MEFs were maintained in DMEM

with 10% FBS, 2 mM glutamax, and 1% primocin (Invivogen). Human skin fibroblasts (HSFs) were isolated as previously described (Brivet et al., 2003) and immortalized by viral transduction with hTERT (Addgene Plasmid 1773) and selection with hygromycin (20 ug/ml). For rescue experiments, HSFs were reconstituted with empty vector or MPC1 by viral transduction and selection with puromycin (1 ug/ml). HSFs were maintained in DMEM with 15% FBS, 2 mM glutamax, and 1% primocin. All viral transductions were performed with pseudotyped retroviral supernatants generated by cotransfection of 293T cells with Vsv-G, Gag-Pol, and a retroviral targeting vector harboring cDNA for the gene of interest. MPC1 cDNA was cloned into (Not1/BamHI) and delivered by the pQCXIP retroviral vector (Clontech).

Knockdown of MPC1 and MPC2 was performed by treating cells with 20 nM siRNA using the Lipofectamine RNAiMax transfection reagent, according to the manufacturers instructions (Invitrogen). The All-Stars nontargeting siRNA (Qiagen) was used as the control for siRNAs targeting MPC1 and MPC2, which were designed with the Dharmacon siDesign Center tool (http://www.dharmacon.com/designcenter /DesignCenterPage.aspx). Sequences of the sense strands of targeting siRNAs, which include a 3' tt DNA overhang are as follows. MPC1: (1) UCAACUACGAGAUGAG UAAtt, (2) GGGAAAACACAGAAUGCUAtt, and (3) CCAUGUAACAAACG AAGUAtt. MPC2: (1) CCGAUAAGGUGAUGCUAAAtt, (2) UGGAUAAAGUGG AGUUGUUtt, and (3) ACCAAGAACUCAAAUCUAAtt. Cells were subjected to knockdown on day zero, again on day 3, and analyzed on day 6.

Measurements of mammalian cellular respiration

Oxygen consumption of MEFs and HSFs was measured with the XF-24 Seahorse Bioanalyzer. The day prior to assays, cells were seeded at densities between 20–30k (MEFs) and 15–25K (HSFs) per well of Seahorse XF-24 plates. At the time of seeding, 12-well plates were seeded proportionally to 1) enable normalization of oxygen consumption data and 2) provide protein lysates for analysis by Western Blot. One hour prior to assays, cells were incubated, after 1 wash, with DMEM without glucose, bicarbonate, or phenol red (SIGMA, D5030), but with either pyruvate at 20 mM (MEFs) or 2 mM (HSFs), or glutamine at 2 mM (HSFs). Basal Oxygen consumption was measured in the incubation media. FCCP-stimulated respiration was measured after injection of FCCP to a final concentration of either 0.5 uM (MEFs) or 1.0 uM (HSFs). For both basal and FCCP-stimulated respiration, a measurement loop was repeated 3 times: 1 minute mixing, 2 minutes waiting, and 3 minutes measuring oxygen consumption. Oxygen consumption data were normalized to total protein. Total protein values were obtained by measuring the protein content, by BCA, of the proportionally seeded wells within 12-well plates and multiplying by the fraction of cells loaded per well in the Seahorse XF-24 plates. Five to eleven biological replicates were analyzed per group in each experiment.

Human genetic mapping

A severe defect of mitochondrial pyruvate oxidation has been found previously in three unrelated consanguineous families of Algerian descent. Key features of the index case in family 1 have been previously reported (Brivet et al., 2003). This female patient

developed a severe neonatal encephalopathy with lactic acidosis and died at 19 months after progressive neurological deterioration. Pyruvate dehydrogenase deficiency was ruled out as in other cases of families 2 and 3. These patients were less severely affected and presented essentially with psychomotor retardation without regression and epilepsy in family 2 or peripheral neuropathy in family 3. Currently these patients are alive aged 5–14 years.

Samples were subjected to a whole genome scan using The GeneChip Human Mapping 250k NspI arrays (Affymetrix, Santa Clara, CA, USA). Homozygosity regions were defined when more than 35 consecutive SNPs were homozygous, using HomoSNP software (http://bips.u-strasbg.fr/HomoSNP/ updated from [Stoetzel et al., 2007]). We selected candidate intervals when homozygous regions were observed for all affected individuals but not for unaffected ones. Homozygous haplotypes were then checked to be either identical for all four affected individuals (hypothesis of a common shared mutation), or identical for both affected individuals of family 1 on one side and identical for the two more mildly affected patients from families 2 and 3 on the other side (hypothesis of one mild and one more severe mutation). Parametric multipoint linkage analysis was performed in family 1 using software ALLEGRO 1.2 via the easyLINKAGE Plus V5.02 interface (Gudbjartsson et al., 2000) and assuming autosomal recessive inheritance, full penetrance, and a disease allelic frequency of 0.0001.

Homozygosity mapping using the three affected families allowed for the identification of four candidate regions, each containing more than 35 consecutive homozygous SNPs in all four affected individuals, but not in unaffected probands from family 1. Haplotype-coherence checking permitted us to discard two regions. Out of the

two remaining candidate regions, the one located on chromosome 7 was 400 kb in length (84,106,464-84,587,114, GRCh37/hg19) and supported the initial hypothesis that a common mutation was shared by all four affected individuals since all homozygous haplotypes were identical. This region contained a single gene (*SEMA3A*), which did not appear to be a functionally relevant candidate. The second region was located on chromosome 6 and of total length 3.2 Mbp (163,607,637-166,842,083, GRCh37/hg19). Haplotypes therein suggested the existence of two different mutations at the same locus, one carried by the more severely affected patients from family 1 and the other by the more mildly affected patients from families 2 and 3. Interestingly, an independent multipoint analysis on family 1 highlighted five regions of linkage reaching the maximal expected LOD score of 2.05 (taking into account first cousin consanguinity), one of them encompassing the entire homozygosity region on chromosome 6. While the LOD score of 2.05 is lower than required for definitive mapping to a single locus, it is the maximal LOD score given the structure of Family 1 that has confirmed first cousin consanguinity. Five other regions in family 1 showed the same LOD score, but the candidate region on chromosome 6 was the only one consistent with homozygosity mapping in the two other families. Improving the confidence in linkage analysis or segregation of mutations would have required the analysis of other family members, who were not accessible to the investigators, despite several attempts to recontact family 2. This interval on chromosome 6 contained 10 potential candidate genes: *PACRG, QKI, C6orf118, PDE10A, SDIM1, T, PRR18, SFT2D1, RPS6KA2*, as well as *BRP44L*, which encodes human MPC1.

Human *MPC1* alleles

The c.289C>T mutation in *MPC1* in family 1, which caused the predicted p.Arg97Trp substitution, also caused an altered splicing pattern of the pre-mRNA, leading to the formation of a truncated mRNA that lacked exon 4 in mutant fibroblasts (Fig. S2.10). Sequence analysis of the other probands from family 1 revealed that the two parents were heterozygous for the c.289C>T mutation and the two unaffected children did not carry the mutation (Fig. S2.4C). Similarly, the two affected children in family 3 were both homozygous for the c.236T>A mutation, which caused the predicted p.Leu79His substitution, and the two parents were both heterozygous (Fig. S2.4C). Sequence analysis of *MPC1* from 80 unaffected donors revealed no evidence of mutations in this gene. Further, the c.236T>A mutation has not been observed in the more than 5200 individuals (European Americans and African Americans) whose exome data are reported in the exome variant server database.

Primers for amplification of aspects of the *MPC1* and *MPC2* genes

The following primers were used to amplify aspects of the MPC1 and MPC2 genes (Table S2.1). Amplification of MPC1 exons and MPC1 cDNAs and ORFs was performed with the Hot-Start Phusion Polymerase (Thermo-Fisher) with the inclusion of Betaine to a final concentration of 1M, and all with annealing temperatures of 72˚C. Primers for the MPC1 ORF include NotI (5') and EcoR1 (3') restriction endonuclease sites that were utilized for cloning. Quantitative PCR (qPCR) was performed with a Roche 480 Light cycler using the Applied BioSystems Sybr Green Master Mix.

Table S2.1. Primers used for quantitative PCR.

Amplicon	Primer	Sequence
hsMPC1 Exon 1	FWD	CCAGCCCCAGCCGTTTTACGGCAG
	REV	CTGAAAGGCGCCCACTGTCACCG
hsMPC1 Exon 2	FWD	GGCACAAACCACCCATGCCCAGC
	REV	GCTGTCACAGAGCTCGTGTCTAGGC
hsMPC1 Exon 3	FWD	GTGTCTGGGGTCCTGGGCATTGATTTC
	REV	GCAAGCAGGAGCTCTACTATGTTGAAAGTCC
hsMPC1 Exon 4	FWD	CAGCCTACTCTTGCTCGGAAATATGTTCC
	REV	CCAGTCCCGCAGCACTCCCTC
hsMPC1 cDNA	FWD	GCCGGGGTGTCATTGGCTCT
	REV	GTGACTCAGCAGCAGCTGGCAAT
hsMPC1 ORF	FWD	GATCGCGGCCGCACCATGGCGGGCGCGTTG
	REV	GATCGGATCCTTATGCAGATGCCGTTTTAGTCATCTC
mmMPC1 qPCR	FWD	GCACGGCCATGGCTGGAGC
	REV	GCAACAGAGGGCGAAAGTCATCCG
mmMPC2 qPCR	FWD	CCGCTTTACAACCACCCGGCA
	REV	CAGCACACACCAATCCCCATTTCA

Mass spectrometric identification of Mpc1 and Mpc2 interacting proteins.

Eluates from TAP purification of Mpc1-His6/HA2 were subjected to trypsin digestion and mass spectrometric protein identification (Table S2.2 and S2.3). Proteins that were absent from a negative control purification and are annotated as mitochondrial are shown, along with the Peptide-Spectral Matches (PSMs). Size of the protein is also shown as this correlates with the number of possible tryptic peptides that can be detected.

Statistical analysis

Quantitative results were analyzed for statistically significant effects. P-values were determined by Student's t test using Microsoft Excel. All quantitative data are reported as mean ± SEM. Significance is denoted as *** $P < 0.001$, ** $P < 0.01$, and * $P < 0.05$.

Table S2.2. Mpc1 TAP purification.

Protein	PSMs	Protein Length (aa)
Ygl080 (Mpc1)	9	139
Mpm1	7	252
Gut2	7	649
Ygr243 (Mpc3)	5	146
Fmp24	4	501
Yhr162 (Mpc2)	4	129

Table S2.3. Mpc2 TAP purification.

Protein	PSMs	Protein Length (aa)
Mdl2	28	773
Yhr162 (Mpc2)	24	129
Ygl080 (Mpc1)	17	130
Nde1	6	560
Cor1	5	457
Ygr243 (Mpc3)	5	146
Gut2	4	649
Qcr2	3	368

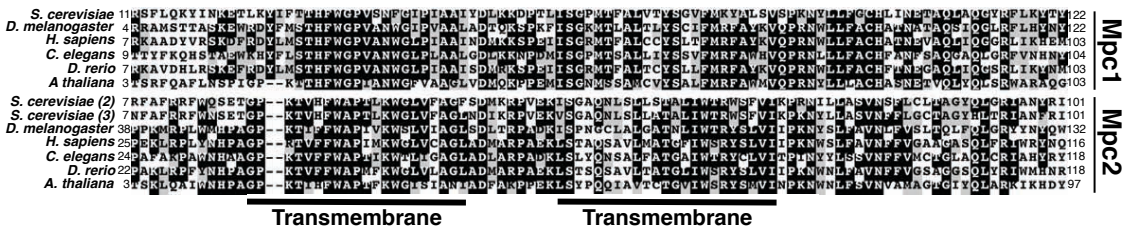

Figure S2.1. MPC1 and MPC2 amino acid alignments.
Mpc protein family sequences were aligned and plotted using the Clustal W and Boxshade programs. The Mpc1 and Mpc2 protein subfamilies were aligned separately first to show conservation within the subfamilies. Yeast Mpc2 (2) and Mpc3 (3), both members of the Mpc2 family, are shown. Subfamily alignments were then aligned manually, to show conservation between the subfamilies. TMHMM and MEMSAT3 transmembrane prediction software predicted the presence of two transmembrane domains in the MPC proteins (shown above) whereas MEMSAT-SVM predicted three transmembrane domains (not shown).

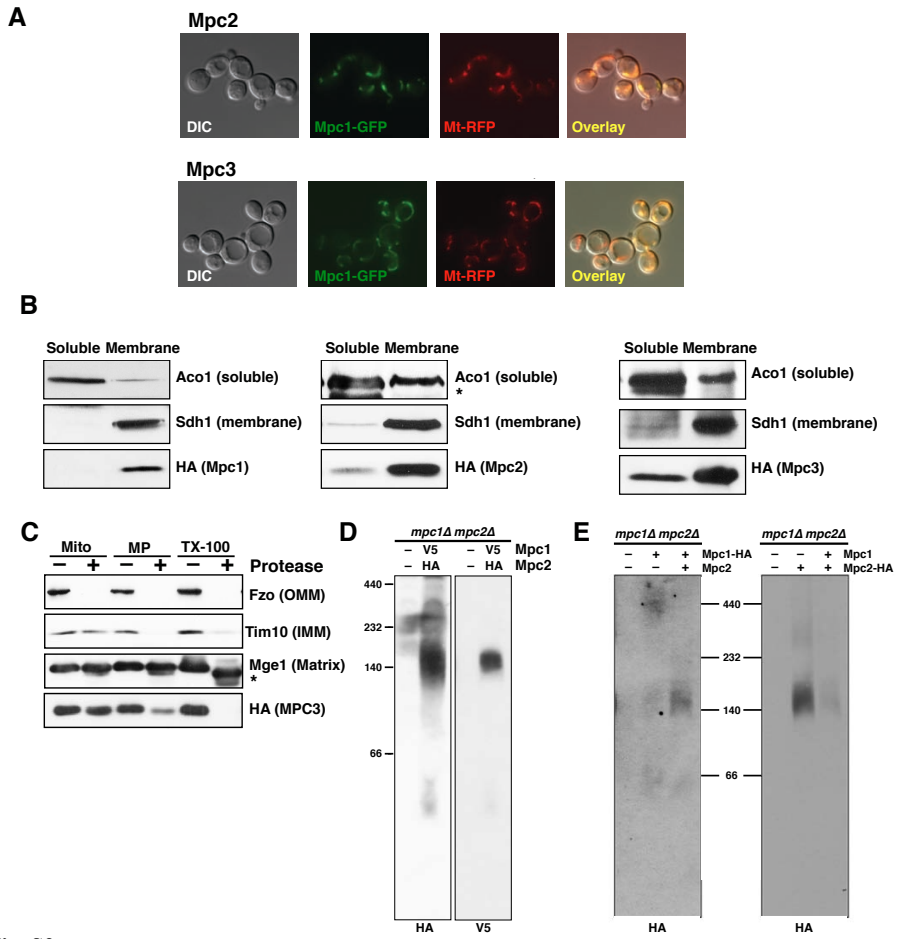

Figure S2.2. Additional characterization of MPC1 and MPC2/MPC3 in yeast. (A) Mpc2-GFP and Mpc3-GFP coexpression with mitochondrial targeted RFP (mtRFP). (B) Soluble and membrane fractions extracted from sonicated mitochondria were analyzed by immunoblot. Mpc proteins were detected by HA antibody. Aco1 is a soluble matrix protein and Sdh1 is a membrane-associated matrix protein. Asterisk indicates a nonspecific signal. (C) Intact mitochondria, hypotonic-swollen mitoplasts, and 1% TritonX-100–solubilized mitochondria of a strain expressing Mpc3-His6/HA3 were treated either with (+) or without (-) Proteinase K and analyzed by immunoblot. Mge1, Tim10, and Fzo1 are matrix, intermembrane space, and outer membrane proteins, respectively. Asterisk indicates a cleaved form of Mge1. (D) Mitochondria extracted from strains harboring either EV or plasmids expressing Mpc1-V5 and Mpc2-HA were solubilized by 1% digitonin and resolved by BN-PAGE followed by immunoblotting with HA and V5 antibodies. (E) Mitochondria extracted from strains harboring plasmids expressing Mpc1-HA in the presence or absence of Mpc2 (left) or Mpc2-HA in the presence or absence of Mpc1 (right) were solubilized by 1% digitonin and resolved by BN-PAGE followed by immunoblotting with an HA antibody. The Mpc1-HA blot was exposed for substantially longer than the Mpc2-HA blot. The remaining Mpc1 assembly is likely a result of Mpc3, which seems to be able to partially compensate for loss of Mpc2.

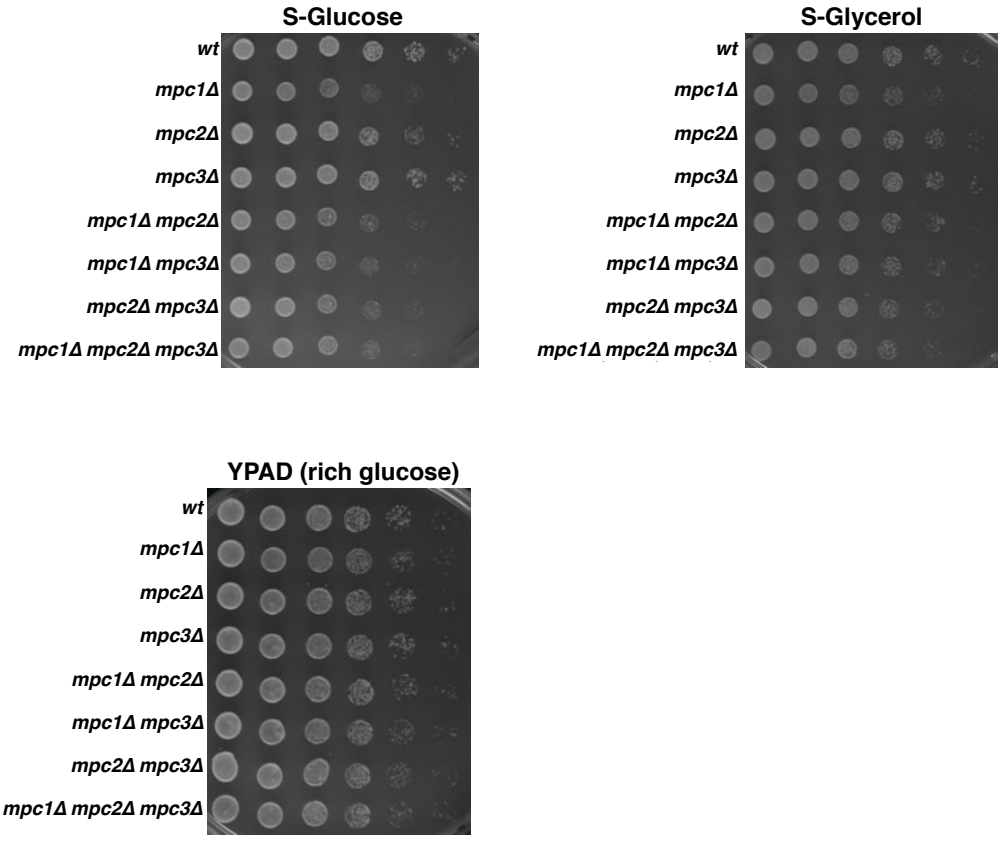

Figure S2.3. Yeast *MPC* mutant growth defects.
Serial dilutions of wild type (*wt*), and the indicated mutant strains were spotted on synthetic complete media, synthetic media containing glycerol, or YPAD media and grown at 30˚C for 24 hours.

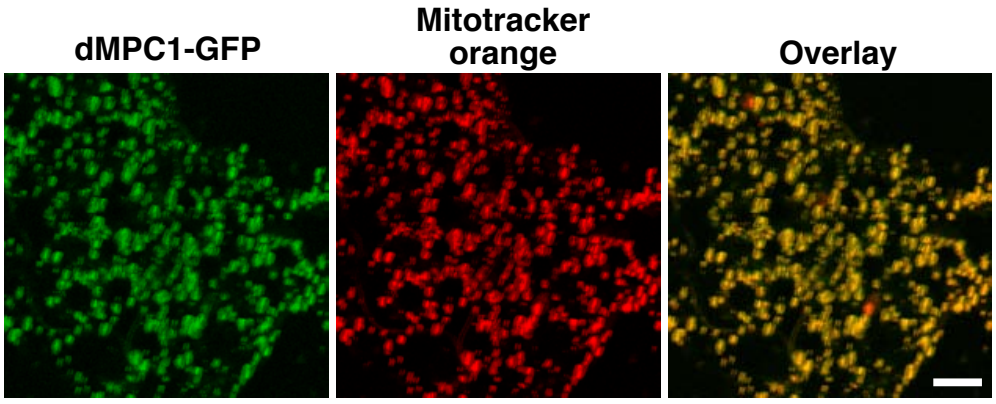

Figure S2.4. *Drosophila* MPC1 is localized to mitochondria.
The adult fat body was dissected from animals expressing a *UAS-dMPC1-eGFP* construct under the control of the ubiquitous driver *Tubulin-GAL4* and subsequently stained with the mitochondria-specific dye Mitotracker Orange. Scale bar = 10μm.

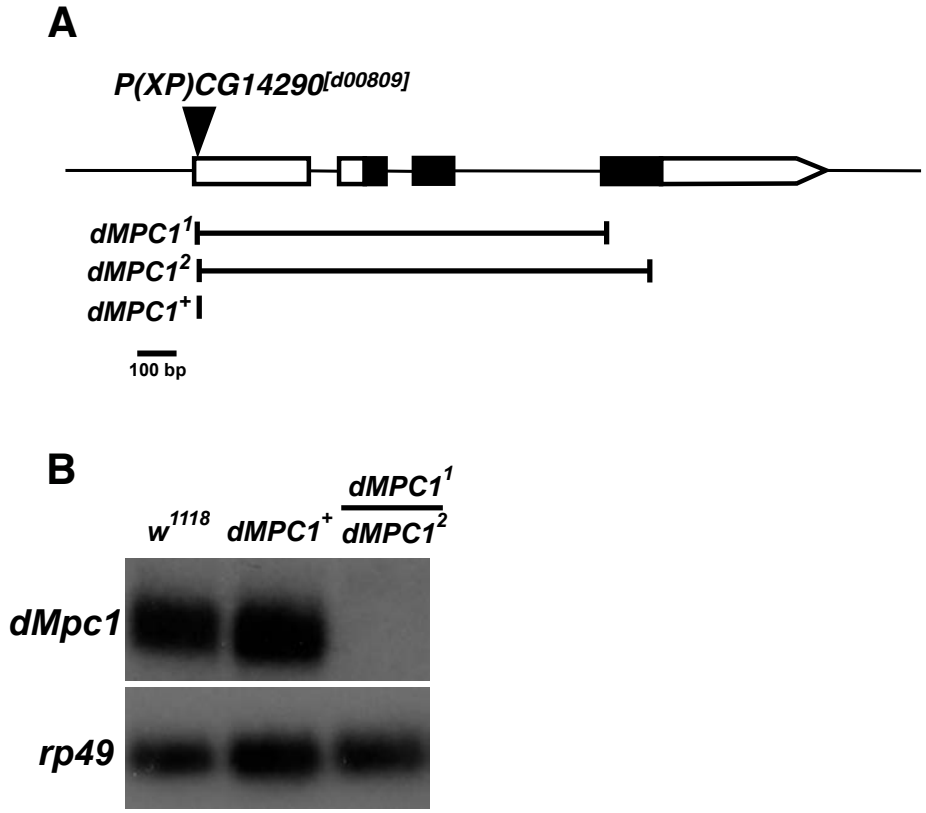

Figure S2.5. *Drosophila MPC1* alleles.
(A) The P-element *P(XP)CG14290[d00809]*, located in the 5'UTR of *dMPC1*, was excised to generate the *dMPC11* and *dMPC12* deletion alleles, which are 999 and 1,352 base pairs in length, respectively. A strain in which *P(XP)CG14290[d00809]* was excised precisely is utilized in this study as a genetically-matched control (*dMPC1+*). All alleles were verified by PCR and DNA sequencing. (B) Northern blot analysis performed using RNA isolated from the wild type *Drosophila* laboratory strain *w*1118 , homozygotes for the *dMPC1* precise excision (*dMPC1+*) and transheterozygotes for the *dMPC11/dMPC12* deletion alleles. RNA was isolated using TriPure extraction reagent (Roche), and the resulting northern blots were probed with radiolabeled oligonucleotides targeted to *dMPC1* and the loading control *Ribosomal protein 49* (*rp49). dMPC1* expression levels are equal to wild type in the precise excision strain, whereas *dMPC1* expression is eliminated in *MPC11/dMPC12* deletion mutants.

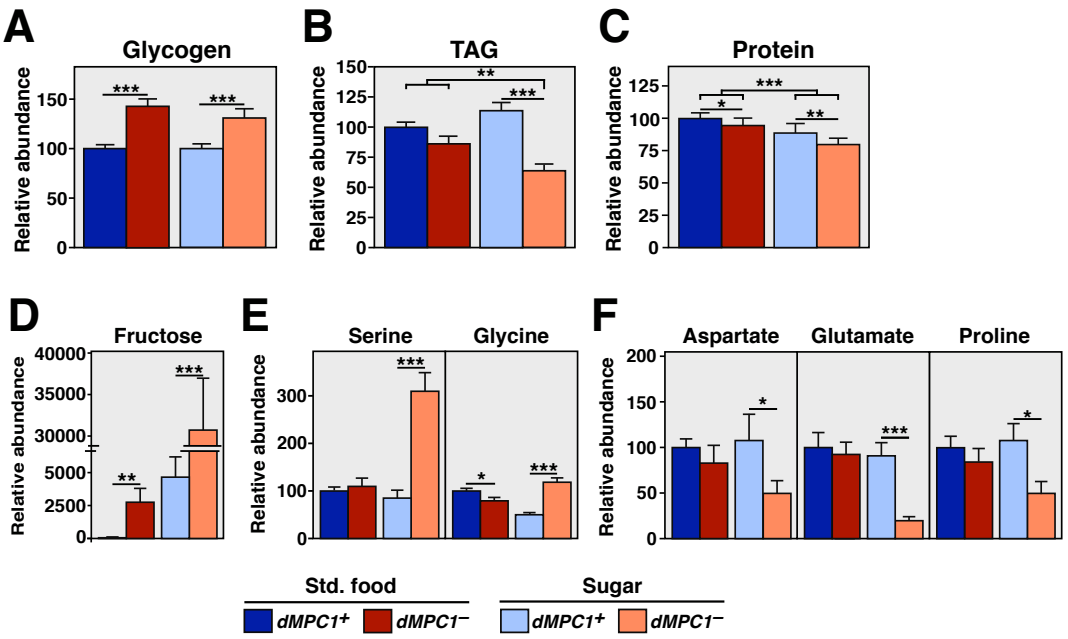

Figure S2.6. *dMPC1* mutants display metabolic defects.
(A–C) Relative abundance of glycogen (A), TAG (B), or protein (C) in extracts from *dMPC1+* or *dMPC–* flies on either a standard laboratory medium (std. food) or a medium containing only sugar after 2 days. (D–F) Relative abundance of fructose (D), amino acids metabolized through glycolysis (E) and amino acids metabolized through the TCA cycle (F) in flies on the indicated diet for two days measured by GC/MS. *p < 0.05, **p < 0.01 and ***p < 0.001 (Student's t test). Data displayed as mean ± SEM.

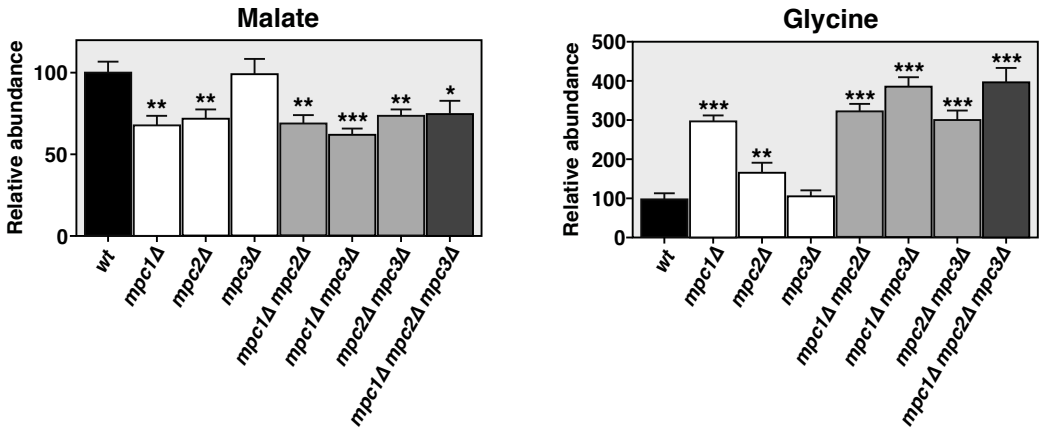

Figure S2.7. Yeast *MPC* mutant metabolomic analysis.
Relative abundance of various metabolites in the indicated strains was measured by GC/MS metabolomics. *p < 0.05; **p < 0.01; ***p < 0.001 relative to *wt* (Student's t test). Data displayed as mean ± SEM.

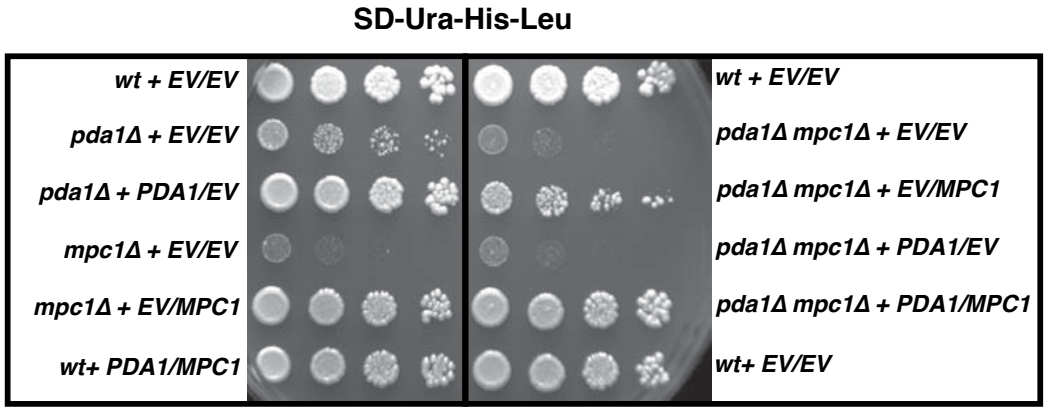

Figure S2.8. Yeast *MPC1* and *PDA1* double mutant analysis.
Serial dilutions of the indicated strains carrying the indicated centromeric expression plasmids were plated on medium lacking leucine and grown at 30˚C for 72 hours.

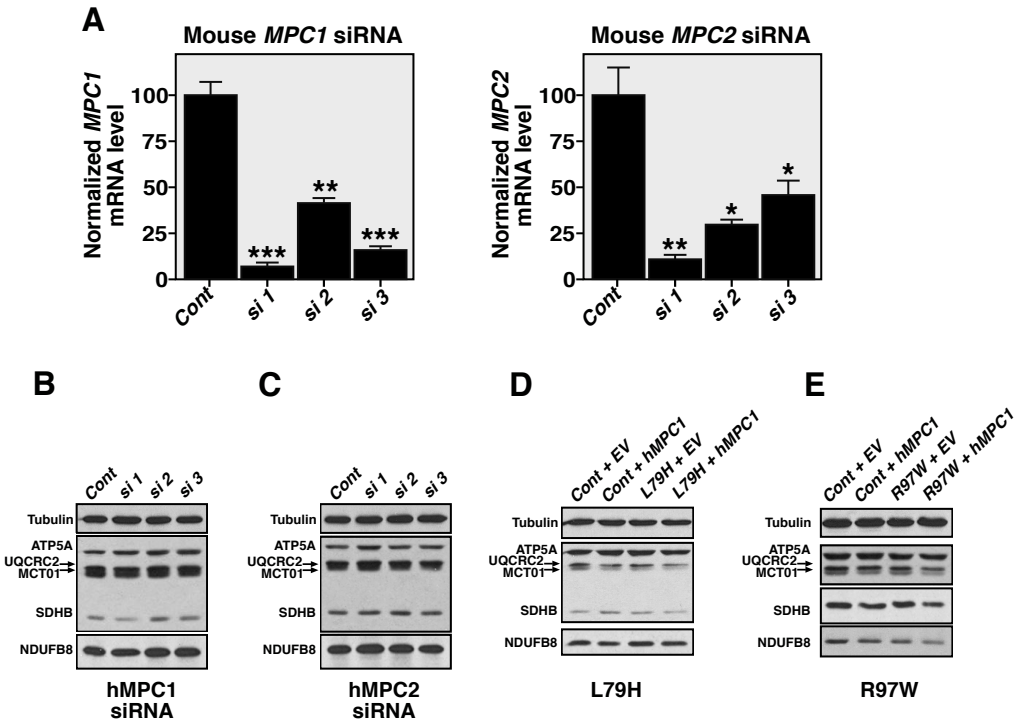

Figure S2.9. Controls for mammalian experiments.
(A) Relative levels of *MPC1* and *MPC2* mRNA after treatment of mouse embryonic fibroblasts (MEFs) with a nontargeting control or siRNAs targeting mouse *MPC1* or *MPC2*. Cont. = control (nontargeting siRNA) (B–E) Western blots for tubulin, ATP5A (Complex V), UQCRC2 (Complex III), MCT01 (Complex IV), SDHB (Complex II), and NDUFB8 (Complex I) performed on cell lysates of (B) MEFs subjected to MPC1 or nontargeting knockdown (cont.), (C) MEFs subjected to MPC2 or nontargeting knockdown, (D) HSFs harboring the wild-type and L79H *MPC1* alleles after retroviral reconstitution with empty vector or wild-type *MPC1* or (E) HSFs harboring the wild-type and R97W *MPC1* alleles, after retroviral reconstitution with empty vector or wild-type *MPC1*. *$p < .05$; **$p < .01$ and ***$p < .001$ relative to controls (Student's t test). Data displayed as mean ± SEM.

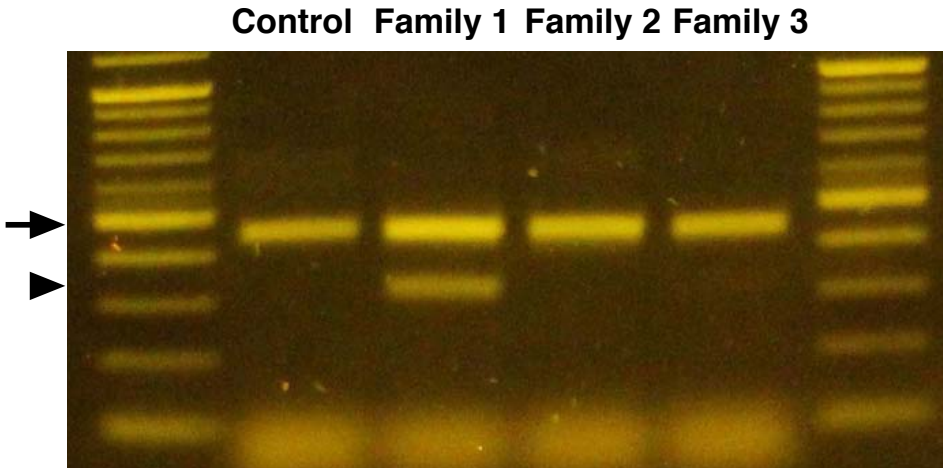

Figure S2.10. Amplification of the *MPC1* cDNA from patient samples.
Amplification of cDNA harboring the *MPC1* ORF derived from human skin fibroblasts that were isolated from a control patient and patients manifesting impaired pyruvate metabolism from families 1, 2, and 3. Amplification of cDNAs from families 1, 2, and 3 resulted in amplicons of the expected size (arrow) that upon sequencing were found to harbor mutations matching those observed when sequencing their *MPC1* genes (Family 1: C289T/R97W; Families 2 and 3: T236A/L79H). Amplification of cDNA from family 1 also produced an unexpected short amplicon (arrowhead). Sequencing revealed that the short *MPC1* mRNA is misspliced and skips exon 4. Exon 4 skipping results in a 2 base pair frame-shift that codes for an Ala58Gly mutation and is followed by a premature stop codon (Ala58GlyfsX2), thereby resulting in a truncated protein.

Supplemental references

Boldogh, I.R., and Pon, L.A. (2007). Purification and subfractionation of mitochondria from the yeast *Saccharomyces cerevisiae*. Methods Cell Biol. *80*, 45–64.

Brivet, M., Garcia-Cazorla, A., Lyonnet, S., Dumez, Y., Nassogne, M.C., Slama, A., Boutron, A., Touati, G., Legrand, A., and Saudubray, J.M. (2003). Impaired mitochondrial pyruvate importation in a patient and a fetus at risk. Mol. Genet. Metab. *78*, 186–192.

Cadwell, R.C., and Joyce, G.F. (1994). Mutagenic PCR. PCR Methods Appl. 3, S136–140.

Canelas, A.B., ten Pierick, A., Ras, C., Seifar, R.M., van Dam, J.C., van Gulik, W.M., and Heijnen, J.J. (2009). Quantitative evaluation of intracellular metabolite extraction techniques for yeast metabolomics. Anal. Chem. *81*, 7379–7389.

Gudbjartsson, D.F., Jonasson, K., Frigge, M.L., and Kong, A. (2000). Allegro, a new computer program for multipoint linkage analysis. Nat. Genet. *25*, 12–13.

Hinman, L.M., and Blass, J.P. (1981). An NADH-linked spectrophotometric assay for pyruvate dehydrogenase complex in crude tissue homogenates. J. Biol. Chem. *256*, 6583–6586.

Palanker, L., Tennessen, J.M., Lam, G., and Thummel, C.S. (2009). Drosophila HNF4 regulates lipid mobilization and beta-oxidation. Cell Metab. *9*, 228–239.

Park, J., Lee, S.B., Lee, S., Kim, Y., Song, S., Kim, S., Bae, E., Kim, J., Shong, M., Kim, J.M., et al. (2006). Mitochondrial dysfunction in Drosophila PINK1 mutants is complemented by parkin. Nature *441*, 1157–1161.

Stoetzel, C., Muller, J., Laurier, V., Davis, E.E., Zaghloul, N.A., Vicaire, S., Jacquelin, C., Plewniak, F., Leitch, C.C., Sarda, P., et al. (2007). Identification of a novel BBS gene (BBS12) highlights the major role of a vertebrate-specific branch of chaperonin-related proteins in Bardet-Biedl syndrome. Am. J. Hum. Genet. *80*, 1–11.

Tennessen, J.M., Baker, K.D., Lam, G., Evans, J., and Thummel, C.S. (2011). The Drosophila estrogen-related receptor directs a metabolic switch that supports developmental growth. Cell Metab. *13*, 139–148.

Wittig, I., Braun, H.P., and Schagger, H. (2006). Blue native PAGE. Nat. Protoc. *1*, 418–428.

CHAPTER 3

DROSOPHILA MPC1 MUTANTS DISPLAY DEFECTS IN CARBOHYDRATE HOMEOSTASIS AND HALLMARKS OF DIABETES

Daniel K. Bricker, Dona R. Wisidagama, and Carl S. Thummel

Summary

Circulating glucose concentrations are maintained at a relatively constant level by the insulin-signaling pathway. Aberrant glucose homeostasis is the main feature of diabetes, which is characterized by chronic hyperglycemia and defective insulin signaling. We describe here a role for the mitochondrial pyruvate carrier (MPC) in the regulation of glucose homeostasis and the prevention of diabetes-like phenotypes. *dMPC1* mutant flies, which lack MPC function, are sensitive to dietary sugar levels and display hyperglycemia, elevated sorbitol, and other metabolic defects. Hyperglycemia can be rescued by specific expression of *dMPC1* in the fat body of *dMPC1* mutants. Moreover, *dMPC1* mutants are glucose intolerant and display reduced activation of insulin signaling in peripheral tissues, possibly caused by a defect in insulin secretion, thus recapitulating key phenotypes associated with diabetes. Taken together, our results support a model in which mitochondrial pyruvate transport facilitates a metabolic state that is required for proper insulin signaling and the maintenance of normal circulating glucose levels.

Introduction

Circulating glucose levels must be maintained within optimal parameters to prevent tissue dysfunction and damage (Negre-Salvayre et al., 2009). This state of euglycemia is achieved through the homeostatic balance of cellular carbohydrate uptake, storage, synthesis, and catabolism (Schrayyef and Gerich, 2010). Carbohydrate homeostasis is primarily regulated by the insulin-signaling pathway, which controls cellular glucose uptake, glycogen synthesis, glycogenolysis, and gluconeogenesis in key

metabolic tissues (Schrayyef and Gerich, 2010; Siddle, 2011). Defects in carbohydrate homeostasis can manifest as diabetes, a disease characterized by a chronic elevation of blood sugar levels (Inzucchi, 2012). Type 2 diabetes, which is defined by peripheral insulin resistance and hyperglycemia, currently affects ~25 million people in the US and represents the seventh leading cause of death nationwide (WHO, 2013). With the spread of dietary excess and a sedentary lifestyle, the increasing incidence of type 2 diabetes is expected to continue at its alarming pace (CDC, 2011). Thus, it is critical that we better understand the basic genetic and molecular mechanisms underlying the regulation of glucose homeostasis and how misregulation of these pathways can lead to diabetes.

Glucose homeostasis is controlled by the secretion of insulin from pancreatic beta cells in response to an increase in circulating glucose (Schrayyef and Gerich, 2010). This process, called glucose-stimulated insulin signaling (GSIS), is characterized by a set of steps that link the oxidative catabolism of glucose to insulin secretion through ATP production and cellular ionic changes. Following a meal, circulating glucose is transported across the beta cell plasma membrane through the glucose transporter GLUT2, rapidly converted to glucose-6-phosphate by glucokinase, and metabolized through glycolysis and the TCA cycle to drive ATP synthesis by the electron transport chain. This spike in ATP results in an increased ATP/ADP ratio, which inhibits the K_{ATP}-dependent channel. The resulting membrane depolarization drives the activation of voltage gated calcium channels, thus increasing the intracellular Ca^{2+} concentration. Ultimately, this Ca^{2+} spike, along with metabolites generated by increased flux of the TCA cycle called coupling factors, trigger insulin secretion (Maechler, 2012; Prentki et al., 2013). Once secreted into the circulation, insulin activates the insulin receptor in

peripheral tissues, such as the liver and skeletal muscle, to activate PI3K and other signaling pathways, driving glucose uptake, metabolism, and storage to maintain euglycemia (Siddle, 2011).

In the fruit fly, *Drosophila melanogaster*, circulating sugar levels are regulated by a signaling pathway orthologous to insulin signaling in humans. Analogous to insulin production by beta cells in the pancreas, several *Drosophila* Insulin Like Peptides (DILPS) are produced in the Insulin Producing Cells (IPCs) of the brain and secreted in response to dietary nutrients (Geminard et al., 2009; Kim and Rulifson, 2004; Nassel et al., 2013). Also similar to beta cells, IPCs in adult flies express the Kir6 and Sur1 subunits of the K_{ATP}-dependent ion channel that is involved in GSIS (Fridell et al., 2009). Consistent with this, drug antagonists of the K_{ATP}-dependent channel used to promote insulin secretion in diabetic patients are functional in *Drosophila* (Fridell et al., 2009; Kim and Rulifson, 2004; Kreneisz et al., 2010). Moreover, IPCs isolated from adult flies depolarize in response to glucose *in vitro*, suggesting that DILP secretion in *Drosophila* adults may be regulated by a similar glucose-sensing mechanism as that used in mammals (Fridell et al., 2009; Kreneisz et al., 2010). Consistent with this model, work from our lab has shown that feeding adult flies glucose alone is sufficient to trigger DILP secretion (Barry et al*.,* manuscript in preparation). Circulating DILPs activate the Insulin Receptor ortholog (InR) in peripheral tissues, including the fat body, which is the fly tissue analogous to both the liver and white adipose tissue (Arrese and Soulages, 2010; Teleman, 2010). DILP binding to the InR ultimately drives the activation of PI3K, the phosphorylation of Akt, and repression of the transcription factor FOXO, thus altering the transcriptional profile of many metabolic genes (Alic et al., 2011; Hwangbo et al., 2004;

Teleman, 2010). DILP signaling regulates aspects of carbohydrate homeostasis in peripheral tissues required to maintain euglycemia through these transcriptional changes and nontranscriptional mechanisms (Alic et al., 2011; Slack et al., 2011; Yamamoto and Tatar, 2011).

Disruption of DILP signaling at multiple levels can lead to metabolic defects in *Drosophila* (Nassel et al., 2013). For example, ablation of the IPCs during development or adulthood results in alterations in TAG storage and an accumulation of glucose, glycogen, and trehalose, which is a disaccharide of glucose that is present in insects (Haselton et al., 2010; Rulifson et al., 2002). Moreover, genetic disruption of *Dilp* genes*, InR,* or a PI3K ortholog *dp110,* results in a similar elevation of carbohydrate levels (Arquier et al., 2008; Murillo-Maldonado et al., 2011; Shingleton et al., 2005; Zhang et al., 2009). Similarly, disruption of DILP secretion from IPCs also results in hyperglycemia (Fridell et al., 2009). Consistent with this observation, *Drosophila* mutants for *Hepatocyte Nuclear Factor 4* (*dHNF4*) recapitulate a monogenic form of diabetes called Maturity Onset Diabetes of the Young 1 (MODY1), which is characterized by defective GSIS and hyperglycemia (Barry et al., manuscript in preparation; Gardner and Tai, 2012; Yamagata et al., 1996). Interestingly, a recent report has shown that increasing dietary sucrose levels to high levels leads to insulin resistance and hyperglycemia in wild type flies (Musselman et al., 2011). In follow up studies, some of the mechanisms underlying insulin resistance in humans were shown to be conserved in this *Drosophila* model of diet-induced diabetes, including dysregulated lipocalin signaling and alterations in lipid metabolism (Law et al., 2010; Musselman et al., 2013; Pasco and Leopold, 2012; Samuel and Shulman, 2012). Thus, studies in *Drosophila*

provide a simple system to understand the genetic and molecular mechanisms governing insulin secretion, insulin resistance, and the regulation of glucose homeostasis.

The glycolytic product pyruvate is positioned at a central node in cellular metabolism, as it can be converted to alanine, lactate, acetyl-CoA, or oxaloacetate, depending on cellular metabolic requirements (Berg et al., 2002). The transport of pyruvate across the inner mitochondrial membrane is critical for fueling the TCA cycle through its conversion to acetyl-CoA or oxaloacetate by the mitochondrial enzymes pyruvate dehydrogenase (PDH) or pyruvate carboxylase (PC), respectively (Gray et al., 2013). Consistent with this central role in cellular metabolism, alterations in pyruvate utilization can affect glucose homeostasis. For example, liver-specific disruption of PC reduces hepatic gluconeogenesis, and loss of either PDH or PC promotes hepatic insulin sensitivity (Choi et al., 2010; Kumashiro et al., 2013). In addition, disrupting PDH in beta cells reduces insulin secretion, demonstrating that the oxidation of glucose-derived pyruvate is required for GSIS *in vivo* (Srinivasan et al., 2010). Taken together, these studies suggest that mitochondrial pyruvate metabolism may represent a critical step in the regulation of glucose homeostasis, insulin resistance, and insulin secretion, all of which are processes known to be dysregulated in the context of diabetes (Inzucchi, 2012).

We recently discovered the identity of the mitochondrial pyruvate carrier (MPC), which functions upstream of PDH and PC by facilitating mitochondrial pyruvate import from the cytosol (Bricker et al., 2012). Interestingly, there is evidence that manipulation of the MPC could be a strategy for treatment for type 2 diabetes as a novel PPAR gamma-sparing thiazolidinedione derivative that inhibits MPC activity was recently identified (Colca et al., 2013; Divakaruni et al., 2013). This MPC-binding drug

can improve insulin sensitivity in flies and cultured human pancreatic islets, but it is not clear if these benefits are the result of MPC inhibition (Colca et al., 2013; Rohatgi et al., 2013). With these recent pharmacological discoveries, it is clear that a better characterization of the role of the MPC in the regulation of glucose homeostasis is required.

In a previous set of experiments, we generated mutations in the *Drosophila* ortholog of *MPC1* (*dMPC1*), an essential subunit of the MPC (Bricker et al*.,* 2012). These mutants are viable to adulthood but display elevated carbohydrate and pyruvate levels, reduced overall ATP production, and a marked sensitivity to amino acid and lipid starvation (Bricker et al., 2012). Using these mutants, we set out to understand the role of mitochondrial pyruvate import in the regulation of glucose homeostasis *in vivo* though genetic studies in *Drosophila melanogaster*. We determined that *dMPC1* mutants exhibit multiple hallmarks of diabetes, including a sensitivity to dietary sugar levels, glucose intolerance, and elevated circulating glucose under both fed and fasted conditions. Accompanying these phenotypes, we found that *dMPC1* mutants display defects in insulin signaling, possibly due to a defect in DILP secretion from the IPCs. Furthermore, we determined that *dMPC1* is required in the fat body to maintain euglycemia when flies are challenged with dietary sugar. Thus, our work defines a role for pyruvate metabolism in carbohydrate homeostasis in *Drosophila* and provides a simple, genetically tractable system for future studies of the role of mitochondrial pyruvate import in the regulation of insulin signaling and glucose homeostasis.

Experimental procedures

Fly strains

Tubulin-Gal4 and *Mef2-Gal4* were obtained from the Bloomington stock center. *Lsp2-Gal4-3.1* (Lazareva et al., 2007) was a gift from Daniela Drummond-Barbosa (Johns Hopkins Bloomberg School of Medicine) and *Dilp2-Gal4* (Wu et al., 2005) was a gift from Ping Shen (University of Georgia). *UAS-dMPC1*, *dMPC1* mutants ($dMPC1^{1}/dMPC1^{2}$ transheterozygotes), and $dMPC1^{+}$ precise-excision control strains were described previously (Bricker, et al., 2012).

Dietary treatments

All flies were maintained at 25˚C. To alter dietary sugar concentrations, media was prepared with a constant 10% yeast concentration, and either low sugar (2% sucrose), intermediate sugar (10% sucrose) or high sugar (18%) concentrations in water. To assay the effect of dietary sugar concentration on metabolite levels, animals were raised on standard Bloomington stock center media and transferred to the indicated diet within 2–4 days of eclosion, and metabolites were measured within 8–12 days of transfer. For lifespan analysis, males were transferred to the indicated diet within 1 day of eclosion. Flies were then transferred to new vials every 2–5 days and dead flies were counted and removed. To assay sugar-induced developmental delay, animals were allowed to lay on egg caps topped with yeast paste, the resulting progeny were transferred at the first instar stage to the indicated diets, and the number of pupariated animals were counted daily.

Metabolite measurements

To directly measure circulating glucose, ~30 adult females were poked in the thorax with a tungsten needle and centrifuged at 13,000 g through DNA columns (Zymo-Spin IIIC #C1006-50) twice in a centrifuge at 4˚C. Hemolymph was then diluted 1/200 in PBS and heat treated at 70˚C for 10 minutes to inactivate enzymes, and the glucose concentration was measured as described previously (Bricker et al., 2012). Whole-animal glucose, trehalose, triacylglycerol (TAG), glycogen, and protein measurements were performed using colorimetric assays and all other metabolites were measured by gas chromatography/mass spectrometry as described previously (Bricker et al., 2012).

Glucose tolerance test

Male adult flies were aged 5–9 days on standard Bloomington stock center media, starved overnight on starvation media (1% agar in H_2O), fed 10% glucose/1% agar for 2 hours, and subsequently transferred to starvation media for 2 or 4 hours. Glucose measurements were performed at each time point as described previously (Bricker et al., 2012).

Assays for activation of peripheral insulin signaling

Flies were aged for 8–12 days on high sugar media prior to western or northern blot analysis. To assay Akt phosphorylation, flies were homogenized and protein from the equivalent of ½ of a fly was resolved by SDS-PAGE and immunoblotted using standard methods with antibodies to Phospho-Akt (Cell Signaling #4691 – 1:1000 dilution), Pan-Akt (Cell Signaling #4054 – 1:1000 dilution), and Beta-Tubulin

(Chemicon MAB380 – 1:100,000 dilution), followed by chemo-luminescent detection. *4eBP* and *rp49* mRNA levels were assayed by northern blot analysis using radiolabeled probes generated using templates amplified using the following primers: *4eBP* – 5'-TGAAGAATCTCCGTGGCTCC-3' and 5'-GACCGAGAGAACAAACAAGGTG-3', *rp49* – 5'-ATTAACCCTCACTAAAG-3' and 5'-AATACGACTCACTATAG-3'. Experiments were repeated several times and representative data is shown.

DILP2 secretion assay

Flies aged 5–9 days were starved overnight followed by 2 hours of feeding on high sugar media (10% yeast/18% sucrose). Brains were dissected from starved or fed animals in cold PBS and fixed for 20 minutes at room temperature (4% paraformaldehyde in PBS). Following several washes in PAT (PBS + 0.5% TritonX-1000) brains were incubated with an antibody targeted to DILP2 (polyclonal antibody generated against the peptide MVCEEYNPVIPH) in PAT+5% normal donkey serum (NDS) at 1:500 concentration for 48 hours at 4˚C. Brains were then washed in PAT and subsequently incubated for 48 hours with Cy2-conjugated secondary antibody in PAT+5% NDS at 4˚C. Brains were mounted in Slowfade Gold^{TM} (Invitrogen) and imaged using an Olympus FV1000 confocal microscope. Z stack images were taken through the entire depth of fluorescence of the IPCs from all brains using identical settings. IPCs were traced in maximum intensity projections and the mean gray value was calculated in Image J to quantify DILP2 staining. Six to eight brains were assayed for each genotype/condition.

Statistics

Prism software was used to graph all quantitative data and perform statistical analysis. P values for pairwise comparisons were calculated using a Student's t test. P values for Kaplan Meyer survival curves were calculated using a log rank test. All quantitative data is shown as mean ± SEM.

Results

Drosophila MPC1 mutants are sensitive to dietary sugar levels

Work from our lab has demonstrated that flies exhibiting defects in carbohydrate homeostasis can be sensitive to the abundance of sugar in their diet (Barry et al., manuscript in preparation). In addition, low carbohydrate diets have been utilized to treat human patients with disorders of pyruvate metabolism (Wexler et al., 1997). Thus, we sought to determine if *dMPC1* mutants are sensitive to dietary sugar levels. To do so, we assayed the developmental timing and adult lifespan of flies fed a diet in which we varied sucrose levels, from low (2%) to intermediate (10%) or high (18%) concentrations in the presence of a constant amount of yeast (10%). The yeast in this food provides the amino acids and lipids required for the *dMPC1* mutants to survive for longer than ~4 days (Bricker et al., 2012). These sucrose concentrations were used such that the highest concentration (18%) is well below the amount (34%) previously shown to cause insulin resistance in wild-type flies (Musselman et al., 2011), and the intermediate level is close to that found in normal *Drosophila* growth media. Control flies raised on these diets experience a developmental delay correlated with increasing dietary sucrose concentrations (Figure 3.1A), whereas *dMPC1* mutants display a similar, but more severe

sugar-induced delay (Figure 3.1B). Adult controls transferred to intermediate or high sugar diets after eclosion live longer than those on low sugar food, consistent with previous reports (Figure 3.1C) (Bass et al., 2007; Skorupa et al., 2008). Conversely, this profile is reversed in *dMPC1* mutant adults, with flies on the low sugar diet living longest, and flies on the high sugar food dying most rapidly (Figure 3.1D). Taken together, these results suggest that *dMPC1* mutants are sensitive to dietary sugar load, especially during the adult stage.

Defects in carbohydrate and lipid homeostasis in *dMPC1* mutants on a high-sugar diet

The sensitivity of *dMPC1* mutants to a high-sugar diet is consistent with an inability to maintain metabolic homeostasis in response to increased sugar intake. To better understand the metabolic changes induced by the high dietary sugar load, we quantified several key metabolites in *dMPC1* mutant adults fed either the low or high sugar diet for 10 days. Interestingly, whole animal trehalose and glucose levels are normal in *dMPC1* mutants on the low sugar diet, and significantly elevated on the high sugar medium (Figures 3.2A and 3.2B). Glycogen levels are increased in *dMPC1* mutants on the low sugar diet, with a further elevation on the high sugar medium (Figure 3.2C). Conversely, TAG levels are normal in *dMPC1* mutants on the low sugar food, and reduced in mutants on the high sugar diet (Figure 3.2D). Moreover, *dMPC1* mutants exhibit a significant accumulation of the sugars inositol, erythrose, and ribose as well as the sugar alcohols sorbitol, mannitol, threitol, and xylitol (or ribitol) when maintained on

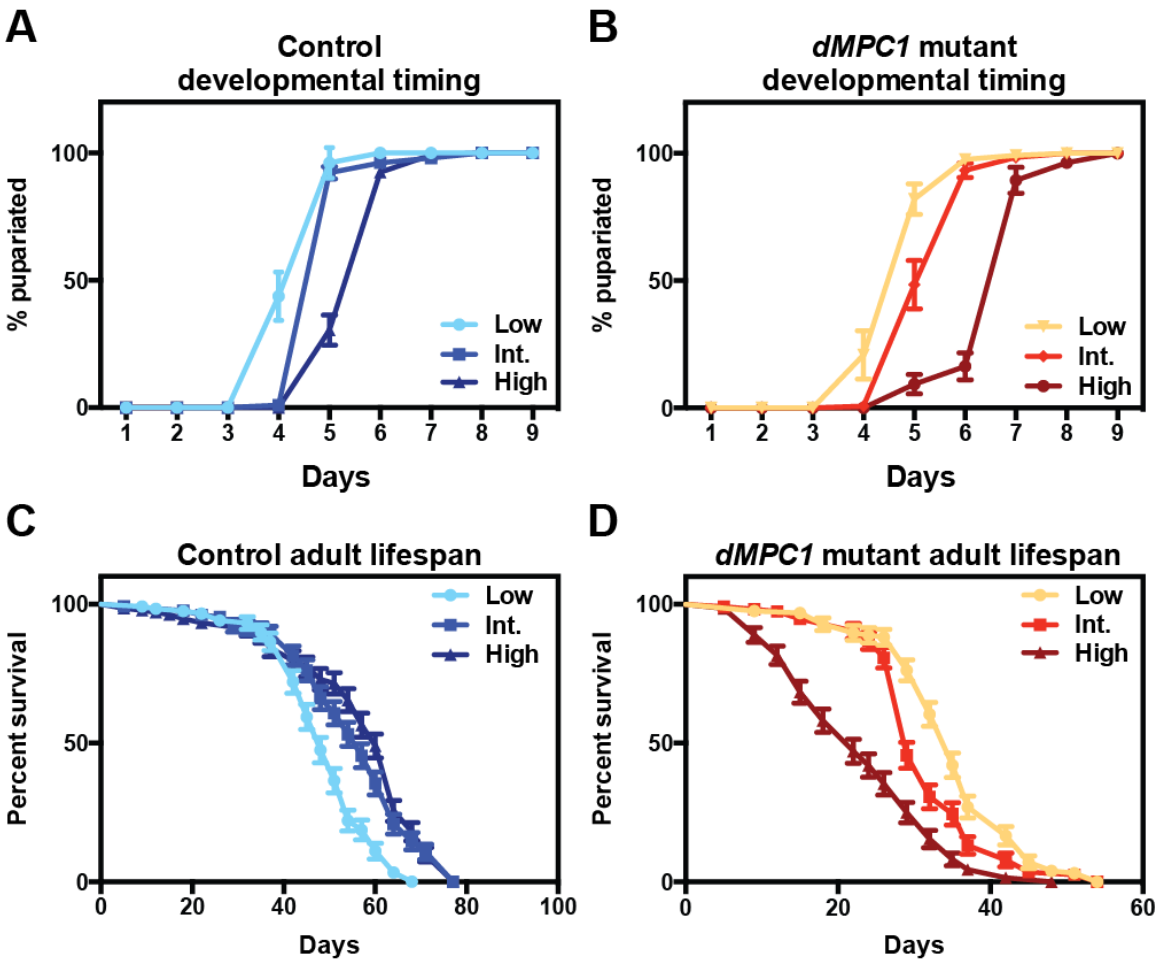

Figure 3.1. *dMPC1* mutants are sensitive to dietary sugar levels.

(A–B) Precise-excision controls or *dMPC1* mutant (*dMPC1*$^{-}$) first instar larvae were transferred to media containing low (2%), intermediate (Int; 10%), or high (18%) sugar concentrations and the number of pupariated flies was counted daily. N > 105 flies per genotype under each feeding condition. Mean ± SEM is shown. Median time to pupariation (days) for each genotype/condition are as follows—Control low = 4.15; Control intermediate = 4.55; Control high = 5.35; Mutant low = 4.48; Mutant intermediate = 5.07; Mutant high = 6.46. (C–D) The percentage of surviving adult control or *dMPC1*$^{-}$ flies fed the low, intermediate, or high sugar diet was assayed every 2–5 days. N > 115 male flies per genotype under each feeding condition. Mean ± SEM is shown. Median lifespan (days) for each genotype/condition–Control low = 48; Control intermediate = 57; Control high = 60; Mutant low = 35; Mutant intermediate = 29; Mutant high = 22. P values for each possible comparison were calculated using a log rank test and are as follows–Control low vs. control intermediate or high: $p < 0.0001$. Control intermediate vs. high: $p = .223$. Mutant low vs. mutant intermediate: $p = 0.0005$. Mutant low vs. mutant high: $p < 0.0001$. Mutant intermediate vs. mutant high: $p < 0.0001$. All control curves vs. all mutant curves: $p < 0.0001$.

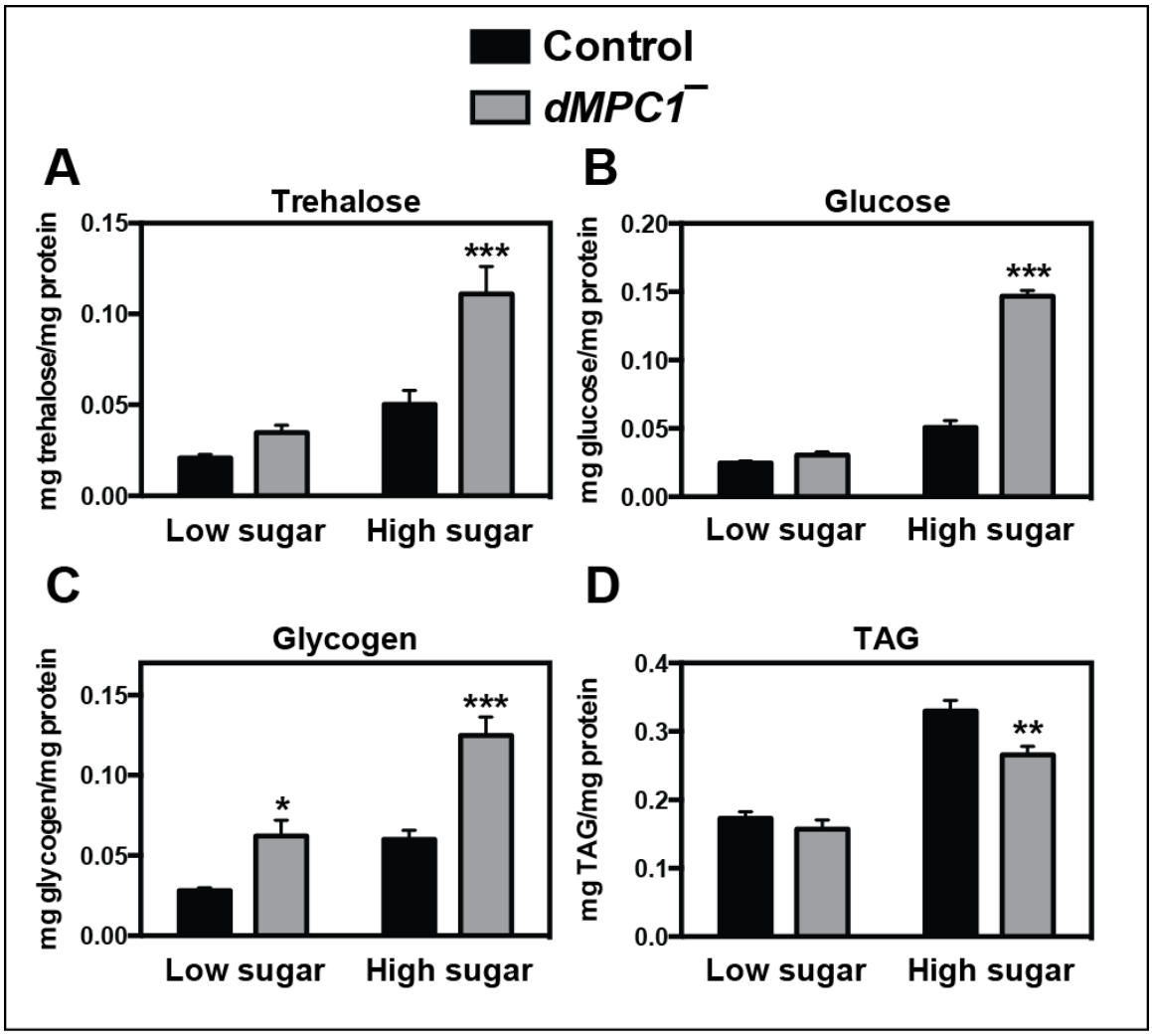

Figure 3.2. Altered carbohydrate and lipid homeostasis in *dMPC1* mutants.
Control or *dMPC1* mutant (*dMPC1*⁻) adults were aged 8–12 days on the low or high sugar diet and whole animal metabolite levels were measured. The abundance of (A) trehalose, (B) glucose, (C) glycogen, or (D) triacylglycerol (TAG) normalized to protein is shown. N = 5–6 samples per genotype. Mean ± SEM is shown. P values calculated by Student's t test. *p < 0.05, **p < 0.01, and ***p < 0.001.

the high sugar diet (Figure 3.3). The sorbitol accumulation is particularly interesting because the conversion of excess intracellular glucose to sorbitol through the polyol pathway is thought to promote neuropathy in diabetic patients (Brownlee, 2001). In addition, we observe a similar sorbitol accumulation in a *Drosophila* model of MODY1 (Barry et al., manuscript in preparation). In contrast, pyruvate accumulates to similar levels in *dMPC1* mutants on both diets (Figure 3.3). These metabolic changes on the high sugar diet demonstrate that *dMPC1* mutants are unable to maintain carbohydrate and lipid homeostasis in response to changes in dietary sugar and, furthermore, that these defects are independent of changes in pyruvate accumulation.

dMPC1 mutants display elevated circulating glucose, increased fasting glucose, and glucose intolerance

Since we observe a sensitivity to dietary sugar and an elevation of glucose and sorbitol in *dMPC1* mutants, we wanted to determine if *dMPC1* mutants exhibit clinically-defined characteristics of diabetes. To do this, we first verified that the increase in *dMPC1* glucose observed in previous experiments does indeed correspond to an increase in the circulating levels of glucose in the hemolymph (Figure 3.4A). Building on that observation, we asked if *dMPC1* mutants exhibit impaired fasting glucose and impaired glucose tolerance, similar to diabetic patients (Inzucchi, 2012). To address this question, we designed a *Drosophila* oral glucose tolerance test that measures the dynamics of postprandial glucose clearance over time. Using this assay, we identified that *dMPC1* mutants display increased fasting glucose levels and a reduced rate of glucose clearance

Figure 3.3. Accumulation of sugars and sugar alcohols in *dMPC1* mutants is influenced by dietary sugar.
Control or *dMPC1* mutant (*dMPC1*$^{-}$) adults were aged 8–12 days on the low or high sugar diet and whole animal small metabolite levels were measured by Gas chromatography/mass spectrometry. The abundance of (A) pyruvate, (B) ribose, (C) inositol, (D) erythrose, (E) sorbitol, (F) mannitol, (G) threitol, or (H) xylitol (or ribitol – cannot differentiate between these two in our analysis) is shown. N = 3 biological replicates per genotype. Mean ± SEM is shown. P values comparing mutants to controls under either condition were calculated by Student's t test. *$p < 0.05$, **$p < 0.01$, and ***$p < 0.001$.

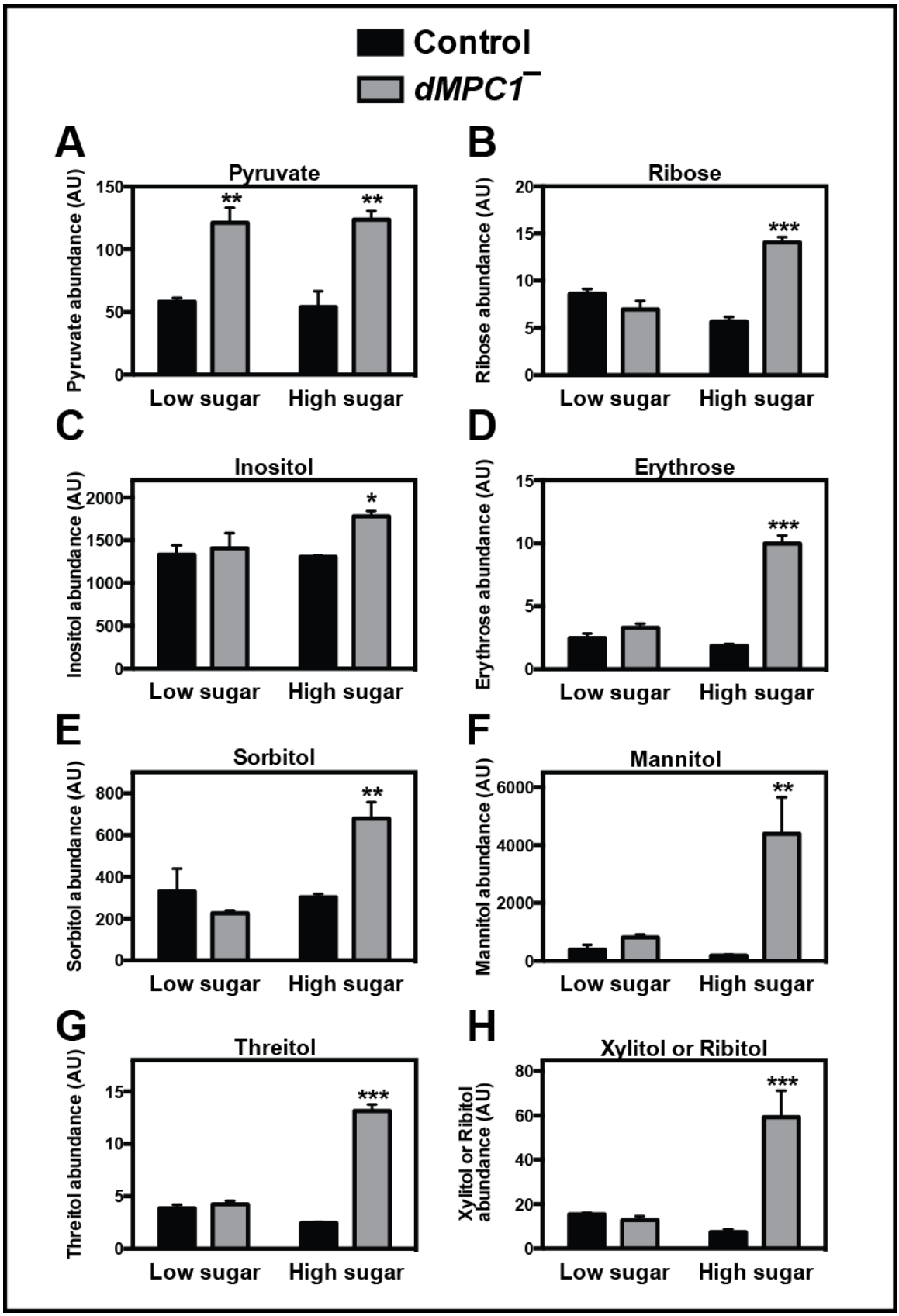
Control
dMPC1¯
A
Pyruvate
Pyruvate abundance (AU)
150
100
50
0
**
**
Low sugar
High sugar
B
Ribose
Ribose abundance (AU)
20
15
10
5
0
***
Low sugar
High sugar
C
Inositol
Inositol abundance (AU)
2000
1500
1000
500
0
*
Low sugar
High sugar
D
Erythrose
Erythrose abundance (AU)
15
10
5
0
***
Low sugar
High sugar
E
Sorbitol
Sorbitol abundance (AU)
800
600
400
200
0
**
Low sugar
High sugar
F
Mannitol
Mannitol abundance (AU)
6000
4000
2000
0
**
Low sugar
High sugar
G
Threitol
Threitol abundance (AU)
15
10
5
0
***
Low sugar
High sugar
H
Xylitol or Ribitol
Xylitol or Ribitol abundance (AU)
80
60
40
20
0
***
Low sugar
High sugar

Figure 3.4. Hallmarks of diabetes in *dMPC1* mutants.
(A) Hemolymph glucose concentrations of either control or *dMPC1* mutant (*dMPC1*$^{-}$) adult flies aged 10 days on high sugar media were determined N = 4 per genotype. (B) Control or *dMPC1*$^{-}$ flies were aged 5–9 days on standard laboratory media and starved overnight for 16 hours. After starvation, whole-animal glucose abundance normalized to protein was determined. N = 5 per genotype. (C) Control or *dMPC1*$^{-}$ flies were aged 5–9 days on standard laboratory media, starved overnight for 16 hours, placed on 10% glucose for 2 hours, and subsequently restarved for either 2 or 4 hours. At each timepoint, whole-animal glucose abundance normalized to protein was assayed. N = 5 biological replicates per genotype at each timepoint. Mean ± SEM is shown. P values were calculated by Student's t test. *$p < 0.05$, *$p < 0.01$, and $p < 0.001$.

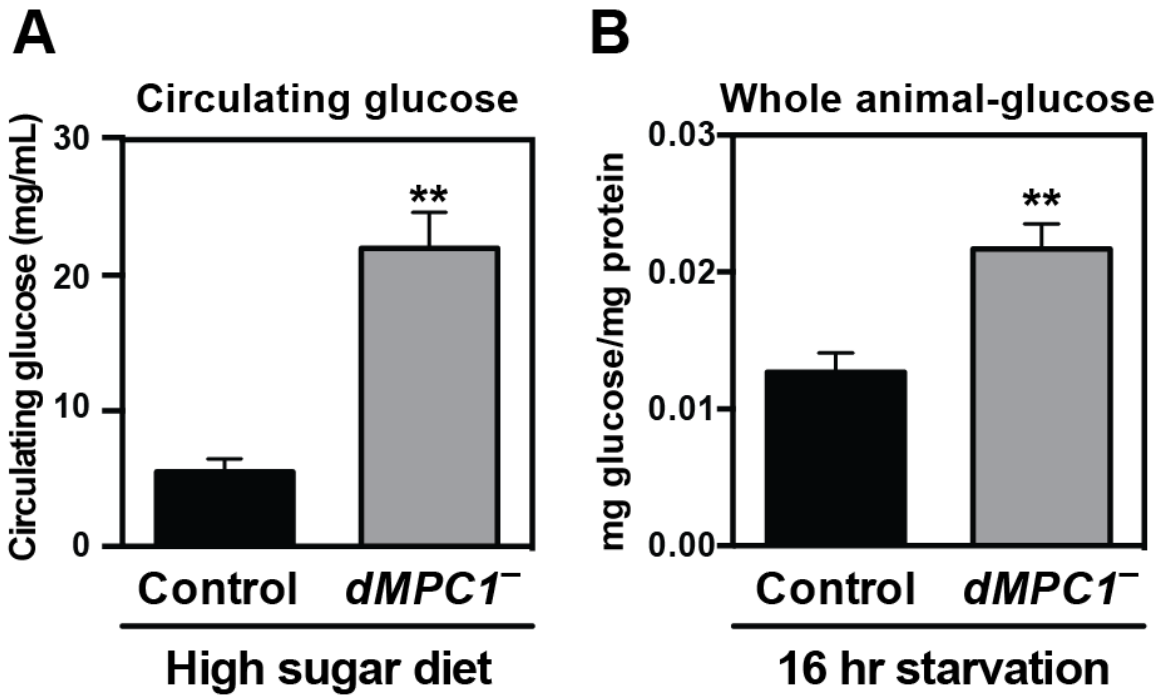
A
Circulating glucose
Circulating glucose (mg/mL)
30
20
10
0
**
Control
dMPC1−
High sugar diet
B
Whole animal-glucose
mg glucose/mg protein
0.03
0.02
0.01
0.00
**
Control
dMPC1−
16 hr starvation

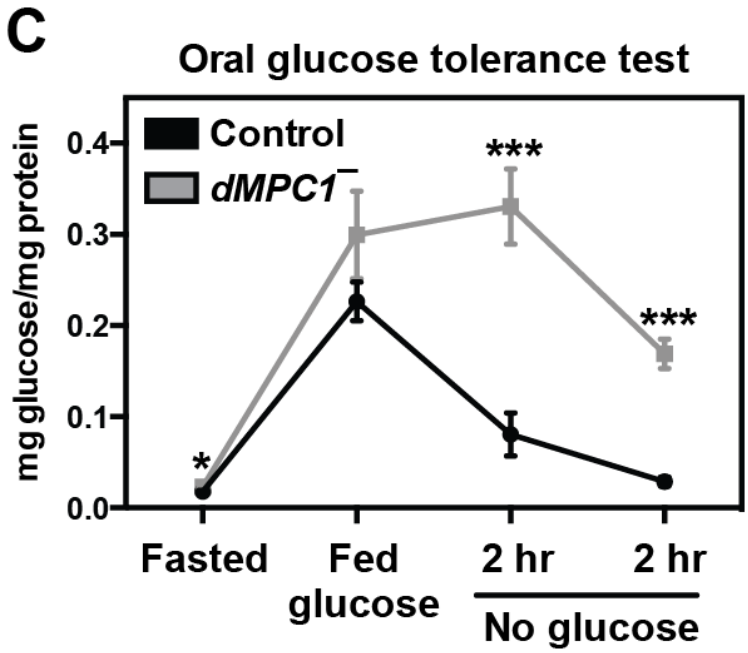
C
Oral glucose tolerance test
Control
dMPC1−
mg glucose/mg protein
0.4
0.3
0.2
0.1
0.0
*
***
***
Fasted
Fed
glucose
2 hr
2 hr
No glucose

following a glucose meal (Figures 3.4B and 3.4C). Taken together, these results establish that *dMPC1* mutants display several key hallmarks of diabetes.

Insulin signaling defects in *dMPC1* mutants

Given the diabetes-like phenotypes observed in *dMPC1* mutants, we predicted that they might also exhibit defects in insulin signaling. To test this prediction, we assayed the phosphorylation state of Akt and the expression level of *4eBP,* a target gene of the transcription factor FOXO (Figure 3.5A)(Alic et al., 2011; Demontis and Perrimon, 2010; Teleman et al., 2008). If insulin signaling is reduced in peripheral tissues, we expect to observe a reduction in Akt phosphorylation and overexpression of *4eBP* due to derepression of FOXO. Consistent with this prediction, *dMPC1* mutants display reduced levels of phosphorylated Akt and increased *4eBP* mRNA levels (Figures 3.5B and 3.5C). Taken together, these results indicate that *dMPC1* is required for normal insulin signaling activity in peripheral tissues.

Partial disruption of DILP2 secretion in *dMPC1* mutants

Reduced insulin signaling in the tissues of *dMPC1* mutants could be caused by a defect in the secretion of DILPs from the IPCs. We hypothesize that mitochondrial pyruvate import would be required for DILP secretion if the release of DILPs from IPCs is controlled by a mechanism similar to GSIS in mammalian beta cells (Prentki et al., 2013; Srinivasan et al., 2010). To address this possibility, we dissected the brains from *dMPC1* mutants following an overnight fast and subsequent refeeding, and assayed the levels of the most abundant of the three DILPs produced in IPCs, DILP2, by

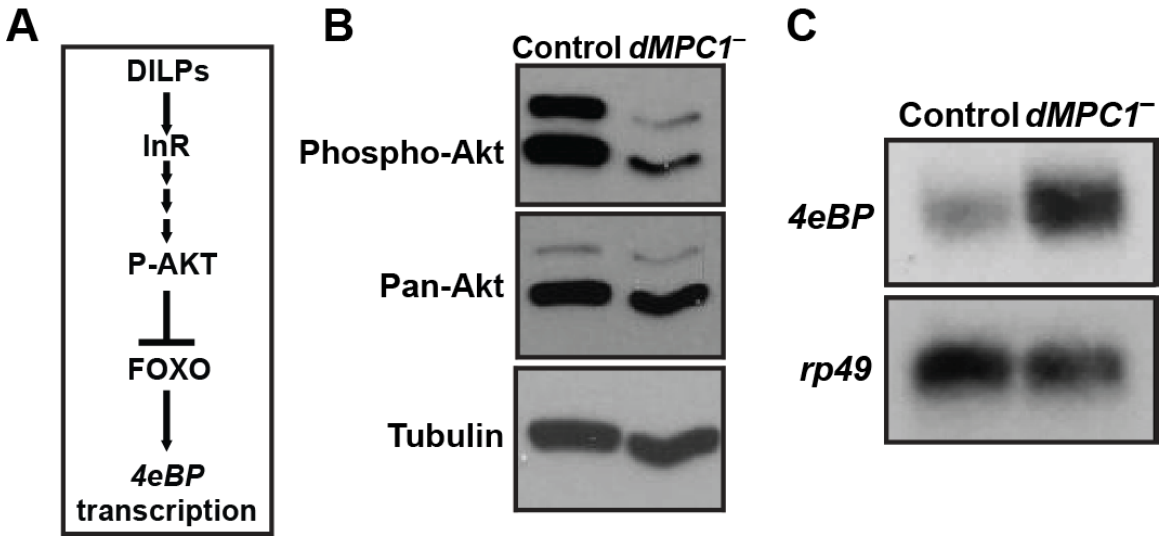

Figure 3.5. Reduction of peripheral insulin signaling activity in *dMPC1* mutants.
(A) A simplified diagram of the *Drosophila* insulin-signaling pathway. (B–C) Control or *dMPC1* mutant adults were aged 8–12 days on the high sugar diet and (B) phosphorylated Akt (phospho-Akt), total Akt, and Tubulin protein levels were determined by western blot analysis, or (C) *4eBP* and *rp49* mRNA levels were assayed by northern blot analysis.

immunofluorescence. In control IPCs, there is a reduction in DILP2 staining upon refeeding due to the secretion of accumulated DILP2, as expected (Figures 3.6A and 3.6B). In contrast, *dMPC1* mutants display an accumulation of DILP2 to higher levels under both fasted and fed conditions, and DILP2 secretion is partially reduced (Figures 3.6A and 3.6B). Thus, although this data is still preliminary, our results indicate that *dMPC1* is required for proper DILP secretion by the IPCs.

dMPC1 is required in the fat body to regulate glucose homeostasis

To determine the tissue specific roles of *dMPC1* in glucose homeostasis, we measured glucose levels in *dMPC1* mutant flies expressing wild type *dMPC1* in critical metabolic tissues. To do this, we combined a Gal4 driver that is expressed ubiquitously (*Tubulin-Gal4*), in the fat body (*Lsp2-Gal4*), the IPCs (*Dilp2-Gal4*), or the muscle (*Mef2-Gal4*), with a *UAS-dMPC1* transgene. Despite the observed defect in DILP secretion in *dMPC1* mutants, *dMPC1* expression in the fat body, but not the IPCs or muscles, is sufficient to rescue hyperglycemia to the same degree as ubiquitous rescue. These results indicate *dMPC1* functions mainly within the fat body to regulate circulating glucose levels (Figure 3.7).

Discussion

Circulating glucose levels are controlled through the coordination of carbohydrate uptake and metabolism by the insulin-signaling pathway in metabolic tissues (Schrayyef and Gerich, 2010). We show here that genetic disruption of mitochondrial pyruvate transport causes defects in glucose homeostasis and insulin signaling. This work provides

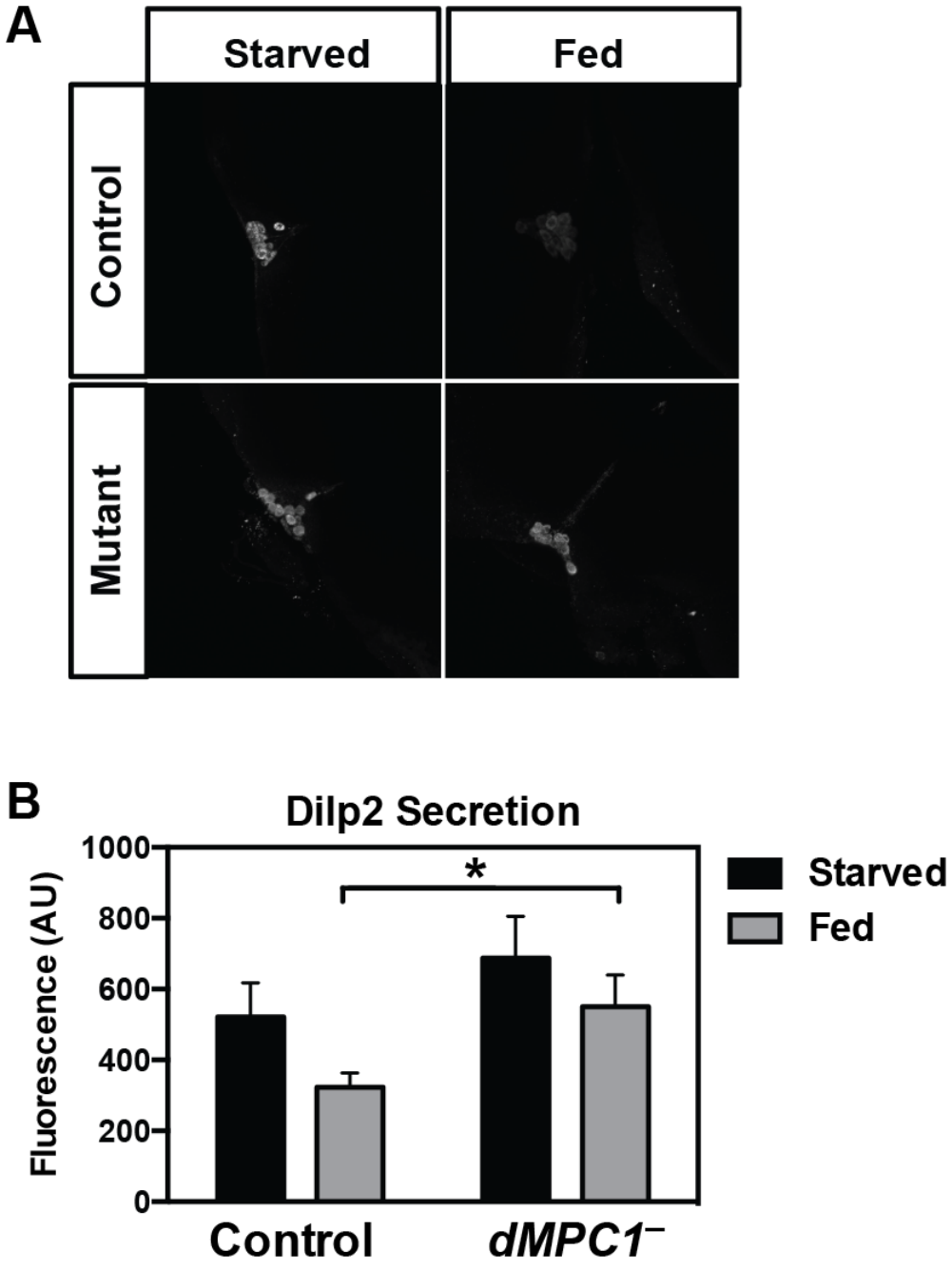

Figure 3.6. Reduced DILP secretion from IPCs in *dMPC1* mutants.
5–9 day old control or *dMPC1* mutant (*dMPC1*$^{-}$) males were starved overnight (16 hr.) and subsequently fed on high sugar media (10% yeast/18% sucrose) for 2 hours. Brains dissected from flies after starvation or subsequent feeding were stained with a Dilp2 antibody. (A) DILP2 staining of representative brains. (B) Quantification of DILP2 staining intensity. N = 6–8 brains per genotype/condition. Mean ± SEM is shown. P value calculated by Student's t test. *$p < 0.05$.

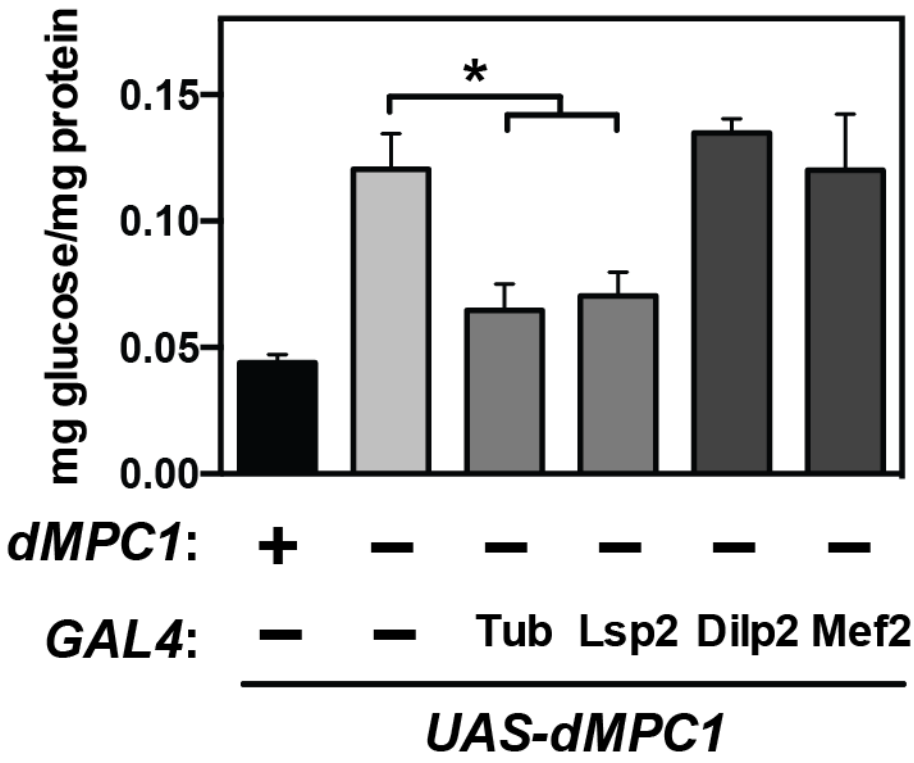

Figure 3.7. Fat body-specific rescue of *dMPC1* ameliorates hyperglycemia in *dMPC1* mutants.
Whole animal glucose levels of controls ($dMPC1^{+}$) or mutant ($dMPC1^{-}$) flies carrying the indicated GAL4 transgenes in the presence of a *UAS-dMPC1* construct after 10 days on high sugar media. GAL4 driver expression patterns: Tubulin (Tub) = ubiquitous; Lsp2 = fat body; Dilp2 = insulin producing cells; Mef2 = muscle. Mean ± SEM is shown. P value calculated by Student's t test. *$p < 0.05$.

new insights into the basic role of mitochondrial pyruvate metabolism in whole-organism physiology. In addition, we have established a new genetic model that can be used to better understand how changes in pyruvate utilization can affect insulin signaling and cause diabetes.

Hallmarks of diabetes in *dMPC1* mutants

We have identified defects associated with diabetes through our phenotypic analysis of *dMPC1* mutants. *dMPC1* mutants are sensitive to dietary sugar levels, as increased sugar correlates with hyperglycemia and a reduction in lifespan. This trend is similar to that observed in the *dHNF4* mutant model of MODY1, although the *dHNF4* mutants have a shorter life span under any dietary condition than *dMPC1* mutant flies (Barry et al., manuscript in preparation). This may be due to the fact that *dHNF4* mutant flies, which exhibit a similar degree of hyperglycemia as that seen in *dMPC1* mutants, also display defects in the regulation of many genes involved in beta-oxidation and the immune response (Barry et al., manuscript in preparation). Our results also translate to humans, as a reduction in dietary carbohydrate levels has been shown to help diabetic patients regulate glycemia and overall health (Kirk et al., 2008). In addition to chronic hyperglycemia, *dMPC1* mutants fed a high-sugar diet display an elevation in fasting glucose levels and reduced glucose clearance in an oral glucose tolerance test. These are key criteria that result in a diabetes diagnosis in the clinic (Inzucchi, 2012). Moreover, these data demonstrate that *dMPC1* mutants display a defect at the level of cellular glucose uptake or retention. Consistent with these defects, we observed reduced peripheral insulin signaling activity, another hallmark of diabetes (Inzucchi, 2012).

We predict that the hyperglycemia observed in *dMPC1* mutants is indirect, however, and ultimately caused by defects in mitochondrial pyruvate import. There are two hypotheses to explain the defects in glucose homeostasis observed in *dMPC1* mutants. First, pyruvate metabolic disruption could cause a general back up of glycolytic intermediates, which could alter the equilibrium of metabolites to reduce the rate at which glucose can be transported across the plasma membrane and phosphorylated (Figure 3.8A). In this model, insulin-signaling defects play a minor role in causing hyperglycemia (Figure 3.8A). Our alternative hypothesis is that the observed reduction in peripheral tissue insulin signaling may be the major factor causing hyperglycemia (Figures 3.8B, 3.8C, and 3.8D). Our metabolomic analysis is inconsistent with the first model (Figure 3.8A) as pyruvate levels are not affected by alterations in dietary sugar concentration. In addition, we do not observe an accumulation of detectable glycolytic intermediates positioned in the pathway between glucose and pyruvate, including glucose-6-phosphate, fructose-6-phosphate, 3-phosphoglycerate, or 2-phosphoglycerate (data not shown). Thus, we predict that the hyperglycemia caused by a loss of *dMPC1* is largely driven by the defect in insulin signaling in peripheral tissues (Figures 3.8B, 3.8C, and 3.8D).

Models for the role of the mitochondrial pyruvate carrier in the regulation of DILP signaling

There are two potentially overlapping models to explain the insulin signaling defects in *dMPC1* mutants. Defective DILP secretion from the IPCs may reduce the concentration of circulating DILPs, resulting in reduced activation of InR in peripheral

Figure 3.8: Models for the role of the MPC in the regulation of insulin signaling and glucose homeostasis.
(A) MPC promotes glycolytic flux and influences glycemia through mitochondrial pyruvate import. In this model, abnormal flux caused by *dMPC1* causes a back up of glycolytic intermediates, such that equilibrium is shifted away from cellular glucose import and Akt phosphorylation in the fat body. Effects on insulin signaling are caused indirectly, possibly by chronic hyperglycemia, instead of glycemia being influenced by MPC-mediated activation of insulin signaling. (B) MPC promotes DILP secretion cell autonomously. In this model, MPC1 facilitates DILP secretion through a metabolic GSIS pathway similar to that of mammals, or by some other mechanism. In *dMPC1* mutants, reduced circulating DILPs cause a reduction in the activity of fat body insulin activation, and thus hyperglycemia and other diabetic phenotypes. (C) MPC promotes DILP secretion non-cell autonomously. This model is similar to that shown in A, except that MPC1 functions in the fat body to promote signaling events that control DILP secretion from the IPCs. In this model, metabolic alterations in the *dMPC1* fat body lead to signaling, either by decreased Unpaired2 (Upd2) expression, increased DILP6 expression, or changes in some other signaling pathway to block DILP secretion. (D) MPC promotes insulin sensitivity. In this model, MPC1 functions primarily in the fat body to promote a metabolic state that is protective against insulin resistance. In *dMPC1* mutants, alteration of lipogenesis, signaling pathways known to affect insulin sensitivity, and/or another mechanism promotes insulin resistance. Insulin resistance in the fat body results in hyperglycemia and other diabetic phenotypes.

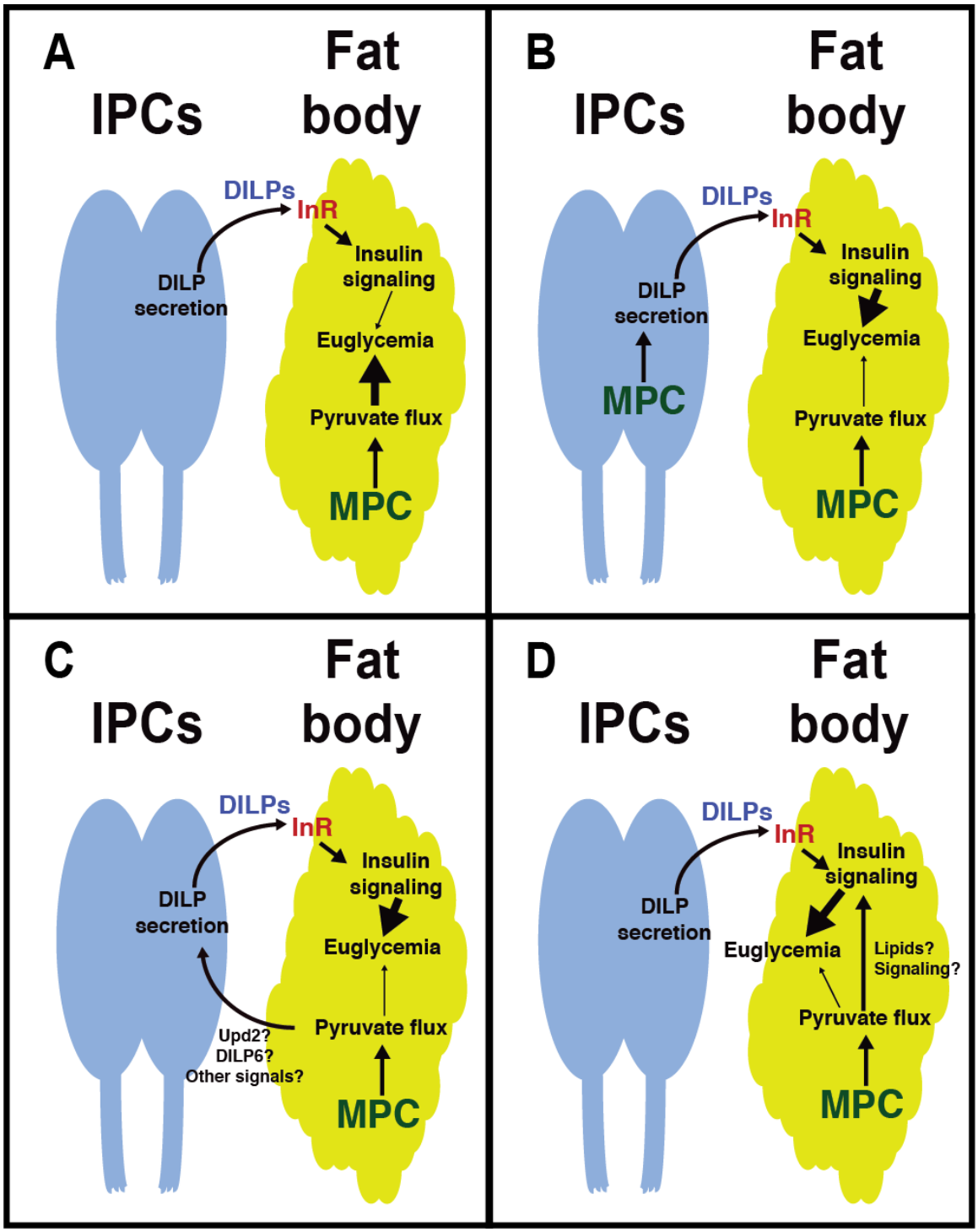
A
IPCs
Fat body
DILPs
InR
DILP secretion
Insulin signaling
Euglycemia
Pyruvate flux
MPC
B
IPCs
Fat body
DILPs
InR
DILP secretion
Insulin signaling
Euglycemia
MPC
Pyruvate flux
MPC
C
IPCs
Fat body
DILPs
InR
DILP secretion
Insulin signaling
Euglycemia
Upd2?
DILP6?
Other signals?
Pyruvate flux
MPC
D
IPCs
Fat body
DILPs
InR
DILP secretion
Insulin signaling
Euglycemia
Lipids?
Signaling?
Pyruvate flux
MPC

tissues (Figures 3.8B and 3.8C). Alternatively, peripheral DILP resistance could decrease the ability of metabolic tissues to efficiently respond to circulating DILPS (Figure 3.8D). Disrupting DILP secretion from IPCs has been shown to cause hyperglycemia (Fridell et al., 2009). IPCs express the Sur1 and Kir6 subunits of the K_{ATP}-dependent potassium channel and thus undergo depolarization and Ca^{2+} influx in response to glucose incubation *ex vivo* (Fridell et al., 2009; Kreneisz et al., 2010). Moreover, glucose feeding alone is sufficient to trigger DILP secretion from the IPCs during adulthood (Barry et al., manuscript in preparation). Taken together, these studies raise the possibility that IPCs may undergo GSIS utilizing a similar glucose sensing mechanism to that seen in mammals (Prentki et al., 2013). If GSIS is controlled by metabolic glucose sensing in flies, then we would predict that mitochondrial pyruvate import would be required for DILP secretion. Consistent with this prediction, we identified a defect in DILP secretion from the IPCs of *dMPC1* mutants. It is unclear, however, if this reduction in DILP secretion is caused by a cell autonomous defect in the IPCs due to effects on glucose sensing or general cellular IPC dysfunction, or non-cell autonomously through a role for the MPC in the fat body. Our data demonstrating that hyperglycemia is rescued by specific expression of *dMPC1* in the fat body, but not the IPCs of *dMPC1* mutant flies, are consistent with the second model (Figure 3.8C). There is precedent for this kind of mechanism, as nutrient sensing pathways in the fat body have been shown to remotely control DILP secretion from the IPCs by production of secreted signaling molecules such as Unpaired 2, Dilp6, or other molecules (Figure 3.8C) (Bai et al., 2012; Geminard et al., 2009; Rajan and Perrimon, 2012). In addition, the functional significance of the observed DILP secretion defect in the reduced activation of insulin signaling in *dMPC1* mutant

tissues remains unknown. This question and the mechanism by which DILP secretion is affected by a loss of *dMPC1* will be explored in future studies. The alternative, but not mutually exclusive explanation for the reduction in peripheral insulin signaling seen in the peripheral tissues of *dMPC1* mutants is insulin resistance (Figure 3.8D). Altered lipid homeostasis is thought to be a major underlying mechanism that drives insulin resistance in mammals (Samuel and Shulman, 2012). Mitochondrial pyruvate import and subsequent conversion to acetyl-CoA would be expected to be critical for carbohydrate-driven fatty acid synthesis (Berg et al., 2002). Consistent with this prediction, we observed an accumulation of TAG in wild-type flies upon transfer to the high sugar diet and found that this response is reduced in *dMPC1* mutants. Fat body lipogenesis was recently shown to be an important protective factor for flies fed a high sugar diet (Musselman et al., 2013). Thus, it is possible that altered lipogenesis in *dMPC1* mutants could affect DILP sensitivity and toxicity associated with high dietary sugar levels (Figure 3.8, D). Alternatively, decreased lipogenesis could also result from impaired insulin signaling, consistent with the role of insulin as an anabolic hormone. Whether the peripheral tissues in *dMPC1* mutants display *bona fide* insulin resistance, however, is unknown and will provide a focus for future studies.

The role of pyruvate metabolism in normal glucose homeostasis and diabetes

Mitochondrial pyruvate metabolism is important in tissues critical for the regulation of glucose homeostasis in mammals, including the pancreatic beta cells and liver. Flux analysis has shown that pyruvate is almost exclusively used to drive the TCA

cycle in beta cells, with ~60% of pyruvate converted to acetyl-CoA by PDH, and ~40% converted to oxaloacetate by PC (Khan et al., 1996; Schuit et al., 1997). PC-derived oxaloacetate, along with citrate, malate and isocitrate, is cycled through cytoplasmic enzymes to regenerate pyruvate (Jensen et al., 2008). This cycling is thought to be important for the production of metabolic coupling factors that promote maximal GSIS (Jensen et al., 2008). Recent evidence, however, suggests that this process is more active in rodents than humans and may not be functionally relevant to human GSIS (MacDonald et al., 2011). Conversion of pyruvate to acetyl-CoA by PDH is critical for ATP production using glucose as an oxidative substrate (Berg et al., 2002). Consistent with this role, GSIS is reduced in mice that carry mutations in PDH in their beta cells, thus resulting in impaired glucose tolerance and hyperglycemia (Srinivasan et al., 2010). This GSIS defect in PDH-deficient beta cells is presumably due to a diminished ability to generate the increase in cellular ATP required to inhibit the K_{ATP}-dependent channel and, thus, promote the depolarization event that drives insulin secretion (Prentki et al., 2013). In the liver, mitochondrial pyruvate is utilized by PDH and PC for lipogenesis and gluconeogenesis (Holness and Sugden, 1990; Merritt et al., 2011). Consistent with these critical roles in liver physiology, defects in pyruvate utilization affect liver glucose metabolism and insulin signaling. For example, a specific loss of PDH or PC in the liver results in improved glycemia and insulin sensitivity (Choi et al., 2010; Kumashiro et al., 2013). Interestingly, these phenotypes are the opposite of those observed in *dMPC1* mutant flies, where we would also expect a reduction in the availability of mitochondrial pyruvate used as a substrate for both PDH and PC. This disparity could be due to the fact that we are studying whole-body *dMPC1* mutants, while mammalian studies of PDH and

PC have focused on tissue-specific genetic disruption (Choi et al., 2010; Kumashiro et al., 2013). Improved insulin sensitivity associated with a hepatic loss of PDH or PC is thought to be driven by reduced hepatic or adipose tissue lipogenesis; however, this mechanism has not been tested directly (Choi et al., 2010; Kumashiro et al., 2013).

Interestingly, the MPC may be a clinically relevant drug target for the treatment of type 2 diabetes. A thiazolidinedione derivative was recently discovered that binds to the MPC via an interaction with the MPC2 subunit (Colca et al., 2013). This drug, which was shown to inhibit mitochondrial pyruvate transport *in vitro*, ameliorates insulin resistance in flies and isolated human beta cells (Colca, et al., 2013; Divakaruni et al., 2013; Rohatgi et al., 2013). Whether inhibition of the MPC is the mechanism underlying how this drug affects insulin sensitivity, however, is unknown. Thus, it is clear that the metabolic fate of pyruvate is critical in the regulation of glucose homeostasis, and defects in pyruvate utilization affect aspects of diabetes pathophysiology. *dMPC1* mutants provide a valuable model to understand how mitochondrial pyruvate import affects these processes.

Future directions

Future studies will be focused on determining the mechanism underlying the defects in insulin signaling and glucose homeostasis in *dMPC1* mutants. To do so, we will perform experiments to differentiate between the DILP secretion and DILP resistance models (Figures 3.8B and 3.8C). First, we will verify that *dMPC1* is required for DILP secretion by repeating our secretion assay. In this experiment, we will drive secretion by glucose feeding so that we can define any observed defects as due to a block

in GSIS. If the secretion defect is reproducible, then we will determine if it is of functional significance. To do this, we will drive the expression of a temperature-sensitive ion channel, TRPA1, specifically in the IPCs of *dMPC1* mutants (Hamada et al., 2008). This tool will allow us to bypass the DILP secretion defect in *dMPC1* mutants by forcing IPC depolarization and consequent DILP secretion in a temporally controlled manner. In these animals, readouts of peripheral insulin signaling activity (phosphorylated Akt and *4eBP* mRNA levels) and glucose levels will be assayed and compared to relevant controls. Alternatively, the low threshold voltage-gated NaChBac Na^+ channel from bacteria that has been shown to constitutively increase neuronal excitability could be expressed in IPCs as described previously (Geminard et al., 2009; Rajan and Perrimon, 2012). Although this latter strategy for forcing DILP secretion has been shown to rescue a DILP secretion defect, it is somewhat limited because it does not allow temporal control of DILP secretion.

If forced DILP secretion is sufficient to fully or partially rescue defects in *dMPC1* mutants, then we will determine the nature of this regulation of DILP secretion by the MPC. To do so, we will determine if DILP secretion from IPCs is regulated by *dMPC1* cell autonomously or non-cell autonomously. We will express *dMPC1* in the IPCs or the fat body of *dMPC1* mutants using the GAL4/UAS system and assay for DILP secretion from the IPCs. Since fat body *dMPC1* rescue is sufficient to rescue hyperglycemia in *dMPC1* mutants, we expect that *dMPC1* in the fat body will also rescue DILP secretion. If this hypothesis is correct, then it will be interesting to measure the expression of fat body signaling molecules previously shown to regulate DILP secretion non-cell autonomously such as Unpaired2 and DILP6 (Bai et al., 2012; Rajan and Perrimon,

2012). Alternatively, GSIS may be regulated by the MPC cell autonomously. The interpretation gained from this result, however, would depend on the experiment described above to determine if forced DILP secretion from the IPCs is sufficient to rescue hyperglycemia and defects in peripheral insulin signaling in *dMPC1* mutants.

If a DILP secretion defect is not the exclusive cause of the insulin signaling defect and hyperglycemia in *dMPC1* mutants, then we will test for insulin resistance. To do this, we will inject bovine insulin into starved adult *dMPC1* mutant flies (Haselton and Fridell, 2011). Since bovine insulin was shown to activate insulin signaling in *Drosophila* tissues, we can measure Phospho-Akt levels and *4eBP* expression in injected animals to determine the sensitivity of peripheral tissues to exogenous insulin (Haselton et al., 2011; Musselman et al., 2011). This approach will bypass any DILP secretion defect present in *dMPC1* mutants. If peripheral tissues display insulin resistance, then we will determine what metabolic or signaling pathways contribute to this defect. Since lipogenesis was previously shown to protect flies from an insulin resistance-inducing diet (Musselman et al., 2013), and *dMPC1* mutants display reduced accumulation of TAG when fed high sugar, we will directly measure glucose incorporation into fatty acids by flux analysis. If, as expected, flux of glucose-derived carbon to fatty acid synthesis is altered in *dMPC1* mutants, then we could validate the functional relevance of this defect by RNA-mediated silencing of *king tubby (ktub)* in the *dMPC1* mutant fat body as described (Musselman et al., 2013). In addition to these metabolic studies, we could determine whether any signaling pathways previously shown to regulate insulin sensitivity are affected in *dMPC1* mutants. To do this, we could measure the expression of several molecules known to regulate DILP sensitivity in *dMPC* mutants, including the InR antagonists

ImPL2 and *SDR* and the lipocalin *Nlaz* (Honegger et al., 2008; Okamoto et al., 2013; Pasco and Leopold, 2012). Based on these results, we could test the functional relevance of any expression changes with double mutant and/or overexpression studies.

Finally, it is possible that hyperglycemia is not entirely caused by the defect in insulin signaling in *dMPC1* mutants (Figure 3.8A). If this is the case, then we will investigate the metabolic mechanisms driving altered glucose homeostasis in *dMPC1* mutants. If the equilibrium of glycolytic intermediates is altered, it may be possible to bypass these defects by overexpressing lactate dehydrogenase in the fat body of *dMPC1* mutants. This enzyme converts cytosolic pyruvate to lactate and thus may enhance glycolytic flux (Yang et al., 1999). Alternatively, we can overexpress upstream rate-limiting enzymes in glycolysis, such as hexokinase and/or phosphofructokinase, to promote glucose uptake and retention (Tennessen et al., 2011). Circulating glucose will be measured in *dMPC1* mutants employing these two strategies for altering glycolytic flux independently and in combination. In addition, we will assay for rescue of insulin signaling defects in these experiments.

Our current data and potential future results combined provide a better understanding of the role of mitochondrial pyruvate metabolism in the maintenance of glucose homeostasis. More specifically, *dMPC1* mutants allow us investigate the role of the MPC in the regulation of insulin signaling and diabetic phenotypes *in vivo*. This understanding is particularly important as it was recently shown that the MPC is a target of PPAR gamma-sparing thiazolidinedione derivatives that improve insulin sensitivity in rodent and fly models. Therefore, our work will likely yield valuable insight into the

mechanism by which altered MPC activity may affect diabetes pathophysiology in humans.

Acknowledgements

We thank Will Barry for his help with experiments and critical reading of this chapter. We also thank James Cox at the University of Utah Metabolomics Core who was instrumental for the GC/MS experiments. This work was supported by NIH R01-GM094232 (Carl S. Thummel) and NIH T32-GM007464 (Daniel K. Bricker).

References

Alic, N., Andrews, T.D., Giannakou, M.E., Papatheodorou, I., Slack, C., Hoddinott, M.P., Cocheme, H.M., Schuster, E.F., Thornton, J.M., and Partridge, L. (2011). Genome-wide dFOXO targets and topology of the transcriptomic response to stress and insulin signalling. Mol. Syst. Biol. *7*, 502.

Arquier, N., Geminard, C., Bourouis, M., Jarretou, G., Honegger, B., Paix, A., and Leopold, P. (2008). Drosophila ALS regulates growth and metabolism through functional interaction with insulin-like peptides. Cell Metab. *7*, 333–338.

Arrese, E.L., and Soulages, J.L. (2010). Insect fat body: energy, metabolism, and regulation. Annu. Rev. Entomol. *55*, 207–225.

Bai, H., Kang, P., and Tatar, M. (2012). Drosophila insulin-like peptide-6 (dilp6) expression from fat body extends lifespan and represses secretion of Drosophila insulin-like peptide-2 from the brain. Aging Cell *11*, 978–985.

Bass, T.M., Grandison, R.C., Wong, R., Martinez, P., Partridge, L., and Piper, M.D. (2007). Optimization of dietary restriction protocols in Drosophila. J. Gerontol. A Biol. Sci. Med. Sci. *62*, 1071–1081.

Berg, J.M., Tymoczko, J.L., and Stryer, L. (2002). Biochemistry. (New York: W. H. Freeman). Accessed online at http://www.ncbi.nlm.nih.gov/books/NBK21154.

Bricker, D.K., Taylor, E.B., Schell, J.C., Orsak, T., Boutron, A., Chen, Y.C., Cox, J.E., Cardon, C.M., Van Vranken, J.G., Dephoure, N., et al. (2012). A mitochondrial pyruvate

carrier required for pyruvate uptake in yeast, Drosophila, and humans. Science *337*, 96–100.

Brownlee, M. (2001). Biochemistry and molecular cell biology of diabetic complications. Nature *414*, 813–820.

CDC (2011). 2011 National Diabetes Fact Sheet. Accessed online at http://www.cdc.gov/diabetes/pubs/pdf/ndfs_2011.pdf.

Choi, C.S., Ghoshal, P., Srinivasan, M., Kim, S., Cline, G., and Patel, M.S. (2010). Liver-specific pyruvate dehydrogenase complex deficiency upregulates lipogenesis in adipose tissue and improves peripheral insulin sensitivity. Lipids *45*, 987–995.

Colca, J.R., McDonald, W.G., Cavey, G.S., Cole, S.L., Holewa, D.D., Brightwell-Conrad, A.S., Wolfe, C.L., Wheeler, J.S., Coulter, K.R., Kilkuskie, P.M., et al. (2013). Identification of a mitochondrial target of thiazolidinedione insulin sensitizers (mTOT)—relationship to newly identified mitochondrial pyruvate carrier proteins. PloS One *8*, e61551.

Demontis, F., and Perrimon, N. (2010). FOXO/4E-BP signaling in Drosophila muscles regulates organism-wide proteostasis during aging. Cell *143*, 813–825.

Divakaruni, A.S., Wiley, S.E., Rogers, G.W., Andreyev, A.Y., Petrosyan, S., Loviscach, M., Wall, E.A., Yadava, N., Heuck, A.P., Ferrick, D.A., et al. (2013). Thiazolidinediones are acute, specific inhibitors of the mitochondrial pyruvate carrier. Proc. Natl. Acad. Sci. USA *110*, 5422–5427.

Du, J., Cleghorn, W.M., Contreras, L., Lindsay, K., Rountree, A.M., Chertov, A.O., Turner, S.J., Sahaboglu, A., Linton, J., Sadilek, M., et al. (2013). Inhibition of mitochondrial pyruvate transport by zaprinast causes massive accumulation of aspartate at the expense of glutamate in the retina. J. Biol. Chem. *288*, 36129–36140.

Fridell, Y.W., Hoh, M., Kreneisz, O., Hosier, S., Chang, C., Scantling, D., Mulkey, D.K., and Helfand, S.L. (2009). Increased uncoupling protein (UCP) activity in Drosophila insulin-producing neurons attenuates insulin signaling and extends lifespan. Aging *1*, 699–713.

Gardner, D.S., and Tai, E.S. (2012). Clinical features and treatment of maturity onset diabetes of the young (MODY). Diabetes Metab. Syndr. Obes. *5*, 101–108.

Geminard, C., Rulifson, E.J., and Leopold, P. (2009). Remote control of insulin secretion by fat cells in Drosophila. Cell Metab. *10*, 199–207.

Gray, L.R., Tompkins, S.C., and Taylor, E.B. (2013). Regulation of pyruvate metabolism and human disease. Cell. Mol. Life Sci. Advanced online publication. PMID: 24363178.

Hamada, F.N., Rosenzweig, M., Kang, K., Pulver, S.R., Ghezzi, A., Jegla, T.J., and Garrity, P.A. (2008). An internal thermal sensor controlling temperature preference in Drosophila. Nature *454*, 217–220.

Haselton, A., Sharmin, E., Schrader, J., Sah, M., Poon, P., and Fridell, Y.W. (2010). Partial ablation of adult Drosophila insulin-producing neurons modulates glucose homeostasis and extends life span without insulin resistance. Cell Cycle *9*, 3063–3071.

Haselton, A.T., and Fridell, Y.W. (2011). Insulin injection and hemolymph extraction to measure insulin sensitivity in adult Drosophila melanogaster. J. Vis. Exp. *52*, e2722.

Holness, M.J., and Sugden, M.C. (1990). Pyruvate dehydrogenase activities and rates of lipogenesis during the fed-to-starved transition in liver and brown adipose tissue of the rat. Biochem. J. *268*, 77–81.

Honegger, B., Galic, M., Kohler, K., Wittwer, F., Brogiolo, W., Hafen, E., and Stocker, H. (2008). Imp-L2, a putative homolog of vertebrate IGF-binding protein 7, counteracts insulin signaling in Drosophila and is essential for starvation resistance. J. Biol. *7*, 10.

Hwangbo, D.S., Gershman, B., Tu, M.P., Palmer, M., and Tatar, M. (2004). Drosophila dFOXO controls lifespan and regulates insulin signalling in brain and fat body. Nature *429*, 562–566.

Inzucchi, S.E. (2012). Clinical practice. Diagnosis of diabetes. N. Engl. J. Med. *367*, 542–550.

Jensen, M.V., Joseph, J.W., Ronnebaum, S.M., Burgess, S.C., Sherry, A.D., and Newgard, C.B. (2008). Metabolic cycling in control of glucose-stimulated insulin secretion. Am. J. Physiol. Endocrinol. Metab. *295*, E1287–1297.

Khan, A., Ling, Z.C., and Landau, B.R. (1996). Quantifying the carboxylation of pyruvate in pancreatic islets. J. Biol. Chem. *271*, 2539–2542.

Kim, S.K., and Rulifson, E.J. (2004). Conserved mechanisms of glucose sensing and regulation by Drosophila corpora cardiaca cells. Nature *431*, 316–320.

Kirk, J.K., Graves, D.E., Craven, T.E., Lipkin, E.W., Austin, M., and Margolis, K.L. (2008). Restricted-carbohydrate diets in patients with type 2 diabetes: a meta-analysis. J. Am. Diet. Assoc. *108*, 91–100.

Kreneisz, O., Chen, X., Fridell, Y.W., and Mulkey, D.K. (2010). Glucose increases activity and Ca2+ in insulin-producing cells of adult Drosophila. Neuroreport *21*, 1116–1120.

Kumashiro, N., Beddow, S.A., Vatner, D.F., Majumdar, S.K., Cantley, J.L., Guebre-Egziabher, F., Fat, I., Guigni, B., Jurczak, M.J., Birkenfeld, A.L., et al. (2013). Targeting

pyruvate carboxylase reduces gluconeogenesis and adiposity and improves insulin resistance. Diabetes *62*, 2183–2194.

Law, I.K., Xu, A., Lam, K.S., Berger, T., Mak, T.W., Vanhoutte, P.M., Liu, J.T., Sweeney, G., Zhou, M., Yang, B., et al. (2010). Lipocalin-2 deficiency attenuates insulin resistance associated with aging and obesity. Diabetes *59*, 872–882.

Lazareva, A.A., Roman, G., Mattox, W., Hardin, P.E., and Dauwalder, B. (2007). A role for the adult fat body in Drosophila male courtship behavior. PLoS Genet. *3*, e16.

MacDonald, M.J., Longacre, M.J., Stoker, S.W., Kendrick, M., Thonpho, A., Brown, L.J., Hasan, N.M., Jitrapakdee, S., Fukao, T., Hanson, M.S., et al. (2011). Differences between human and rodent pancreatic islets: low pyruvate carboxylase, ATP citrate lyase, and pyruvate carboxylation and high glucose-stimulated acetoacetate in human pancreatic islets. J. Biol. Chem. *286*, 18383–18396.

Maechler, P. (2012). Mitochondrial signal transduction in pancreatic beta-cells. Best practice & research. J. Clin. Endocrinol. Metabol. *26*, 739–752.

Merritt, M.E., Harrison, C., Sherry, A.D., Malloy, C.R., and Burgess, S.C. (2011). Flux through hepatic pyruvate carboxylase and phosphoenolpyruvate carboxykinase detected by hyperpolarized 13C magnetic resonance. Proc. Natl. Acad. Sci. USA *108*, 19084–19089.

Murillo-Maldonado, J.M., Sanchez-Chavez, G., Salgado, L.M., Salceda, R., and Riesgo-Escovar, J.R. (2011). Drosophila insulin pathway mutants affect visual physiology and brain function besides growth, lipid, and carbohydrate metabolism. Diabetes *60*, 1632–1636.

Musselman, L.P., Fink, J.L., Narzinski, K., Ramachandran, P.V., Hathiramani, S.S., Cagan, R.L., and Baranski, T.J. (2011). A high-sugar diet produces obesity and insulin resistance in wild-type Drosophila. Dis. Model. Mech. *4*, 842–849.

Musselman, L.P., Fink, J.L., Ramachandran, P.V., Patterson, B.W., Okunade, A.L., Maier, E., Brent, M.R., Turk, J., and Baranski, T.J. (2013). Role of fat body lipogenesis in protection against the effects of caloric overload in Drosophila. J. Biol. Chem. *288*, 8028–8042.

Nassel, D.R., Kubrak, O.I., Liu, Y., Luo, J., and Lushchak, O.V. (2013). Factors that regulate insulin producing cells and their output in. Front. Physiol. *4*, 252.

Negre-Salvayre, A., Salvayre, R., Auge, N., Pamplona, R., and Portero-Otin, M. (2009). Hyperglycemia and glycation in diabetic complications. Antiox. Redox. Signal. *11*, 3071–3109.

Okamoto, N., Nakamori, R., Murai, T., Yamauchi, Y., Masuda, A., and Nishimura, T. (2013). A secreted decoy of InR antagonizes insulin/IGF signaling to restrict body growth in Drosophila. Genes Dev. *27*, 87–97.

Pasco, M.Y., and Leopold, P. (2012). High sugar-induced insulin resistance in Drosophila relies on the lipocalin Neural Lazarillo. PloS One *7*, e36583.

Prentki, M., Matschinsky, F.M., and Madiraju, S.R. (2013). Metabolic signaling in fuel-induced insulin secretion. Cell Metab. *18*, 162–185.

Rajan, A., and Perrimon, N. (2012). Drosophila cytokine unpaired 2 regulates physiological homeostasis by remotely controlling insulin secretion. Cell *151*, 123–137.

Rohatgi, N., Aly, H., Marshall, C.A., McDonald, W.G., Kletzien, R.F., Colca, J.R., and McDaniel, M.L. (2013). Novel insulin sensitizer modulates nutrient sensing pathways and maintains beta-cell phenotype in human islets. PloS One *8*, e62012.

Rulifson, E.J., Kim, S.K., and Nusse, R. (2002). Ablation of insulin-producing neurons in flies: growth and diabetic phenotypes. Science *296*, 1118–1120.

Samuel, V.T., and Shulman, G.I. (2012). Mechanisms for insulin resistance: common threads and missing links. Cell *148*, 852–871.

Schrayyef, M.Z., and Gerich, J.E. (2010). Normal Glucose Homeostasis. Principles of Diabetes Mellitus. 16th Edition. (New York, NY: Springer Publishing) L. Poretsky (ed.) pp. 19–34.

Schuit, F., De Vos, A., Farfari, S., Moens, K., Pipeleers, D., Brun, T., and Prentki, M. (1997). Metabolic fate of glucose in purified islet cells. Glucose-regulated anaplerosis in beta cells. J. Biol. Chem. *272*, 18572–18579.

Shingleton, A.W., Das, J., Vinicius, L., and Stern, D.L. (2005). The temporal requirements for insulin signaling during development in Drosophila. PLoS Biol. *3*, e289.

Siddle, K. (2011). Signalling by insulin and IGF receptors: supporting acts and new players. J. Mol. Endocrinol. *47*, R1–10.

Skorupa, D.A., Dervisefendic, A., Zwiener, J., and Pletcher, S.D. (2008). Dietary composition specifies consumption, obesity, and lifespan in Drosophila melanogaster. Aging Cell *7*, 478–490.

Slack, C., Giannakou, M.E., Foley, A., Goss, M., and Partridge, L. (2011). dFOXO-independent effects of reduced insulin-like signaling in Drosophila. Aging Cell *10*, 735–748.

Srinivasan, M., Choi, C.S., Ghoshal, P., Pliss, L., Pandya, J.D., Hill, D., Cline, G., and Patel, M.S. (2010). Beta-cell-specific pyruvate dehydrogenase deficiency impairs glucose-stimulated insulin secretion. Am. J. Phisiol. Endocrinol. Metab. *299*, E910–917.

Teleman, A.A. (2010). Molecular mechanisms of metabolic regulation by insulin in Drosophila. Biochem. J. *425*, 13–26.

Tennessen, J.M., Baker, K.D., Lam, G., Evans, J., and Thummel, C.S. (2011). The Drosophila estrogen-related receptor directs a metabolic switch that supports developmental growth. Cell Metab. *13*, 139–148.

Wexler, I.D., Hemalatha, S.G., McConnell, J., Buist, N.R., Dahl, H.H., Berry, S.A., Cederbaum, S.D., Patel, M.S., and Kerr, D.S. (1997). Outcome of pyruvate dehydrogenase deficiency treated with ketogenic diets. Studies in patients with identical mutations. Neurology *49*, 1655–1661.

WHO (2013). Diabetes Fact Sheet. Accessed online at http://www.who.int/mediacentre /factsheets/fs312/en/.

Wu, Q., Zhang, Y., Xu, J., and Shen, P. (2005). Regulation of hunger-driven behaviors by neural ribosomal S6 kinase in Drosophila. Proc. Natl. Acad. Sci. USA *102*, 13289–13294.

Yamagata, K., Furuta, H., Oda, N., Kaisaki, P.J., Menzel, S., Cox, N.J., Fajans, S.S., Signorini, S., Stoffel, M., and Bell, G.I. (1996). Mutations in the hepatocyte nuclear factor-4alpha gene in maturity-onset diabetes of the young (MODY1). Nature *384*, 458–460.

Yamamoto, R., and Tatar, M. (2011). Insulin receptor substrate chico acts with the transcription factor FOXO to extend Drosophila lifespan. Aging Cell *10*, 729–732.

Yang, Y.T., San, K.Y., and Bennett, G.N. (1999). Redistribution of metabolic fluxes in Escherichia coli with fermentative lactate dehydrogenase overexpression and deletion. Metab. Eng. *1*, 141–152.

Zhang, H., Liu, J., Li, C.R., Momen, B., Kohanski, R.A., and Pick, L. (2009). Deletion of Drosophila insulin-like peptides causes growth defects and metabolic abnormalities. Proc. Natl. Acad. Sci. USA *106*, 19617–19622.

CHAPTER 4

SDHAF4 PROMOTES MITOCHONDRIAL SUCCINATE DEHYDROGENASE ACTIVITY AND PREVENTS NEURODEGENERATION

Daniel K. Bricker*, Jonathan G. Van Vranken*, Noah Dephore, Steven P. Gygi, James E. Cox, Jared Rutter, Carl S. Thummel

*Jonathan G. Van Vranken and myself are co-first authors on this chapter, which has been submitted to Cell Metabolism for publication

Summary

Succinate dehydrogenase (SDH) occupies a central place in cellular energy production, linking the tricarboxylic cycle with the electron transport chain. These critical functions are consistent with the causal role of SDH loss of function in a subset of cancer and neuromuscular disorders. In spite of these unique activities, only two factors have been identified that are required for proper SDH assembly and the prevention of disease. Herein we characterize a novel evolutionarily conserved mitochondrial protein designated Sdh8/SDHAF4, using yeast, *Drosophila*, and mammalian cells. We show that Sdh8 interacts specifically with Sdh1 in the mitochondrial matrix, facilitating its association with Sdh2 and the subsequent assembly of the SDH holocomplex. These roles for Sdh8 are critical for preventing motility defects and neurodegeneration in *Drosophila* as well as the excess ROS generated by free Sdh1. These studies provide insights into the mechanisms by which SDH is assembled and raise the possibility that some forms of neuromuscular disease may be associated with mutations that affect this SDH assembly factor.

Introduction

Mitochondria are dynamic organelles that are essential for many cellular processes including metabolism, signal transduction, and apoptosis. Consistent with these broad cellular functions, mitochondrial dysfunction is associated with a wide range of human diseases, including diabetes, neurodegeneration, and cancer. These important roles have led to comprehensive characterization of the mitochondrial proteome, identifying more than 1,000 nuclear-encoded proteins (Mercer et al., 2011; Pagliarini et

al., 2008; Sickmann et al., 2003). In spite of these efforts, however, many mitochondrial proteins remain uncharacterized, including proteins that are conserved throughout eukaryotic evolution. We are studying this subset of proteins as part of a systematic effort to comprehensively understand mitochondrial physiology. Herein, we describe the function of one of these evolutionarily conserved proteins and demonstrate that it is essential for proper succinate dehydrogenase (SDH) complex assembly and activity in yeast, flies, and mammalian cells.

SDH is unique in that it functions in both the tricarboxylic acid (TCA) cycle and the electron transport chain (ETC), wherein it is referred to as Complex II. SDH links the oxidation of succinate to fumarate in the TCA cycle with the reduction of ubiquinone to ubiquinol in the ETC, which contributes to the establishment of the mitochondrial membrane potential and ATP synthesis. SDH is a heterotetrameric protein complex that is embedded in the inner mitochondrial membrane (IMM), with its catalytic domain facing the mitochondrial matrix. The complex is anchored to the IMM by two integral membrane proteins, Sdh3 (SDHC in humans) and Sdh4 (SDHD), which coordinate a heme cofactor at their interface. The Sdh3/Sdh4 dimer binds the peripheral membrane protein Sdh2 (SDHB), which tethers the catalytic Sdh1 (SDHA) subunit to the complex. Sdh1 harbors a covalently bound FAD cofactor that is required for the oxidation of succinate (Hao et al., 2009; Robinson et al., 1994). The two electrons that result from this activity are channeled through the three iron-sulfur clusters in Sdh2 to ubiquinone, which interacts with SDH via the Sdh3/Sdh4 membrane anchor (Rutter et al., 2010).

The assembly of complexes like SDH presents the cell with the problem of coordinating the synthesis and stepwise interactions of individual subunits to form an

intricate membrane bound complex. This problem is exacerbated in the case of ETC complexes as individual subunits contain redox-active cofactors that can perform inappropriate and deleterious reactions when they are not properly secluded within the native complex. As a result, a number of dedicated factors assist the assembly of these complexes by facilitating cofactor insertion, preventing nonproductive interactions, and stabilizing assembly intermediates.

While the importance of assembly factors for Complex I and Complex IV is well established (Diaz et al., 2011; Fernandez-Vizarra et al., 2009), dedicated SDH assembly factors have only recently begun to emerge with the discovery of SDHAF1 (Sdh6 in yeast) and SDHAF2 (Sdh5) (Ghezzi et al., 2009; Hao et al., 2009). Human patients with loss of function mutations in *SDHAF1* or *SDHAF2* display reduced SDH complex levels and activity and present with infantile leukoencephalopathy and neuroendocrine tumors, respectively (Ghezzi et al., 2009; Hao et al., 2009). This is consistent with the spectrum of diseases that associate with mutations affecting the core subunits of SDH—*SDHA*, *SDHB*, *SDHC*, and *SDHD* (Bardella et al., 2011; Rutter et al., 2010)—and with a series of additional diseases that are characterized by loss of SDH activity, but which lack mutations in known SDH genes (Jain-Ghai et al., 2013; Pantaleo et al., 2014). Disruption of the yeast orthologs for *SDHAF1* or *SDHAF2* (*SDH5* or *SDH6*) prevents respiratory-dependent growth, with a clear defect in SDH activity. While the precise mechanism by which Sdh6 supports SDH biogenesis has remained elusive, Sdh5 was shown to be required for the covalent attachment of the FAD cofactor to Sdh1 (Ghezzi et al., 2009; Hao et al., 2009). The current model proposes that Sdh1 is flavinated by Sdh5 and then binds iron-sulfur loaded Sdh2, which then docks onto the pre-assembled membrane

bound Sdh3-Sdh4 dimer to form the holocomplex (Rutter et al., 2010). We hypothesized that the complexity of this assembly process likely necessitates the action of additional dedicated assembly factors and that the genes encoding these factors may contribute to the currently idiopathic SDH-associated genetic diseases.

With the goal of discovering new human disease genes and gaining a better understanding of SDH assembly and activity, we have focused on our ongoing functional elucidation of uncharacterized mitochondrial proteins. These studies led us to identify an evolutionarily conserved SDH assembly factor, Ybr269, which we have renamed Sdh8 in yeast and SDHAF4 in higher organisms. Utilizing yeast, flies, and mammalian cells, we have defined the molecular function of the SDHAF4 protein family in SDH assembly and an important role for SDHAF4 in metazoan physiology.

Experimental procedures

Drosophila strains

The following stocks were obtained from the Bloomington Stock Center: *ElaV-Gal4* (Luo et al., 1994)*, Daughterless-Gal4* (Wodarz et al., 1995)*, Frt82B,CoVa^{tend}/TM6B* (Mandal et al., 2005), *SdhB$^{[12081]}$/CyO* (Walker et al., 2006) and *SdhA$^{[HP21216]}$/CyO*. *Sdhaf4* mutants and transgenic lines were generated as described below. All fly stocks were maintained at 25˚C on standard cornmeal/molasses/agar food ambient O_2 concentrations unless otherwise noted.

Generation of *dSdhaf4* mutant lines

DSdhaf4 mutants were generated by targeting the second exon of *dSdhaf4* using TALENs, as described (Cermak et al., 2011; Dahlem et al., 2012; Hu et al., 2013). The specificity of potential TALEN target sequences was determined using Target Finder (https://tale-nt.cac.cornell.edu) and a BLAST analysis. TALEN pairs were designed and constructed by the Mutation Generation and Detection Core Research Facility at the University of Utah (http://www.cores.utah.edu/) with the following specifications: Left binding site—5'-CGAGATCAAGGAACCAAA-3'; Right binding site—5'-AATGGCCTTCCAGAAGA-3'; Spacer—5'-GACGCGCACCGAGAAGCT-3'. The TALEN Golden Gate kit described by Cermak et al. was used with modifications, and TALENs were assembled as described by Dahlem et al. and Hu et al. Plasmid DNAs carrying the *dSdhaf4* TALEN construct were then purified with a Qiagen maxi-prep kit and concentrated by ethanol precipitation. RNAs were generated by digesting the TALEN construct with NotI, repurifying, and directing in vitro transcription using the AmpliScribe SP6 High Yield Transcription Kit (Epicentre), followed by the ScriptCap m7G Capping System (Epicentre). The TALEN RNAs were concentrated and 250 μg/ml of each RNA was combined in 0.1X PBS. We used the obligate heterodimer architecture DDD/RRR and injected ~200 *Canton S* embryos. ~35 surviving injected G_0 animals were crossed individually to a strain carrying a *CyO* balancer. ~5 F_1 progeny males from each cross were then outcrossed to a strain carrying a *CyO* balancer marked with GFP, and individual strains were isolated. Flies were screened for mutations in *dSdhaf4* by high resolution melt analysis (Dahlem et al., 2012). Two putative mutant strains (*dSdhaf4*^{1} and *dSdhaf4*^{2}) were verified by DNA sequencing. Flies carrying a wild type *dSdhaf4* locus

derived from the same G_0 animals as the *dSdhaf4*^{1} and *dSdhaf4*^{2} alleles were carried through the same series of crosses and used as genetically matched controls. This control is labeled *dSdhaf4*$^{+}$ or *dSdhaf4*$^{+/+}$ in all figures. The transposable P-element insertion p*CG7224*^{KG07581} was also used to generate a *dSdhaf4* allele by imprecise excision. The *dSdhaf4*^{3} allele, which was verified by Southern blotting, PCR and DNA sequencing, contains an unexcised fragment of the p*CG7224*^{KG07581} element. A precise excision was also isolated (*dSdhaf4*$^{Ex32+}$) and is used as a control for *dSdhaf4*^{3} in all relevant experiments. All mutant and control genotypes analyzed are in a *w*^{1118} background.

Generation of transgenic fly lines

To generate *UAS-dSdhaf4* rescue construct, the *CG7224* cDNA (GH 06541) was excised using XhoI and BglII and inserted into a pUAST vector. To generate the *UAS-hSdhaf4* construct, the *hSdhaf4* cDNA was PCR amplified from pJR3455A, which contains an *hSdhaf4* cDNA amplified from HepG2 cells using the primers 5'-CGAG ATCTATGACCCCATCGAGGCTT-3' and 5'-CGCTCGAGTTAAAAATCAA TACAGCGTCCTTTT-3'. This amplicon was then cut with BglII and XhoI and cloned into an pUAST-AttB plasmid. All plasmids used to generate transgenic lines were verified by restriction digestion and DNA sequencing. *UAS-dShdaf4* transgenic lines were generated using standard P-element mediated transformation, and *UAS-hSdhaf4* transgenic lines were targeted to AttP2 by site-directed transformation (Bateman et al., 2006; Pfeiffer et al., 2010). *Elav-Gal4*, *UAS-dSdhaf4*, and *UAS-hSdhaf4* on the third chromosome were crossed into the *dSdhaf4*^{1} or *dSdhaf4*^{2} background using balanced crossing schemes. *Da-Gal4* on the third chromosome was recombined onto the same

chromosome as the *dSdhaf4*^{2} allele. The presence of the *dSdhaf4* mutant alleles in transgenic lines was verified by DNA sequencing and complementation tests.

Drosophila genetic interactions

To assay whether combining the lethal allele of *SdhA* or the viable hypomorphic allele of *SdhB* with *dSdhaf4* mutations affects viability, the *SdhA*$^{[HP21216]}$ or *SdhB*$^{[12081]}$ insertions were recombined with the either *dSdhaf4*^{1} or *dSdhaf4*^{2} alleles. Flies carrying these recombinant chromosomes, *dSdhaf4*^{1} allele alone, *Sdh* allele alone, or a wild type chromosome over an SM5 balancer marked with *Cy*$^{-}$ were intercrossed in various combinations. All crosses were performed in triplicate. The number of expected progeny resulting from these crosses was calculated based on mendelian ratios. To determine if the expected number of progeny of non-SM5 chromosomes reached adulthood, the total number of eclosed *Cy*$^{+}$ adult flies was counted, and that number was compared to 1/2 or 1/3 of the total number of progeny depending on whether a 1:1 or 1:2 ratio was expected. The N values for genetic interactions shown between *dSdhaf4* and *SdhA/B* represent the total number of progeny counted from the pertinent cross. Since *CoVa*$^{[tend]}$ mutation is on the third chromosome, *dSdhaf4*^{1}*/SM5;CoVa*$^{[tend]}$*/TM3* or *dSdhaf4*$^{+}$*/SM5;CoVa*$^{[tend]}$*/TM3* flies were crossed to *dSdhaf4*^{2}*/dSdhaf4*^{2} or *dSdhaf4*$^{+}$*/dSdhaf4*$^{+}$ flies, respectively. A normal 1:1 distribution of *Cy*$^{-}$*:Cy*$^{+}$ flies were observed (Data not shown), so only the *Cy*$^{+}$ flies were counted. Since TM3 is marked with *Sb*$^{-}$, the total number of *Cy*$^{+}$;*Sb*$^{-}$ or *Cy*$^{+}$*;Sb*$^{+}$ flies was counted and compared to the 1:1 ratio expected. The N values shown for the genetic interaction experiment concering *dSdhaf4* and *CoVa* represent the total number of *Cy*$^{+}$ progeny assayed.

Drosophila lifespan analyses

For lifespan measurements, flies were allowed to eclose for one day and were separated into vials containing ~20 flies. Every 2–4 days dead flies were counted/removed and surviving flies transferred to new food vials. >100 flies were assayed for each genotype. For starvation assays, 2–4 day old females were transferred to starvation media (1% agar in H_2O), and the number of surviving flies was assayed every 12 hours. >90 flies were assayed per genotype. To measure sensitivity to hyperoxia, vials containing 2–4 day old females were placed in polyethylene bags (Scienceware 12”x16”), which were subsequently filled with 100% O_2 and sealed using a Quick Seal bag sealer. Bags were refilled with fresh O_2 2–3 times daily and the number of surviving flies was assayed every 24 hours. >40 flies were assayed per genotype. A similar degree of hyperoxia sensitivity was observed in *dSdhaf* mutants placed in a styrofoam box with a continuous flow of 100% O_2 as described (Walker et al., 2006); however, we could not maintain this experimental paradigm long enough to assay the full lifespan of controls (data not shown). Survival during hyperoxia was assayed at room temperature, whereas flies for all other lifespan experiments were kept at 25˚C. Experiments on female flies are presented for all survival curves, but similar results were observed when assaying males (data not shown).

Drosophila metabolomic analysis and enzyme activity assays

Adult male flies were aged 5–7 days, washed with PBS, and snap frozen in liquid nitrogen. Metabolites were extracted from frozen flies and GC/MS was performed as previously described (Bricker et al., 2012). Succinate dehydrogenase activity was

measured in mitochondrial extracts as previously described, by examining the reduction of iodonitrotetrazolium at 500 nm in the presence of succinate (Celotto et al., 2011). Citrate synthase activity was measured in mitochondrial extracts by examining the reduction of 5,5'-5 dithiobis-2-nitrobenzoic acid in the presence of oxaloacetate and acetyl-CoA, as previously described (Tang et al., 2009). Enzyme activity per gram of mitochondrial protein was calculated.

Drosophila paralytic assays

Bang sensitivity was measured as previously described (Ganetzky and Wu, 1982). Flies were collected in groups of 5–8 females per vial and allowed to recover from CO_2 anesthesia for at least 2 hours. Flies were then vortexed for 15 seconds and the time it takes to return to a standing position was assayed. At least 3 vials were assayed per condition in each experiment, and all experiments were repeated at least twice. Experiments on female flies are presented, but similar results were observed when assaying males (data not shown).

Electron microscopy

Heads were removed from 8–12 day old female flies, the proboscis was removed, and heads were fixed overnight in EM grade 3% glutaraldehyde/3% paraformaldehyde in PBS at 4˚C. After fixation, heads were rinsed three times in 10 mM cacodylate buffer and postfixed in 2% OsO_4 for 2 hours at room temperature. The heads were then washed in the same buffer, followed by a wash in dH2O, and then poststained in 1% uranyl acetate for 1 hour at room temperature. After washing with dH2O, heads were dehydrated in a

graded series of acetone (25%, 50%, 75%, 90% and 3 x 100% for 20 min each step), and then infiltration was conducted over 3 days followed by embedding in epoxy resin (Embed 812, Electron Microscopy Sciences). For the infiltration step, specimens were incubated in 30% resin and acetone for 6 hours, then in placed in 70% resin and acetone overnight. The next day, the specimens were placed into 90% resin and acetone for 8 hrs and 100% resin for another overnight incubation. On the following day, after two incubations in freshly prepared 100% resin over 6 hrs, specimens were embedded and polymerized at 60˚C for 48 hrs. Ultrathin (70 nm) sections were obtained with diamond knife (Diatome) and an ultratome Leica UC6 (Leica Microsystems, Bannockburn,IL). Grids with sections were poststained with saturated uranyl acetate in dH_2O for 20 min and with lead citrate for 10 min and imaged at 120kV using a Technai T 12 electron microscope. N = 3 flies assayed per genotype.

Immunoblotting

The following antibodies were used for immunoblotting: anti-SdhA (Abcam 137756; rabbit polyclonal to human SdhA), anti-SdhB (Abcam 14714; mouse monoclonal to human SdhB), anti-Atp synthase α (Abcam 14748; mouse monoclonal to bovine Atp5) and anti-beta Tubulin (Chemicon MAB380; mouse monoclonal), anti-VDAC (Abcam 15895), anti-Sdh1 (rabbit polyclonal to yeast Sdh1; was a generous gift from Dennis Winge), anti-Sdh2 (rabbit polyclonal to yeast Sdh2; was a generous gift from Dennis Winge), anti-Porin (Abcam 110326).

SdhA/Sdh1 flavination assay

To visualize flavinated SdhA, mitochondrial extracts were fractionated by SDS-PAGE and the gel was incubated for 20 minutes in 10% acetic acid. Autofluorescent flavo-SdhA was imaged using an ethidium bromide filter, as previously described (Hao et al., 2009). The gel was stained with Coomassie Blue to visualize total protein as a control for loading in *Drosophila* experiments. In yeast experiments, immunoblot for Sdh1 was used to control for loading.

Yeast strains and growth conditions

Saccharomyces cerevisiae (BY4741 *MATa, his3 leu2 met15 ura3*) and *Saccharomyces cerevisiae* (W303a *MATa, his3 leu2 met15 trp1 ura3*) were used as the wild-type strains where indicated. Each mutant was derived from a BY4741 or W303 diploid using a standard PCR-based homologous recombination method. Each haploid was generated by sporulation and tetrad dissection. The genotypes of all strains used in this study are shown (Table 4.1). Yeast transformation was performed by the standard TE/LiAc method and transformed cells were recovered and grown in synthetic complete glucose (SD) medium lacking the appropriate amino acid(s) for selection purposes. Medium used in this study includes YPA and synthetic minimal medium supplemented with 2% glucose, 2% raffinose, 2% glycerol, 2% ethanol, or 2% acetate.

Growth assays were performed using synthetic minimal media supplemented with the appropriate amino acids and indicated carbon source. Overnight cultures were back-diluted equivalent ODs and spotted as 10-fold serial dilutions.

Table 4.1. Yeast strains used in this study.

Strain	Genotype	Source
WT (BY4741)	*Mat A his3 leu2 ura3 met15*	Open Biosystems
*sdh1*Δ	*Mat A his3 leu2 ura3 met15 sdh1::his3MX*	This Study
*sdh2*Δ	*Mat A his3 leu2 ura3 met15 sdh2::kanMX*	This Study
*sdh4*Δ	*Mat A his3 leu2 ura3 met15 sdh4::natMX*	This Study
*sdh8*Δ	*Mat A his3 leu2 ura3 met15 sdh8::hygMX*	This Study
*sdh1*Δ*sdh2*Δ	*Mat A his3 leu2 ura3 met15 sdh1::his3MX sdh2::kanMX*	This Study
*sdh1*Δ*sdh4*Δ	*Mat A his3 leu2 ura3 met15 sdh1::his3MX sdh4::natMX*	This Study
*sdh1*Δ*sdh8*Δ	*Mat A his3 leu2 ura3 met15 sdh1::his3MX sdh8::hygMX*	This Study
*sdh2*Δ*sdh4*Δ	*Mat A his3 leu2 ura3 met15 sdh2::kanMX sdh4::natMX*	This Study
*sdh2*Δ*sdh8*Δ	*Mat A his3 leu2 ura3 met15 sdh2::kanMX sdh8::hygMX*	This Study
*sdh4*Δ*sdh8*Δ	*Mat A his3 leu2 ura3 met15 sdh4::natMX sdh8::hygMX*	This Study
*sdh1*Δ*sdh2*Δ*sdh4*Δ	*Mat A his3 leu2 ura3 met15 sdh1::his3MX sdh2::kanMX sdh4::natMX*	This Study
*sdh1*Δ*sdh2*Δ*sdh8*Δ	*Mat A his3 leu2 ura3 met15 sdh1::his3MX sdh2::kanMX sdh8::hygMX*	This Study
*sdh1*Δ*sdh4*Δ*sdh8*Δ	*Mat A his3 leu2 ura3 met15 sdh1::his3MX sdh4::natMX sdh8::hygMX*	This Study
*sdh2*Δ*sdh4*Δ*sdh8*Δ	*Mat A his3 leu2 ura3 met15 sdh2::kanMX sdh4::natMX sdh8::hygMX*	This Study
*sdh1*Δ*sdh2*Δ*sdh4*Δ*sdh8*Δ	*Mat A his3 leu2 ura3 met15 sdh1::his3MX sdh2::kanMX sdh4::natMX sdh8::hygMX*	This Study
WT (W303)	*Mat A his3 leu2 ura3 met15 trp1*	David Stillman
*sdh1*Δ	*Mat A his3 leu2 ura3 met15 trp1 sdh1::kanMX*	This Study
*sdh2*Δ	*Mat A his3 leu2 ura3 met15 trp1 sdh2::kanMX*	This Study
*sdh5*Δ	*Mat A his3 leu2 ura3 met15 trp1 sdh5::kanMX*	This Study
*sdh8*Δ	*Mat A his3 leu2 ura3 met15 trp1 sdh8::hygMX*	
*sdh1*Δ*sdh8*Δ	*Mat A his3 leu2 ura3 met15 trp1 sdh1::kanMX sdh8::hygMX*	This Study
*sdh2*Δ*sdh8*Δ	*Mat A his3 leu2 ura3 met15 trp1 sdh2::kanMX sdh8::hygMX*	This Study
*sdh5*Δ*sdh8*Δ	*Mat A his3 leu2 ura3 met15 trp1 sdh5::kanMX sdh8::hygMX*	This Study

Plasmid construction

The plasmids expressing internal His_6HA_3 or GFP tagged Sdh8 were generated by PCR amplification of SDH8 (NC_001134.8) flanked by its upstream promoter and downstream terminator regions off genomic DNA. The untagged gene along with its regulatory elements were ligated into pRS415 using XhoI and SpeI. Sewing PCR was used to add NheI and SalI restriction sites between the codons encoding residues N82 and S83 of SDH8. The His_6HA_3 tag, which was chemically synthesized, and the GFP tag, which was amplified by PCR, were each ligated between N82 and S83 using the NheI and SalI yielding the final SDH8-His_6HA_3 and SDH8-GFP constructs. The sequence of each construct was confirmed by sequencing (Genewiz).

Human and *Drosophila SDHAF4* were cloned such that the expression of each gene was under the control of the SDH8 promoter. Sewing PCR was used to clone the SDH8 promoter and terminator separated by NheI and SalI restriction sites into pRS415. SDHAF4 from each species was PCR amplified from cDNA and ligated between the SDH8 promoter and terminator using NheI and SalI. $Sdh1^{H90A}$ and $Sdh1^{H90S}$ constructs were generated by sewing PCR. The mutants were ligated into pRS416 using XhoI and XmaI. Both constructs were expressed under the control of the native *SDH1* promoter and terminator.

Isolation of yeast mitochondria

Yeast cells were harvested in midlog phase. Preparation of crude mitochondria was as described previously (Boldogh and Pon, 2007). Cell pellet was washed once with ddH_2O and incubated in TD buffer (100 mM Tris-SO_4, pH 9.4 and 100 mM DTT) for 15

min at 30˚C. Spheroplasts were obtained by incubating cells in SP buffer (1.2 M Sorbitol and 20 mM potassium phosphate, pH 7.4), supplemented with 0.3 mg/mL lyticase for 1 hour at 30˚C to remove the cell wall. Spheroplasts were gently washed once and homogenized in ice-cold SEH buffer (0.6 M sorbitol, 20 mM HEPES-KOH, pH 7.4, 2 mM $MgCl_2$, 1mM EGTA) using a dounce homogenizer applied with 30–40 strokes. Crude mitochondria were further purified using differential centrifugation. When needed, pure mitochondria were isolated by ultracentrifugation through a continuous nycodenz gradient.

Fluorescence microscopy

The sdh8 mutant strain transformed with plasmids expressing Sdh8-GFP and MtRFP was grown in SD medium overnight. Cells were back-diluted in fresh media to 0.1 OD and allowed to grow for several hours. Images were captured using a Zeiss Axioplan 2 Imaging microscope (Carl Zeiss).

Steady-state protein analysis

Yeast mitochondria were solubilized in Laemmli buffer. Samples were resolved by SDS-PAGE and assessed by immunoblot. *Drosophila* extracts from either 20 μg isolated mitochondria or the equivalent of half of a fly were analyzed in each lane of a Western blot.

Assessment of submitochondrial localization and solubility

Submitochondrial fractionation was performed using a protocol adapted from Boldogh and Pon (2007). Mitochondria were incubated in the isotonic SH buffer (20mM HEPES-KOH, pH 7.4, 0.6M Sorbitol) of hypotonic H buffer (20mM HEPES-KOH, pH 7.4) with and without 1% Tritin-X100. Samples were treated with Protease K (New England BioLabs) on ice for 30 min. Addition of PMSF to each sample was used to terminate protease digestion. Samples were resolved by SDS-PAGE and assessed by immunoblot.

Solubility of Sdh8 was assessed by ultracentrifugation. Mitochondria were suspended in SH buffer and subjected to sonication. Mitochondrial membranes were isolated by ultracentrifugation at 100,000 x g for 30 min (MLA-130, Beckman Coulter). The membrane (membrane fraction) was resuspended in 2X Laemmli buffer. The supernatant (soluble fraction) was precipitated in 20% TCA and resuspended in 2X Laemmli buffer. Samples were resolved by SDS-PAGE and assessed by immunoblot.

Yeast enzyme activity assays

SDH and MDH activity assays were performed on mitochondria isolated from yeast cells as previously described in Hao et al. (2009).

Yeast metabolomic analysis

Metabolomic analysis was carried out in the Metabolomics Core Research Facility at the University of Utah School of Medicine. Yeast cultures were grown to an OD of 1 in synthetic media containing 2% glycerol and 2% ethanol.

Mammalian cell culture

C2C12 myoblasts (ATCC CLR-1772) were maintained in DMEM with 10% FBS, 2mM Glutamax (Gibco), and 1% Primocin (Invitrogen). All knockdowns were performed by treating cells with 5 nM total siRNA, using the Lipofectamine RNAiMax tranfection reagent (Invitrogen). The All-Stars nontargeting siRNA (Qiagen) was used as a control for siRNAs targeting *SDHAF4* (NM_026503), which were designed using Dharmacon siDesign Center tool (http://www.dharmacon.com/designcenter/DesignCenterPage.aspx). Sequences of the sense strands of targeting siRNAs, which include a 3' tt DNA overhang, are as follows: (si1) UGAGUUAUCAGGAAGGAAA and (si3) UCUCACAACUGCAGAAUCA. Cells were subjected to knockdown on day 0, again on day 3, and harvested for analysis on day 6. Total RNA was isolated with the RNeasy Mini Kit (Qiagen) and reverse transcribed to cDNA using the High Capacity cDNA Reverse Transcriptase Kit (Applied Biosystems). Quantitative PCR was performed on cDNA with a Roche 480 LightCycler using LightCycler 480 SYBR Green 1 Master Mix (Roche) to confirm knockdown.

Isolation of mammalian mitochondria

The procedure was adapted from (Bozidis et al., 2007). C2C12 cells were trypsinized, washed twice with ice cold PBS, and pelleted. The cell pellet was resuspended in 2 mL ice cold MTE buffer and lysed by sonication (Branson Model 250, continuous pulse, power setting 3.5, 3 cycle, 10 s. each). Cell debris and nuclei were pelleted at 1,400 x g for 10 min. Mitochondria were recovered from the supernatant by centrifugation at 10,000 x g for 10 min. Mitochondria were resuspended in MTE.

Protein concentration was determined by Advanced Protein Assay Reagent (Cytoskeleton).

Immunoprecipitation of Sdh8-His_6HA_3 and Sdh2-His_6HA_3

Crude mitochondria were isolated and resuspended to a concentration of 5 mg/mL in XWA buffer. Soluble proteins were extracted by sonication and centrifugation at 20,000 x g for 20 mins. Membrane proteins were extracted in buffer containing 0.7% digitonin for 1 hour and centrifugation at 20,000 x g for 20 minutes. Cleared mitochondrial lysates were incubated with anti-HA antibody conjugated agarose (Sigma) for 2 hours at 4˚C. The agarose was washed 3–5 times and eluted in buffer containing 1 mg/mL HA peptide. Elution samples were precipitated in 20% TCA, resolved by SDS-PAGE, and assessed by mass spectroscopy and/or immunoblot.

Blue native polyacrylamide gel electrophoresis (BN-PAGE)

BN-PAGE was performed as described previously (Wittig et al., 2006). Mitochondria were resuspended in lysis buffer (50 mM NaCl, 5 mM 6-aminocaproic acid, 50 mM imidazole, 1 mM AEBSF, and protease inhibitor cocktail). Yeast and *Drosophila* mitochondria were solubilized with 1% digitonin and mammalian mitochondria with 2% digitonin. Lysates were resolved on a 3%–13% gradient native gel using a PROTEAN®II xi Cell gel running system (Bio-Rad). Western blot performed as described elsewhere using a Trans-blot transfer cell (Bio-Rad) and PVDF membranes.

Statistics

PRISM software was used to graph all quantitative data and perform statistical analyses. P values for pairwise comparisons were determined using a Student's t test and p values for multiple comparisons were calculated using one-way analysis of variance (ANOVA) with a Bonferroni correction. Metabolomics data is presented in box-plot form, where the box represents the 25^{th}–75^{th} percentile, the line is the median, and the whiskers represent the range of the data. All other quantitative data is shown as the mean ± SEM. P values for Kaplan-Meier survival curves were calculated using a log-rank test.

Results

Yeast Sdh8 is a conserved mitochondrial matrix protein required for maximal SDH activity

Sdh8 is a small protein of approximately 15 kDa that belongs to a paneukaryotic protein family, which we have named the SDHAF4 family (Figure 4.1A). We confirmed the published annotation of Sdh8 as a mitochondrial protein by assaying the subcellular localization of an Sdh8-GFP fusion protein expressed under the control of the native *SDH8* promoter and terminator (Reinders et al., 2006). Although fusion proteins with GFP at the N- and C-terminus were unable to complement the phenotype of an *sdh8*Δ mutant strain and were therefore deemed to be nonfunctional, efficient rescue was seen when GFP was fused into a predicted unstructured region within Sdh8, between residues S82 and N83 (Figure 4.1E). Sdh8-GFP exhibited complete colocalization with a mitochondrially localized RFP in an *sdh8*Δ strain, confirming the mitochondrial localization of Sdh8 (Figure 4.1B).

Figure 4.1. Yeast Sdh8 is a conserved matrix protein required for maximal SDH activity.
(A) Sequence alignment of the SDHAF4 protein family (Clustal Omega). (B) Intact mitochondria, hypotonic-swollen mitoplasts, and Triton X-100-solubilized mitochondria of a *sdh8*Δ strain expressing Sdh8-His_6HA_3 were treated either with (+) or without (-) proteinase K and analyzed by immunoblot along with the whole-cell lysate (WCL) and postmitochondrial supernatant (PMS). Fzo1, Cyb2, and Mge1 are outer mitochondrial membrane, inner-membrane space, and matrix proteins, respectively. (C) Mitochondria isolated from *sdh8*Δ mutant cells expressing Sdh8-His_6HA_3 were separated into soluble and membrane fractions. Each fraction was assessed by SDS-PAGE and immunoblot. Sdh5 and Porin are used as controls and represent soluble and membrane bound proteins, respectively. (D) The *sdh8*Δ mutant expressing Sdh8-GFP and MitoRFP were grown to early log phase and imaged by fluorescent microscopy. (E) Ten fold serial dilutions of wild-type (WT) yeast transformed with an empty vector (EV), *sdh8*Δ mutants transformed with EV, or *sdh8*Δ transformed with SDH8-His_6HA_3, all in a W303 background, were grown on different carbon sources and incubated at 30˚C. (F–H) GC/MS was used to measure the abundance of metabolites in WT and *sdh8*Δ yeast (W303 background). The data is depicted in box plot format, with the box representing the lower and upper quartiles, the horizontal line representing the median, and the bars representing the minimum and maximum data points. (N = 6 biological replicates. $^{**}p < 0.005$; $^{*}p < 0.05$).

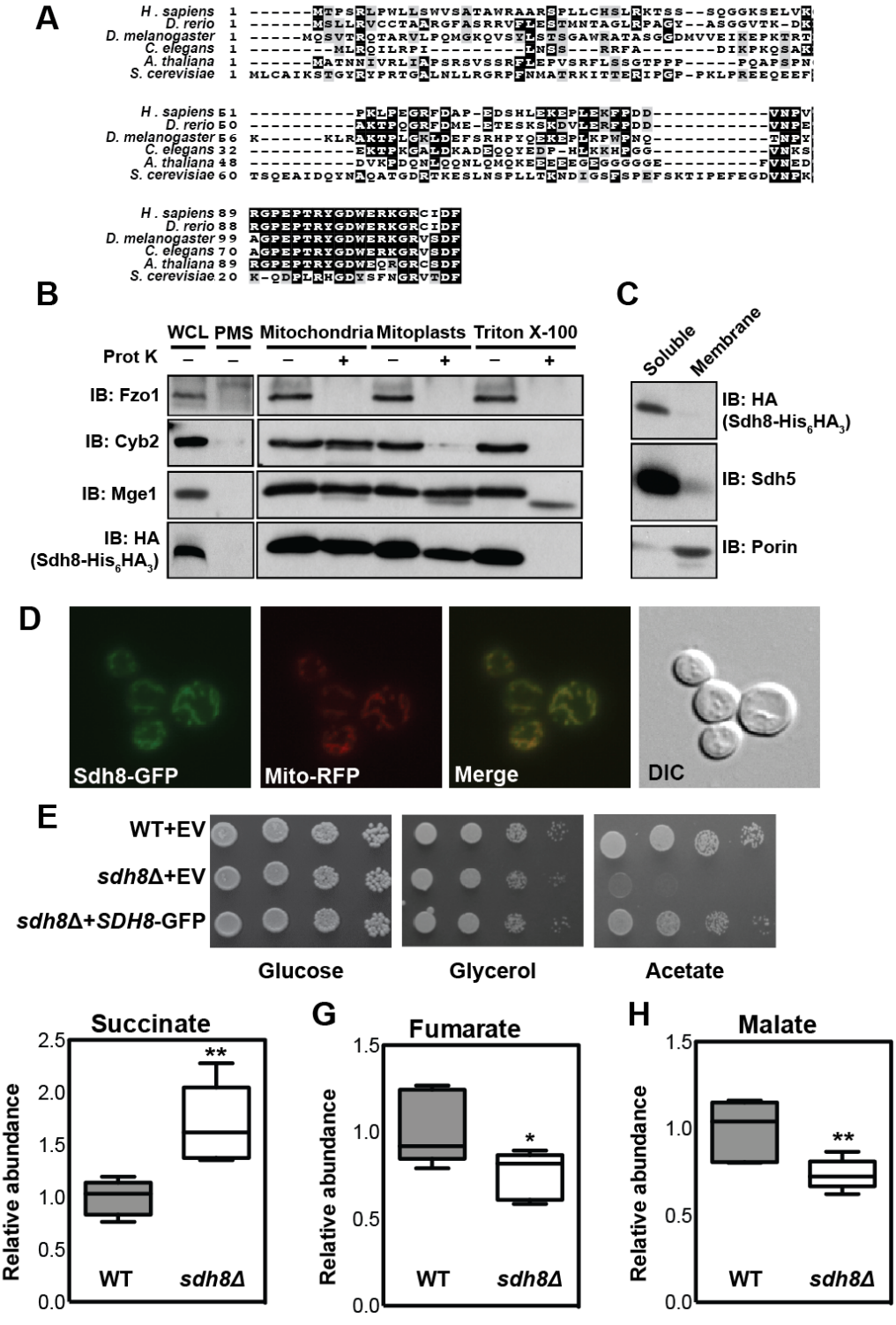
A
H. sapiens
D. rerio
D. melanogaster
C. elegans
A. thaliana
S. cerevisiae
B
WCL
PMS
Mitochondria
Mitoplasts
Triton X-100
Prot K
IB: Fzo1
IB: Cyb2
IB: Mge1
IB: HA (Sdh8-His6HA3)
C
Soluble
Membrane
IB: HA (Sdh8-His6HA3)
IB: Sdh5
IB: Porin
D
Sdh8-GFP
Mito-RFP
Merge
DIC
E
WT+EV
sdh8Δ+EV
sdh8Δ+SDH8-GFP
Glucose
Glycerol
Acetate
F
Succinate
Relative abundance
WT
sdh8Δ
G
Fumarate
Relative abundance
WT
sdh8Δ
H
Malate
Relative abundance
WT
sdh8Δ

The subcellular and submitochondrial localization of this protein was further investigated using biochemical fractionation. We generated an Sdh8-His_6HA_3 fusion analogous to the internal Sdh8-GFP fusion and confirmed it to be fully functional (Figure 4.2A). Upon biochemical fractionation, Sdh8-His_6HA_3 was readily detected in the whole cell lysate but was undetectable in the postmitochondrial supernatant (Figure 4.1B, left panel). Sdh8-His_6HA_3 was present in purified mitochondria and was protected from Proteinase K except in the presence of Triton X-100, consistent with its localization to the mitochondrial matrix (Figure 4.1B, right panel). Sdh8-His_6HA_3 appears to not be stably associated with membranes as it was soluble following sonication, like the soluble Sdh5 protein and unlike the integral membrane protein porin (Figure 4.1C). Taken together, these results demonstrate that Sdh8 is a soluble protein localized to the mitochondrial matrix.

To begin to assess the role of Sdh8 in mitochondrial function, an *sdh8*Δ mutant was established in two strains (BY4741 and W303), both of which were used for key experiments to control for genetic background. While *sdh8*Δ mutants grew normally in glucose medium, growth was impaired on glycerol and acetate, demonstrating a defect in mitochondrial respiration (Figures 4.2A and 4.1E). Interestingly, growth was particularly impaired on acetate-containing medium, which is a hallmark of mutants that affect SDH activity. Consistent with this possibility, metabolomic analysis of *sdh8*Δ mutants revealed an apparent block in the TCA cycle at SDH, with an accumulation of succinate and depletion of the two TCA cycle intermediates downstream of SDH, fumarate and malate, in both strain backgrounds (Figures 4.2B and 4.1F–4.1H). We also measured the enzymatic activity of SDH in mitochondria harvested from wild-type (WT) and *sdh8*Δ

Figure 4.2. Yeast Sdh8 is a conserved mitochondrial matrix protein required for maximal SDH activity and assembly.
(A) Ten-fold serial dilutions of wild-type (WT) yeast transformed with an empty vector (EV) or *sdh8*Δ mutants transformed with either EV or a plasmid expressing SDH8-His_6/HA_3, all in a BY4741 background, were grown on the indicated carbon sources at 30˚C for 2 days (glucose) or 4 days (glycerol, acetate). (B) GC/MS was used to measure the abundance of metabolites in WT and *sdh8*Δ yeast (BY4741 background). The data is depicted in box plot format, with the box representing the lower and upper quartiles, the horizontal line representing the median, and the bars representing the minimum and maximum data points. N = 6 biological replicates. ****$p < 0.0001$; **$p < 0.005$; *$p < 0.05$). (C) SDH and (D) malate dehydrogenase enzyme assays were performed on mitochondrial extracts of WT, *sdh8*Δ, and *sdh1*Δ strains, normalized to total protein (± SEM; N = 3 biological replicates. **, $p < 0.005$). (E) Mitochondria from WT and *sdh8*Δ cells were solubilized in digitonin, fractionated by BN-PAGE, and analyzed by immunoblotting to detect Atp2 (complex V), Cor1/2 (complex III), Cox3 (complex IV), Sdh1 (complex II), or Por1 (Porin). (F) Ten-fold serial dilutions of the indicated strains were grown on the indicated carbon sources at 30˚C as in (A). *SDHAF4* and *dSdhaf4* are the human and *Drosophila* orthologs of *SDH8*, respectively, and were each expressed under the control of the endogenous *SDH8* promoter and terminator.

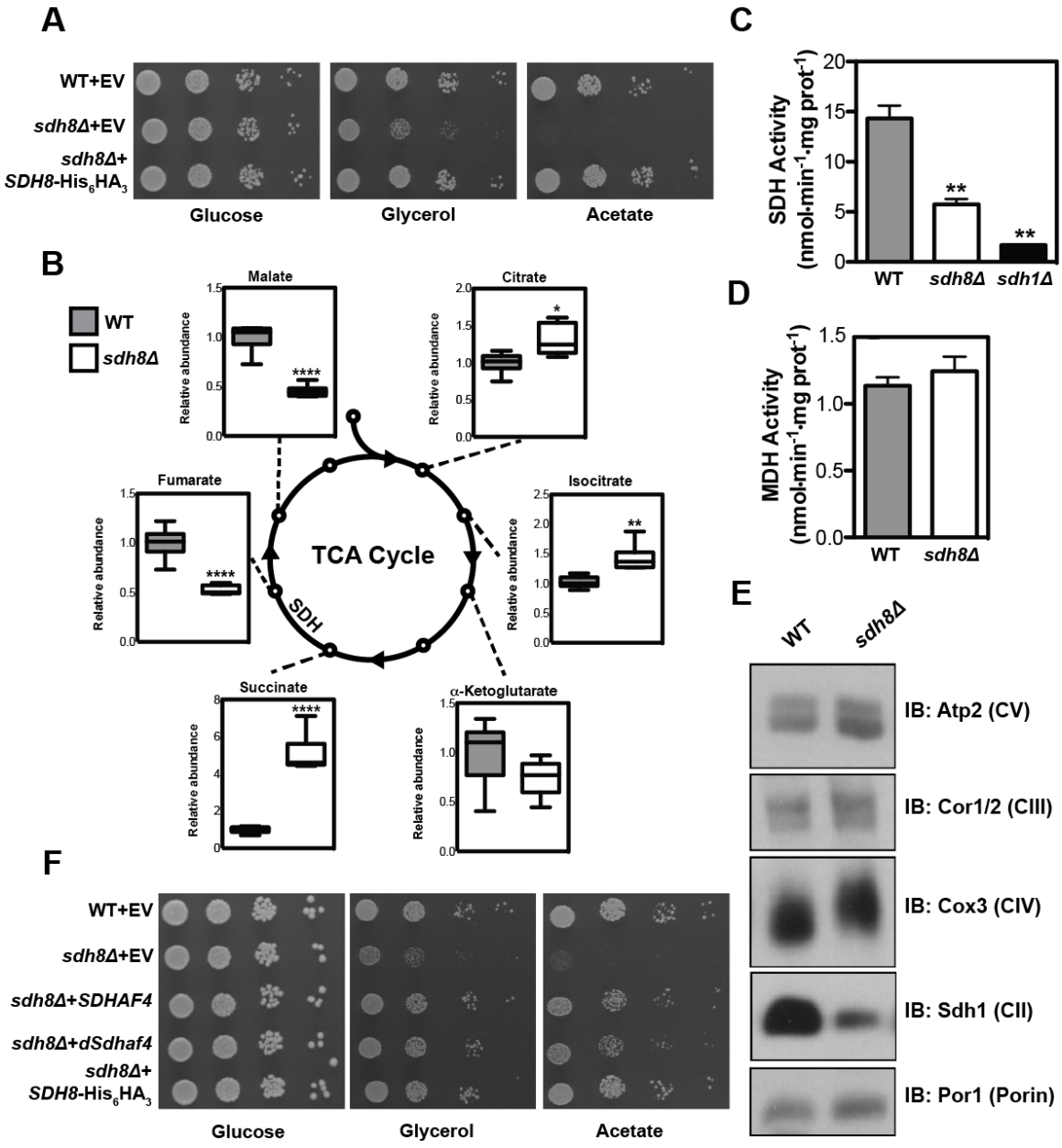
A
WT+EV
sdh8Δ+EV
sdh8Δ+
SDH8-His6HA3
Glucose
Glycerol
Acetate
B
WT
sdh8Δ
Malate
Citrate
Fumarate
Isocitrate
Succinate
α-Ketoglutarate
Relative abundance
TCA Cycle
SDH
C
SDH Activity
(nmol·min-1·mg prot-1)
WT
sdh8Δ
sdh1Δ
D
MDH Activity
(nmol·min-1·mg prot-1)
WT
sdh8Δ
E
WT
sdh8Δ
IB: Atp2 (CV)
IB: Cor1/2 (CIII)
IB: Cox3 (CIV)
IB: Sdh1 (CII)
IB: Por1 (Porin)
F
WT+EV
sdh8Δ+EV
sdh8Δ+SDHAF4
sdh8Δ+dSdhaf4
sdh8Δ+
SDH8-His6HA3
Glucose
Glycerol
Acetate

cells. SDH activity in *sdh8*Δ cells was decreased 60% relative to WT (Figure 4.2C), while malate dehydrogenase (MDH) activity was unaffected (Figure 4.2D). Finally, the steady state level of the SDH holocomplex was assessed by blue native polyacrylamide gel electrophoresis (BN-PAGE). Mitochondria purified from either WT or *sdh8*Δ cells were solubilized in digitonin, resolved by BN-PAGE, and probed by immunoblot. We observed a marked decrease in assembled SDH complexes of similar magnitude to the decrease in SDH activity (Figure 4.2E). Taken together, these data demonstrate that Sdh8 is required for the stability and activity of SDH.

Based on sequence alignments, Sdh8 appears to be a member of a broadly evolutionarily conserved protein family (Figure 4.1A). As a first step toward determining if its function is conserved across eukaryotic species, the human and *Drosophila* orthologs of *SDH8* (*SDHAF4* and *dSdhaf4*, respectively) were expressed in the *sdh8*Δ mutant under the control of the native *SDH8* promoter and terminator. Both orthologs complement the *sdh8Δ* growth defects (Figure 4.2F), suggesting that the role of Sdh8 in SDH assembly is an evolutionarily conserved feature of the SDHAF4 family.

Mammalian SDHAF4 is required for maximal SDH activity

To assess a possible role for mammalian SDHAF4 in SDH function, we transfected C2C12 mouse myoblasts with a nontargeting control siRNA (control) or either of two siRNAs targeting mouse SDHAF4 (si1 and si2). Knockdown of *SDHAF4* mRNA was confirmed (Figure 4.3A) and mitochondria were harvested from cells transfected with control, si1, and si2 siRNAs. Immunoblot of the isolated mitochondria revealed that depletion of SDHAF4 did not affect the steady state abundance of SDHA

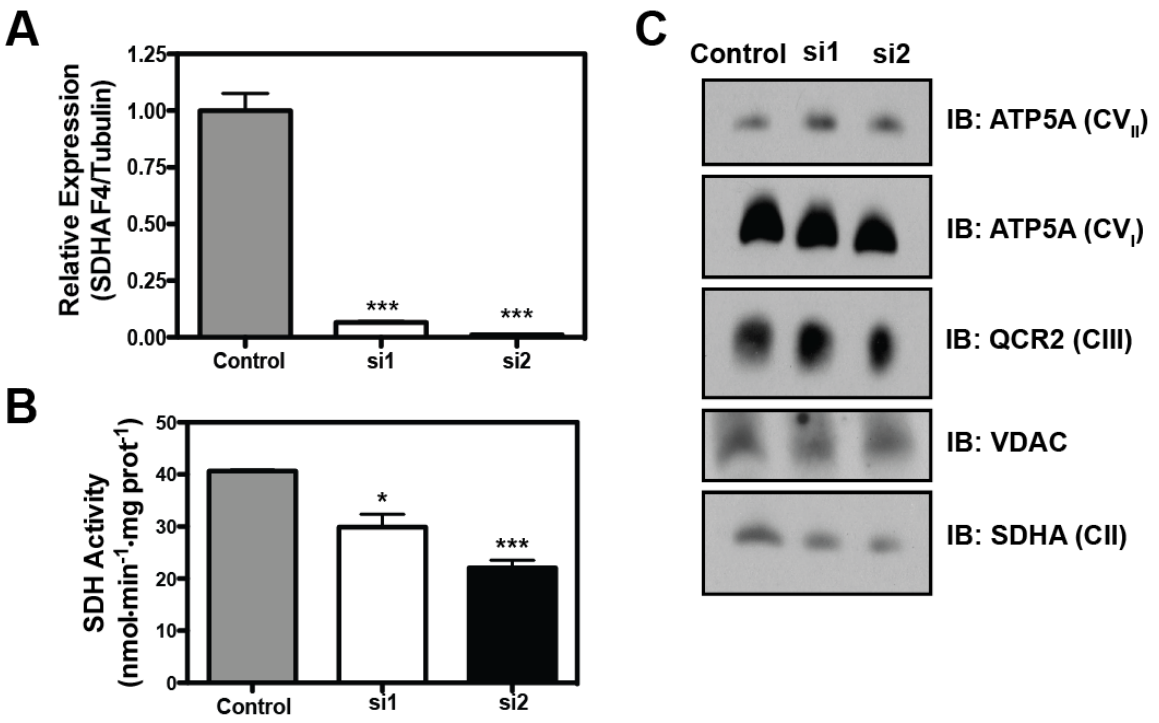

Figure 4.3. Mammalian SDHAF4 is required for maximal SDH activity.
(A) C2C12 cells were transfected with either a control nontargeting siRNA or either of two siRNAs directed against *SDHAF4* (si1 and si3), and *SDHAF4* mRNA abundance was assayed by quantitative RT-PCR and normalized to tubulin mRNA (± SEM. N = 3 biological replicates. ***, $p < 0.0001$). (B) SDH enzyme activity was measured in mitochondria harvested from C2C12 cells treated as in (A) (± SEM. N = 3 biological replicates. ***$p < 0.0005$; *$p < 0.05$). (C) Mitochondria extracted C2C12 cells treated as in (A) were solubilized in digitonin, fractionated by BN-PAGE, and analyzed by immunoblotting for ATP5A (complex V monomers (CV_I) or dimers (CV_{II}), QCR2 (complex III), VDAC, or SDHA (complex II).

(mammalian ortholog of yeast Sdh1) or SDHB (mammalian ortholog of yeast Sdh2; Figure 4.4A). We detected, however, a dose-dependent decrease in SDH enzymatic activity in *SDHAF4* knockdown cells (Figure 4.3B), with no significant change in MDH activity (Figure 4.4B). In addition, cells transfected with si1 or si2 showed a reproducible and specific decrease in steady-state SDH complexes as assayed by BN-PAGE, of a magnitude similar to that seen in SDH activity (Figure 4.3C). We conclude that SDHAF4 is required for the proper assembly and activity of SDH in both yeast and mammalian cells.

Drosophila Sdhaf4 is required for succinate dehydrogenase activity

To further define the function of Sdh8 and to examine its role in the context of a multicellular organism, we extended our analysis to *Drosophila*. Three mutations were generated in the gene encoding the *Drosophila* ortholog of *SDH8* (*CG7224*) that we have renamed *Drosophila Sdhaf4* (*dSdhaf4*). Two of these alleles were deletion/insertion mutations generated using TALEN endonuclease-mediated gene targeting ($dSdhaf^{1}$ and $dSdhaf4^{2}$) that are predicted to cause a frameshift and premature stop codon in the N-terminal half of the protein (Figure 4.5A). Genetically matched control strains for these alleles were also generated in a w^{1118} genetic background. The third allele ($dSdhaf^{3}$) is an independently derived deletion that removes most of the *dSdhaf4* coding region, generated by imprecise excision of a P-element (Figure 4.5A). A stock that carries a precise excision of this P-element was used as a genetically matched control for this strain.

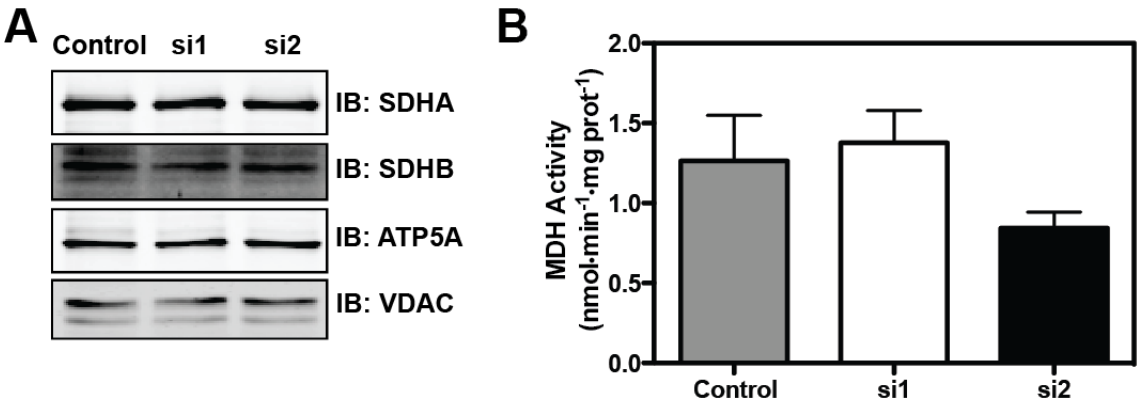

Figure 4.4. **Mammalian SDHAF4 is required for maximal SDH activity.**
(A) Mitochondria extracted C2C12 cells transfected with AS, si1, or si2 were subjected to SDS-PAGE and analyzed by immunoblot of SDHA, SDHB, ATP5A, and VDAC. (B) MDH enzyme activity was measured in mitochondria harvested from C2C12 cells transfected with AS, si1, or si2 (± SEM. N = 3 biological replicates).

Figure 4.5. Metabolomic analysis of multiple *dSdhaf4* mutants reveals changes in several metabolic pathways.
(A) *dSdhaf4* alleles generated and used in this study. TALEN induced alleles (*dSdhaf4*^{1} and *dSdhaf4*^{2}) are shown in red, while the deletion generated by imprecise excision (*dSdhaf4*^{3}) of the p*CG7224*$^{[KG07581]}$ P element, is shown in blue. The *dSdhaf4*^{3} allele contains a remnant of the p*CG7224*$^{[KG07581]}$ element that was not excised. Another strain in which the p*CG7224*$^{[KG07581]}$ element was precisely excised (*Ex32+*) was generated, confirmed by PCR, and used as a control for all studies with the *dSdhaf4*^{3} allele. (B) Either LC/MS or GC/MS was used to measure the abundance of metabolites in transheterozygous *dSdhaf4*$^{1/3}$ mutants compared to genetically matched *dSdhaf4*$^{+/Ex32+}$ controls. (C) Changes in non-TCA cycle metabolites in *dSdhaf4*$^{1/2}$ or *dSdhaf4*$^{1/3}$ flies compared to their respective controls measured using GC/MS. The data is depicted in box plot format, with the box representing the lower and upper quartiles, the horizontal line representing the median, and the bars representing the minimum and maximum data points. Eight to twelve biological replicates from two independent experiments were combined per genotype. *$p < 0.05$; **$p < 0.01$; ***$p < 0.001$.

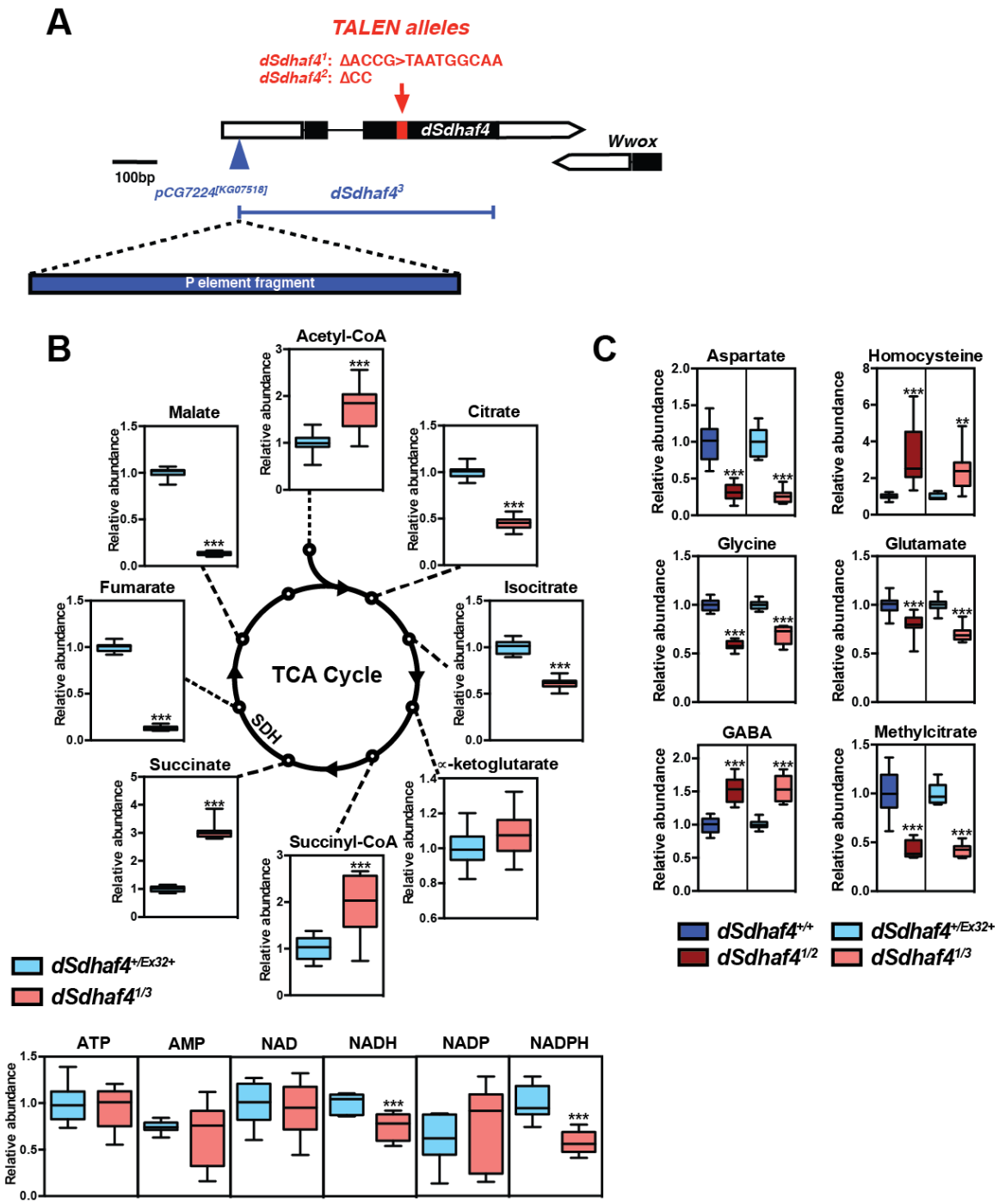
A
TALEN alleles
dSdhaf4¹: ΔACCG>TAATGGCAA
dSdhaf4²: ΔCC
dSdhaf4
Wwox
100bp
pCG7224[KG07518]
dSdhaf4³
P element fragment
B
Acetyl-CoA
Malate
Citrate
Fumarate
Isocitrate
TCA Cycle
SDH
Succinate
∝-ketoglutarate
Succinyl-CoA
Relative abundance
dSdhaf4+/Ex32+
dSdhaf41/3
ATP
AMP
NAD
NADH
NADP
NADPH
C
Aspartate
Homocysteine
Glycine
Glutamate
GABA
Methylcitrate
dSdhaf4+/+
dSdhaf41/2
dSdhaf4+/Ex32+
dSdhaf41/3

Similar to our findings in yeast, metabolomic analysis of *dSdhaf4* mutants revealed a significant accumulation of succinate and depletion of malate and fumarate (Figures 4.5B and 4.6A). Acetyl-CoA was also elevated, while citrate and isocitrate were reduced in the mutants (Figures 4.5B and 4.6A). These effects may be due to a reduction in oxaloacetate (which was undetectable in our experiments) that is required for the formation of citrate from acetyl-CoA. Consistent with this, aspartate, which is interconvertible with oxaloacetate, is depleted in *dSdhaf4* mutants (Figure 4.5C). Interestingly, NADH and NADPH are reduced in *dSdhaf4* mutants, while ATP levels are unaffected (Figures 4.5B and 4.6A). *dSdhaf4* mutants also display significant changes in the abundance of several other metabolites, including homocysteine, glycine, glutamate, the neurotransmitter gamma aminobutyrate (GABA) and methylcitrate (Figure 4.5C). Similar changes were observed upon metabolomic analysis of flies carrying a *dSdhaf4* TALEN-induced allele over the independently derived imprecise excision, indicating that these results are consistent across genetic backgrounds (Figures 4.5B, 4.5C, and 4.6A). Consistent with this metabolomic profile, *dSdhaf4* mutant mitochondria display an 85% reduction in SDH activity compared to controls (Figure 4.6B). No significant effect, however, was seen on citrate synthase (CS) activity, indicating that the reduced SDH activity is not associated with general mitochondrial dysfunction (Figure 4.6C). Based on these data, we conclude that, like yeast *sdh8*Δ mutants, *dSdhaf4* mutants have a specific impairment in SDH function.

Figure 4.6. *Drosophila Sdhaf4* is required for SDH activity.
(A) Either LC/MS (acetyl-CoA, succinyl-CoA, ATP, AMP, NAD, NADH, NADP, and NADPH) or GC/MS (citrate, isocitrate, alpha-ketoglutarate, succinate, fumarate and malate) was used to measure the abundance of metabolites in transheterozygous *dSdhaf4*$^{1/2}$ (*dSdhaf4*$^{-}$) mutants compared to genetically matched w^{1118} controls (*dSdhaf4*$^{+}$). The data are depicted in box plot format, with the box representing the lower and upper quartiles, the horizontal line representing the median, and the bars representing the minimum and maximum data points. Eight to twelve biological replicates from two independent experiments were combined per genotype. (B) Succinate dehydrogenase or (C) citrate synthase enzymatic activity was measured in extracts from mitochondria isolated from either control or *dSdhaf4* mutant flies (± SEM. N = 4–6 biological replicates. **$p < 0.01$ and ***$p < 0.001$). Two independent experiments were performed with similar results.

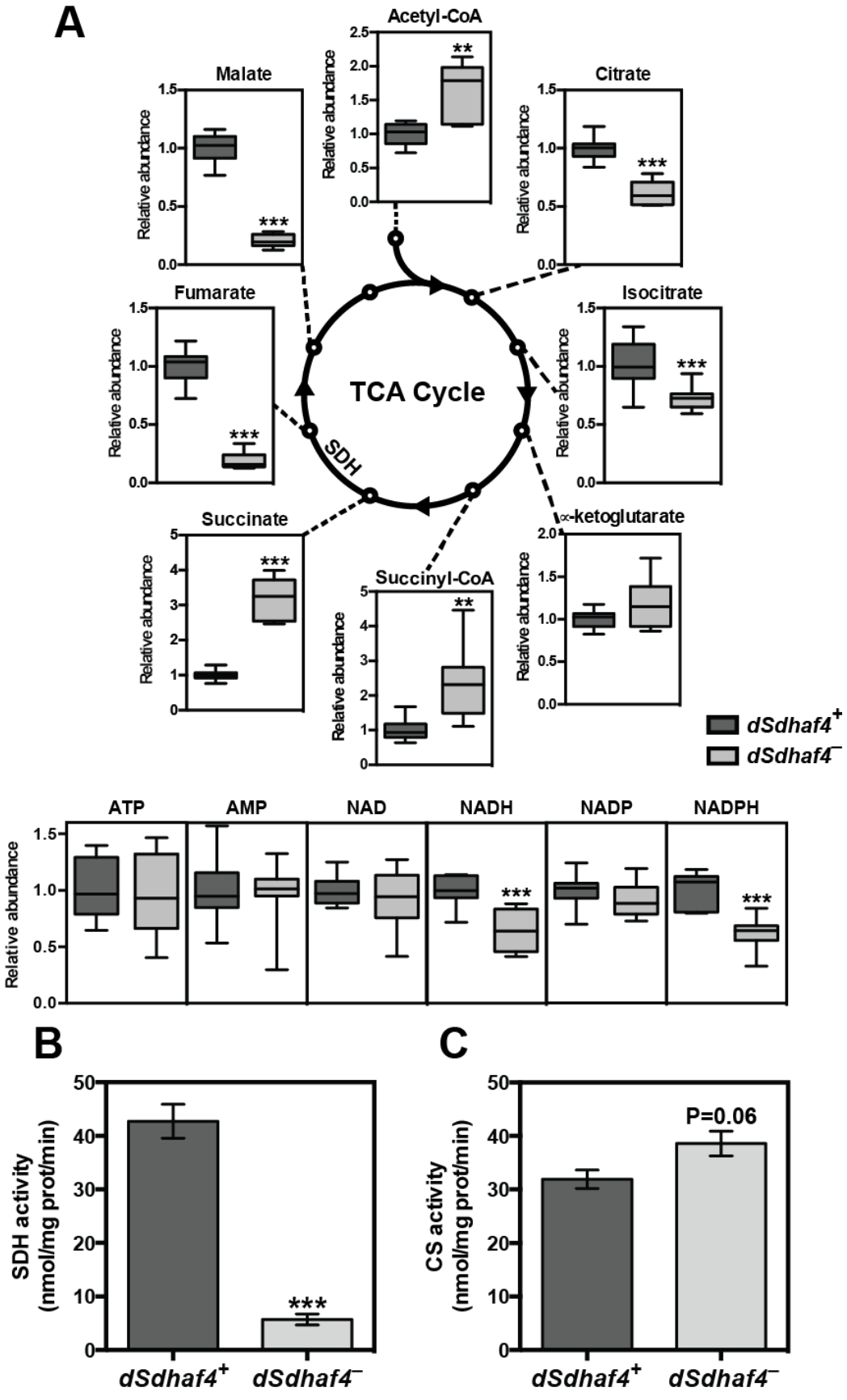
A
Acetyl-CoA
Malate
Citrate
Fumarate
Isocitrate
TCA Cycle
SDH
Succinate
∝-ketoglutarate
Succinyl-CoA
Relative abundance
dSdhaf4+
dSdhaf4–
ATP
AMP
NAD
NADH
NADP
NADPH
B
SDH activity (nmol/mg prot/min)
C
CS activity (nmol/mg prot/min)
P=0.06

Drosophila Sdhaf4 is required for the stability of SdhA and SdhB

The decrease in SDH activity in *dSdhaf4* mutants is greater than that seen in yeast *sdh8*Δ mutants, suggesting that there might be a more profound effect on the steady-state level of SDH. Consistent with this, the SDH holocomplex was undetectable in BN-PAGE experiments, whereas the levels of Complex V were unaffected (Figure 4.7A). This lack of SDH holocomplex was accompanied by an apparent reduction in the stability of the SdhA and SdhB subunits in *dSdhaf4* mutants (Figures 4.7B, 4.8A, and 4.8B). We also examined whether loss of one copy of *dSdhaf4* or *dSdhaf4* overexpression could affect SDH function. *dSdhaf4* heterozygous mutants, however, displayed similar SDH activity to controls (Figure 4.8C), and *dSdhaf4* overexpression had no effect on SDH activity or SDH subunit protein levels (Figures 4.8D and 4.8E).

The reduced levels of SDH subunits in the *dSdhaf4* mutant suggest that we might see genetic interactions between *dSdhaf4* alleles and mutations in SDH subunit-encoding genes. Consistent with this, we found that *dSdhaf4* mutant flies heterozygous for a strong loss-of-function mutation in *SdhA* or homozygous for a hypomorphic mutation in *SdhB* displayed reduced viability compared to controls (Figures 4.7C and 4.8F). This genetic interaction is specific for SDH subunit-encoding genes, as *dSdhaf4* mutants heterozygous for a null allele of *Cytrochrome oxidase Va subunit* (*CoVa*) (Mandal et al., 2005) displayed normal viability (Figure 4.7C). Taken together, these biochemical and genetic studies indicate that dSdhaf4 is required for SDH assembly and activity, likely through maintaining the stability of SdhA and SdhB.

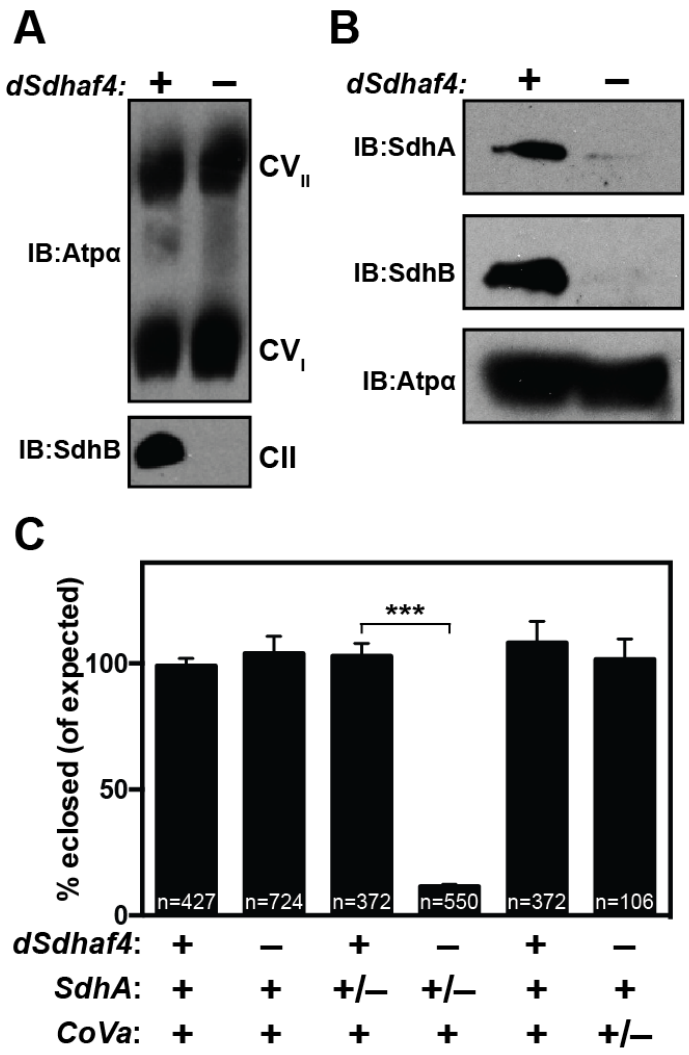

Figure 4.7. *Drosophila Sdhaf4* is required for SdhA and SdhB stability.
(A) Mitochondrial extracts from either w^{1118} controls (*dSdhaf4*$^{+}$) or *dSdhaf4*$^{1/2}$ mutants (*dSdhaf4*$^{-}$) were fractionated by BN-PAGE and analyzed by immunoblotting to detect Atpα (Complex V monomers or dimers) or SdhB (Complex II). (B) Total protein from mitochondria isolated from either control or *dSdhaf4* mutant flies was resolved using SDS-PAGE, followed by immunoblotting to detect SdhA, SdhB, or ATPα. (C) Flies carrying either control or *dSdhaf4* mutant chromosomes over a balancer chromosome were crossed to flies carrying a strong loss-of-function allele for either *SdhA* or *Cytochrome c oxidase Va subunit* (*CoVa*) over a balancer. The resulting progeny were scored for the absence or presence of the marker linked to the balancer chromosome. The proportion of the expected progeny that eclosed, based on Mendelian ratios of the indicated genotypes, is shown. (± SEM. N = number of progeny assayed from each cross. *** $p < 0.001$ (Student's t test).

Figure 4.8. *Drosophila Sdhaf4* is required for the stability of SdhA and SdhB, but is not a rate-limiting factor in SDH assembly.
(A) Mitochondrial extracts from w^{1118} control (*dSdhaf4*$^{+}$) or *dSdhaf4*$^{1/2}$ (*dSdhaf4*$^{-}$) flies were resolved by SDS-PAGE; the gel was washed and then either exposed to ultraviolet light to visualize flavinated SdhA (top) or stained with Coomassie Blue (bottom) to visualize total protein. Two biological replicates are shown. The reduction in flavinated SdhA reflects the overall reduction in SdhA protein levels, indicating little if any effect of the mutation on flavination. (B) Protein from whole-fly homogenates was resolved by SDS-PAGE followed by immunoblotting to detect SdhB or tubulin. The asterisk denotes a nonspecific band. Two biological replicates are shown. (C) Mitochondria were isolated from either control w^{1118} (*dSdhaf4*$^{+/+}$) or heterozygous *dSdhaf4*$^{+/1}$ (*dSdhaf4*$^{+/-}$) flies and SDH enzymatic activity was assayed. (D) Mitochondria were isolated from flies carrying a ubiquitous *Tubulin-GAL4* driver or a *UAS-dSdhaf4* element alone or in combination, and SDH enzymatic activity was assayed. (E) Mitochondria were isolated from flies carrying a ubiquitous *Tubulin-GAL4* driver or a *UAS-dSdhaf4* element alone or in combination, and SdhA, SdhB or ATP∝ subunit levels were assayed by western blot analysis. (F) Flies harboring either control (*dSdhaf4*$^{+}$) or *dSdhaf4*$^{1/2}$ (*dSdhaf4*$^{-}$) mutant chromosomes linked to a hypomorphic *SdhB* allele or wild type *SdhB* locus over a balancer were crossed to each other in various combinations. The resulting progeny from these crosses were then assayed for the absence or presence of the marker linked to the balancer chromosome. The proportion of the expected progeny eclosed based on Mendelian ratios of the indicated genotype is shown. The n values displayed in parentheses in the graph represent the total number of progeny assayed resulting from each cross. The mean ± SEM is shown in D–F.

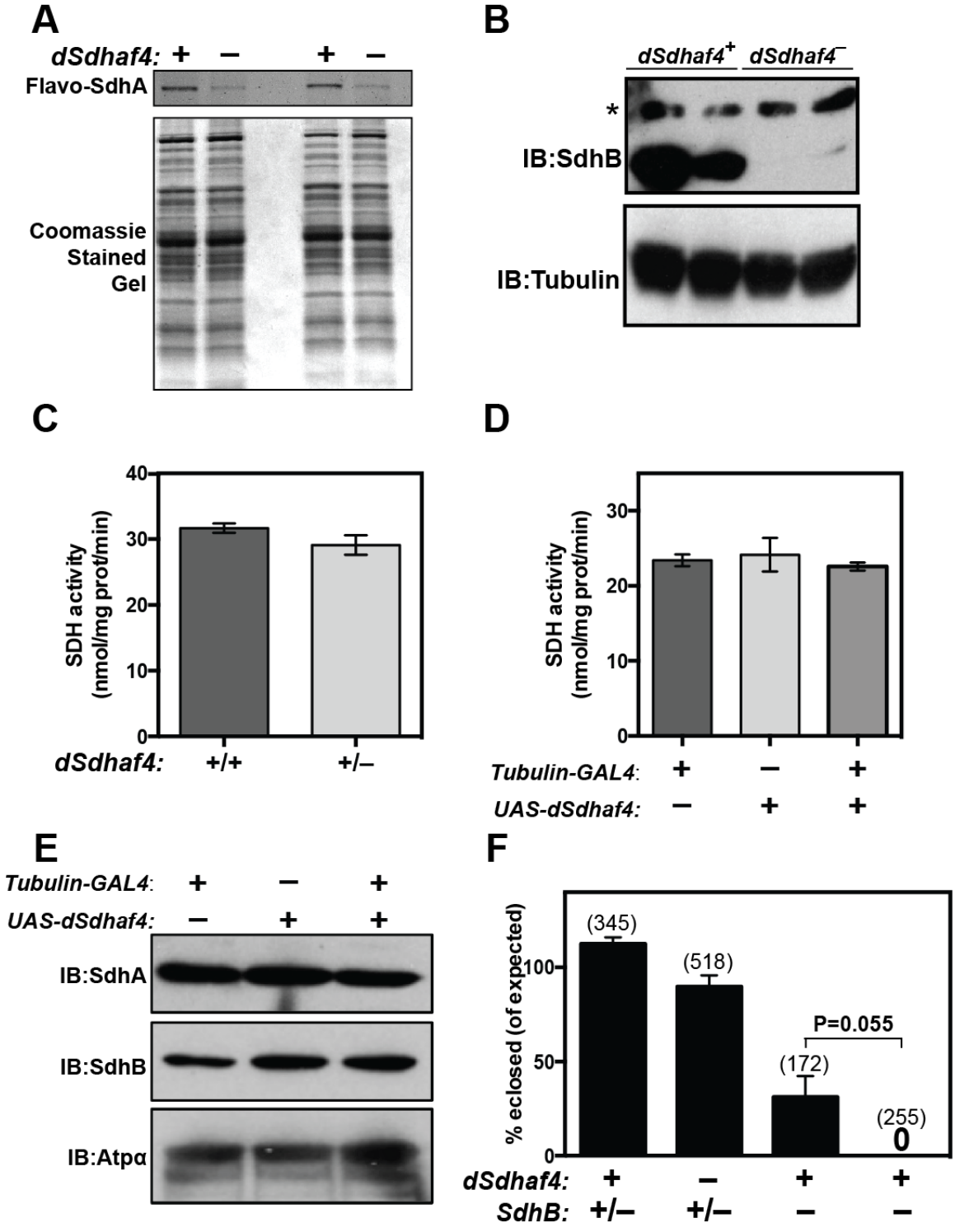
A
dSdhaf4: + – + –
Flavo-SdhA
Coomassie Stained Gel
B
dSdhaf4+ dSdhaf4–
*
IB:SdhB
IB:Tubulin
C
SDH activity (nmol/mg prot/min)
40
30
20
10
0
dSdhaf4: +/+ +/–
D
SDH activity (nmol/mg prot/min)
30
20
10
0
Tubulin-GAL4: + – +
UAS-dSdhaf4: – + +
E
Tubulin-GAL4: + – +
UAS-dSdhaf4: – + +
IB:SdhA
IB:SdhB
IB:Atpα
F
% eclosed (of expected)
100
50
0
(345)
(518)
(172)
(255)
P=0.055
0
dSdhaf4: + – + +
SdhB: +/– +/– – –

dSdhaf4 mutants display neurodegenerative phenotypes, early-adult lethality, and sensitivity to oxidative stress

Consistent with their metabolic defects, *dSdhaf4* mutants died earlier than controls, with a median lifespan of 12 days compared to a median lifespan of 69 days for control flies (Figure 4.9A). Interestingly, these mutants also displayed two phenotypes that are hallmarks of mitochondrial dysfunction, bang sensitivity, and erect wings (Figures 4.9B, 4.9C, 4.10A, and 4.10B) (Fergestad et al., 2006; Greene et al., 2003). Since bang sensitivity is often associated with neurodegeneration (Celotto et al., 2006a; Gnerer et al., 2006; Liu et al., 2007), we examined the photoreceptors of *dSdhaf4* mutant compound eyes by transmission electron microscopy. This study revealed that *dSdhaf4* mutant retinas displayed a marked disorganization of retinal architecture (Figure 4.9D, asterisks) consistent with a neurodegenerative phenotype (Feany and Bender, 2000). The photoreceptors were also highly vesicularized (Figure 4.9D, arrows) (Kiselev et al., 2000), with aberrant mitochondrial morphology (Figure 4.9D, arrowheads). This neurodegeneration phenotype is tissue-autonomous as specific expression of wild-type *dSdhaf4* in neurons was sufficient to rescue the bang sensitivity of *dSdhaf4* mutants (Figures 4.9E, 4.10C, and 4.10D). Moreover, global expression of human *Sdhaf4* in *dSdhaf4* mutants partially rescued the bang sensitivity of these animals, providing further evidence of a conserved function for *Sdhaf4* (Figures 4.9E, 4.10C, and 4.10D). Taken together, these results demonstrate that dSdhaf4 is required in neurons to maintain tissue structure and function. Defects in mitochondrial ATP production and ROS homeostasis have been previously shown to cause neurodegenerative phenotypes similar to those observed in *dSdhaf4* mutants

Figure 4.9. *Drosophila Sdhaf4* mutants display neurodegenerative phenotypes, early-adult lethality, and sensitivity to oxidative stress.
(A) The number of surviving w^{1118} control (*dSdhaf4*$^{+}$) or *dSdhaf4*$^{1/2}$ mutant (*dSdhaf4*$^{-}$) females maintained on standard laboratory food at normoxia was assayed at 2–4 day intervals. Each data point is the percentage of surviving flies ± SEM, with at least 110 flies assayed per genotype. (B) Control or *dSdhaf4* mutant females aged 6–8 hours, 2–4 days, or 8–12 days were vortexed for 15 seconds and the percentage of paralyzed flies was counted as described (Ganetzky and Wu, 1982). (±SEM. N > 32 flies per age per genotype. ** $p < 0.01$ and *** $p < 0.001$ [ANOVA]). (C) The length of time required for the *dSdhaf4* mutant flies in (A) to recover from paralysis is presented as a bar graph, with the number of paralyzed *dSdhaf4* mutants analyzed from each age group depicted above the bar. (D) Cross sections of compound eyes from 8–12 day old control or *dSdhaf4* mutant flies visualized by transmission electron microscopy. Arrows point to aberrant vesicularization of *dSdhaf4* mutant photoreceptors, arrowheads point to mitochondria, and asterisks denote vacuoles. (E) Control or *dSdhaf4* mutant flies at 8–12 days of age carrying either the ubiquitous *Daughterless-Gal4* (*Da-GAL4*) driver, the pan-neuronal *Elav*-Gal4 driver, or no driver, in the presence or absence of either a *UAS-dSdhaf4* transgene or a *UAS-human Sdhaf4* (*hSdhaf4*) transgene, were vortexed as in (A). Note that *UAS-dSdhaf4* alone has leaky *dSdhaf4* activity since it partially rescues in the absence of a GAL4 driver. (±SEM. N = 15–40. *** $p < 0.001$ [ANOVA]). (F) Control or *dSdhaf4* mutant females at 2–4 days of age were transferred to 100% oxygen and the number of surviving animals was counted each day. The median lifespan of controls under hypoxia is 9 days and the median lifespan of *dSdhaf4* mutants under hypoxia is 1 day. Data is shown as the percentage of surviving flies ± SEM. At least 40 flies were assayed per genotype. P values for both survival curves (panels A and F) were calculated using a log-rank test.

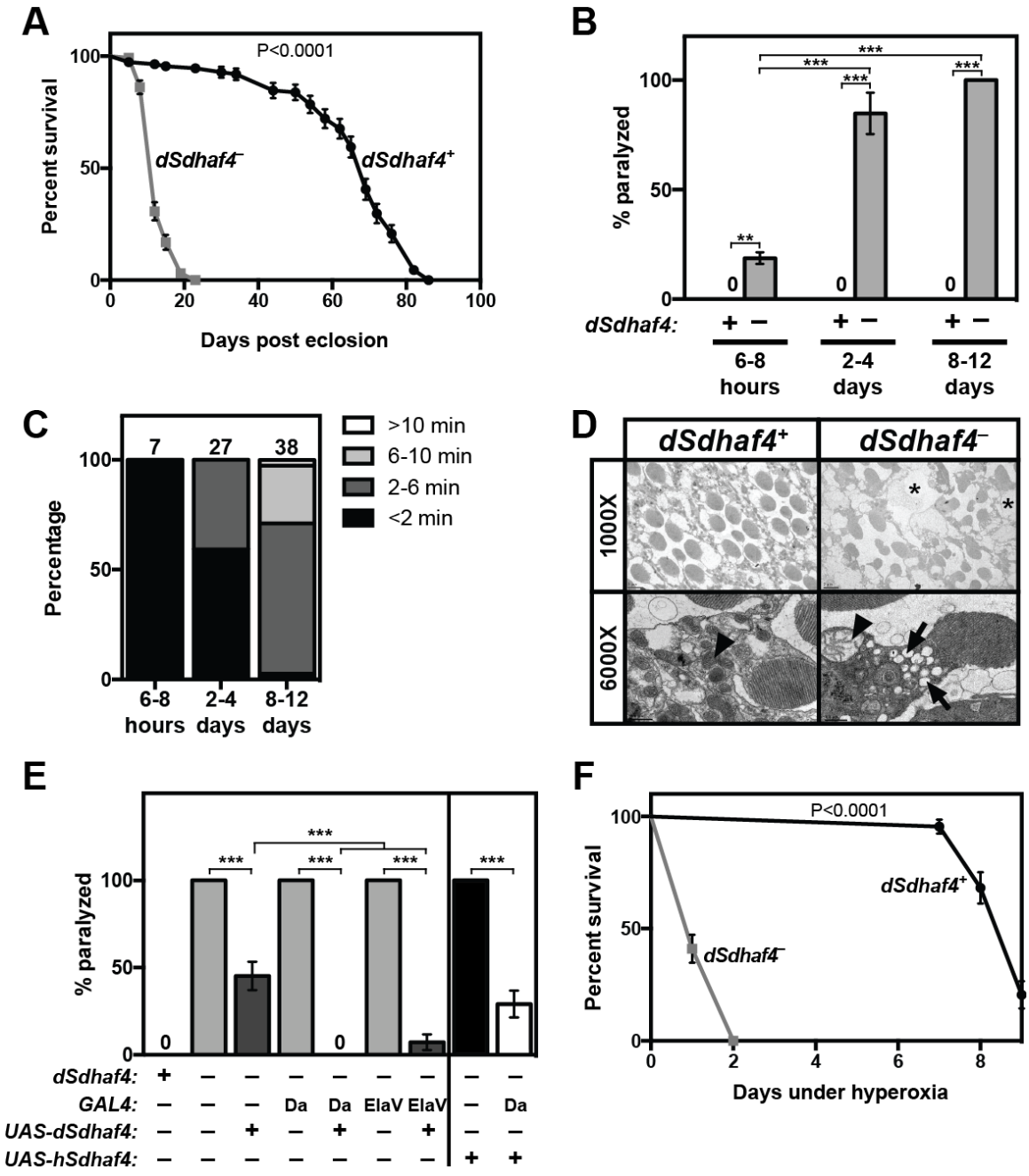
A
P<0.0001
Percent survival
dSdhaf4⁻
dSdhaf4⁺
Days post eclosion
B
% paralyzed
dSdhaf4:
6-8 hours
2-4 days
8-12 days
C
Percentage
>10 min
6-10 min
2-6 min
<2 min
7
27
38
6-8 hours
2-4 days
8-12 days
D
dSdhaf4⁺
dSdhaf4⁻
1000X
6000X
E
% paralyzed
dSdhaf4:
GAL4:
UAS-dSdhaf4:
UAS-hSdhaf4:
Da
ElaV
F
P<0.0001
Percent survival
dSdhaf4⁺
dSdhaf4⁻
Days under hyperoxia

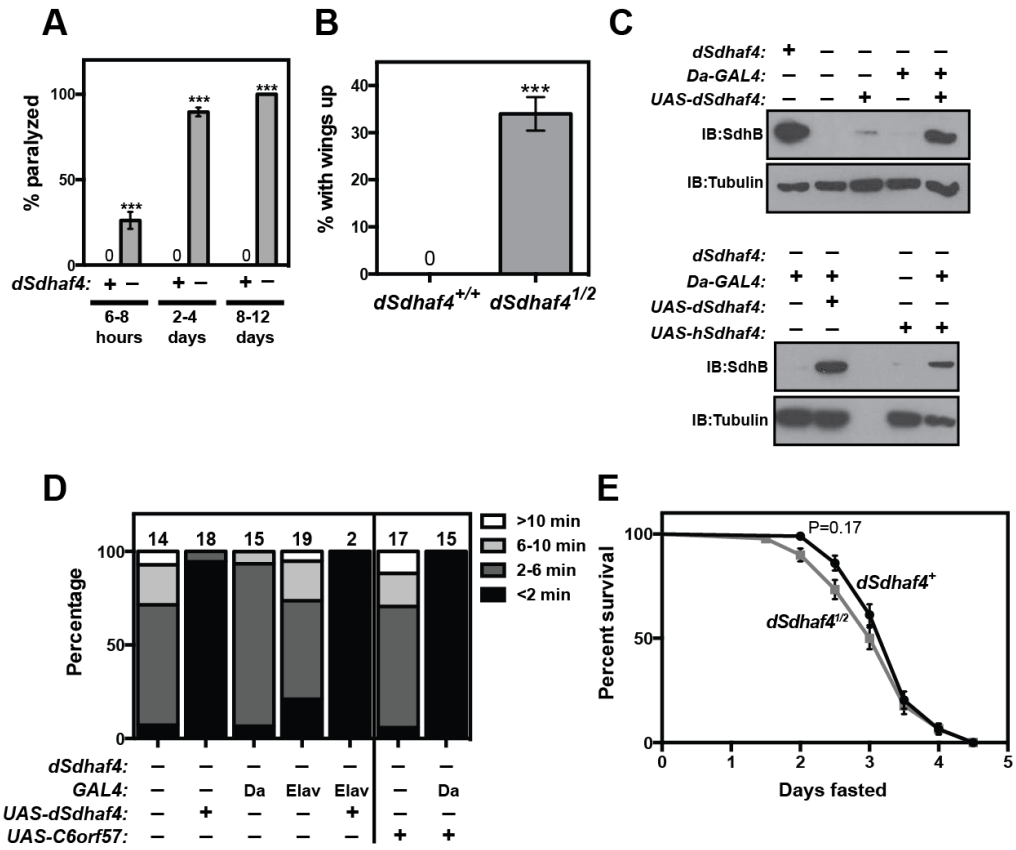

Figure 4.10. *dSdhaf4* mutants are sensitive to bang induced paralysis, but not starvation.

(A) Adult $dSdhaf4^{+/Ex32+}$ ($dSdhaf4^{+}$) or $dSdhaf4^{1/3}$ ($dSdhaf4^{-}$) females aged 6–8 hours, 2–4 days, or 8–12 days were vortexed for 15 seconds and the percentage of paralyzed flies was counted. N > 35 flies at each age per genotype. ***p < 0.001 (ANOVA). (B) The percentage of 3–7 day old w^{1118} control or $dSdhaf4^{1/2}$ females that hold their wings in an upright position is shown. N > 180 flies per genotype. ***p < 0.001 (Student's t test). The mean ± SEM is shown in A and B. (C) Controls or *dSdhaf4* mutant flies carrying the ubiquitous *Daughterless* driver (*Da-GAL4*) or no driver in the presence or absence of either a *UAS-dSdhaf4* transgene or a *UAS-human Sdhaf4* (*hSdhaf4*) transgene were homogenized. Proteins from these homogenates were resolved by SDS-PAGE followed by immunoblotting to detect either SdhB or tubulin. Note that *UAS-dSdhaf4* is leaky since it partially rescues in the absence of a GAL4 driver. (D) The amount of time 8–12 day old flies paralyzed in Figure 4.9E take to recover from paralysis was quantified. The percentage of flies paralyzed <2 minutes, 2–6 minutes, 8–10 minutes or > 10 minutes are shown. The number above each bar represents the total number of flies of the indicated genotype paralyzed and is the sample size from which each data set is based. (E) Two to four day old controls or *dSdhaf4* mutant females were starved and the number of surviving animals was counted every 12 hours. The median lifespan under starvation 3.5 days for controls and 3.25 days for *dSdhaf4* mutants. Data shown as the percentage of surviving flies ± SEM. At least 90 flies were assayed per genotype. P value calculated using a log-rank test.

(Celotto et al., 2012; Fergestad et al., 2006; Liu et al., 2007). Since loss of *dSdhaf4* does not appear to affect steady state ATP levels (Figures 4.6A and 4.5B), we hypothesized that dSdhaf4 may be required for protection against ROS toxicity. Consistent with this, *dSdhaf4* mutants were highly sensitive to oxidative stress induced by hyperoxia (Figure 4.9F), but showed no sensitivity to starvation, which is unassociated with ROS production (Figure 4.10E). These data suggest a connection between the role of dSdhaf4 in SDH assembly and oxidative stress resistance.

Yeast Sdh8 is a chaperone for soluble and covalently flavinated Sdh1

Data from three distinct eukaryotic systems indicate that the SDHAF4 protein family plays an evolutionarily conserved role in SDH assembly and activity. Turning back to yeast, we sought to understand the mechanism by which Sdh8 supports SDH biogenesis. To identify proteins interacting with Sdh8, we performed a large scale HA immunoprecipitation from either WT or Sdh8-His_6HA_3 containing mitochondria. The final eluates were resolved by SDS-PAGE, revealing a band of ~70 kDa that was present only in the Sdh8-His_6HA_3 immunoprecipitation. Using mass spectrometry, we found that this band contained Msd1, a nuclear-encoded mitochondrial tRNA synthetase for aspartate (Gampel and Tzagoloff, 1989) and Sdh1, the catalytic subunit of SDH (Figure 4.11A). Due to the strong connection with SDH assembly and function, we focused on this putative interaction between Sdh8 and Sdh1, which was confirmed by immunoprecipitation of Sdh8 followed by identification of Sdh1 in the eluate using an Sdh1-specific antibody (Figure 4.12A, lanes 1 and 6 vs. 2 and 7). This experiment also demonstrated that Sdh8 occupies a minor, but significant portion of Sdh1 in the matrix

Figure 4.11. Yeast Sdh8 is a cochaperone for unbound and covalently flavinated Sdh1.
(A) A large scale HA immunoprecipitation of mitochondria isolated from *sdh8*Δ cells expressing Sdh8-His_6HA_3 and WT cells as a control. The final eluates were resolved by SDS-PAGE and visualized by silver stain (Thermo Scientific). The proteins present in each band were identified by mass-spectroscopy. (B) WT, *sdh8*Δ, and *sdh5*Δ mitochondria were resolved by SDS-PAGE and imaged for covalent FAD (ultraviolet light) or immunoblotted for Sdh1. (C) Sdh8-His_6HA_3 was immunoprecipitated using anti-HA conjugated agarose from digitonin-solublilized mitochondria. Mitochondria were extracted from *sdh8*Δ cells expressing Sdh8-His_6HA_3 or *sdh1*Δ*sdh8*Δ cells expressing Sdh8-His_6HA_3 and $Sdh1^{H90S}$ mutant (BY4741 background). (D) Sdh8-His_6HA_3 was immunoprecipitated from WT and *sdh5*Δ mitochondria using anti-HA conjugated agarose (W303 background). (E) Mitochondrial lysates isolated from control cells (WT), *sdh8*Δ cells expressing Sdh8-His_6HA_3, *sdh1*Δ*sdh8*Δ cells expressing Sdh8-His_6HA_3, *sdh2*Δ*sdh8*Δ cells expressing Sdh8-His_6HA_3, *sdh8*Δ cells, *sdh2*Δ*sdh8*Δ cells, and *sdh5*Δ*sdh8*Δ cells expressing Sdh8-His_6HA_3 were fractionated by SDS-PAGE. Levels of each protein were assessed by immunoblot for Sdh1, Sdh2, and HA (Sdh8-His_6HA_3). Immunoblot of Porin was used as a loading control (W303 background). (F) Sdh2- His_6HA_3 was immunoprecipitated from digitonin-solubilized mitochondria. Mitochondria were extracted from control cells (WT), *sdh2*Δ*sdh4*Δ cells expressing Sdh2-His_6HA_3, or *sdh2*Δ*sdh4*Δ*sdh8*Δ cells expressing Sdh2-His_6HA_3 (BY4741 background).

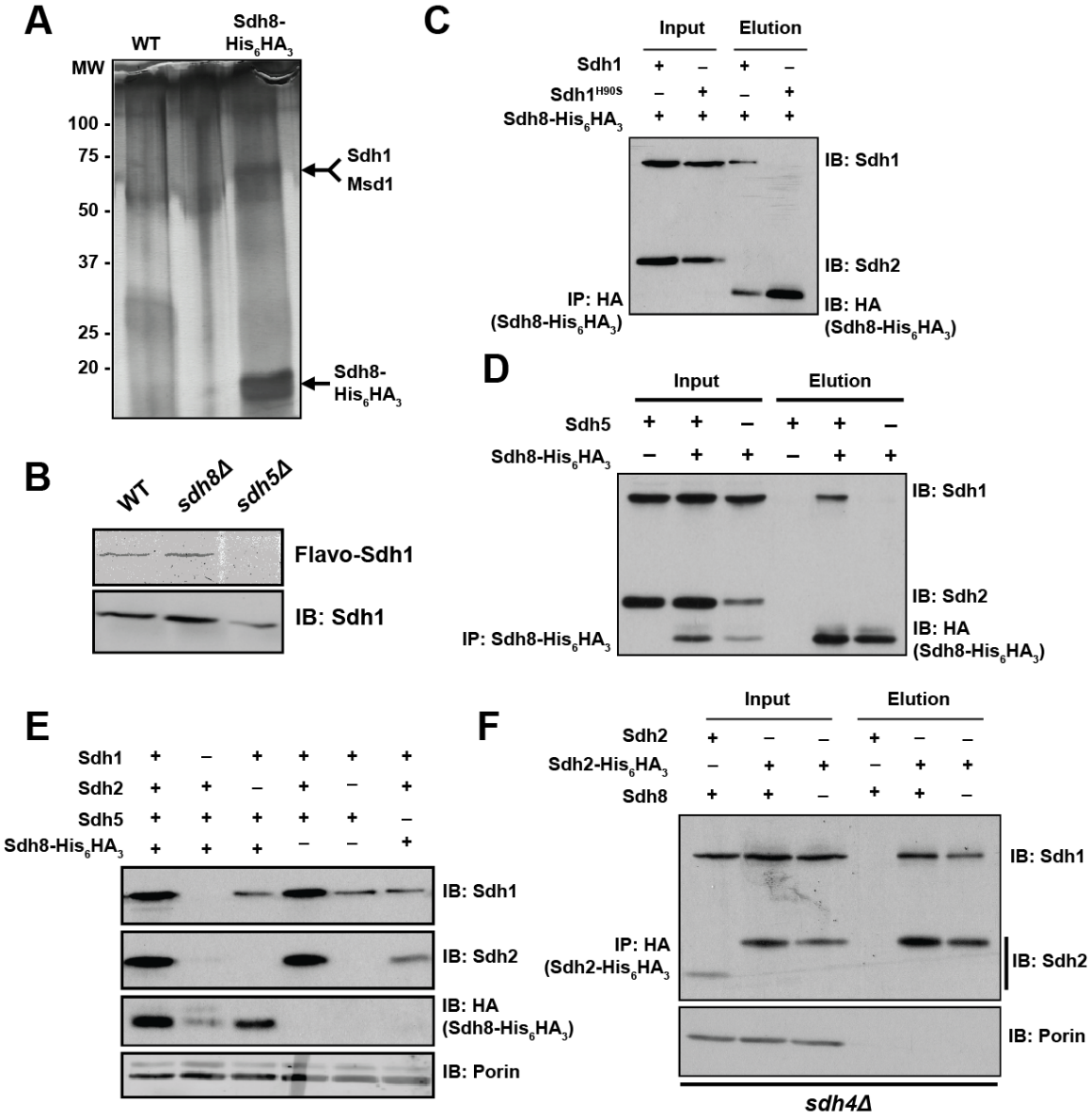
A
WT
Sdh8-His6HA3
MW
100
75
50
37
25
20
Sdh1
Msd1
Sdh8-His6HA3
B
WT
sdh8Δ
sdh5Δ
Flavo-Sdh1
IB: Sdh1
C
Input
Elution
Sdh1
Sdh1H90S
Sdh8-His6HA3
IB: Sdh1
IB: Sdh2
IP: HA (Sdh8-His6HA3)
IB: HA (Sdh8-His6HA3)
D
Input
Elution
Sdh5
Sdh8-His6HA3
IB: Sdh1
IB: Sdh2
IP: Sdh8-His6HA3
IB: HA (Sdh8-His6HA3)
E
Sdh1
Sdh2
Sdh5
Sdh8-His6HA3
IB: Sdh1
IB: Sdh2
IB: HA (Sdh8-His6HA3)
IB: Porin
F
Input
Elution
Sdh2
Sdh2-His6HA3
Sdh8
IB: Sdh1
IP: HA (Sdh2-His6HA3)
IB: Sdh2
IB: Porin
sdh4Δ

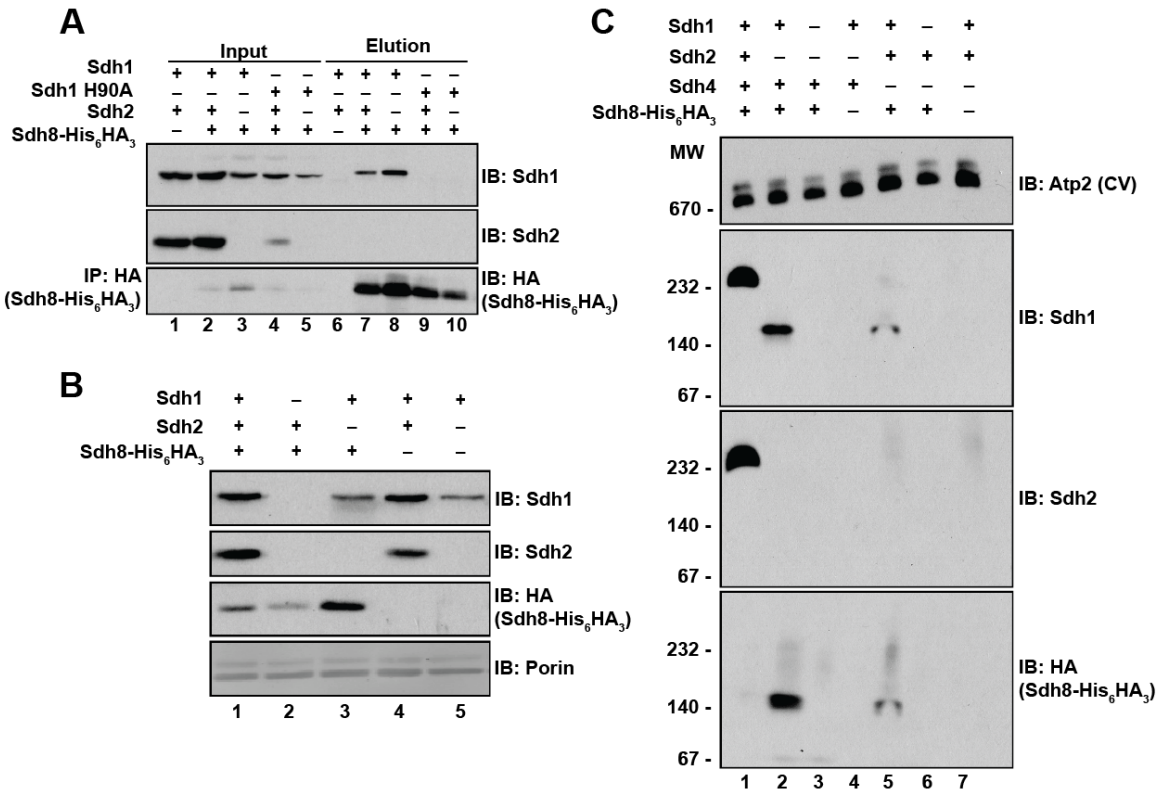

Figure 4.12. Yeast Sdh8 is a cochaperone for unbound and covalently flavinated Sdh1.

(A) Sdh8-His_6HA_3 was immunoprecipitated using anti-HA antibody-conjugated agarose from digitonin-solubilized mitochondria isolated from the yeast strains described as follows. Lanes 1 and 6, WT cells; Lanes 2 and 7, *sdh8*Δ cells expressing Sdh8-His_6HA_3; Lanes 3 and 8, *sdh2*Δ *sdh8*Δ cells expressing Sdh8-His_6HA_3; Lanes 4 and 9 *sdh1*Δ *sdh8*Δ cells expressing Sdh8-His_6HA_3 and $Sdh1^{H90A}$; Lanes 5 and 10, *sdh1*Δ *sdh2*Δ *sdh8*Δ cells expressing Sdh8-His_6HA_3 and $Sdh1^{H90A}$. (B) Mitochondrial lysates isolated from the following strains were fractionated by SDS-PAGE. Lane 1, *sdh8*Δ cells expressing Sdh8-His_6HA_3; Lane 2, *sdh1*Δ *sdh8*Δ cells expressing Sdh8-His_6HA_3; Lane 3, *sdh2*Δ *sdh8*Δ cells expressing Sdh8-His_6HA_3; Lane 4, *sdh8*Δ cells; Lane 5, *sdh2*Δ *sdh8*Δ cells (BY4741 background). Steady state protein abundance was assessed by immunoblot using antibodies against Sdh1, Sdh2, and HA (Sdh8-His_6HA_3). (C) Mitochondria isolated from the following yeast strains were solubilized in digitonin and fractionated by BN-PAGE. Lane 1, *sdh8*Δ cells expressing Sdh8-His_6HA_3; Lane 2, *sdh2*Δ *sdh8*Δ cells expressing Sdh8-His_6HA_3; Lane 3, *sdh1*Δ *sdh2*Δ *sdh8*Δ cells expressing Sdh8-His_6HA_3; Lane 4, *sdh2*Δ *sdh8*Δ; Lane 5, *sdh4*Δ *sdh8*Δ cells expressing Sdh8-His_6HA_3; Lane 6, *sdh1*Δ *sdh4*Δ *sdh8*Δ cells expressing Sdh8-His_6HA_3; Lane 7, *sdh4*Δ *sdh8*Δ cells. Immunoblotting was used to detect Atp2 (complex V) as a control and complexes containing Sdh1, Sdh2, and HA (Sdh8-His_6HA_3). SDH complex (~232 kDa), Sdh1/Sdh8 subcomplex (~150 kDa).

under WT conditions and that Sdh2 is likely not a member of this complex as it is undetectable in the eluate (Figure 4.12A).

Since Sdh8 binds Sdh1 independent of Sdh2, we hypothesized that Sdh8 may be acting as a chaperone for a free soluble pool of Sdh1 in the mitochondrial matrix. If this is true, then deletion of *SDH2* might shift Sdh1 to a free soluble form, which would increase the demand for Sdh8 function. Consistent with this possibility, *sdh2*Δ mutant mitochondria exhibit an accumulation of Sdh8 (Figure 4.12B, lane 1 vs. lane 3), while *sdh1*Δ mutant mitochondria exhibit a depletion of Sdh8 (Figure 4.12B, lane 1 vs. lane 2). Furthermore, this accumulation of Sdh8-His_6HA_3 results in enhanced Sdh1-Sdh8 association in the *sdh2*Δ mutant (Figure 4.12A, lanes 2 and 7 vs 3 and 8) despite an approximately two-fold decrease in steady state Sdh1 levels (Figure 4.12B, lane 1 vs. lane 3). Although the stability of Sdh8 depends on Sdh1, Sdh1 abundance is unaffected by the deletion of *SDH8* (Figure 4.12B). However, Sdh2 levels are reduced in an *sdh8*Δ mutant, likely due to decreased Sdh1 competence for interaction with Sdh2 (Figure 4.12B). This is further supported by the observation that the formation of the Sdh1-Sdh2 soluble dimer, which is readily apparent in a mutant lacking the Sdh4 membrane anchor, is impaired in an *sdh8*Δ mutant (Figure 4.11F). Interpretation of this experiment is complicated by the decreased Sdh2 steady state level in the *sdh1*Δ mutant, but the data are most consistent with the hypothesis that Sdh8 is required to maintain Sdh1 in a state that is fully competent to bind Sdh2 and assemble in the SDH holocomplex. Sdh1 is known to be covalently flavinated at H90 in a reaction that requires the activity of Sdh5 (Hao et al., 2009). Initially, we found that deletion of *SDH8* does not impact the flavination of Sdh1 (Figure 4.11B).

We reasoned, however, that Sdh8 might act specifically on the flavinated form of free Sdh1. Accordingly, we immunoprecipitated Sdh8-His_6HA_3 from mitochondria that express wild-type Sdh1, $Sdh1^{H90A}$, or $Sdh1^{H90S}$, which are Sdh1 mutants that cannot covalently bind FAD. Indeed, $Sdh1^{H90A}$ and $Sdh1^{H90S}$ both failed to copurify with Sdh8-His_6HA_3 (Figures 4.12A, lanes 2 and 7 vs. lanes 4 and 9, and 4.11C) even in the absence of Sdh2 (Figure 4.12A, lanes 2 and 7 vs. lanes 5 and 10). In further support of this hypothesis, we found that Sdh1 failed to interact with Sdh8-His_6HA_3 in *sdh5*Δ mutant cells (Figure 4.11D), which lack covalent Sdh1 flavination (Figure 4.11B) (Hao et al., 2009). Furthermore, Sdh8-His_6HA_3 was destabilized in the *sdh5*Δ mutant as was observed for the *sdh1*Δ mutant (Figure 4.11E, lane 1 vs. 6). Finally, Sdh8-His_6HA_3 is not present in the SDH holocomplex, as assayed by BN-PAGE (Figure 4.12C, lane 1). We also observed that deletion of *SDH2* or *SDH4*, which ablates the SDH holocomplex, causes the emergence of a subcomplex of ~150 kDa, which lacks Sdh2 but clearly contains both Sdh1 and Sdh8 (Figure 4.12C, lanes 2 and 5). This is not coincidental comigration as loss of either Sdh1 or Sdh8 causes this subcomplex to disappear from *sdh2*Δ and *sdh4*Δ mutant strains (Figure 4.12C, lanes 3, 4, 6, and 7). Taken together, these data demonstrate that Sdh8 interacts specifically with flavo-Sdh1, independent of other components of the SDH complex, and its stability depends upon this interaction.

Sdh8 protects the cell from oxidative stress

The data presented thus far demonstrate that Sdh8 acts as a chaperone for Sdh1 to promote formation of the Sdh1/Sdh2 dimer. We found that overexpression of Sdh1 does not rescue the growth defects of *sdh8*Δ mutants but, rather, is toxic to both WT and

*sdh8*Δ cells on respiratory carbon sources, with the *sdh8*Δ mutant being particularly sensitive (Figures 4.13A and 4.14A). Within the mitochondrial matrix, Sdh1 can form soluble complexes with two proteins — Sdh2 and Sdh8. To further interrogate potential toxicity associated with unbound Sdh1 we assayed the growth of *sdh2*Δ*sdh8*Δ mutant cells compared to each single mutant. In this double mutant all Sdh1 will be in the free unbound state. Indeed, deletion of both *SDH2* and *SDH8* causes a synthetic growth phenotype, while no apparent phenotype was observed for either single deletion strain (Figure 4.13B). These observations raise the possibility that free Sdh1 is toxic and that this toxicity may be alleviated by Sdh8. To test this, we cooverexpressed Sdh8 with Sdh1 and observed a significant rescue of the Sdh1 toxicity (Figure 4.13C). We conclude that, in addition to promoting assembly of the Sdh1/Sdh2 dimer; Sdh8 also prevents the toxicity associated with free Sdh1.

In considering possible mechanisms for toxicity of free Sdh1, we hypothesized that the exacerbated *sdh8*Δ phenotype on acetate compared to glycerol medium (Figure 4.2A) may be the result of increased oxidative stress. This is consistent with previous reports using acetate to trigger ROS-dependent cell death in yeast (Carmona-Gutierrez et al., 2010), as well as the sensitivity of *dSdhaf4* mutants to hyperoxia (Figure 4.9F). In support of this hypothesis, we found that the *sdh8*Δ mutant is profoundly hypersensitive to paraquat in glycerol media relative to WT cells (Figure 4.13D). If this impaired growth is the result of elevated ROS, then overexpression of genes involved in ROS detoxification might suppress the growth phenotype. In fact, overexpression of *YAP1*, a transcription factor that stimulates the expression of many genes important for oxidative stress defense (including *TRR1*, *TRX2*, *GSH1,* and *GLR1*), as well as the mitochondrial

Figure 4.13. Sdh8 protects the cell from oxidative stress.
(A) Ten-fold serial dilutions of WT and *sdh8*Δ yeast either transformed with an empty vector or overexpressing Sdh1 were plated on media containing the indicated carbon source and incubated at 30˚C (W303 background) for 2 days (glucose), 3 days (raffinose) or 4 days (glycerol, acetate). (B) WT, *sdh2*Δ, *sdh8*Δ, and *sdh2*Δ *sdh8*Δ cells were back-diluted in synthetic complete media with 2% glucose and incubated at 30˚C. Growth was assessed by measuring the optical density (600 nm) of each culture at various time points. (±SEM. N = 3. Time point (TP) 1—*sdh2*Δ vs. *sdh2*Δ*sdh8*Δ p = .007, *sdh8*Δ vs. *sdh2*Δ*sdh8*Δ p = .01; TP 2—*sdh2*Δ vs. *sdh2*Δ*sdh8*Δ p = .03, *sdh8*Δ vs. *sdh2*Δ*sdh8*Δ p = .03; TP 3—*sdh2*Δ vs. *sdh2*Δ*sdh8*Δ p = .01, *sdh8*Δ vs. *sdh2*Δ*sdh8*Δ p = .02; TP 4—*sdh2*Δ vs. *sdh2*Δ*sdh8*Δ p < .0001, *sdh8*Δ vs. *sdh2*Δ*sdh8*Δ p = .0003; TP 5—*sdh2*Δ vs. *sdh2*Δ*sdh8*Δ p = .001, *sdh8*Δ vs. *sdh2*Δ*sdh8*Δ p < .0001; TP 6—*sdh2*Δ vs. *sdh2*Δ*sdh8*Δ p = .004, *sdh8*Δ vs. *sdh2*Δ*sdh8*Δ p = .0025). (C) Ten-fold serial dilutions of WT yeast transformed with an empty vector, WT yeast overexpressing Sdh1, and WT yeast overexpressing Sdh1 and Sdh8 were plated on media containing acetate and incubated at 30˚C (W303 background) as in (A). (D) Ten-fold serial dilutions of WT yeast transformed with an empty vector, *sdh8*Δ cells transformed with an empty vector, and *sdh8*Δ cells expressing Sdh8-His_6HA_3 were plated on media containing glycerol with and without 1mM paraquat and incubated at 30˚C (W303 background) as in (A). (E) Ten-fold serial dilutions of WT yeast transformed with an empty vector, *sdh8*Δ cells transformed with an empty vector, and *sdh8*Δ cells overexpressing YAP1 were plated on media containing the indicated carbon source and incubated at 30˚C (BY4741 background) as in (A). (F) Shown here is an updated model of the assembly of SDH. Upon entry into the mitochondrial matrix, apo-Sdh1 is rapidly flavinated in a reaction that requires Sdh5 (Hao et al., 2009). Acting as a cochaperone, Sdh8 binds and occupies Sdh1 forming an important intermediate subcomplex that prevents Sdh1 autoxidation (2). Sdh8 occupies Sdh1 until it is ready to further proceed through the assembly pathway and presumably facilitates the formation of Sdh1/Sdh2 soluble dimers upon the import of a freshly translated Sdh2 (3). In the end, the Sdh1/Sdh2 dimer is free to dock on the IMM via interactions with Sdh3 and Sdh4 which have previously assembled on the IMM (4).

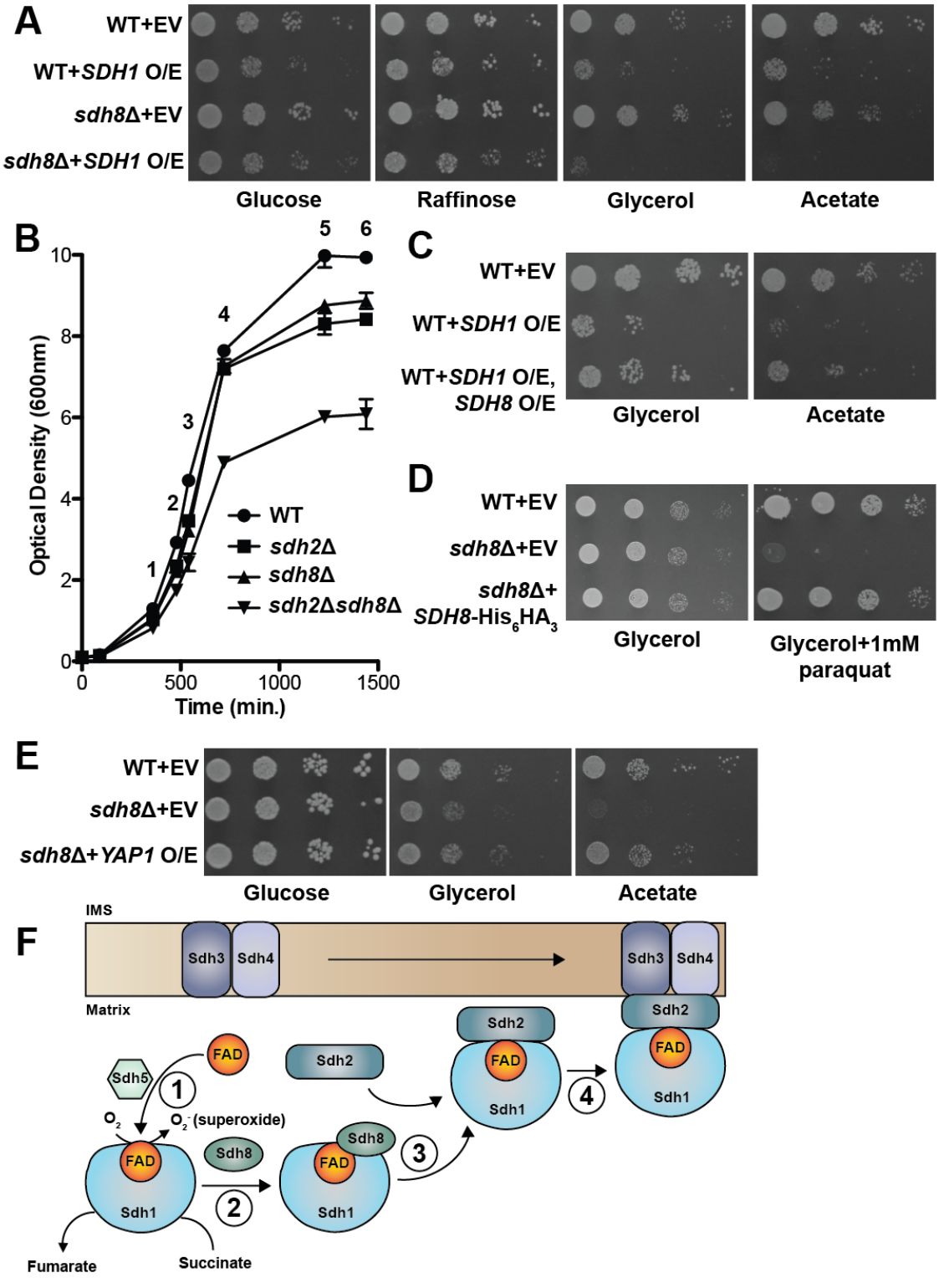
A
WT+EV
WT+SDH1 O/E
sdh8Δ+EV
sdh8Δ+SDH1 O/E
Glucose
Raffinose
Glycerol
Acetate
B
Optical Density (600nm)
Time (min.)
WT
sdh2Δ
sdh8Δ
sdh2Δsdh8Δ
C
WT+EV
WT+SDH1 O/E
WT+SDH1 O/E, SDH8 O/E
Glycerol
Acetate
D
WT+EV
sdh8Δ+EV
sdh8Δ+ SDH8-His6HA3
Glycerol
Glycerol+1mM paraquat
E
WT+EV
sdh8Δ+EV
sdh8Δ+YAP1 O/E
Glucose
Glycerol
Acetate
F
IMS
Matrix
Sdh3
Sdh4
Sdh2
Sdh5
FAD
Sdh1
Sdh8
O2
O2- (superoxide)
Fumarate
Succinate

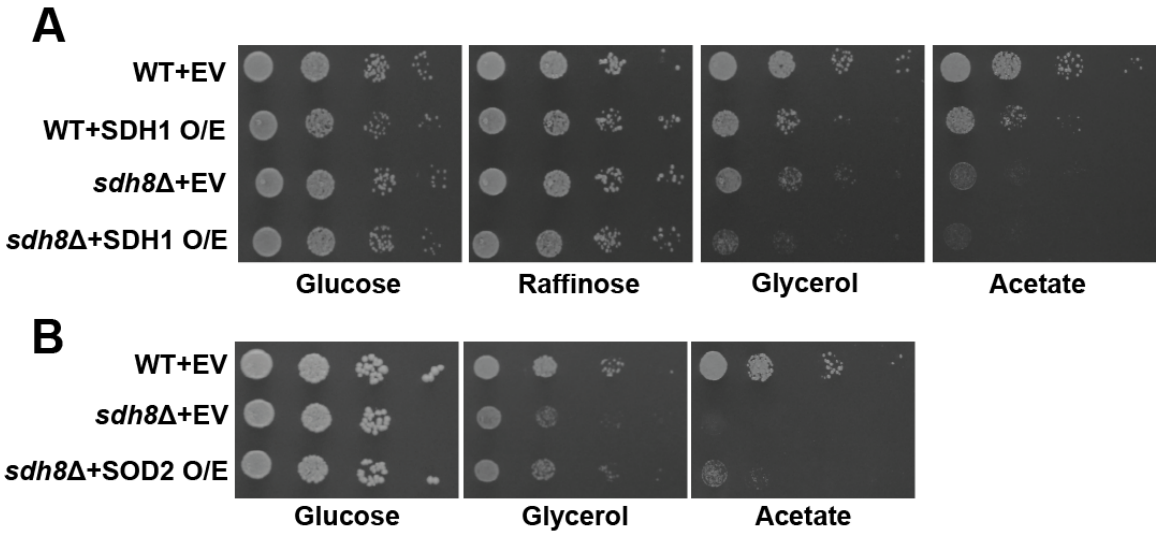

Figure 4.14. Sdh8 protects the cell from oxidative stress.
(A) Ten-fold serial dilutions of WT yeast transformed with an empty vector, WT yeast overexpressing SDH1, *sdh8*Δ cells transformed with an empty vector, and *sdh8*Δ cells overexpressing SDH1 were plated on media containing the indicated carbon source and incubated at 30˚C (BY4741 background). (B) Ten fold serial dilutions of WT yeast transformed with an empty vector, sdh8Δ cells transformed with an empty vector, and *sdh8*Δ cells overexpressing SOD2 were plated on media containing the indicated carbon source and incubated at 30˚C (BY4741 background).

superoxide dismutase *SOD2*, completely or partially rescued the growth phenotype of *sdh8*Δ cells (Figures 4.13E and 4.14B).

Discussion

The critical role of SDH in primary cellular metabolism is reflected by the variety of diseases associated with its dysfunction. Unlike other ETC complexes, which require multiple factors for their assembly, only two factors have been identified that are required for the assembly of the SDH holocomplex within the inner mitochondrial membrane. Herein we use three distinct eukaryotic model systems, yeast, *Drosophila*, and mammalian cells, to demonstrate that the SDHAF4 protein family consists of evolutionarily conserved SDH assembly factors. We show that SDHAF4 binds directly to flavinated Sdh1, blocking the generation of excess ROS and facilitating its interaction with Sdh2 and the subsequent assembly of the SDH holocomplex. These functions for SDHAF4 appear to be conserved in metazoans and suggest a role for this factor in disease, as *Drosophila Sdhaf4* mutants display muscular and neuronal dysfunction as well as neurodegeneration. Yeast and *Drosophila Sdhaf4* mutants exhibit the classic metabolomic phenotype of SDH deficiency, with an apparent block in the TCA cycle that results in an accumulation of succinate and a depletion of fumarate and malate, the two TCA cycle intermediates downstream of SDH (Figures 4.2B and 4.6A). Consistent with these effects, the yeast and fly mutants display a reduction in the steady-state levels of the SDH holocomplex and reduced SDH enzyme activity, indicating an important role for SDHAF4 in SDH stability and activity (Figures 4.2C, 4.2E, 4.6B, and 4.7A). siRNA-mediated knockdown of SDHAF4 in mammalian cells leads to similar defects (Figures

4.3B and 4.3C). Moreover, expression of either fly or human SDHAF4 is sufficient to rescue the growth defects of an *sdh8*Δ mutant yeast strain (Figure 4.2F). Taken together, these results demonstrate that the central requirement for SDHAF4 in SDH assembly has been conserved through evolution, from yeast to mammals.

Our biochemical studies in yeast provide a mechanistic context for understanding the role of SDHAF4 in SDH assembly. An unbiased proteomic analysis of SDHAF4-associated proteins revealed a physical interaction between Sdh8 and Sdh1, the catalytic subunit of SDH (Figure 4.11A). We confirmed the specificity of this interaction by co-immunoprecipitation and demonstrated that an Sdh1/Sdh8 subcomplex of ~150 kDa can be detected in unstressed WT cells, albeit at very low levels (Figure 4.12A). Increased levels of this subcomplex, however, become readily detectable upon genetic disruption of the SDH complex through deletion of either Sdh2 or Sdh4 (Figure 4.12C). Taken together, these results support the model that Sdh8 interacts with a soluble pool of Sdh1 prior to the formation of the Sdh1/Sdh2 soluble dimer and assembly of the holocomplex. Moreover, Sdh8 interacts specifically with the flavinated form of Sdh1, indicating that this association follows Sdh1 flavination by Sdh5/SDHAF2 (Figures 4.12A, 4.11C, and 4.11D) (Hao et al., 2009). This model is consistent with the localization of Sdh8 to the mitochondrial matrix where it can readily access free flavo-Sdh1, which is subsequently tethered to the IMM through its association with Sdh2 and the membrane-bound Sdh3/Sdh4 dimer (Figure 4.13F).

We observed that Sdh8 stability directly relates to its association with Sdh1, further supporting the centrality of its role as an Sdh1 chaperone (Figure 4.12B). Thus, deletion of Sdh1 leads to a dramatic reduction in Sdh8 levels while deletion of Sdh2,

which causes greatly increased availability of free Sdh1, leads to an increase in Sdh8 (Figure 4.12B). Although Sdh1 protein levels are unperturbed in *sdh8*Δ cells, we observed considerable destabilization of Sdh2, which is consistent with impaired formation of Sdh1/Sdh2 dimers (Figure 4.12B). Therefore, we hypothesize that the occupation of free Sdh1 by Sdh8 facilitates the formation of Sdh1/Sdh2 dimers. This dimer fails to form efficiently in the absence of Sdh8, and Sdh2 is destabilized as it is in mutants lacking Sdh1 altogether.

Interestingly, the loss of dSdhaf4 appears to have more severe consequences in *Drosophila* than in yeast or mammalian cells. *dSdhaf4* mutants display a profound reduction in SDH enzyme activity, destabilization of both SdhA and SdhB, and a significant loss of SDH holocomplexes (Figures 4.6B, 4.7A, and 4.7B). In contrast, yeast *sdh8*Δ mutants and C2C12 mouse myoblasts treated with SDHAF4 siRNA maintain ~40–50% of wild-type SDH activity and preserve a similar fraction of assembled SDH holocomplexes (Figures 4.2C, 4.2E, 4.3B, and 4.3C). This difference may be caused by a greater dependence of SdhA on its SDHAF4 chaperone in *Drosophila*. While yeast *sdh8*Δ mutants have relatively normal levels of Sdh1, *dSdhaf4* mutants have greatly reduced levels of SdhA, which probably underlies the nearly complete loss of SDH holocomplexes. It is possible that yeast and mammalian cells express an additional SDHA chaperone that can function in the absence of SDHAF4, maintaining the levels of SDHA to support holocomplex assembly. Identification of the mechanism that underlies this discrepancy, however, will require further study of SDH assembly in both yeast and flies. Regardless, it is important to note that *dSdhaf4* mutants retain some SDH activity (~15%) and that this is sufficient to support limited viability, albeit with both muscular

(erect wings) and behavioral (neurodegeneration) dysfunction. In contrast, *SdhA* null mutants are lethal, demonstrating that a further reduction in SDH activity cannot be tolerated (Mast et al., 2008). Thus, while the SDHAF4 protein family is clearly involved in SDH stability and activity, it does not appear to be an absolute requirement as some level of SDH activity remains in the absence of the respective SDHAF4 ortholog in all three model systems.

Our demonstration that Sdh8 acts through Sdh1 to facilitate formation of the Sdh1/Sdh2 dimer and subsequently the SDH holocomplex further emphasizes the importance of dedicated chaperones for ETC complex assembly. We propose that this unique demand might relate to the need to protect the redox-active cofactors present in many ETC complex subunits (Messner and Imlay, 2002). Prior to assembly, these cofactors are exposed to solvent and, therefore, susceptible to damaging chemical reactions. Interestingly, a cosubmitted report characterized two additional SDH assembly factors, Sdh6/SDHAF1 and Sdh7/SDHAF3, which appear to serve a similar role for Sdh2 as Sdh8 serves for Sdh1 (Na et al., Submitted manuscript; Chapter 5). These factors chaperone monomeric Sdh2, and potentially the Sdh1-Sdh2 dimer, protecting the Sdh2 Fe-S clusters during assembly. Taken together with the previous discovery of Sdh5, which is required for Sdh1 flavination (Hao et al., 2009), these studies suggest that a series of dedicated chaperones play important roles in the assembly of SDH as they do for other ETC complex members (Figure 4.13F).

The susceptibility of free cofactors to damaging chemical reactions is exemplified by our data suggesting that free flavinated Sdh1 is toxic and that this toxicity is alleviated by Sdh8. The modest phenotype of both *sdh2*Δ and *sdh8*Δ single mutant cells grown in

glucose is greatly enhanced when these two deletions are combined (Figure 4.13B). Furthermore, overexpression of Sdh1 causes growth defects in WT cells, but this phenotype is exacerbated in *sdh8*Δ mutants and ameliorated by co-overexpression of Sdh8 (Figures 4.13A and 4.13C). Thus, we conclude that the chaperone activity of Sdh8 protects the cell from potentially damaging effects of unbound Sdh1, which are likely due to the generation of reactive oxygen species enabled by solvent-accessible FAD. Sdh1, which contains a covalently bound, redox active FAD cofactor is capable of oxidizing succinate to fumarate independent of the SDH complex. This oxidation of succinate leads to the reduction of FAD, which is then auto-oxidized by molecular oxygen to yield superoxide (Guzy et al., 2008; Messner and Imlay, 2002). The observation that Sdh8 interacts specifically with covalently flavinated Sdh1, but not with apo-Sdh1, is consistent with Sdh8 acting to prevent this mechanism of oxidative stress. Further, *sdh8*Δ mutant cells were unable to grow on respiratory medium in the presence of the superoxide producer paraquat (Figure 4.13D). Similarly, *dSdhaf4* mutant flies are highly sensitive to oxidative stress induced by hyperoxia (Figure 4.9F). More importantly, overexpression of two genes involved in the detoxification of reactive oxygen species—*YAP1* and *SOD2*—rescued the *sdh8*Δ growth defects in yeast (Figures 4.13E and 4.14B). We conclude that, in addition to promoting Sdh2 binding and holocomplex assembly, Sdh1 protects the redox-active FAD cofactor from potentially deleterious solvent interactions.

These biochemical aberrations resulted in profound physiological defects in *Drosophila* lacking *dSdhaf4*, all of which are hallmarks of mitochondrial dysfunction and which suggest possible links to human disease. Most notably, *dSdhaf4* mutants display

bang sensitivity, a phenotype characterized by a susceptibility to mechanically induced paralytic seizures, which is commonly elicited by defects in mitochondrial function (Fergestad et al., 2006; Liu et al., 2007). *dSdhaf4* mutants also display neurodegeneration and reduced lifespan, which often accompanies bang sensitivity (Fergestad et al., 2008). In addition, we observed abnormal wing posture in *dSdhaf4* mutants, which is characteristic of muscular dysfunction (Greene et al., 2003). Similar phenotypes have been reported in flies harboring mutations in several known disease-causing genes that impact mitochondrial function. For example, *Pink* and *Parkin* mutants display abnormal wing posture, and *mtATP6* mutants are bang sensitive (Celotto et al., 2006b; Fernandes and Rao, 2011). Human mutations in *Pink/Parkin* and *mtATP6* are known to cause familial Parkinson's disease and mitochondrial encephalopathy, respectively (Schapira, 2012). Moreover, as described in more detail below, some neurodegenerative diseases such as Leigh's syndrome are known to be associated with a loss of SDH activity. Our studies of *dSdhaf4* thus provide a genetic model for better understanding the pathophysiology of neurodegenerative disorders that are caused by SDH deficiency (Hoekstra and Bayley, 2013; Rutter et al., 2010).

Similar to *dSdhaf4* mutants, *SdhB* hypomorphic mutants that retain ~40% of normal SDH activity are sensitive to oxidative stress and display a reduced lifespan (Walker et al., 2006). The *SdhB* hypomorphs, however, were not reported to undergo mechanically induced paralytic seizures or display neurodegenerative phenotypes (Walker et al., 2006). This lack of neuronal phenotypes in *SdhB* mutants could be due to the higher overall SDH activity seen in these partial loss-of-function mutants relative to a complete loss of *dSdhaf4* activity. It is also possible, however, that the neurodegeneration

phenotype is driven by increased ROS production rather than a defect in mitochondrial ATP production. In support of this model, clones generated using a lethal null allele of *SdhA* in the eye display retinal degeneration similar to that seen in *dSdhaf4* mutants, which was shown to be specifically caused by increased ROS production (Mast et al., 2008). This is also consistent with our finding that *dSdhaf4* mutants are not depleted of ATP (Figures 4.5B and 4.6A), possibly enabled by metabolic compensation (Celotto et al., 2011) and/or decreased movement (data not shown). Thus, our study of *dSdhaf4*, and other work characterizing *SdhA, SdhB,* and *dSdhaf3* mutants in *Drosophila*, suggests that tissue dysfunction induced by a loss of SDH appears to be largely driven by increased ROS production (Mast et al., 2008; Na et al., Submitted manuscript; Walker et al., 2006). This is consistent with our hypothesis that SDH assembly factors may have evolved as a mechanism to protect cells and organisms from ROS production during SDH assembly.

Mutations in all genes encoding previously published SDH subunits and assembly factors have been shown to cause human disease. These include neurodegenerative diseases (Leigh's Syndrome, Leukodystrophy, and Leukoencephalopathy), which have been linked to mutations in *SDHA*, *SDHB*, and *SDHAF1* (Alston et al., 2012; Ghezzi et al., 2009; Horvath et al., 2006; Ohlenbusch et al., 2012). Mutations in *SDHA, SDHB, SDHC, SDHD,* and *SDHAF2* have also been shown to cause paragangliomas and pheochromocytomas—two classes of neuroendocrine tumors (Astuti et al., 2001; Fishbein and Nathanson, 2012; Hao et al., 2009). Recently, several cases of wild-type gastrointestinal stromal tumors (WT GIST) have been linked to germline loss-of-function mutations in *SDHA* and *SDHB* (Celestino et al., 2012; Italiano et al., 2012; Janeway et al., 2011; Oudijk et al., 2013). This wealth of evidence linking SDH dysfunction to disease

raises the possibility that damaging mutations in *SDHAF4* may cause human disease. In fact, several cases of SDH-deficient diseases, including Leigh's Syndrome and WT GIST, lack mutations in the genes encoding all known SDH subunits (Horvath et al., 2006; Jain-Ghai et al., 2013; Janeway et al., 2011). Our phenotypic studies raise the important possibility that *SDHAF4* is a candidate gene for these and other diseases characterized by SDH deficiency. Our future efforts will focus on determining the incidence of these possible causative *SDHAF4* mutations.

On the basis of the data presented in this report, we conclude that the SDHAF4 gene family encodes a novel SDH assembly factor. Insights gained in our studies of this protein have allowed us to propose a more complete model of SDH assembly (Figure 4.13F). Upon import into the matrix by TOM and TIM apo-Sdh1 is flavinated in a reaction that requires Sdh5 (Hao et al., 2009). Free flavo-Sdh1 is then bound by Sdh8 to form a ~150 kDa subcomplex. This subcomplex occupies Sdh1, preventing auto-oxidation and supporting its ability to dimerize with Sdh2. The Sdh1/Sdh2 soluble dimer is then recruited to the IMM via interactions with Sdh3 and Sdh4 to form the SDH holocomplex (Figure 4.13F). This model highlights the importance of subunit-specific chaperones in the process of assembly. Indeed, failure of SDHAF4 to occupy free SdhA prevents normal SDH assembly in three eukaryotic systems and has profound physiological consequences. The identification and characterization of the SDHAF4 protein family thus provide important new insights into the process of SDH assembly, the mechanisms by which SDH subunits are protected for generating ROS, and a new candidate gene to understand human disease associated with a loss of SDH activity.

Acknowledgements

We thank Dana Carroll, Kelly Beumer, and Tim Dahlem at the University of Utah Mutation and Detection Core for generating the TALEN gene-targeting constructs, Linda Nikolova at the University of Utah Electron Microscopy core for assistance performing TEM, the Bloomington Stock Center for providing stocks, FlyBase for critical information that made these studies possible, and Dennis Winge for providing antibodies and other reagents. This research was supported by NIH grant NIH 1R01 GM094232 (JR and CST), and we acknowledge support of funds in conjunction with the grant P30CA042014 awarded to the Huntsman Cancer Institute. DKB was supported by the NIH Genetics Predoctoral Training Grant T32 GM007464. JGV was supported by the Huntsman Cancer Institute Multidisciplinary Cancer Research Training Program.

References

Alston, C.L., Davison, J.E., Meloni, F., van der Westhuizen, F.H., He, L., Hornig-Do, H.T., Peet, A.C., Gissen, P., Goffrini, P., Ferrero, I., et al. (2012). Recessive germline SDHA and SDHB mutations causing leukodystrophy and isolated mitochondrial complex II deficiency. J. Med. Genet. *49*, 569–577.

Astuti, D., Latif, F., Dallol, A., Dahia, P.L., Douglas, F., George, E., Skoldberg, F., Husebye, E.S., Eng, C., and Maher, E.R. (2001). Gene mutations in the succinate dehydrogenase subunit SDHB cause susceptibility to familial pheochromocytoma and to familial paraganglioma. Am. J. Hum. Genet. *69*, 49–54.

Bardella, C., Pollard, P.J., and Tomlinson, I. (2011). SDH mutations in cancer. Biochim. Biophys. Acta *1807*, 1432–1443.

Bateman, J.R., Lee, A.M., and Wu, C.T. (2006). Site-specific transformation of *Drosophila* via phiC31 integrase-mediated cassette exchange. Genetics *173*, 769–777.

Boldogh, I.R., and Pon, L.A. (2007). Purification and subfractionation of mitochondria from the yeast *Saccharomyces cerevisiae*. Methods Cell. Biol. *80*, 45–64.

Bozidis, P., Williamson, C.D., and Colberg-Poley, A.M. (2007). Isolation of endoplasmic reticulum, mitochondria, and mitochondria-associated membrane fractions from transfected cells and from human cytomegalovirus-infected primary fibroblasts. Curr. Prot. Cell Biol. *37*, 3.27.1–3.27.23.

Bricker, D.K., Taylor, E.B., Schell, J.C., Orsak, T., Boutron, A., Chen, Y.C., Cox, J.E., Cardon, C.M., Van Vranken, J.G., Dephoure, N., et al. (2012). A mitochondrial pyruvate carrier required for pyruvate uptake in yeast, *Drosophila*, and humans. Science *337*, 96–100.

Carmona-Gutierrez, D., Eisenberg, T., Buttner, S., Meisinger, C., Kroemer, G., and Madeo, F. (2010). Apoptosis in yeast: triggers, pathways, subroutines. Cell Death Differ. *17*, 763–773.

Celestino, R., Lima, J., Faustino, A., Maximo, V., Gouveia, A., Vinagre, J., Soares, P., and Lopes, J.M. (2012). A novel germline SDHB mutation in a gastrointestinal stromal tumor patient without bona fide features of the Carney-Stratakis dyad. Fam. Cancer *11*, 189–194.

Celotto, A.M., Chiu, W.K., Van Voorhies, W., and Palladino, M.J. (2011). Modes of metabolic compensation during mitochondrial disease using the *Drosophila* model of ATP6 dysfunction. PloS One *6*, e25823.

Celotto, A.M., Frank, A.C., McGrath, S.W., Fergestad, T., Van Voorhies, W.A., Buttle, K.F., Mannella, C.A., and Palladino, M.J. (2006a). Mitochondrial encephalomyopathy in *Drosophila*. J. Neurosci. *26*, 810–820.

Celotto, A.M., Frank, A.C., Seigle, J.L., and Palladino, M.J. (2006b). *Drosophila* model of human inherited triosephosphate isomerase deficiency glycolytic enzymopathy. Genetics *174*, 1237–1246.

Celotto, A.M., Liu, Z., Vandemark, A.P., and Palladino, M.J. (2012). A novel *Drosophila* SOD2 mutant demonstrates a role for mitochondrial ROS in neurodevelopment and disease. Brain Behav. *2*, 424–434.

Cermak, T., Doyle, E.L., Christian, M., Wang, L., Zhang, Y., Schmidt, C., Baller, J.A., Somia, N.V., Bogdanove, A.J., and Voytas, D.F. (2011). Efficient design and assembly of custom TALEN and other TAL effector-based constructs for DNA targeting. Nucleic Acids Res. *39*, e82.

Dahlem, T.J., Hoshijima, K., Jurynec, M.J., Gunther, D., Starker, C.G., Locke, A.S., Weis, A.M., Voytas, D.F., and Grunwald, D.J. (2012). Simple methods for generating and detecting locus-specific mutations induced with TALENs in the zebrafish genome. PLoS Genet. *8*, e1002861.

Diaz, F., Kotarsky, H., Fellman, V., and Moraes, C.T. (2011). Mitochondrial disorders caused by mutations in respiratory chain assembly factors. Semin. Fetal Neonatal Med. *16*, 197–204.

Feany, M.B., and Bender, W.W. (2000). A *Drosophila* model of Parkinson's disease. Nature *404*, 394–398.

Fergestad, T., Bostwick, B., and Ganetzky, B. (2006). Metabolic disruption in *Drosophila* bang-sensitive seizure mutants. Genetics *173*, 1357–1364.

Fergestad, T., Olson, L., Patel, K.P., Miller, R., Palladino, M.J., and Ganetzky, B. (2008). Neuropathology in *Drosophila* mutants with increased seizure susceptibility. Genetics *178*, 947–956.

Fernandes, C., and Rao, Y. (2011). Genome-wide screen for modifiers of Parkinson's disease genes in *Drosophila*. Mol. Brain *4*, 17.

Fernandez-Vizarra, E., Tiranti, V., and Zeviani, M. (2009). Assembly of the oxidative phosphorylation system in humans: what we have learned by studying its defects. Biochim. Biophys. Acta *1793*, 200–211.

Fishbein, L., and Nathanson, K.L. (2012). Pheochromocytoma and paraganglioma: understanding the complexities of the genetic background. Cancer Genet. *205*, 1–11.

Gampel, A., and Tzagoloff, A. (1989). Homology of aspartyl- and lysyl-tRNA synthetases. Proc. Natl. Acad. Sci. USA *86*, 6023–6027.

Ganetzky, B., and Wu, C.F. (1982). Indirect suppression involving behavioral mutants with altered nerve excitability in *Drosophila melanogaster*. Genetics *100*, 597–614.

Ghezzi, D., Goffrini, P., Uziel, G., Horvath, R., Klopstock, T., Lochmuller, H., D'Adamo, P., Gasparini, P., Strom, T.M., Prokisch, H., et al. (2009). SDHAF1, encoding a LYR complex-II specific assembly factor, is mutated in SDH-defective infantile leukoencephalopathy. Nat. Genet. *41*, 654–656.

Gnerer, J.P., Kreber, R.A., and Ganetzky, B. (2006). Wasted away, a *Drosophila* mutation in triosephosphate isomerase, causes paralysis, neurodegeneration, and early death. Proc. Natl. Acad. Sci. USA *103*, 14987–14993.

Greene, J.C., Whitworth, A.J., Kuo, I., Andrews, L.A., Feany, M.B., and Pallanck, L.J. (2003). Mitochondrial pathology and apoptotic muscle degeneration in *Drosophila* parkin mutants. Proc. Natl. Acad. Sci. USA *100*, 4078–4083.

Guzy, R.D., Sharma, B., Bell, E., Chandel, N.S., and Schumacker, P.T. (2008). Loss of the SdhB, but Not the SdhA, subunit of complex II triggers reactive oxygen species-

dependent hypoxia-inducible factor activation and tumorigenesis. Mol. Cell. Biol. *28*, 718–731.

Hao, H.X., Khalimonchuk, O., Schraders, M., Dephoure, N., Bayley, J.P., Kunst, H., Devilee, P., Cremers, C.W., Schiffman, J.D., Bentz, B.G., et al. (2009). SDH5, a gene required for flavination of succinate dehydrogenase, is mutated in paraganglioma. Science *325*, 1139–1142.

Hoekstra, A.S., and Bayley, J.P. (2013). The role of complex II in disease. Biochim. Biophys. Acta *1827*, 543–551.

Horvath, R., Abicht, A., Holinski-Feder, E., Laner, A., Gempel, K., Prokisch, H., Lochmuller, H., Klopstock, T., and Jaksch, M. (2006). Leigh syndrome caused by mutations in the flavoprotein (Fp) subunit of succinate dehydrogenase (SDHA). J. Neuol. Neurosurg. Phsychiatry *77*, 74–76.

Hu, R., Wallace, J., Dahlem, T.J., Grunwald, D.J., and O'Connell, R.M. (2013). Targeting human microRNA genes using engineered Tal-effector nucleases (TALENs). PloS One *8*, e63074.

Italiano, A., Chen, C.L., Sung, Y.S., Singer, S., DeMatteo, R.P., LaQuaglia, M.P., Besmer, P., Socci, N., and Antonescu, C.R. (2012). SDHA loss of function mutations in a subset of young adult wild-type gastrointestinal stromal tumors. BMC Cancer *12*, 408.

Jain-Ghai, S., Cameron, J.M., Al Maawali, A., Blaser, S., MacKay, N., Robinson, B., and Raiman, J. (2013). Complex II deficiency—a case report and review of the literature. Am. J. Med. Genet. *161A*, 285–294.

Janeway, K.A., Kim, S.Y., Lodish, M., Nose, V., Rustin, P., Gaal, J., Dahia, P.L., Liegl, B., Ball, E.R., Raygada, M., et al. (2011). Defects in succinate dehydrogenase in gastrointestinal stromal tumors lacking KIT and PDGFRA mutations. Proc. Natl. Acad. Sci. USA *108*, 314–318.

Kiselev, A., Socolich, M., Vinos, J., Hardy, R.W., Zuker, C.S., and Ranganathan, R. (2000). A molecular pathway for light-dependent photoreceptor apoptosis in *Drosophila*. Neuron *28*, 139–152.

Liu, W., Gnanasambandam, R., Benjamin, J., Kaur, G., Getman, P.B., Siegel, A.J., Shortridge, R.D., and Singh, S. (2007). Mutations in cytochrome c oxidase subunit VIa cause neurodegeneration and motor dysfunction in *Drosophila*. Genetics *176*, 937–946.

Luo, L., Liao, Y.J., Jan, L.Y., and Jan, Y.N. (1994). Distinct morphogenetic functions of similar small GTPases: *Drosophila* Drac1 is involved in axonal outgrowth and myoblast fusion. Genes Dev. *8*, 1787–1802

.

Mandal, S., Guptan, P., Owusu-Ansah, E., and Banerjee, U. (2005). Mitochondrial regulation of cell cycle progression during development as revealed by the tenured mutation in *Drosophila*. Dev. Cell *9*, 843–854.

Mast, J.D., Tomalty, K.M., Vogel, H., and Clandinin, T.R. (2008). Reactive oxygen species act remotely to cause synapse loss in a *Drosophila* model of developmental mitochondrial encephalopathy. Development *135*, 2669–2679.

Mercer, T.R., Neph, S., Dinger, M.E., Crawford, J., Smith, M.A., Shearwood, A.M., Haugen, E., Bracken, C.P., Rackham, O., Stamatoyannopoulos, J.A., et al. (2011). The human mitochondrial transcriptome. Cell *146*, 645–658.

Messner, K.R., and Imlay, J.A. (2002). Mechanism of superoxide and hydrogen peroxide formation by fumarate reductase, succinate dehydrogenase, and aspartate oxidase. J. Biol. Chem. *277*, 42563–42571.

Ohlenbusch, A., Edvardson, S., Skorpen, J., Bjornstad, A., Saada, A., Elpeleg, O., Gartner, J., and Brockmann, K. (2012). Leukoencephalopathy with accumulated succinate is indicative of SDHAF1 related complex II deficiency. Orphanet J. Rare Dis. *7*, 69.

Oudijk, L., Gaal, J., Korpershoek, E., van Nederveen, F.H., Kelly, L., Schiavon, G., Verweij, J., Mathijssen, R.H., den Bakker, M.A., Oldenburg, R.A., et al. (2013). SDHA mutations in adult and pediatric wild-type gastrointestinal stromal tumors. Mod. Path. *26*, 456–463.

Pagliarini, D.J., Calvo, S.E., Chang, B., Sheth, S.A., Vafai, S.B., Ong, S.E., Walford, G.A., Sugiana, C., Boneh, A., Chen, W.K., et al. (2008). A mitochondrial protein compendium elucidates complex I disease biology. Cell *134*, 112–123.

Pantaleo, M.A., Astolfi, A., Urbini, M., Nannini, M., Paterini, P., Indio, V., Saponara, M., Formica, S., Ceccarelli, C., Casadio, R., et al. (2014). Analysis of all subunits, SDHA, SDHB, SDHC, SDHD, of the succinate dehydrogenase complex in KIT/PDGFRA wild-type GIST. Eur. J. Hum. Genet. *22*, 32–39.

Pearl, P.L., Gibson, K.M., Cortez, M.A., Wu, Y., Carter Snead, O., 3rd, Knerr, I., Forester, K., Pettiford, J.M., Jakobs, C., and Theodore, W.H. (2009). Succinic semialdehyde dehydrogenase deficiency: lessons from mice and men. J. Inherit. Metab. Dis. *32*, 343–352.

Pfeiffer, B.D., Ngo, T.T., Hibbard, K.L., Murphy, C., Jenett, A., Truman, J.W., and Rubin, G.M. (2010). Refinement of tools for targeted gene expression in *Drosophila*. Genetics *186*, 735–755.

Reinders, J., Zahedi, R., Pfanner, N., Meisinger, C., and Sickmann, A. (2006). Toward the Complete Yeast Mitochondrial Proteome: Multidimensional Separation Techniques for Mitochondrial Proteomics. J. Proteome. Res. *5*, 1543–1554.

Robinson, K., Rothery, R., Weiner, J., and Lemire, B. (1994). The covalent attachment of FAD to the flavoprotein of *Saccharomyces cerevisiae* succinate dehydrogenase is not necessary for import and assembly into mitochondria. Eur. J. Biochem. *222*, 983–990.

Rutter, J., Winge, D.R., and Schiffman, J.D. (2010). Succinate dehydrogenase - Assembly, regulation and role in human disease. Mitochondrion *10*, 393–401.

Schapira, A.H. (2012). Mitochondrial diseases. Lancet *379*, 1825–1834.

Sickmann, A., Reinders, J., Wagner, Y., Joppich, C., Zahedi, R., Meyer, H.E., Schonfisch, B., Perschil, I., Chacinska, A., Guiard, B., et al. (2003). The proteome of *Saccharomyces cerevisiae* mitochondria. Proc. Natl. Acad. Sci. USA *100*, 13207–13212.

Tang, S., Le, P.K., Tse, S., Wallace, D.C., and Huang, T. (2009). Heterozygous mutation of Opa1 in *Drosophila* shortens lifespan mediated through increased reactive oxygen species production. PloS One *4*, e4492.

Walker, D.W., Hajek, P., Muffat, J., Knoepfle, D., Cornelison, S., Attardi, G., and Benzer, S. (2006). Hypersensitivity to oxygen and shortened lifespan in a *Drosophila* mitochondrial complex II mutant. Proc. Natl. Acad. Sci. USA *103*, 16382–16387.

Wodarz, A., Hinz, U., Engelbert, M., and Knust, E. (1995). Expression of crumbs confers apical character on plasma membrane domains of ectodermal epithelia of *Drosophila*. Cell *82*, 67–76.

CHAPTER 5

TWO LYR ASSEMBLY FACTORS MEDIATE MATURATION OF THE FES SUBUNIT OF SUCCINATE DEHYDROGENASE

Un Na*, Wendou Yu*, James E. Cox, Daniel K. Bricker, Knut Brockman, Jared Rutter, Carl S. Thummel, and Dennis R. Winge

*Un Na and Wendou Yu are co-first authors on this chapter, which has been submitted to Cell Metabolism for publication.

Summary

Disorders arising from impaired assembly of succinate dehydrogenase (SDH) result in a myriad of pathologies, consistent with its unique role in linking the citric acid cycle and electron transport chain. In spite of this critical function, however, only a few factors are known to be required for SDH assembly and function. We show here that two factors, Sdh6 (SDHAF1) and Sdh7 (SDHAF3), mediate maturation of the FeS cluster SDH subunit (Sdh2/SDHB). Yeast, *Drosophila* and mammalian cells lacking SDHAF3 are impaired in SDH activity with reduced levels of Sdh2. *Drosophila* lacking the Sdh7 ortholog SDHAF3 are hypersensitive to oxidative stress and exhibit muscular and neuronal dysfunction. Yeast studies revealed that Sdh6 and Sdh7 act together to promote Sdh2 maturation by binding to a Sdh1:Sdh2 intermediate, protecting it from the deleterious effects of oxidants. These studies in yeast, *Drosophila*, and mammalian cells raise the possibility that SDHAF3 mutations may be associated with idiopathic SDH-associated diseases.

Introduction

Succinate dehydrogenase (SDH) is an integral component of the mitochondrial respiratory chain and a component of the tricarboxylic acid (TCA) cycle. It catalyzes the two-electron oxidation of succinate to fumarate with the reduction of ubiquinone to ubiquinol (succinate:ubiquinone oxidoreductase). SDH is embedded within the inner membrane (IMM) of mitochondria and consists of four nuclear-encoded subunits, designated Sdh1 through Sdh4 in yeast and SDHA through SDHD in mammalian cells. SDH deficiency in humans results in infant encephalomyopathy and optic atrophy, myopathy or tumorigenesis in the adult (Finsterer, 2008; Rustin and Rotig, 2002). Germ

line loss-of-function mutations in human genes for SDHA, SDHB, SDHC, and SDHD are strongly linked with susceptibility to familial paraganglioma, pheochromocytoma, gastrointestinal stromal tumors, renal cell carcinoma, and neuroblastoma (Bardella et al., 2011; Baysal et al., 2000; Feichtinger et al., 2010; Janeway et al., 2011). Tumorigenesis arising from SDH-deficiency is purportedly related to the deleterious effects of supraphysiological levels of succinate, which is a known inhibitor of a myriad of a-ketoglutarate (aKG)-dependent enzymes including prolyl hydroxylases, histone demethylases, and DNA demethylases (Selak et al., 2005; Xiao et al., 2012).

The tetrameric enzyme contains five redox cofactors including a covalently bound FAD and three iron-sulfur clusters in a hydrophilic segment consisting of two subunits Sdh1 and Sdh2 and a membrane anchor domain consisting of Sdh3 and Sdh4 subunits with a heme moiety bound at the subunit interface (Robinson and Lemire, 1996). The Fe/S clusters form an electron wire to facilitate electron transfer to the ubiquinone-binding site formed between Sdh2 and the membrane anchor subunits (Sun et al., 2005).

Assembly factors are frequently used to facilitate cofactor insertion in mitochondrial respiratory complexes and mitigate unwanted reactions during biogenesis. Recently, two SDH assembly factors associated with human pathogenesis were identified. SDHAF1 was found in a study of infantile mitochondrial diseases in which two families presented with multiple afflicted children with leukoencephalopathy (Ghezzi et al., 2009). Biochemical analyses revealed a SDH deficiency in muscle samples and fibroblasts from these patients along with missense mutations in SDHAF1. Deletion of the yeast ortholog of *SDHAF1* (*SDH6*) resulted in a respiratory deficiency and a specific reduction in SDH activity (Ghezzi et al., 2009). SDH deficiency has subsequently been

reported in other patients that carry *SDHAF1* mutations (Ohlenbusch et al., 2012). SDHAF2 was shown to be required for the covalent attachment of FAD to the catalytic Sdh1 subunit (Hao et al., 2009). Yeast lacking Sdh5 were respiratory deficient due to the lack of SDH activity. Germline loss-of-function mutations in *SDHAF2* were identified in SDH-deficient, neuroendocrine paraganglioma tumors (Hao et al., 2009). A number of SDH-deficient pathologies, including Leigh syndrome, gastrointestinal stromal tumors, and neuroblastomas, have also been reported that lack mutations in known SDH assembly factors or SDH structural subunits (Feichtinger et al., 2010; Janeway et al., 2011). Thus, additional SDH assembly factors may remain to be discovered, potentially providing insights into the causes of idiopathic SDH-associated diseases.

Sdh6 is a member of the LYR protein family that consists of 10 proteins in the human proteome and four in the yeast proteome (Figure 5.1A). Within yeast, the founding member is the mitochondrial Isd11 protein that functions in the matrix FeS biogenesis pathway as an effector of the Nfs1 cysteine desulfurase (Adam et al., 2006; Wiedemann et al., 2006). We demonstrated that a second LYR protein Mzm1 is a chaperone for the Rieske FeS subunit of OXPHOS Complex III (Atkinson et al., 2011; Cui et al., 2012). The remaining yeast LYR proteins are Sdh6 and Acn9 (human ortholog Q9NRP4). Although Sdh6 is required for proper SDH activity, its molecular mechanisms remain unknown. Moreover, Acn9 (designated Sdh7 in yeast and SDHAF3 in humans) has no known function. Here we show that these two factors are required for SDH biogenesis in eukaryotes. Both Sdh6 and Sdh7 function in the maturation of the Fe/S cluster subunit Sdh2 in yeast and shields Sdh2 maturation from the deleterious effects of endogenous reactive oxygen species. We also report that loss of *SDHAF3* in *Drosophila*

Figure 5.1. Succinate dehydrogenase deficiency in cells lacking two LYR motif family proteins, Sdh6 and Sdh7.
(A) L-X-L/A-Y-R-X-X-L/I-R/K motif conserved in four LYR motif family proteins in yeast. Isd11, a chaperone required for cysteine desulfurase activity of Nfs1 in Fe/S biogenesis pathway (Adam et al., 2006); Mzm1, a protein facilitating the Rieske FeS protein insertion into bc_1 (Cui et al., 2012); Sdh6, an ortholog of human SDHAF1; Sdh7, a protein originally identified for normal acetate utilization in yeast (B) Ten-fold serial dilutions of cells starting from $OD_{600} = 0.5$ were spotted on synthetic complete (SC) media containing different carbon sources as indicated, and incubated at 30˚C. (C) Ten-fold serial dilutions of cells starting from $OD_{600} = 0.5$ were spotted on uracil (-) SC media and incubated at 30˚C. EV, empty vector (D) Metabolites extracted from cells cultured in synthetic minimal media containing 2% raffinose / 0.2% glucose were analyzed using GC/MS. Cells were harvested at $OD_{600} = 2$. Relative levels of metabolites to WT are represented as mean ± SEM ($N \geq 4$ biological replicates; *$p < 0.05$; **$p < 0.005$). (E) Relative SDH activity in isolated mitochondria compared to WT. Mitochondria were isolated from cells grown in SC media plus 2% raffinose / 0.2% glucose for 24 h (midlog) and 48 h (stationary). Succinate-dependent/quinone-mediated reduction of DCPIP was measured at 600 nm for SDH activity. Oxaloacetate-dependent oxidation of NADH was measured at 340 nm for MDH activity. Data are shown as mean ± SD is shown ($N = 3$; ** $p < 0.05$). (F) Blue-Native (BN) PAGE analysis to visualize protein complexes. Mitochondria isolated from the strains harvested at late-log phase were solubilized with 1% digitonin. After clarification, soluble fractions were separated on BN-PAGE and then transferred to membranes for detection of protein complexes using appropriate antibodies. Sdh1, a FAD-containing subunit of SDH; F1β, a subunit of ATP synthase in oxidative phosphorylation.

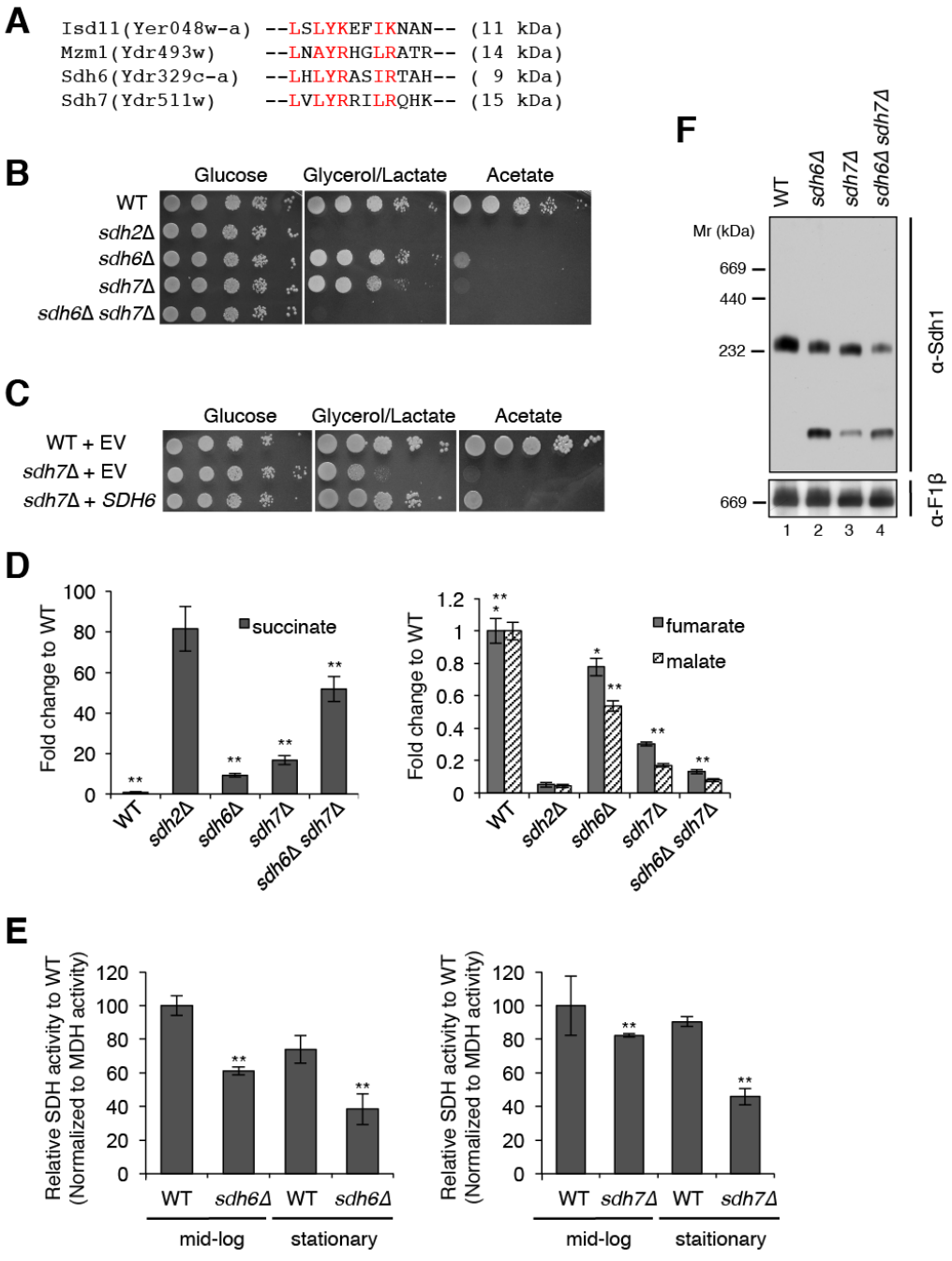
A
Isd11(Yer048w-a) --LSLYKEFIKNAN-- (11 kDa)
Mzm1(Ydr493w) --LNAYRHGLRATR-- (14 kDa)
Sdh6(Ydr329c-a) --LHLYRASIRTAH-- (9 kDa)
Sdh7(Ydr511w) --LVLYRRILRQHK-- (15 kDa)
B
Glucose
Glycerol/Lactate
Acetate
WT
sdh2Δ
sdh6Δ
sdh7Δ
sdh6Δ sdh7Δ
C
Glucose
Glycerol/Lactate
Acetate
WT + EV
sdh7Δ + EV
sdh7Δ + SDH6
D
Fold change to WT
succinate
fumarate
malate
WT
sdh2Δ
sdh6Δ
sdh7Δ
sdh6Δ sdh7Δ
E
Relative SDH activity to WT
(Normalized to MDH activity)
WT
sdh6Δ
WT
sdh6Δ
mid-log
stationary
Relative SDH activity to WT
(Normalized to MDH activity)
WT
sdh7Δ
WT
sdh7Δ
mid-log
staitionary
F
WT
sdh6Δ
sdh7Δ
sdh6Δ sdh7Δ
Mr (kDa)
669
440
232
669
α-Sdh1
α-F1β
1 2 3 4

or mammalian cells leads to a marked SDH-deficiency analogous to that in yeast, with defects in muscular and neuronal function in mutant flies. This study identifies two new SDH assembly factors, providing a more complete understanding of its critical role in cellular energy production and a potential molecular framework for defining currently idiopathic SDH-associated diseases.

Experimental procedures

Yeast strains and plasmids

S. cerevisiae strains used in this study are listed in Table 5.1. Yeast cells were grown in synthetic complete or minimal media containing 2% raffinose and 0.2% glucose unless indicated otherwise. Deletion strains were generated by homologous recombination and confirmed by PCR analysis of locus as described earlier (Longtine et al., 1998). Plasmids used in this study are listed in Table 5.2 and were constructed using general subcloning techniques.

Mammalian cell culture and siRNA

HEK293 cells fibroblasts were maintained in DMEM supplemented with 10% FBS, 100 units/ml penicillin, 100 mg/ml streptomycin, and 2 mM Glutamax at 37˚C in a humidified incubator with 5% CO_2. Transfection of siRNA was performed by treating cells with 10 nM total siRNA with Lipofectamine RNAiMax transfection reagent, according to the manufacturer's instructions (Invitrogen). ON-TARGETplus SDHAF1 siRNA SMARTpool and ON-TARGETplus Non-Targeting Pool were purchased from Dharmacon. Total RNA was isolated using the standard Trizol method. Total cDNA was

Table 5.1. Yeast strains used in this study.

Strain	Genotype	Source
WT (W303)	*MATa ade2-1 can1-100 his3-11,15 leu2-3,112 trp1-1 ura3-1*	
sdh6Δ	*MATa ade2-1 can1-100 his3-11,15 leu2-3,112 trp1-1 ura3-1 sdh6::KanMX6*	This study
sdh7Δ	*MATα ade2-1 can1-100 his3-11,15 leu2-3,112 trp1-1 ura3-1 sdh7::KanMX6*	This study
sdh6Δ sdh7Δ	*MATa ade2-1 can1-100 his3-11,15 leu2-3,112 trp1-1 ura3-1 sdh6::KanMX6 sdh7::URA3*	This study
sdh6Δ sdh7Δ	*MATa ade2-1 can1-100 his3-11,15 leu2-3,112 trp1-1 ura3-1 sdh6::KanMX6 sdh7::TRP1*	This study
sdh1Δ	*MatA his3 leu2 lys2 met15 trp1 ura3 sdh1::KanMX4*	Hao et al. 2009
sdh2Δ	*MATa ade2-1 can1-100 his3-11,15 leu2-3,112 trp1-1 ura3-1 sdh2::His3MX6*	This study
sdh2Δ sdh6Δ	*MATa ade2-1 can1-100 his3-11,15 leu2-3,112 trp1-1 ura3-1 sdh2::His3MX6 sdh6::KanMX6*	This study
sdh2Δ sdh7Δ	*MATa ade2-1 can1-100 his3-11,15 leu2-3,112 trp1-1 ura3-1 sdh2::His3MX6 sdh7::TRP1*	This study
sdh4Δ	*MATa ade2-1 can1-100 his3-11,15 leu2-3,112 trp1-1 ura3-1 sdh4::KanMX6*	This study
sdh4Δ sdh6Δ	*MATa ade2-1 can1-100 his3-11,15 leu2-3,112 trp1-1 ura3-1 sdh4::KanMX6 sdh6::His3MX6*	This study
sdh4Δ sdh7Δ	*MATa ade2-1 can1-100 his3-11,15 leu2-3,112 trp1-1 ura3-1 sdh4::KanMX6 sdh7::URA3*	This study
sdh3Δ	*MATa ade2-1 can1-100 his3-11,15 leu2-3,112 trp1-1 ura3-1 sdh3::KanMX6*	This study
sdh5Δ	*MATα ade2-1 can1-100 his3-11,15 leu2-3,112 trp1-1 ura3-1 sdh5::His3MX6*	Kim et al. 2012
sdh4Δ sdh5Δ	*MATα ade2-1 can1-100 his3-11,15 leu2-3,112 trp1-1 ura3-1 sdh4::KanMX6 sdh5::His3MX6*	This study
mzm1Δ	*MATα ade2-1 can1-100 his3-11,15 leu2-3,112 trp1-1 ura3-1 mzm1::URA3*	Dr. Aaron Atkinson

Table 5.2. Plasmids used in this study.

Plasmid	Source
pRS416 Sdh6-His_6-3HA	This study
pRS416 Sdh7-His_6-3HA	This study
pRS416 Sdh6-His_6-2Myc	This study
pRS415 Sdh7-His_6-2Myc	This study
pRS426 Sdh6-His_6-2Myc	This study
pRS426 Sdh7-His_6-2Myc	This study
pRS413 Sdh7-Myc	This study
pRS416 EV	Dr. David Stillman
pRS426 EV	Dr. David Stillman
pRS424 Sdh2	Dr. Jared Rutter
pRS424 EV	Dr. David Stillman
YEp351 EV	Dr. David Stillman
YEp351 Yap1	Dr. W. Scott Moye-Rowley

obtained using a High Capacity cDNA Reverse Transcription Kit with random oligomers (Applied Biosystems). TaqMan Probe-Based Gene Expression Analysis was performed to evaluate knockdown efficiency with probes purchased from Applied Biosystems using ABI PRISM 7000.

Metabolomic analysis

Metabolite profiling analysis was performed as described previously (Bricker et al., 2012). For yeast, overnight starter cultures in YPD medium were washed with sterile water, and then re-inoculated in synthetic minimal media containing 2% raffinose/0.2% glucose with appropriate auxotrophy if strains contained exogenous plasmids. The initial inoculation was at OD_{600} = 0.01. The cultures were grown to OD_{600} = 1 or 2 and metabolites were extracted as described (Canelas et al., 2009) for GC/MS analysis. For *Drosophila*, control wild-type *Canton S* flies and *dSdhaf3* mutants were collected at 5 days after eclosion and snap frozen in liquid nitrogen, using 20 male animals per sample and collecting six samples for each experiment, and the results presented are combined from two independent experiments.

Proteinase K assay

Mitochondrial aliquots (30 μg protein) were treated with 20 mM HEPES (pH 7.4) hypotonic buffer for swelling or lysised with hypotonic buffer containing 1% Triton X-100 for 30 min on ice in the presence or absence of proteinase K, respectively. Intact mitochondria were kept in 20 mM HEPES plus 0.6 M sorbitol in the presence or absence of proteinase K for 30 min on ice. Proteins were recovered by TCA precipitation and then

analysed by general procedures for immunoblotting.

High-copy suppressor screening

Genomic DNA isolated from *sdh6*Δ strains was partially digested with Sau3AI. 1 to 12 Kb fragments were recovered by gel extraction, which was subjected to ligation with high-copy pRS424 digested with BamH1. Approximately 60,000 colonies were recovered with ampicillin selection after *E. coli* transformation, and 40% of plasmids appeared to contain genomic DNA inserts based on blue-white screening and plasmid mapping. High copy plasmids were isolated as a pRS424 library using a Qiagen Maxi prep kit. The library was transformed to *sdh6*Δ strains. Approximately 30,000 colonies were obtained on synthetic complete (SC) glucose media lacking tryptophan. Colonies showing enhanced growths on SC acetate media lacking tryptophan after replica plating were selected and kept as a master collection. In order to verify that enhanced growth on acetate media was dependent on plasmids, drop-test was performed after plasmid shedding with 5-fluoroanthranilic acid (Toyn et al., 2000). Plasmids were recovered and sequenced only from colonies showing that their enhanced growths were dependent on plasmids.

Mitochondrial enzymatic activity assay

Succinate dehydrogenase (SDH) and aconitase activity assays were performed as described previously (Atkinson et al., 2011). To measure SDH activity, isolated mitochondria were incubated in 40 mM potassium phosphate (pH 7.4) buffer with 0.5% Tween 80, 20 mM succinate, and 20 μM antimycin A for 5 min at RT. The reaction was

initiated by adding 90 μM decylubiquinone and 120 μM dichlorophenolindophenol (DCPIP), and then the rate of reduction of DCPIP was measured spectrophotometrically at 600 nm for 5 min. Aconitase activity measured in soluble fractions of mitochondria disrupted by repetitive freeze-thaw with 100 μM cis-aconitate in 50 mM Tris (pH 7.4) at 240 nm. For malate dehydrogenase (MDH) activity assay, soluble mitochondrial fractions were obtained using sonication followed by centrifugation. Oxidation of 0.2 mM NADH was monitored in the presence of 2 mM oxaloacetate in 100 mM Tris (pH 7.4) at 340 nm (Hayes et al., 1991).

Mitochondrial protein import assay

Mitochondrial protein import assay was performed as described previously (Wagener et al., 2011). Briefly, *SDH2* and *RIP1* open reading frames were subcloned in pGEM-4Z for *in vitro* transcription/translation, respectively. Radiolabeled precursor proteins were obtained using reticulocyte lysate (Promega) in the presence of ^{35}S-Met. Precursors were imported into 75 μg of isolated mitochondria in 50 mM HEPES-KOH (pH 7.2) buffer containing 0.6 M sorbitol, 0.5 mg/ml BSA, 2 mM potassium phosphate, 75 mM KCl, 10 mM magnesium acetate, 2 mM EDTA, 2.5 mM $MnCl_2$, 2 mM ATP, 2 mM NADH, 10 mM creatine phosphate, 0.1 mg/ml creatine kinase, 2.5 mM malate, and 2.5 mM succinate for 30 min at 25˚C for pulse. Import was stopped by adding 5 μM valinomycin and then chased for the periods of time indicated. Nonimported precursors were removed by degradation using proteinase K after dilution with 20 mM HEPES-KOH (pH 7.2) plus 0.6 M sorbitol on ice. Samples were separated on SDS-PAGE and detected by autoradiography.

Co-immunoprecipitation

Mitochondria were solubilized in 10 mM sodium phosphate (pH 7.4), 500 mM NaCl, 1 mM EDTA, 1% digitonin and 1X protease inhibitor cocktail (Roche) for 30 min on ice. Crosslink was performed simultaneously with solubilization by adding 1 mM of Dithiobis[succinimidylpropionate] (Pierce) for 30 min at RT. Supernatants after centrifugation at 14,000 x g were incubated with magnetic anti-Myc beads (Cell Signaling Tech.) for 4 h at 4˚C. Beads were washed with 10 mM sodium phosphate (pH 7.4), 500 mM NaCl, 1 mM EDTA, 0.1 % digitonin, and 1 mM PMSF. After washing three times, bound substances were recovered by boiling with 2X SDS-PAGE sample buffer, which was subjected to immunoblotting.

Hydrogen peroxide sensitivity assay

Hydrogen peroxide sensitivity assay was performed as described previously (Khalimonchuk et al., 2007). Briefly, strains were precultured in YPD media up to late-log phase. Precultures were diluted by 2-fold in YPD and incubated for 2 h in the presence or absence of 6 mM H_2O_2. After washing with sterile water, 10-fold serial dilutions starting from OD_{600} = 0.5 were spotted on YPD plates and then incubated at 30^{o}C.

Miscellaneous Procedures

Yeast mitochondria isolation was performed using the method of Glick and Pon (Glick and Pon, 1995), and mammalian mitochondria isolation was performed as described previously (Chen et al., 2012). Standard procedures were performed for SDS-

PAGE and immunoblotting. BN-PAGE was performed as described previously with mitochondrial lysates in 1% digitonin solution (Wittig et al., 2006). Samples were separated on 4%–16% NativePAGE Bis-Tris Gel (Life technology) and transferred to PVDF membrane for immunodetection. Anti-Sdh1, Sdh2, and Sdh3 were from the previous study (Kim et al., 2012). Antibodies to Por1 were from Molecular Probes, and SDHA, SDHB, SDHC, and ATP5a were from Abcam. Protein concentration was determined by the Bradford assay.

Drosophila strains

Flies were maintained on standard Bloomington Stock Center medium with malt at 25˚C. The following stocks were obtained from the Bloomington Stock Center: *SdhA*^{HP21216}*/CyO* (Bloomington # 22087)*, SdhB*^{12081}*/CyO* (Walker et al., 2006) *da-Gal4* (Wodarz et al., 1995), *Act5C-Gal4/CyO* (Bloomington # 25374).

Generation of *dSdhaf3* mutant

dSdhaf3 mutants were generated using "ends-out" homologous recombination essentially as previously described (Maggert et al., 2008). The targeting vector was designed with 3 kb homology arms corresponding to the genomic sequence upstream of the *dSdhaf3* start codon and downstream of *dSdhaf3* exon 2, such that homologous recombination would cause the replacement of *dSdhaf3* exons 1–2 with the *miniwhite* marker. First, homology arms were amplified by PCR using Phusion Taq Polymerase (NEB) with the following primers: 5'' HA—CGGGCGCGCCAATACGAGCGAA TAACAACTGTT and CGCCTAGGGGAGCACTCCGTTCGTACT; 3' HA—

CGGCGGCCGCTTGTGCGATTCTTCAGCAAC and CGGGATCCAAAAGGCGC CATACTAAGCA. PCR products were then subcloned into Topo TA (Invitrogen) cloning vectors, after which, the presence of the correct flanking homology arms was verified by restriction digestion and DNA sequencing. Next, the 3' homology arm was excised from the Topo TA vector using BamHI and NotI, and ligated into a pW25.2 vector cut with the same enzymes. Following this step, the 5' homology arm was excised from the Topo TA vector using AvrII and AscI and ligated into the pW25.2 vector containing the 3' homology arm cut with the same enzymes. The presence of both homology arms was then verified by restriction digestion and used to generate transgenic flies using P-element mediated transformation.

Two strains containing the *dSdhaf3* targeting construct on the second chromosome over *CyO* (donor strain 1 and donor strain 2) were isolated and crossed to *yw; Flp, SceI, Noc/CyO* flies. Third instar progeny resulting from this cross were heat-shocked at 38˚C for 1 hr to induce *Flp* and *SceI* expression to drive target construct linearization and subsequent homologous recombination at the *dSdhaf3* locus. Once the heat-shocked larvae completed metamorphosis, *w+* mosaic females were crossed to *Flp; TM3/TM6, Ubx* flies. Individual *w+* progeny from these crosses were crossed to a Ap^{Xa} */SM5; TM3* stock to determine if the *miniwhite* marker had translocated to the 3rd chromosome. Two lines from donor strain 1, and five lines from donor strain 2 with *miniwhite* on chromosome 3 were isolated. The replacement of exons 1 and 2 in the *dSdhaf3* gene was then verified in one line derived from donor strain 2 strain by DNA sequencing and by Southern blot analysis. The ^{32}P-labeled probe for the Southern blot

experiment was generated by PCR amplification the using 5'-AACAAGTGATCCCA CCAAGC-3' and 5'-GGTGCAGAGCGTGTGTGTAT-3' oligonucleotide primers.

Generation of the *UAS-dSdhaf3* transgenic flies

The *dSdhaf3* cDNA was amplified from a commercially available plasmid (BDGP DGC gold RE23580) using the primers CGGAATTCTGAGTTTTTAGCCGGCTG and CGCTCGAGTACACTGATTTATTTGCCTTGC. The *dSdhaf3* cDNA amplicon was then cut with EcoRI and XhoI, and subsequently ligated into the pUAST plasmid cut with the same enzymes. The presence of the *dSdhaf3* cDNA in the pUAST plasmid was verified by restriction digestion and DNA sequencing, and was then used to generate transgenic lines by P-element mediated transformation.

Isolation of mitochondria from *Drosophila*

Mitochondria for western blot studies or SDH assays were purified from flies as described with modifications (Schwarze et al., 1998). Briefly, 200–300 flies per sample were homogenized gently 20 times with an A type dounce pestle in cold mitochondrial isolation media (250 mM sucrose, 10 mM Tris pH 7.4, 1 mM EDTA). These homogenates were centrifuged at 1000 g for 1 min through a 40 μM cell strainer (#352340, BD Falcon Franklin Lakes, NJ) in a 50 ml tube to remove cuticle debris, followed by a second centrifugation at 1000 g at 4˚C for 5 min to remove cell debris. Mitochondrial pellets were obtained by centrifugation at 13,000 g at 4˚C for 5 min and then resuspended in 1 ml mitochondrial isolation medium. The protein concentration was determined using Bio-Rad Protein Assay Dye Reagent (Cat#: 500-0006). Mitochondrial

pellets were stored frozen for western blot analysis or resuspended in incubation medium (220 mM sucrose, 5 mM KH_2PO_4, 20 mM KCl, 10 mM HEPES, pH 7.2) for enzyme activity assays and stored at -80˚C.

Drosophila SDH activity assay

Succinate dehydrogenase activity in mitochondrial extracts was measured using a colorimetric-continuous method, essentially as described (Munujos et al., 1993). This method uses iodonitrotetrazolium chloride as an electron acceptor and measures its reduction at 500 nm in the presence or absence of succinate. Enzyme activity is presented as the percentage of control w^{1118} flies from three independent experiments, using six replicates for each sample.

Western blot analysis of *Drosophila* mitochondrial proteins

Purified mitochondrial pellets were resuspended in RIPA buffer (50 mM Tris–HCl, pH 7.4, 150 mM NaCl, 1 mM EDTA, 1% Triton X-100, 0.5% sodium deoxycholate, 0.1% sodium dodecyl sulfate) and dissolved in sample buffer (50 mM Tris–HCl, pH 6.8, 2% SDS, 10% glycerol, 1% β-mercaptoethanol, 12.5 mM EDTA, 0.02 % bromophenol blue) for SDS-PAGE. Western blot and chemiluminescence were performed as described (Yu et al., 2012). Rabbit anti-Human SdhA polyclonal antibody (1:1500) and mouse anti-Bovine ATP5 monoclonal antibody (1:10,000) were purchased from Abcam. Rabbit anti-SdhB antibody (1:1500) was raised against yeast Sdh2 for use in this study.

Drosophila motility assays

The climbing assay was performed essentially as described (Gargano et al., 2005). Briefly, 20 animals per vial were raised on standard medium and transferred to empty vials, with a line drawn four centimeters from the bottom of the vial. Flies were then tapped down gently to the bottom of the vial and allowed to climb for 10 seconds. Videos of the climbing flies were replayed for quantification, scoring the number of flies that climbed above the line after 5 seconds. Flies in four vials were assayed under each condition, and all experiments were repeated three times. Recovery from paralysis was assayed essentially as described previously (Ganetzky and Wu, 1982). Briefly, 20 animals per vial were raised on standard medium and transferred to empty vials. The vials were vortexed for 30 seconds after which the flies were allowed to recover. Videos were replayed for quantification, scoring the number of flies that moved away from the bottom of the vials after 10 sec. Flies in four vials were assayed under each condition, and all experiments were repeated three times.

Drosophila lifespan analyses

Vials containing 20 five-day old male or female control w^{1118} flies or *dSdhaf3* mutants were transferred to vials with 1% agar in PBS for starvation, 5% ethanol, 1% agar in PBS for alcohol treatment, or 30 mM paraquat in semidefined medium (Backhaus et al., 1984) for paraquat treatment (Rzezniczak et al., 2011). Surviving animals were scored every 24 h except animals subjected to starvation, which were assayed at 12 h intervals. The hyperoxia experiments were performed by transferring flies to vials with fresh medium and then sealing the vials in a polyethylene bag (Scienceware 12” x 16”)

filled with 100% oxygen. Surviving animals were scored every 24 h and the bags were filled with fresh oxygen. In all experiments, flies were scored from 15–20 vials of flies per experiment, from 3–5 independent experiments.

Statistics

Yeast data were analyzed using Microsoft Excel 2011. Data are presented as mean ± SD or mean ± SEM as indicated. Statistical significance was evaluated using Student's test. $p < 0.05$ was considered significant. Statistical analysis and graphical presentation for *Drosophila* studies were performed using PRISM software. Student's t test was used for pairwise comparisons, and one-way analysis of variance (ANOVA) was used for multiple comparisons. Fly metabolomic data are graphically represented as box plots, with the box representing the lower and upper quartiles, the horizontal line representing the median, and the bars representing the minimum and maximum data points. All other data are shown as the mean ± SEM.

Results

Cells lacking Sdh6 and Sdh7 exhibit SDH deficiency

As a first step toward characterizing Sdh6 and Sdh7 function, we examined the growth phenotypes of *sdh6*Δ or *sdh7*Δ mutants on nonfermentable carbon sources using *S. cerevisiae*. Cells lacking Sdh6 or Sdh7 exhibit a partial growth defect on glycerol/lactate media and a severe growth defect on acetate medium compared to wild-type cells (Figure 5.1B), which is consistent with previous studies (Ghezzi et al., 2009; McCammon, 1996). We confirmed that the respiratory growth defects of *sdh6*Δ and

*sdh7*Δ mutants were attributed to deletions of *SDH6* and *SDH7,* as respiratory growth of *sdh6*Δ and *sdh7*Δ cells was restored with epitope-tagged Sdh6 and Sdh7, respectively (Figure 5.2). Since both Sdh6 and Sdh7 belong to the LYR motif protein family, we looked for genetic interactions between their encoded proteins (Figure 5.1A). The *sdh6*Δ *sdh7*Δ double deletion strain exhibited a marked synthetic growth defect on glycerol/lactate medium (Figure 5.1B). In addition, the overexpression of *SDH6* partially suppressed the respiratory growth defect of *sdh7*Δ cells (Figure 5.1C); however, overexpression of *SDH7* failed to restore respiratory function of *sdh6*Δ cells (data not shown).

Metabolomic profiling was used to identify the biological process impaired in *sdh6*Δ and *sdh7*Δ mutants, assaying the levels of approximately 100 polar metabolites. We cultured cells in synthetic minimal medium with 2% raffinose and 0.2% glucose up to stationary phase. Metabolites extracted from cells were analyzed using gas chromatography-mass spectrometry (GC/MS) (Figure 5.1D). Cells lacking either Sdh6 or Sdh7 exhibited elevated succinate levels and attenuated fumarate and malate levels consistent with impaired conversion of succinate to fumarate by SDH in the citric acid cycle. These observations in *sdh6*Δ cells are consistent with the previous study in fibroblasts harboring mutations in *SDHAF1* gene, which is the human *SDH6* ortholog (Ghezzi et al., 2009). Moreover, the *sdh6*Δ *sdh7*Δ double mutant showed an enhanced accumulation in succinate, consistent with the synergistic respiratory growth defects in these cells.

To confirm that the increased succinate/fumarate ratio in *sdh7*Δ mutants was due to impaired SDH function, we quantified SDH activity in mitochondria purified from

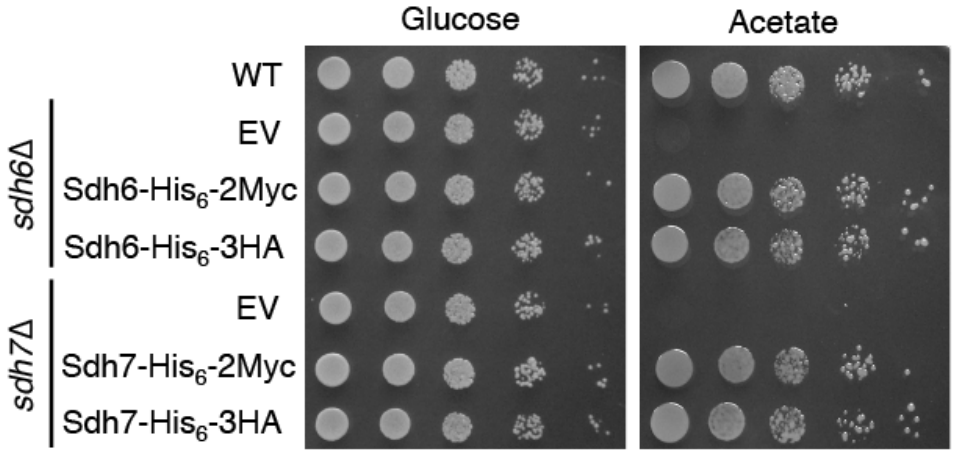

Figure 5.2. Complementation of *sdh6*Δ and *sdh7*Δ mutants with exogenously expressed epitope-tagged Sdh6 and Sdh7, respectively.
Low-copy plasmids with either *MET25* promoter for His_6-2Myc or own endogenous promoters for His_6-3HA were transformed. Ten-fold dilutions starting from OD_{600} = 0.5 were spotted on synthetic complete media containing carbon sources indicnated, and then incubated at 30˚C.

wild-type (WT) and mutant cells lacking Sdh6 or Sdh7. Mitochondria isolated from *sdh6*Δ and *sdh7*Δ cells harvested at midlog phase exhibited modest diminutions of SDH activity, but the deficit was magnified in stationary phase cells (Figure 5.1E). In addition, *sdh6*Δ *sdh7*Δ double mutants showed markedly decreased SDH activity (34% of WT, data not shown) relative to the single mutants in accordance with the synergistic respiratory growth defect and TCA cycle intermediates in *sdh6*Δ *sdh7*Δ double mutants. Enzymatic activities of pyruvate dehydrogenase, α-ketoglutarate dehydrogenase, aconitase, malate dehydrogenase, and bc_1 Complex III were unaffected in cells lacking Sdh6 or Sdh7 (data not shown).

A moderate diminution of the assembled tetrameric SDH complex was seen in mitochondria isolated from late-log cultures of *sdh6*Δ or *sdh7*Δ mutants as visualized by BN-PAGE (Figure 5.1F). The abundance of the SDH complex was further attenuated in *sdh6*Δ *sdh7*Δ double mutant cells. Thus, Sdh6 and Sdh7 are required to maintain normal SDH levels and activity in yeast. In addition to reduced levels of tetrameric SDH in the mutant cells, a Sdh1 subcomplex is evident, and the same subcomplex is seen in cells lacking Sdh2 or Sdh4 (Figures 5.1F and 5.2). Therefore, Sdh6 and Sdh7 may function in SDH assembly rather than the regulation of SDH activity.

Maturation of Sdh2, an SDH subunit containing Fe/S clusters, is impaired in the absence of Sdh6 or Sdh7

To further characterize the roles of Sdh6 and Sdh7, the steady-state levels of SDH subunits were quantified in mitochondria isolated from mutant cells. The levels of Sdh2 were attenuated in both *sdh6*Δ and *sdh7*Δ mutants and further diminished in the *sdh6*Δ

*sdh7*Δ double mutant (Figure 5.3A). Sdh1 levels were unchanged in the mutant cells and covalent flavinylation of Sdh1 was not significantly altered (Figures 5.3A and 5.4). We demonstrated previously that cells lacking Sdh5 were compromised in Sdh1 flavinylation leading to a reduced stability of Sdh1 (Hao et al., 2009; Kim et al., 2012).

A mitochondrial *in vitro* protein import assay was used to address a role of Sdh6 and Sdh7 in Sdh2 maturation. The import assay consisted of the *in vitro* import of ^{35}S-methionine labeled Sdh2 into purified mitochondria isolated from *sdh2*Δ cells. Sdh2-deficient mitochondria were used to ensure that unassociated Sdh1 pool would be available for a stabilizing interaction with imported Sdh2. Furthermore, any changes in the mitochondrial membrane potential, which drives protein import, due to already decreased SDH activities in *sdh6*Δ mutants and *sdh7*Δ mutants are negated by using *sdh2*Δ cells. The stability of ^{35}S-Sdh2 as monitored during the chase phase of the reaction was compromised in cells lacking Sdh6 or Sdh7 especially in mitochondria isolated from stationary phase cultures (Figure 5.3B). This result is consistent with the exacerbated defect in SDH activity seen in mutant cells at late stages of growth. Unlike Sdh2, radioisotope-labeled Rip1, a target of the LYR protein Mzm1, remained unaffected by loss of either Sdh6 or Sdh7.

A subcomplex of Sdh1 and Sdh2 is known to accumulate in cells lacking the membrane anchor subunits Sdh3 and/or Sdh4 (Kim et al., 2012) (Figure 5.3D, compare lanes 1 and 3). We observed that cells depleted of the membrane anchor contain increased steady-state levels of both Sdh6 and Sdh7 (Figure 5.3C). The increased levels of Sdh6 and Sdh7 in cells accumulating an Sdh1/Sdh2 subcomplex led us to speculate

Figure 5.3. Sdh6 or Sdh7 functions are linked to the Fe/S Sdh2 subunit.
(A) Steady-state levels of mitochondrial proteins. FAD-containing Sdh1 was visualized by UV excitation. Other proteins visualized by immunoblotting include Mdh1, malate dehydrogenase and Por1 (a protein constituting voltage-dependent anion channel). (B) ^{35}S-methionine labeled proteins were incubated with isolated mitochondria for 30 min (pulse), followed by blocking protein import with valinomycin for 30 and 60 min (chase), respectively. Radiolabeled proteins were resolved on SDS-PAGE and detected by autoradiography. (C) Functional Sdh6-His_6-3HA or Sdh7-His_6-3HA under their own endogenous promoters was expressed from plasmids in cells lacking either Sdh2 or Sdh4 along with endogenous Sdh6 or Sdh7 depleted, respectively. Steady-state levels are shown by immunoblotting. (D) Co-immunoprecipitation of Sdh6-His_6-2Myc after crosslinking. Mitochondria were solubilized with 1% digitonin in the presence of 1 mM dithiobis[succinimidylpropionate]. The crosslinking reaction was stopped with Tris buffer (pH 7.4), and the supernatants were absorbed to anti-Myc antibody-conjugated magnetic beads. Bound substances to Myc beads were resolved on SDS-PAGE and detected by immunoblotting. Input, 4% of total lysates; Aco1, 4Fe-4S aconitase. (E) Standard co-immunoprecipitation of Sdh7-His_6-2Myc was performed with isolated mitochondria without crosslinking. Input, 2% of total lysates. (F) Steady-state levels of Sdh2 in *sdh1*Δ mutants with overexpression of proteins indicated. Yap1, transcription factor up-regulating oxidative stress response genes. (G) SDH activity in *sdh6*Δ mutants with *SDH2* overexpression was detected spectroscopically as described in Figure 5.1E. Data are represented as mean ± SD (N = 3). (H) Succinate levels in *sdh7*Δ mutants with *SDH2* overexpression were measured as described in Figure 5.1D. Mean ± SEM is shown (N=6).

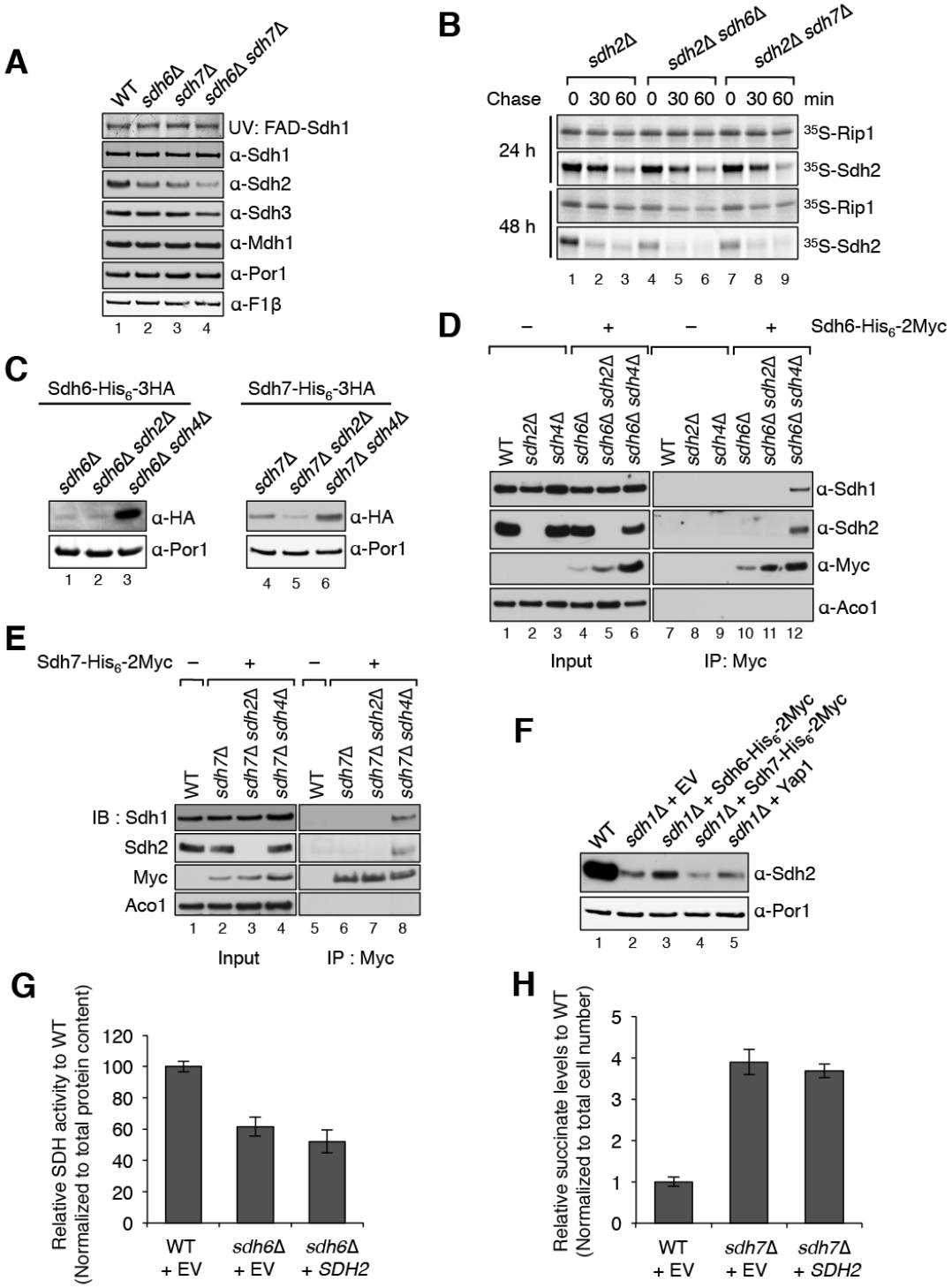
A
WT
sdh6Δ
sdh7Δ
sdh6Δ sdh7Δ
UV: FAD-Sdh1
α-Sdh1
α-Sdh2
α-Sdh3
α-Mdh1
α-Por1
α-F1β
1 2 3 4
B
sdh2Δ
sdh2Δ sdh6Δ
sdh2Δ sdh7Δ
Chase 0 30 60 0 30 60 0 30 60 min
24 h
48 h
35S-Rip1
35S-Sdh2
35S-Rip1
35S-Sdh2
1 2 3 4 5 6 7 8 9
C
Sdh6-His6-3HA
Sdh7-His6-3HA
sdh6Δ
sdh6Δ sdh2Δ
sdh6Δ sdh4Δ
sdh7Δ
sdh7Δ sdh2Δ
sdh7Δ sdh4Δ
α-HA
α-Por1
1 2 3
4 5 6
D
Sdh6-His6-2Myc
WT
sdh2Δ
sdh4Δ
sdh6Δ
sdh6Δ sdh2Δ
sdh6Δ sdh4Δ
α-Sdh1
α-Sdh2
α-Myc
α-Aco1
1 2 3 4 5 6 7 8 9 10 11 12
Input
IP: Myc
E
Sdh7-His6-2Myc
WT
sdh7Δ
sdh7Δ sdh2Δ
sdh7Δ sdh4Δ
IB : Sdh1
Sdh2
Myc
Aco1
1 2 3 4 5 6 7 8
Input
IP : Myc
F
WT
sdh1Δ + EV
sdh1Δ + Sdh6-His6-2Myc
sdh1Δ + Sdh7-His6-2Myc
sdh1Δ + Yap1
α-Sdh2
α-Por1
1 2 3 4 5
G
Relative SDH activity to WT
(Normalized to total protein content)
120
100
80
60
40
20
0
WT + EV
sdh6Δ + EV
sdh6Δ + SDH2
H
Relative succinate levels to WT
(Normalized to total cell number)
5
4
3
2
1
0
WT + EV
sdh7Δ + EV
sdh7Δ + SDH2

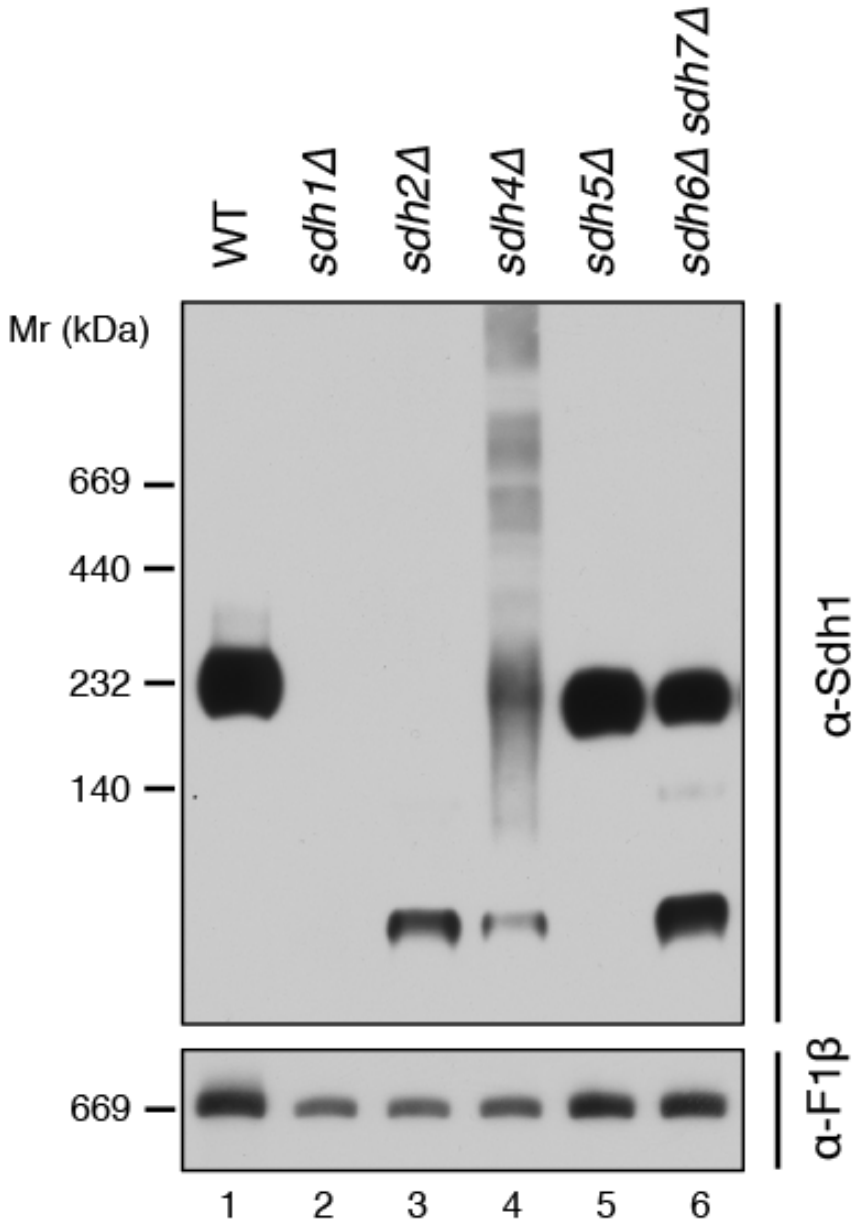

Figure 5.4. BN-PAGE analysis of respiratory complexes.
Mitochondria from the strains were solubilized with 1% digitonin. Soluble fractions were separated on BN-PAGE and transferred to membranes for detection of protein complexes using appropriate antibodies. Sdh1, a subunit of SDH; F1β, a subunit of Complex V.

that Sdh6 and Sdh7 may interact with the Sdh1/Sdh2 subcomplex. We performed co-immunoprecipitation on epitope-tagged Sdh6 and Sdh7 in mitochondria from WT cells and cells stalled in SDH assembly. A fraction of Sdh1 and Sdh2 were copurified with either Sdh6 or Sdh7 from cells lacking the membrane anchor domain but not in cells devoid of Sdh2 (Figures 5.3D, 5.3E, and 5.5A). These interactions are seen in the presence and absence of crosslinking prior to resin adsorption. These results suggest that Sdh6 and Sdh7 interact with Sdh2 within a Sdh1/Sdh2 subcomplex. Moreover, these interactions appear to occur in the mitochondrial matrix, consistent with the known matrix location of Sdh1, Sdh2, and Sdh6 (Ghezzi et al., 2009). Sdh7 is also a matrix protein as revealed by proteinase K treatment of purified mitochondria, which degrades Sdh7 only in the presence of detergents and not upon hypotonic disruption of only the outer membrane (Figure 5.5B).

The physical interactions of Sdh6 and Sdh7 with Sdh2 prompted the hypothesis that Sdh6 and Sdh7 may be chaperones for Sdh2. To test this, we first examined the ability of overexpressed Sdh6 or Sdh7 to stabilize the highly labile Sdh2 present in *sdh1*Δ cells (Kim et al., 2012). Elevated levels of Sdh6, but not Sdh7, led to increased steady-state Sdh2 levels under these conditions (Figure 5.3F). This result raised a possibility that Sdh6 may function as a chaperone for Sdh2 prior to its interaction with Sdh1. We tested whether *SDH2* overexpression in *sdh6*Δ mutants or *sdh7*Δ mutants would restore SDH activity and suppress the respiratory growth defects. However, *SDH2* overexpression neither restored SDH activity nor reversed succinate accumulation or rescued respiratory growth of *sdh6*Δ mutants and *sdh7*Δ mutants (Figure 5.3G, 5.3H, and 5.6A–5.6C).

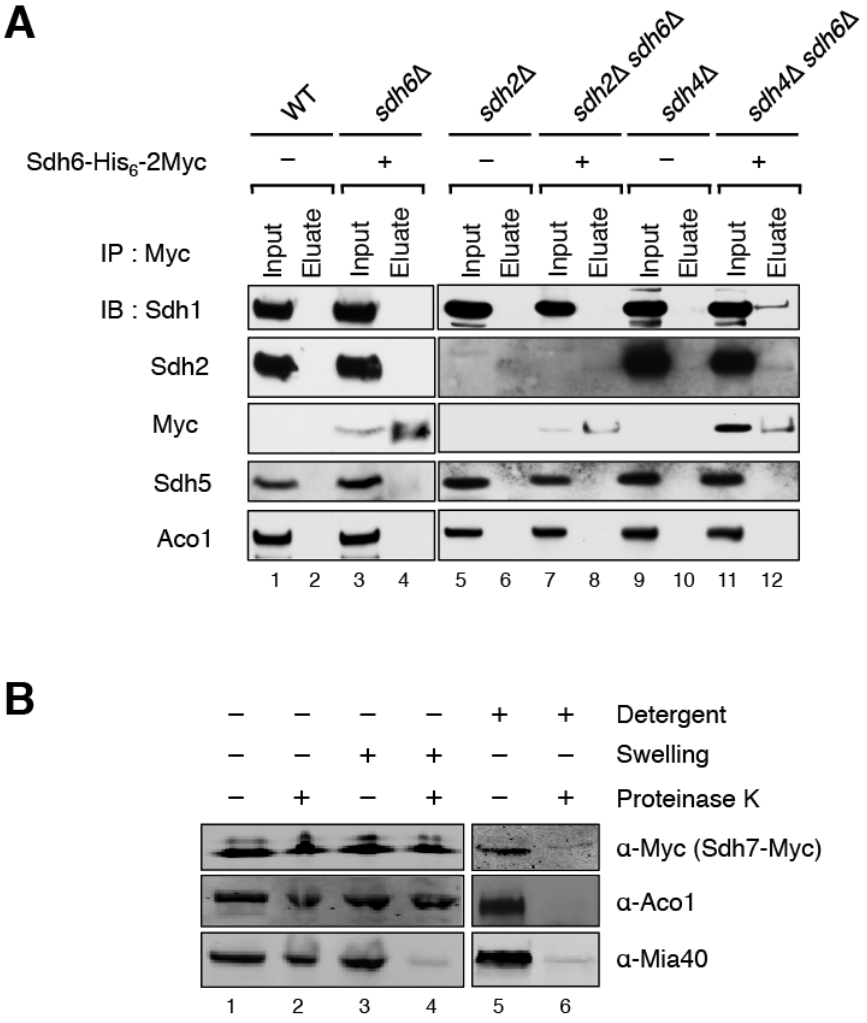

Figure 5.5. Co-immunoprecipitation of Sdh6-His$_6$-2Myc in various strains and localization study of Sdh7.
(A) Mitochondrial lysates were obtained after solubilization with 1% digitonin, which were subjected to anti-Myc antibody-conjugated magnetic beads. Bound substances to Myc antibody beads were resolved on SDS-PAGE and detected by immunoblotting. Load, 4% of total lysates. (B) Proteinase K assay to assess the localization of Sdh7. Sdh7-Myc was expressed in *sdh7*Δ mutants and mitochondria were isolated. Intact mitochodria, hyoptonic buffer treated mitochondria, and 1% Triton X-100 treated mitochondria were incubated with proteinase K for 30 min on ice. Sample were resolved on SDS-PAGE. Aco1, a soluble mitochondrial matrix protein; Mia40, a mitochondrial intermembrane space protein.

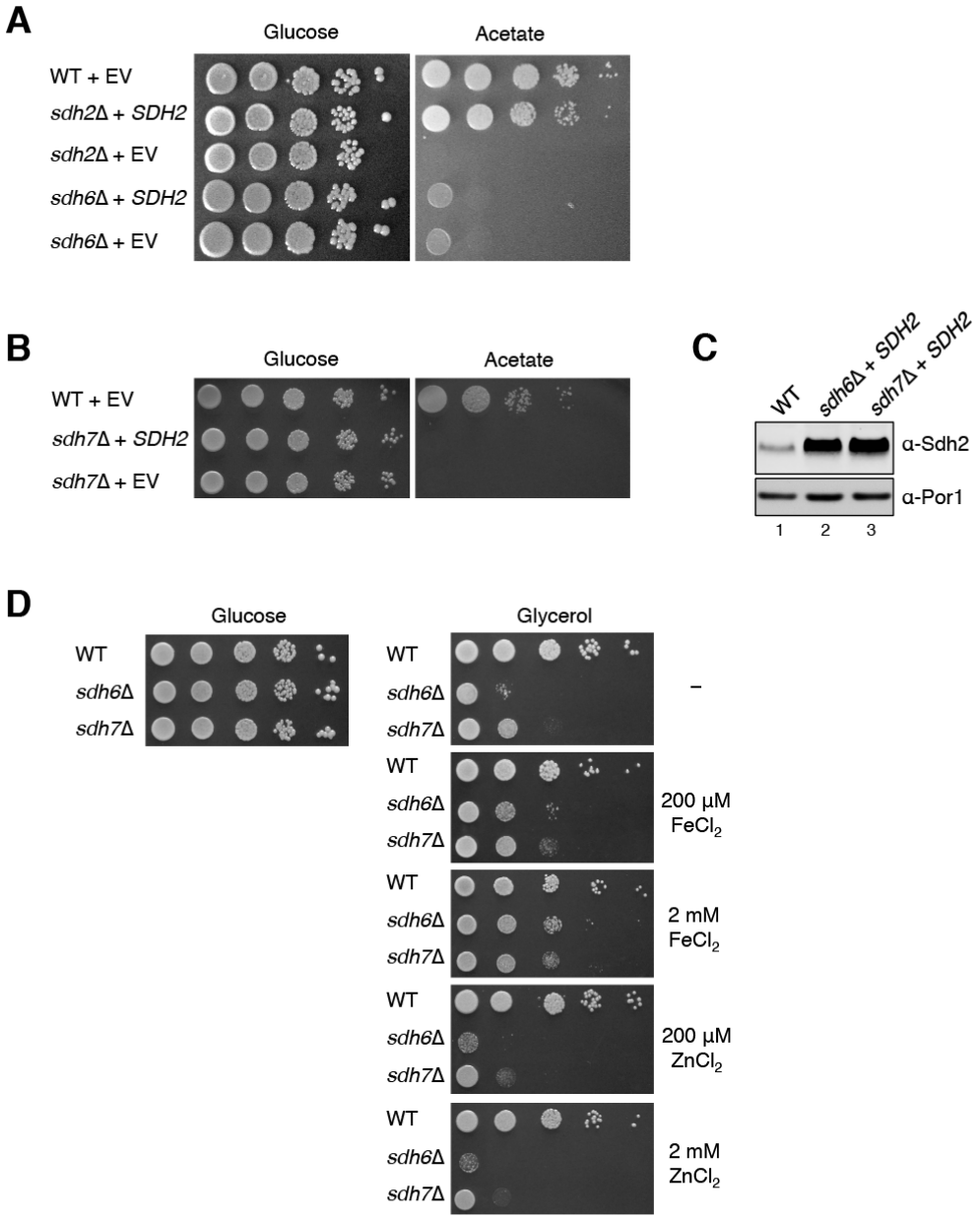

Figure 5.6. Growth tests of *sdh6*Δ mutants and *sdh7*Δ mutants with *SDH2* overexpression and iron supplementation

(A,B). Cell harboring either high-copy *SDH2* plasmid or empty vector (EV) were spotted on synthetic complete media by 10-fold serial dilutions, and incubated at 30˚C. (C) Steady-state levels of Sdh2 overexpressed. (D) Enhanced respiratory growths of *sdh6*Δ mutants and *sdh7*Δ mutants with iron supplementation 10-fold serial dilutions of cells starting from $OD_{600} = 0.5$ were spotted on synthetic complete media ± $FeCl_2$ or $ZnCl_2$ as concentrations indicated, and then incubated at 30˚C.

These results suggest that Sdh6 and Sdh7 may have a more active role in Sdh2 maturation.

Antioxidants ameliorate defects in *sdh6*Δ mutants and *sdh7*Δ mutants

Further clues to the function of Sdh6 emerged from a genetic suppressor study in which extragenic suppressors of the acetate growth defect of *sdh6*Δ mutants were recovered. We generated a high-copy plasmid library with partially digested genomic DNA from *sdh6*Δ mutants. This library was transformed to *sdh6*Δ mutants and the transformants that exhibited enhanced growth on acetate medium were collected. Interestingly, multiple independent suppressors were recovered that encoded Yap1, which is a transcriptional activator that induces the expression of a battery of antioxidant genes, including thioredoxin, thioredoxin reductase and glutathione reductase, in response to oxidative stress (Fernandes et al., 1997). The overexpression of *YAP1* in subcloned vectors robustly suppressed the acetate growth defect of cells lacking Sdh6 (Figure 5.7A). Consistent with the antioxidant role of Yap1 expression, supplemental glutathione or N-acetyl-cysteine also restored limited respiratory growth in *sdh6*Δ mutants (Figure 5.7B).

Since we observed a genetic interaction between *SDH6* and *SDH7*, we tested whether overexpression of *YAP1* could also restore respiratory growth in *sdh7*Δ mutants. Indeed, *YAP1* overexpression suppressed the respiratory growth defect of *sdh7*Δ mutants, although the suppression was less pronounced compared to *sdh6*Δ mutants (Figure 5.7A). Moreover, the addition of exogenous reductants restored limited respiratory growth of

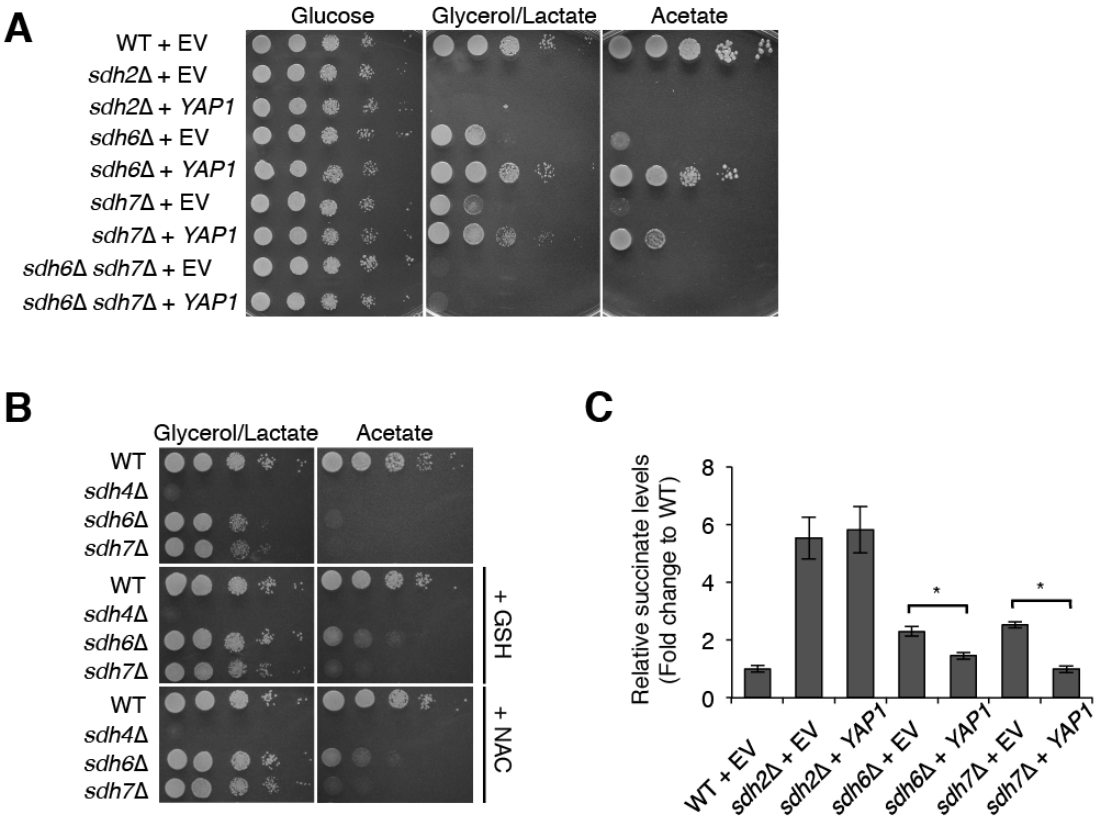

Figure 5.7. Exogenous antioxidants rescue the growth defect of *sdh6*Δ and *sdh7*Δ mutants.

(A) Cells harboring either empty vector (EV) or high-copy *YAP1* plasmid were spotted on SC media lacking leucine by 10-fold serial dilutions and incubated at 30˚C. (B) 10-fold serial dilutions of cells were spotted on SC media ± 5 mM N-acetyl cysteine or 2 mM glutathione and incubated at 30˚C. (C) Succinate levels in cells overexpressing *YAP1* were measured as described in Figure 5.1D. Cells were harvested at OD_{600} = 1. Mean ± SEM is shown (N = 6; *p < 0.005).

*sdh7*Δ mutants (Figure 5.7B). To confirm that *YAP1* overexpression restored SDH activity in *sdh6*Δ and *sdh7*Δ single mutant cells, we assessed SDH activity by measuring succinate levels using metabolomics. Indeed, *YAP1* overexpression decreased succinate levels in both *sdh6*Δ and *sdh7*Δ mutants significantly, while *YAP1* overexpression did not affect succinate levels in *sdh2*Δ mutants as a negative control (Figure 5.7C). Therefore, we conclude that *YAP1* overexpression contributes to the restoration of SDH activity in *sdh6*Δ and *sdh7*Δ mutants. Elevated levels of Yap1, however, have no effect on the respiratory growth defects in *sdh6*Δ *sdh7*Δ double mutants (Figure 5.7A).

Stabilization of Sdh2 by Sdh6 and Sdh7 is manifested under oxidative stress conditions

We hypothesized that Sdh6 and Sdh7 may be important for Sdh2 maturation under oxidative stress conditions. Initially, we tested whether cells lacking Sdh6 or Sdh7 were hypersensitive to the superoxide anion generator paraquat. The respiratory growth defect of *sdh6*Δ and *sdh7*Δ single mutants was dramatically exacerbated in the presence of paraquat (Figure 5.8A). Likewise, steady-state levels of Sdh2 were markedly attenuated in paraquat-treated *sdh6*Δ and *sdh7*Δ mutants compared to WT cells (Figure 5.8B). In contrast, steady-state levels of other mitochondrial Fe/S containing proteins were not significantly altered by paraquat in the mutant cells (Figure 5.8B).

The paraquat sensitivity of *sdh6*Δ and *sdh7*Δ mutants may arise from either enhanced ROS damage or the accumulation of a pro-oxidant in the mutants. We observed that ROS levels were not changed in untreated *sdh6*Δ and *sdh7*Δ mutants using

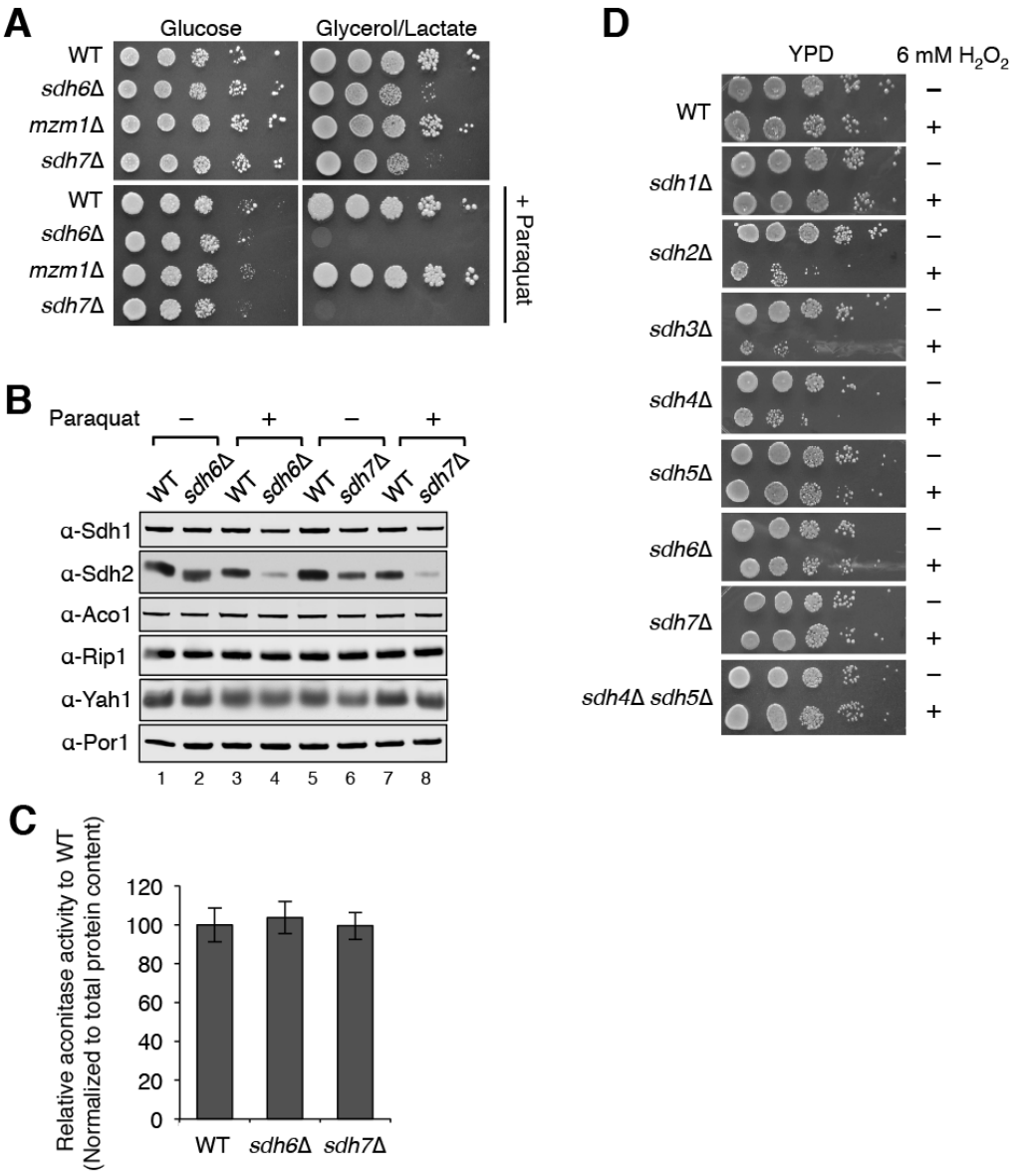

Figure 5.8. *sdh6*Δ and *sdh7*Δ mutants are sensitive to oxidative stress.
(A) Ten-fold serial dilutions of cells were spotted on SC media ± 2 mM paraquat with indicated carbon sources and incubated at 30˚C. (B) Steady-state levels of proteins in mitochondria isolated from strains cultured in SC media with 2% raffinose / 0.2% glucose supplemented with 2 mM paraquat. Yah1, ferredoxin of the mitochondrial matrix. (C) Aconitase activity specific to *cis*-aconitate conversion in isolated mitochondria. Data are shown as mean ± SD (N = 3). (D) Precultures grown up to late-log phase in YPD media were diluted 2-fold, followed by addition of 6 mM H_2O_2 and incubated for 2 h at 30˚C. Cells were washed with sterile water and 10-fold serial dilutions were spotted on YPD plate, followed by incubation at 30˚C.

two different assays. First, we quantified aconitase (Aco1) activity. The 4Fe-4S cluster in aconitase is susceptible to ROS damage (Gardner, 2002); thus aconitase activity is an indicator of ROS stress *in vivo*. We did not observe a diminution of aconitase activity in *sdh6*Δ and *sdh7*Δ mutants compared to WT (Figure 5.8C). Second, we tested the mutant cells for hydrogen peroxide sensitivity on rich glucose medium. As cells accumulate ROS, they become sensitized to exogenous ROS and subsequently lose viability (Khalimonchuk et al., 2007). After a 2-hour treatment of cells with 6 mM H_2O_2, the viability of *sdh2*Δ, *sdh3*Δ, and *sdh4*Δ mutant strains was significantly compromised (Figure 5.8D). However, *sdh6*Δ and *sdh7*Δ mutant cells exhibited no growth defects. The lack of impairment in aconitase activity and hydrogen peroxidase sensitivity suggest that ROS levels are not elevated in *sdh6*Δ and *sdh7*Δ mutants as compared to WT cells. It is noteworthy that *sdh1*Δ and *sdh5*Δ single mutants and the *sdh4*Δ *sdh5*Δ double mutant did not show hydrogen peroxide sensitivity compared to *sdh2*Δ, *sdh3*Δ, and *sdh4*Δ strains, which suggests that an assembly intermediate containing FAD-Sdh1 may be the source for electron leakage for the generation of ROS in *sdh2*Δ, *sdh3*Δ, and *sdh4*Δ single mutants.

<u>*Drosophila Sdhaf3* mutants are sensitive to oxidative stress</u>

The *Drosophila* genome encodes a close ortholog of Sdh7 (Figure 5.9A), but has only a weak candidate homolog of Sdh6. Accordingly, we examined the functions of Sdh7 in *Drosophila* to determine if its roles in SDH assembly and activity have been conserved through evolution and to define its possible physiological functions. Gene targeting was used to generate a null mutation in the *Drosophila sdh7* ortholog

Figure 5.9. Generation and characterization of *dSdhaf3* null mutants
(A) Amino acid sequence alignment of Sdh7 orthologs in eukaryotes using Clustal Omega. (B) Gene targeting was used to disrupt the *dSdhaf3* locus. A *miniwhite* selectable marker was flanked by two 3 kb regions of homology to the *dSdhaf3* locus (5'HA and 3'HA), resulting in the deletion of 339 bp of *dSdhaf3* coding region upon homologous recombination. (C) The structure of the mutated *dSdhaf3* locus was confirmed by Southern blot hybridization. Genomic DNA was isolated from three genetic backgrounds: (1) w^{1118} control flies, (2) two independent transformant lines that carry the *dSdhaf3* targeting construct integrated randomly in the genome (donor strains 1 and 2), and (3) the *dSdhaf3* deletion mutant generated using donor strain #2 (see Supplemental Experimental Procedures). The DNA was cut using *HindII* and *EcoRV* restriction endonucleases and analyzed by Southern blot hybridization using probes to detect the 5' and 3' regions of the dSdhaf3 locus. These probes will detect a 2.8 kb fragment from the wild-type locus, and 0.73 and 3.4 kb fragments from the disrupted gene containing the miniwhite marker. The Southern blot shows that only the 2.8 kb fragment is present in the w^{1118} control, as expected (lane 1). The two donor strains carry both the wild-type locus and the 3.4 kb and 0.73 kb fragments from the targeting construct (lanes 2 and 3). The homozygous *dSdhaf3* mutant has only the 3.4 kb and 0.73 kb fragments, as expected (lane 4). Note that the ~7 kb fragment in donor strain #1 is of unknown origin. Donor strain #2 was used to generate the *dSdhaf3* mutant used in this study. (D) GC/MS was used to compare the relative levels of small metabolites in wild-type controls (grey boxes) and *dSdhaf3* mutants (white boxes). N = 12 samples from two independent experiments with 20 flies/sample (5-day old). ***$p < 0.001$. (E) Proteins from purified mitochondria were extracted from w^{1118} controls (+) and *dSdhaf3* mutants (–), fractionated by non-denaturing PAGE, and analyzed for total protein by Commassie Blue staining or for flavinylated SdhA. A SdhA marker is included as a control (M). (F) Control w^{1118} flies and *dSdhaf3* mutants were tested for paralysis as described in Supplemental Experimental Procedures, scoring for the number of flies that moved off the bottom of the vial after vortexing. Results are from three independent experiments using a total of 12 vials with 20 adults/vial at 1, 2, 3, or 4 weeks of age. ***$p < 0.001$

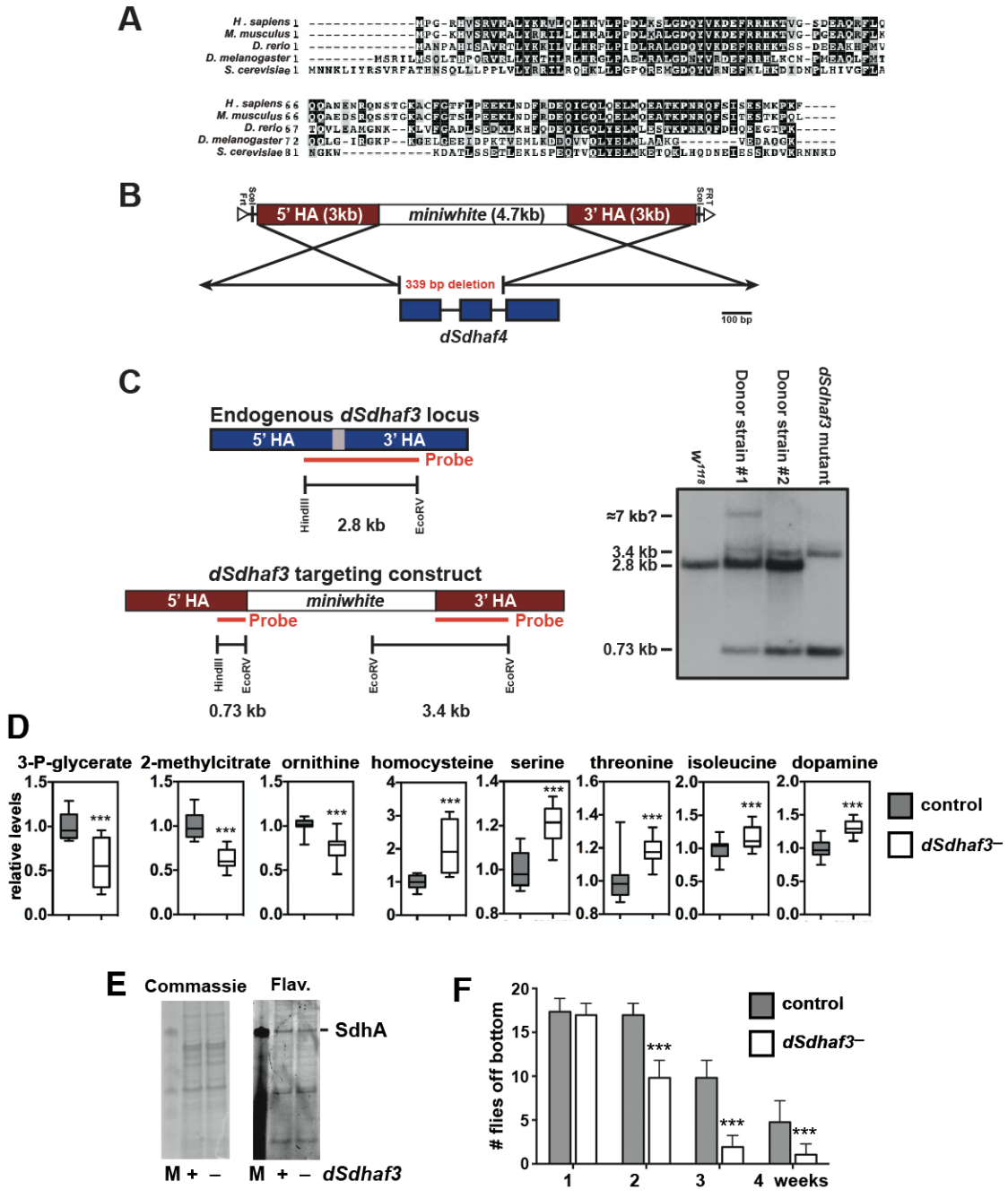
A
H. sapiens
M. musculus
D. rerio
D. melanogaster
S. cerevisiae
B
5' HA (3kb)
miniwhite (4.7kb)
3' HA (3kb)
339 bp deletion
100 bp
dSdhaf4
C
Endogenous dSdhaf3 locus
5' HA
3' HA
Probe
HindIII
2.8 kb
EcoRV
dSdhaf3 targeting construct
miniwhite
0.73 kb
3.4 kb
w1118
Donor strain #1
Donor strain #2
dSdhaf3 mutant
≈7 kb?
3.4 kb
2.8 kb
0.73 kb
D
3-P-glycerate
2-methylcitrate
ornithine
homocysteine
serine
threonine
isoleucine
dopamine
relative levels
control
dSdhaf3–
E
Commassie
Flav.
SdhA
M + –
M + – dSdhaf3
F
flies off bottom
control
dSdhaf3–
1
2
3
4 weeks

(*CG14898*), which we refer to here as *dSdhaf3* (Figures 5.9B–5.9D). These mutants were outcrossed for six generations to w^{1118}, which was used as a control for most studies. *dSdhaf3* mutants progress normally through development and have a normal lifespan when maintained on standard growth media. These animals are, however, sensitive to ethanol (Figure 5.10A) and oxidative stress, resulting from either paraquat treatment (Figure 5.10B) or hyperoxia (Figure 5.10C). The response to hyperoxia is most pronounced, with a 50% reduction in lifespan relative to controls, although $SdhB^{12081}$ hypomorphic mutants display a more severe effect (Walker et al., 2006). Interestingly, most *Sdhaf3* mutants exposed to 100% oxygen for 4 days held their wings erect, a hallmark of mitochondrial dysfunction and muscle degeneration (DeSimone et al., 1996; Greene et al., 2003). A similar abnormal wing posture was observed in $SdhB^{12081}$ mutants maintained under normal conditions (10–15%) or exposed to hyperoxia (80–100%).

dSdhaf3 mutants display reduced SdhB protein levels and SDH activity

If the function of *dSdhaf3* has been conserved through evolution, then *dSdhaf3* mutants should display a specific defect in SDH function. Consistent with this possibility, metabolomic profiling of *dSdhaf3* mutants revealed relatively few significant changes in metabolite levels, with elevated succinate and reduced levels of citrate, fumarate, and malate (Figure 5.10D). Biochemical analysis of mitochondrial extracts from *dSdhaf3* mutants demonstrated that *dSdhaf3* mutants have normal levels of SdhA, but significantly reduced levels of SdhB (Figure 5.10E), resulting in an approximate 50% reduction in SDH enzymatic activity (Figures 5.10F and 5.10G), similar to the phenotypes of *sdh7*Δ yeast. SdhA is also flavinylated normally in *dSdhaf3* mutants, as expected (Figure 5.9E).

Figure 5.10. *dSdhaf3* mutants are sensitive to oxidative stress and display reduced levels of SdhB, reduced SDH activity, and motility defects.

Five-day old w^{1118} control (solid line) and *dSdhaf3* mutant (dotted line) males were transferred to vials with (A) 5% ethanol, 1% agar in PBS, (B) 30 mM paraquat in semi-defined medium, or (C) 100% O_2 with standard medium, and living animals were scored daily. Homozygous $SdhB^{12081}$ mutants (dashed line) were included in the hyperoxia experiment. Each graph was compiled from 3–5 experiments, using a total of 15–21 vials with 20 animals per vial. Error bars represent ±SEM. *p < 0.05, **p < 0.01, ***p < 0.001. (D) GC/MS was used to compare the relative levels of small metabolites in wild-type controls (grey boxes) and *dSdhaf3* mutants (white boxes). N = 12 samples from two independent experiments with 20 flies/sample (5-day old). ***p < 0.001. (E) Proteins were extracted from mitochondria isolated from w^{1118} controls, *dSdhaf3* mutants, or *UAS-dSdhaf3/+* transformants, and analyzed by immunoblotting to detect SdhA, SdhB, and ATPα, (a subunit of complex V). (F) A continuous colorimetric assay was used to measure SDH enzyme activity in extracts of purified mitochondria from w^{1118} controls, *dSdhaf3* mutants, and *UAS-dSdhaf3/+* transformants. ***p < 0.001. (G) Proteins from purified mitochondria were extracted from w^{1118} controls and *dSdhaf3* mutants, fractionated by nondenaturing PAGE, and analyzed for SDH and Complex IV activity. (H) Control w^{1118} flies and *dSdhaf3* mutants were tested for motility in three independent experiments using a total of 18 vials with 20 adults/vial at 1, 2, 3, or 4-weeks of age. *p < 0.05, ***p < 0.001

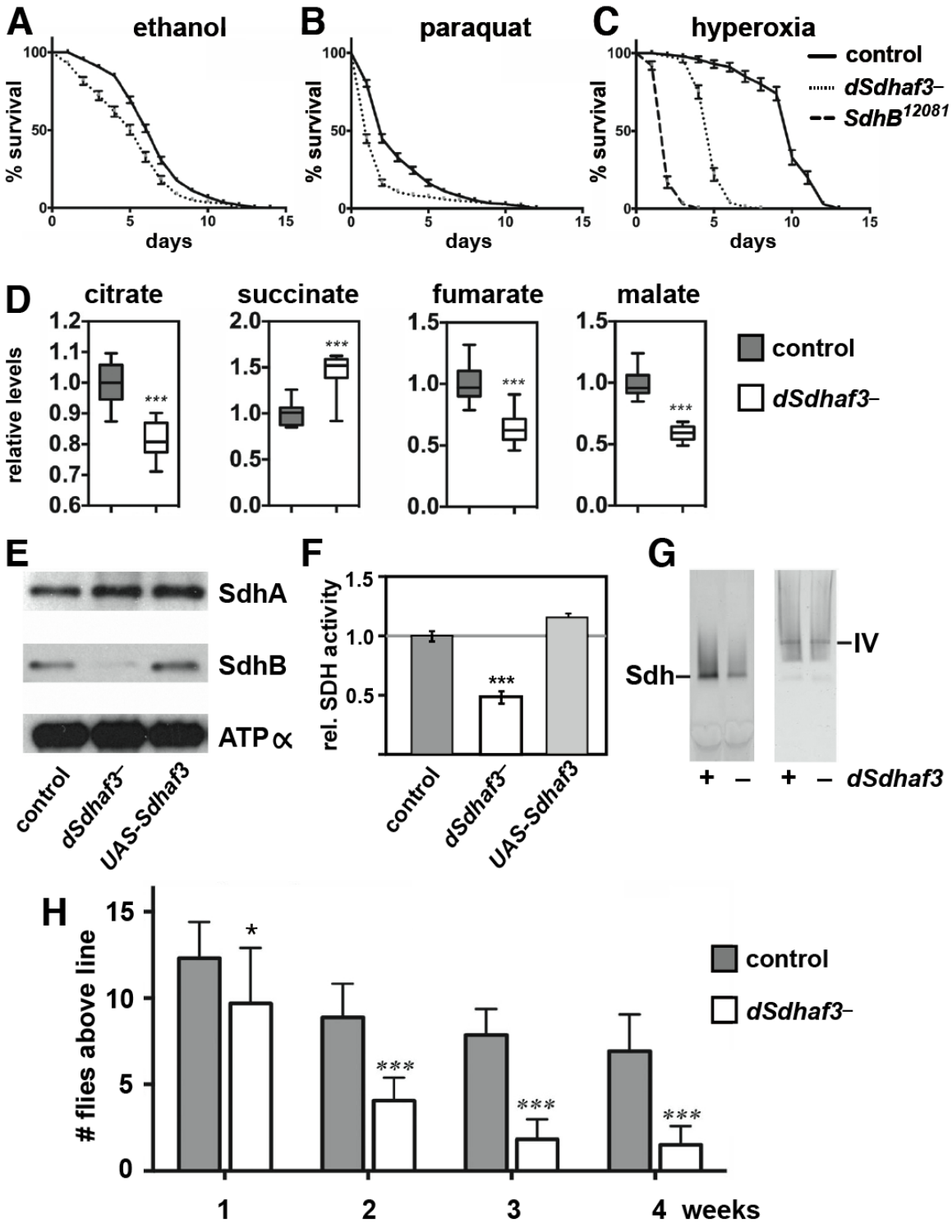
A
ethanol
% survival
days
B
paraquat
% survival
days
C
hyperoxia
% survival
days
control
dSdhaf3–
SdhB12081
D
citrate
succinate
fumarate
malate
relative levels
control
dSdhaf3–
E
SdhA
SdhB
ATPα
control
dSdhaf3–
UAS-Sdhaf3
F
rel. SDH activity
control
dSdhaf3–
UAS-Sdhaf3
G
Sdh–
–IV
+ – + – dSdhaf3
H
flies above line
control
dSdhaf3–
1
2
3
4 weeks

Combining the hypomorphic *SdhB*^{12081} allele with the *dSdhaf3* mutation resulted in a dramatic decrease in viability, demonstrating a strong genetic interaction, consistent with the reduced levels of SdhB in *dSdhaf3* mutants and confirming the functional interaction between dSdhaf3 and SDH (Figure 5.11A).

Interestingly, although *dSdhaf3* mutants are fully viable and fertile, they display a clear age-dependent reduction in movement (Figure 5.10H). While mutants at 1 week of adult life show no difference in motility relative to controls, mutants display an approximate 50% reduction in movement by 2 weeks of age and a more severe motility defect at later stages (Figure 5.10H). Mutants are also significantly more sensitive to paralysis by 2 weeks of age, relative to controls (Figure 5.9F). Thus, like its counterpart in yeast, dSdhaf3 is required to maintain normal SDH levels and activity and is required for proper wing muscle function and motility in *Drosophila*.

Antioxidant and genetic rescue of *dSdhaf3* mutants

Consistent with the ability of antioxidants to suppress the growth defects in *sdh7*Δ yeast mutants, either a dietary (N-acetyl cysteine) or genetic (Sod2 expression) reduction in oxidative stress rescued the hyperoxia sensitivity of *dSdhaf3* mutants (Figures 5.12A and 5.2B). Unlike the yeast studies, however, overexpression of the putative Sdh6 homolog (encoded by *CG34229*), using *Act5C-GAL4* to drive a *UAS-CG34229* transgene in *dSdhaf3* mutants, had no effect on their sensitivity to hyperoxia (Figure 5.11B). This result, however, is difficult to interpret because there is only limited sequence homology between CG34229 and Sdh6. We conclude that this functional interaction between Sdh6 and Sdh7 may not be conserved through evolution or, alternatively, that CG34229 is not a

Figure 5.11. *dSdhaf3* interacts with *SdhB* and overexpression of *CG34229* fails to rescue the hyperoxia sensitivity of *dSdhaf3* mutants.
(A) Flies carrying either control or *dSdhaf3* mutant chromosomes over a balancer chromosome were crossed to flies carrying a hypomorphic allele for SdhB over a balancer. The resulting progeny were scored for the absence or presence of the marker linked to the balancer chromosome. The proportion of the expected progeny that eclosed, based on Mendelian ratios of the indicated genotypes, is shown. "+" represents a *TM3* balancer for *dSdhaf3* and a *CyO* balancer for $SdhB^{12081}$. (N) = number of progeny assayed from each cross in a total of four independent experiments. The mean ± SEM is shown and ***$p < 0.001$ (B) A BLAST search for a *Drosophila* Sdh6 homolog identified CG34229, which shares limited sequence similarity with both the yeast protein and human LYR proteins. Widespread overexpression of *CG34229* using *Act5C-GAL4* to drive a *UAS-CG34229* transgene in *dSdhaf3* mutants (orange line), however, had no effect on their sensitivity to hyperoxia. We conclude that the functional interaction between Sdh6 and Sdh7 may not be conserved through evolution or that the true *Drosophila* homolog of Sdh6 remains to be discovered.

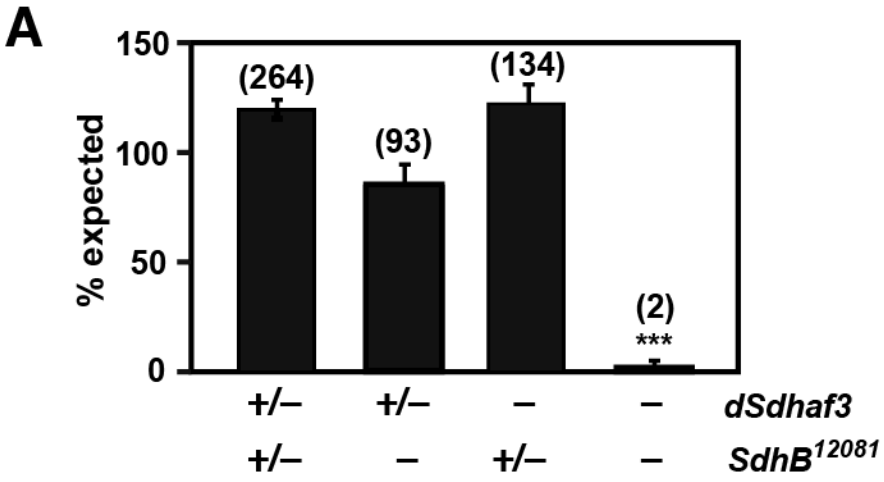
A
150
100
50
0
% expected
(264)
(93)
(134)
(2)
***
+/–
+/–
–
–
dSdhaf3
+/–
–
+/–
–
SdhB12081

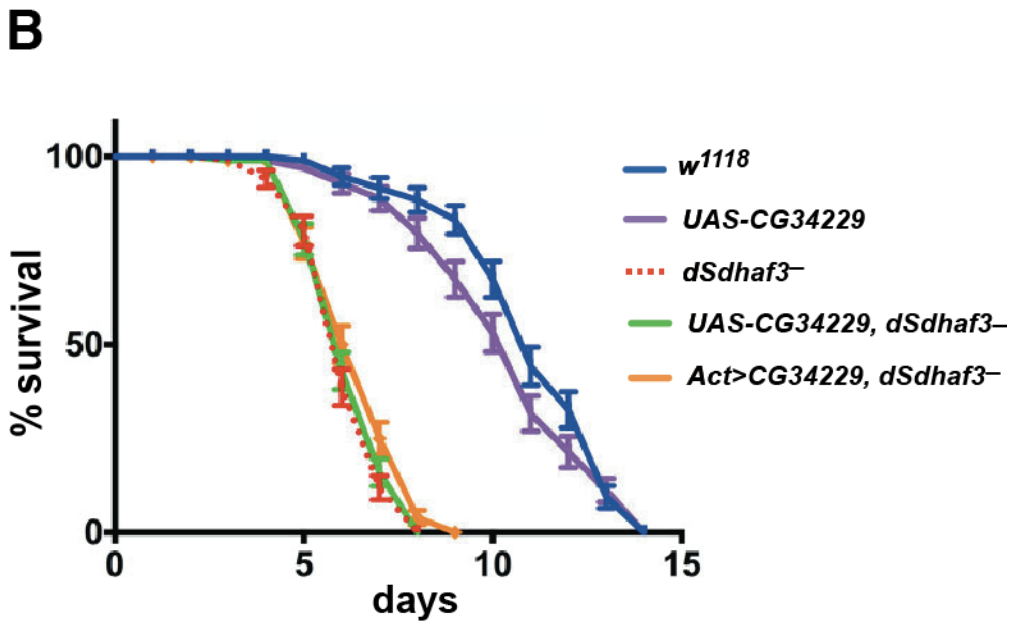
B
100
50
0
% survival
0
5
10
15
days
w1118
UAS-CG34229
dSdhaf3–
UAS-CG34229, dSdhaf3–
Act>CG34229, dSdhaf3–

Figure 5.12. *dSdhaf3* function is required in the muscles and nervous system.
Five-day old w^{1118} control (solid line) and *dSdhaf3* mutant (dotted line) males were transferred to vials with 100% O_2 with standard medium, and living animals were scored daily. (A) 0.1% N-acetyl cysteine was added to the culture medium for a quarter of the vials. (B) Expression of *Sod2* using the ubiquitous *Act5C-GAL4* driver (*Act > Sod2*; purple line) partially rescues the hyperoxia sensitivity of *dSdhaf3* mutants. (C) Expression of wild-type *dSdhaf3* using the ubiquitous *Act5C-GAL4* driver (*Act > dSdhaf3*; purple line) rescues the hyperoxia sensitivity of *dSdhaf3* mutants. (D) The muscle-specific *C57-GAL4* driver provides minor, but significant, rescue of the hyperoxia sensitivity of *dSdhaf3* mutants (purple line) relative to the control that carries the *UAS-dSdhaf3* transgene alone (green line), while the CNS-specific *elav-GAL4* driver provides more efficient rescue (orange line). Expression of wild-type *dSdhaf3* by using either the ubiquitous *Act5C-GAL4* driver (E, purple), the muscle-specific *C57-GAL4* driver (F, purple), or the CNS-specific *elav-GAL4* driver (F, orange) rescues the climbing defect in *dSdhaf3* mutants. The *Act > dSdhaf3* rescue in C and E was performed in females; other rescue studies were performed in males (A, B, D, F). The apparent partial rescue of *dSdhaf3* mutants by a single copy of the *UAS-dSdhaf3* transgene (C, D, green line) appears to be due to genetic background since *UAS-dSdhaf3* transformants have normal levels of SdhB and SDH activity (E, F). Each graph was compiled from two experiments with a total of 10 vials with 20 animals per vial.

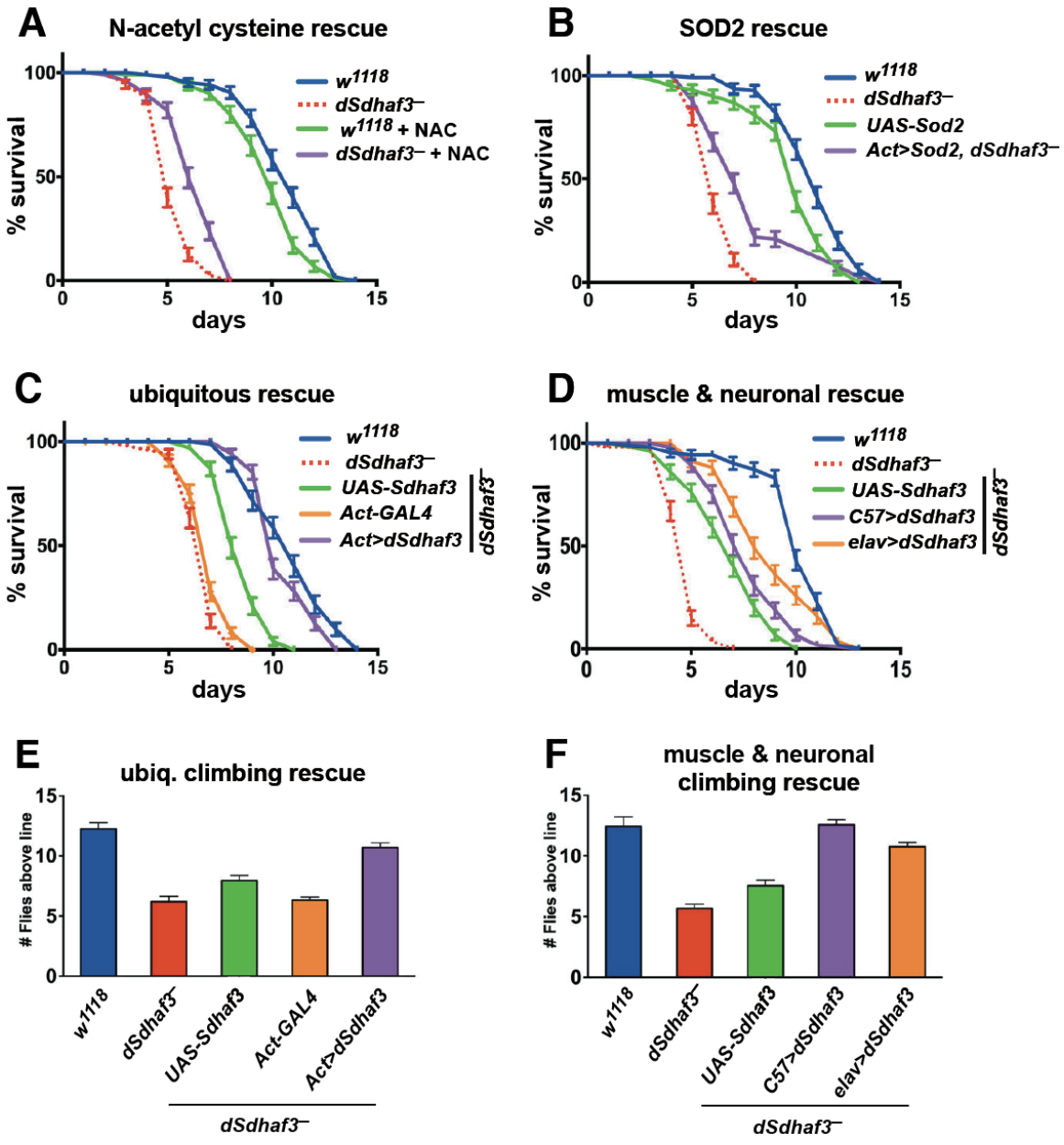
A
N-acetyl cysteine rescue
% survival
days
w1118
dSdhaf3–
w1118 + NAC
dSdhaf3– + NAC
B
SOD2 rescue
% survival
days
w1118
dSdhaf3–
UAS-Sod2
Act>Sod2, dSdhaf3–
C
ubiquitous rescue
% survival
days
w1118
dSdhaf3–
UAS-Sdhaf3
Act-GAL4
Act>dSdhaf3
dSdhaf3–
D
muscle & neuronal rescue
% survival
days
w1118
dSdhaf3–
UAS-Sdhaf3
C57>dSdhaf3
elav>dSdhaf3
dSdhaf3–
E
ubiq. climbing rescue
Flies above line
w1118
dSdhaf3–
UAS-Sdhaf3
Act-GAL4
Act>dSdhaf3
dSdhaf3–
F
muscle & neuronal climbing rescue
Flies above line
w1118
dSdhaf3–
UAS-Sdhaf3
C57>dSdhaf3
elav>dSdhaf3
dSdhaf3–

functional homolog of Sdh6. The wing posture and motility defects in *dSdhaf3* mutants suggested that these animals suffer from muscular and neuronal dysfunction. Consistent with this model, widespread expression of WT *dSdhaf3* (*Act > dSdhaf3)* in *dSdhaf3* mutants fully rescues their sensitivity to hyperoxia (Figure 5.12C), while muscle-specific (*C57 > dSdhaf3*) or neuronal-specific (*elav > dSdhaf3*) expression provides partial rescue (Figure 5.12D). Similar effects are seen on the climbing defects in *dSdhaf3* mutants (Figures 5.12E and 5.12F). Genetic rescue in the fat body (*Cg-GAL4*) or intestine (*Mex-GAL4*), however, provided no significant rescue (data not shown). Widespread overexpression of *dSdhaf3* in wild-type flies has no significant effect on their resistance to hyperoxia (data not shown). Taken together, we conclude that dSdhaf3 function is conserved through evolution and that proper SDH levels and activity are required for resistance to oxidative stress as well as muscular and neuronal function, consistent with their dependence on mitochondrial oxidative phosphorylation.

SDHB, but not SDHA, is specifically impaired in human cells deficient in wild-type SDHAF1

Although the original study of the human Sdh6 ortholog, SDHAF1, demonstrated that it is required for SDH activity and abundance in fibroblasts (Ghezzi et al., 2009), its mechanism of action remained undefined. We therefore addressed whether SDHAF1 protects SDHB (the human Sdh2 ortholog) from ROS damage similar to yeast Sdh6. First, we determined steady-state levels of SDH structural subunits in SDHAF1-depleted HEK293 cells by siRNA knockdown. SDHB and SDHC levels were significantly reduced upon SDHAF1 depletion (Figure 5.13A). SDHA levels, however, remained

Figure 5.13. SDHB is destabilized in human cells with reduced levels of SDHAF1.
(A) Relative *SDHAF1* mRNA levels in HEK293 cells 72 h after *SDHAF1* knockdown using siRNA (left panel) and steady-state levels of proteins from total cell lysates (right panel). (B) HEK293 cells were treated with either control siRNA or *SDHAF1* siRNA. Paraquat was added to cultures 24 h after siRNA transfection. Total cell lysates were obtained 48 h after paraquat supplementation. (C) Steady-state levels of proteins in mitochondria isolated from control fibroblasts and patient fibroblasts harboring mutations on *SDHAF1* (Ohlenbusch et al., 2012). (D) Model of the role of Sdh6(SDHAF1) and Sdh7(SDHAF3) in maturation of the FeS centers in Sdh2(SDHB). Sdh6 and Sdh7 associate with Sdh2 within a Sdh2/Sdh1 intermediate. Sdh1 maturation requires covalent flavinylation by Sdh5 followed by formation of the Sdh1/Sdh2 subcomplex that is chaperoned by Sdh8 (see Chapter 4).

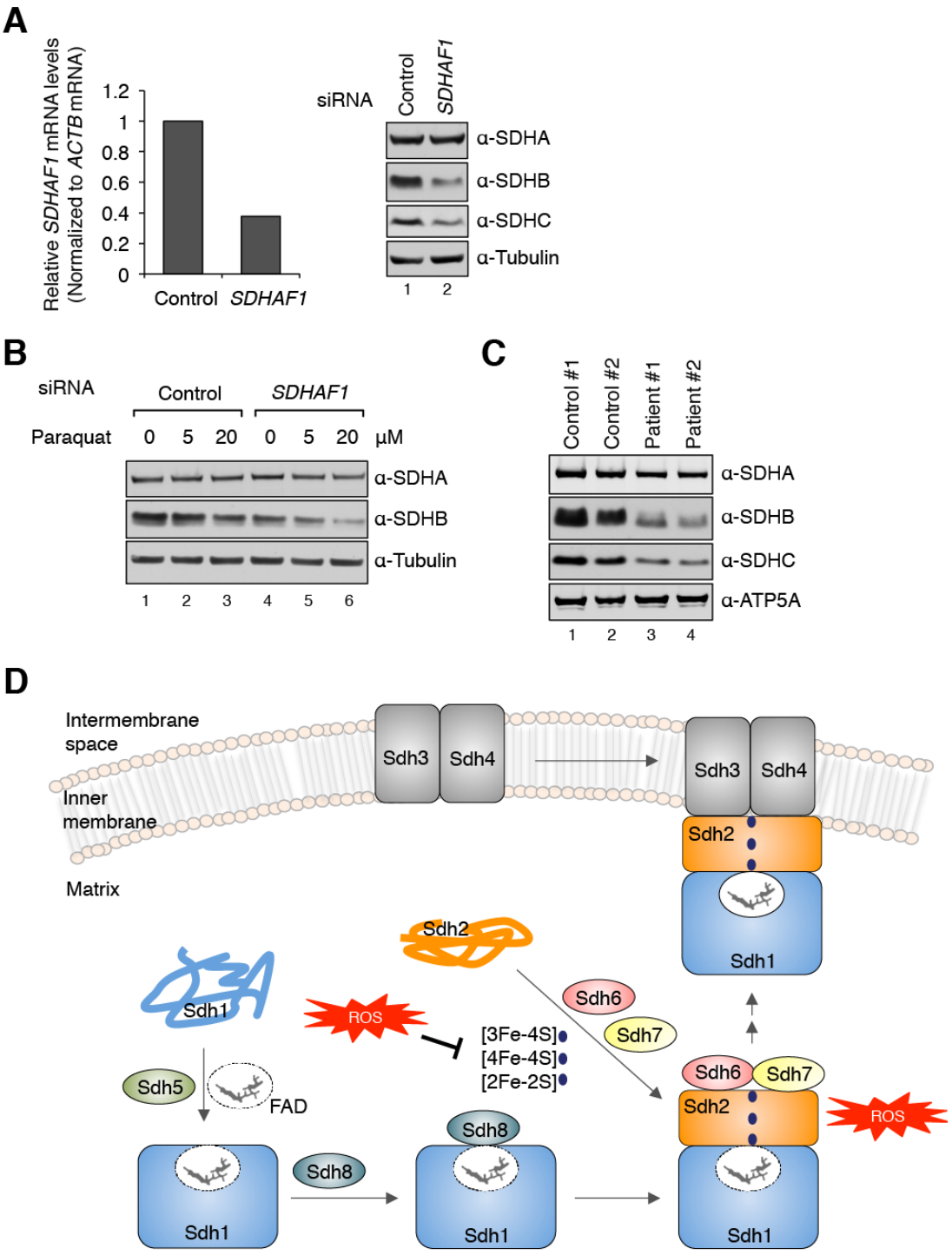
A
Relative SDHAF1 mRNA levels (Normalized to ACTB mRNA)
1.2
1
0.8
0.6
0.4
0.2
0
Control
SDHAF1
siRNA
Control
SDHAF1
α-SDHA
α-SDHB
α-SDHC
α-Tubulin
1 2
B
siRNA
Control
SDHAF1
Paraquat 0 5 20 0 5 20 μM
α-SDHA
α-SDHB
α-Tubulin
1 2 3 4 5 6
C
Control #1
Control #2
Patient #1
Patient #2
α-SDHA
α-SDHB
α-SDHC
α-ATP5A
1 2 3 4
D
Intermembrane space
Inner membrane
Matrix
Sdh3
Sdh4
Sdh2
Sdh1
Sdh6
Sdh7
Sdh5
Sdh8
FAD
ROS
[3Fe-4S]
[4Fe-4S]
[2Fe-2S]

unaffected. Next, we tested the effects of paraquat on SDHAF1-depleted HEK293 cells. In accordance with the yeast and fly data, SDHB levels were further attenuated in SDHAF1-deficient cells exposed to paraquat (Figure 5.13B), which suggests that SDHAF1 resembles Sdh6 in protecting the FeS SDH subunit from ROS damage.

We also examined the steady-state SDHB levels in patient fibroblasts with a known *SDHAF1* mutation. Both SDHB and SDHC levels were diminished in mitochondria isolated from the patient fibroblasts, whereas SDHA levels remained unaffected compared to controls (Figure 5.13C). It is noteworthy that the degree of diminution in SDHB levels was comparable to SDH activity as patient #1 fibroblasts and patient #2 retained 52% and 40% SDH activity of control fibroblasts, respectively.

Discussion

The present work demonstrates that maturation of the FeS subunit of Sdh2 (SDHB) requires the participation of two assembly factors, Sdh6 (SDHAF1) and Sdh7 (SDHAF3). These factors are shown to guide Sdh2 maturation within the mitochondrial matrix in the midst of endogenous oxidants. Yeast, flies and mammalian cells lacking one of these factors are impaired in SDH activity and assembly with Sdh2 exhibiting a heightened susceptibility to oxidants. Endogenous oxidants arising from the respiratory chain are deleterious to FeS cluster stability. Oxidative metabolism in the mitochondria leads to the formation of superoxide anions from the one electron reduction of O_2. Superoxide anions can readily dissociate FeS clusters, so the assembly of FeS cluster centers in mitochondrial enzymes is susceptible to oxidative damage. The present studies in yeast, flies, and mammalian cells suggest that Sdh6 and Sdh7 exert a conserved

function in the assembly of the three FeS cluster centers in Sdh2 and shield the centers from oxidants.

Yeast studies reveal that Sdh6 and Sdh7 act in concert in the maturation of Sdh2 with a limited redundancy in function. Yeast lacking either factor show a marked SDH deficiency in late-log cultures that rely on oxidative metabolism. Under these conditions, the mutant cells contain a reduced level of the assembled tetrameric enzyme. These cells exhibit a hypersensitivity to the superoxide generator paraquat. The respiratory defect of these mutants is readily suppressed by overexpression of the Yap1 transcriptional activator of oxidative stress genes or exogenous reductants. These studies highlight the role of Sdh6 and Sdh7 in shielding Sdh2 maturation from deleterious effects of oxidants.

Flies lacking the Sdh7 ortholog SDHAF3, likewise, are hypersensitive to paraquat and hyperoxia. The mutant flies show diminished levels of active SDH and as a result accumulate succinate. The *dSdhaf3* mutants are viable and fertile, yet display impaired movement that intensifies with age. The erect wing phenotype exhibited under hyperoxic conditions and the motility defects evident in aged mutant flies are consistent with muscular and neuronal dysfunction. Moreover, neuronal or muscle-specific expression of wild-type *dSdhaf3* is sufficient to partially rescue the hyperoxia sensitivity of the mutants, demonstrating the importance of SDH function in these tissues that rely heavily on OXPHOS. The hyperoxia sensitivity of *dSdhaf3* mutants is also partially suppressed by dietary N-acetyl cysteine or overexpression of the matrix mangano-superoxide dismutase encoded by *Sod2*. These effects of antioxidants mimic the rescue of yeast *sdh7*Δ mutant oxidative growth and demonstrate the apparent close conservation of Sdh7/SDHAF3 function through evolution.

Conservation in SDH6/SDHAF1 function between yeast and humans also exists. Attenuation of SDHAF1 in HEK293 culture cells leads to a hypersensitivity in the stability of the FeS SDHB subunit to paraquat. SDHB instability is also seen in two SDHAF1 patient fibroblast lines. One implication of the observed antioxidant rescue of the defect of *sdh6*Δ yeast cells and *dSdhaf3* mutant flies is the potential use of antioxidant therapeutics for patients afflicted with SDHAF1 (and perhaps SDHAF3) mutations. Patients with SDHAF1 mutations have presented with SDH-deficient leukoencephalopathy (Ghezzi et al., 2009; Ohlenbusch et al., 2012) and have a survival window that may be amenable to antioxidant therapy. Two case studies were reported that attempted to alleviate clinical symptoms in SDH-deficient patients harboring SDHAF1 mutations by supplementing riboflavin and CoQ10. The clinical outcomes, however, were not significantly improved (Jain-Ghai et al., 2013). More recently, a candidate therapeutic, EPI-743, is being tested for treatment of Leigh syndrome patients (Martinelli et al., 2012). EPI-743 is a vitamin E quinone, which is orally bioavailable and crosses the blood-brain barrier (Shrader et al., 2011). Future studies will focus on the efficacy of antioxidants with SDHAF1 patient fibroblasts. In addition, it is important to note that every gene encoding an SDH subunit or known assembly factor is causally associated with human disease. We thus anticipate that SDHAF3 mutations will be associated with one or more previously idiopathic SDH-associated diseases and propose that SDHAF1 and SDHAF3 are candidate susceptibility factors for undefined SDH-deficient tumors.

The present work provides insights into the physiological function of Sdh6 and Sdh7 in Sdh2 maturation. Sdh6 and Sdh7 are shown to bind to the Sdh1:Sdh2 assembly

intermediate that accumulates in mutants lacking the SDH membrane anchor. In addition, both Sdh6 and Sdh7 accumulate in the membrane anchor mutant cells. Sdh6 was found to impart stabilization to Sdh2 in cells lacking the FAD subunit Sdh1, suggesting that at least Sdh6 has a specific interface for Sdh2. These assembly factors do not appear to be mere Sdh2 chaperones since elevated levels of Sdh2 do not suppress the respiratory defects of *sdh6*Δ or *sdh7*Δ mutants. Rather, a role in Sdh2 maturation is implicated by the observed accumulation of an Sdh1 assembly intermediate in *sdh6*Δ or *sdh7*Δ mutants. Sdh2 maturation requires the insertion of three distinct FeS clusters. A 2Fe-2S cluster exists in the N-terminal domain of Sdh2, which forms an interface with Sdh1 (Sun et al., 2005). The C-terminal domain of Sdh2 contains both 4Fe-4S and 3Fe-4S clusters. FeS cluster synthesis in the mitochondrial matrix occurs on the ISU/ISA scaffold complexes and the preformed clusters are transferred to client proteins. The transfer of labile preformed FeS clusters may be sensitive to the deleterious effects of endogenous oxidants, so Sdh6 and Sdh7 may serve a role in chaperoning this transfer step. The two proteins are likely to have separate roles in this transfer step since the proteins are not completely redundant. A candidate role in the FeS cluster insertion step is supported by the observed partial suppression of respiratory growth defect of *sdh6*Δ or *sdh7*Δ mutants by supplemental iron (Figure 5.6D). Superoxide inactivation of the 4Fe-4S center in aconitase leads to a dissociation of one iron ion forming an inactive 3Fe-4S center that can be reactivated by supplemental iron salts (Gardner and Fridovich, 1992)**.** Future studies will focus on the detailed mechanism by which Sdh6 and Sdh7 participate in FeS cluster maturation of Sdh2. Moreover, the observation that the two LYR proteins Sdh6 and Sdh7 function with the FeS cluster Sdh2 subunit has significant implications for the

uncharacterized LYR proteins present in the human proteome. Our studies raise the possibility that future functional studies of LYRM1, LYRM2, LYRM5, and LYRM9 will reveal novel roles in the assembly of FeS clusters in mammalian-specific FeS cluster enzymes.

Acknowledgements

We thank James Cox and the University of Utah Metabolomics Core facility for the metabolomic analyses, the Bloomington Stock Center for providing fly stocks, and FlyBase for information used for this study. We acknowledge pilot support from the Huntsman Cancer Institute (Nuclear Control of Cell Growth and Differentiation Program). DKB was supported by the NIH Genetics Predoctoral Training Grant T32 GM007464. This research was supported by NIH RO1 ES03817 (DRW) and 1R01 GM094232 (CST).

References

Adam, A.C., Bornhovd, C., Prokisch, H., Neupert, W., and Hell, K. (2006). The Nfs1 interacting protein Isd11 has an essential role in Fe/S cluster biogenesis in mitochondria. EMBO J. *25*, 174–183.

Atkinson, A., Smith, P., Fox, J.L., Cui, T.Z., Khalimonchuk, O., and Winge, D.R. (2011). The LYR Protein Mzm1 Functions in the Insertion of the Rieske Fe/S Protein in Yeast Mitochondria. Mol. Cell. Biol. *31*, 3988–3996.

Backhaus, B., Sulkowski, E., and Schlote, F. (1984). A semi-synthetic general purpose medium for D. melanogaster. Dros. Info. Serv. *60*, 210–212.

Bardella, C., Pollard, P.J., and Tomlinson, I. (2011). SDH mutations in cancer. Biochim. Biophys. Acta *1807*, 1432–1443.

Baysal, B.E., Ferrell, R.E., Willett-Brozick, J.E., Lawrence, E.C., Myssiorek, D., Bosch, A., van der Mey, A., Taschner, P.E., Rubinstein, W.S., Myers, E.N., Richard, C.W., 3rd,

Cornelisse, C.J., Devilee, P., and Devlin, B. (2000). Mutations in SDHD, a mitochondrial complex II gene, in hereditary paraganglioma. Science *287*, 848–851.

Bricker, D.K., Taylor, E.B., Schell, J.C., Orsak, T., Boutron, A., Chen, Y.C., Cox, J.E., Cardon, C.M., Van Vranken, J.G., Dephoure, N., Redin, C., Boudina, S., Gygi, S.P., Brivet, M., Thummel, C.S., and Rutter, J. (2012). A mitochondrial pyruvate carrier required for pyruvate uptake in yeast, *Drosophila*, and humans. Science *337*, 96–100.

Canelas, A.B., ten Pierick, A., Ras, C., Seifar, R.M., van Dam, J.C., van Gulik, W.M., and Heijnen, J.J. (2009). Quantitative evaluation of intracellular metabolite extraction techniques for yeast metabolomics. Anal. Chem *81*, 7379–7389.

Chen, Y.C., Taylor, E.B., Dephoure, N., Heo, J.M., Tonhato, A., Papandreou, I., Nath, N., Denko, N.C., Gygi, S.P., and Rutter, J. (2012). Identification of a protein mediating respiratory supercomplex stability. Cell Metab. *15*, 348–360.

Cui, T.Z., Smith, P.M., Fox, J.L., Khalimonchuk, O., and Winge, D.R. (2012). Late-stage maturation of the rieske Fe/S protein: Mzm1 stabilizes Rip1 but does not facilitate its translocation by the AAA ATPase Bcs1. Mol. Cell. Biol. *32*, 4400–4409.

DeSimone, S., Coelho, C., Roy, S., VijayRaghavan, K., and White, K. (1996). ERECT WING, the *Drosophila* member of a family of DNA binding proteins is required in imaginal myoblasts for flight muscle development. Development *122*, 31–39.

Feichtinger, R.G., Zimmermann, F., Mayr, J.A., Neureiter, D., Hauser-Kronberger, C., Schilling, F.H., Jones, N., Sperl, W., and Kofler, B. (2010). Low aerobic mitochondrial energy metabolism in poorly or undifferentiated neuroblastoma. BMC Cancer *10*, 149.

Fernandes, L., Rodrigues-Pousada, C., and Struhl, K. (1997). Yap, a novel family of eight bZIP proteins in *Saccharomyces cerevisiae* with distinct biological functions. Mol. Cell. Biol. *17*, 6982–6993.

Finsterer, J. (2008). Leigh and Leigh-like syndrome in children and adults. Pediatr. Neurol. *39*, 223–235.

Ganetzky, B., and Wu, C.F. (1982). Indirect suppression involving behavioral mutants with altered nerve excitability in *Drosophila melanogaster*. Genetics *100*, 597–614.

Gardner, P.R. (2002). Aconitase: sensitive target and measure of superoxide. Methods in Enzymol. *349*, 9–23.

Gardner, P.R., and Fridovich, I. (1992). Inactivation-reactivation of aconitase in Escherichia coli. A sensitive measure of superoxide radical. J. Biol. Chem. *267*, 8757–8763.

Gargano, J.W., Martin, I., Bhandari, P., and Grotewiel, M.S. (2005). Rapid iterative negative geotaxis (RING): a new method for assessing age-related locomotor decline in Drosophila. Exp. Gerontol. *40*, 386–395.

Ghezzi, D., Goffrini, P., Uziel, G., Horvath, R., Klopstock, T., Lochmuller, H., D'Adamo, P., Gasparini, P., Strom, T.M., Prokisch, H., Invernizzi, F., Ferrero, I., and Zeviani, M. (2009). SDHAF1, encoding a LYR complex-II specific assembly factor, is mutated in SDH-defective infantile leukoencephalopathy. Nat. Genet. *43*, 259–265.

Glick, B.S., and Pon, L.A. (1995). Isolation of highly purified mitochondria from *Saccharomyces cerevisiae*. Meth. Enzymol. *260*, 213–223.

Greene, J.C., Whitworth, A.J., Kuo, I., Andrews, L.A., Feany, M.B., and Pallanck, L.J. (2003). Mitochondrial pathology and apoptotic muscle degeneration in *Drosophila* parkin mutants. Proc. Natl. Acad. Sci. USA *100*, 4078–4083.

Hao, H.X., Khalimonchuk, O., Schraders, M., Dephoure, N., Bayley, J.P., Kunst, H., Devilee, P., Cremers, C.W., Schiffman, J.D., Bentz, B.G., Gygi, S.P., Winge, D.R., Kremer, H., and Rutter, J. (2009). SDH5, a gene required for flavination of succinate dehydrogenase, is mutated in paraganglioma. Science *325*, 1139–1142.

Hayes, M.K., Luethy, M.H., and Elthon, T.E. (1991). Mitochondrial malate dehydrogenase from corn : purification of multiple forms. Plant Physiol. *97*, 1381–1387.

Jain-Ghai, S., Cameron, J.M., Al Maawali, A., Blaser, S., MacKay, N., Robinson, B., and Raiman, J. (2013). Complex II deficiency—a case report and review of the literature. Am. J. Med. Genet. Part A *161A*, 285–294.

Janeway, K.A., Kim, S.Y., Lodish, M., Nose, V., Rustin, P., Gaal, J., Dahia, P.L., Liegl, B., Ball, E.R., Raygada, M., Lai, A.H., Kelly, L., Hornick, J.L., O'Sullivan, M., de Krijger, R.R., Dinjens, W.N., Demetri, G.D., Antonescu, C.R., Fletcher, J.A., Helman, L., and Stratakis, C.A. (2011). Defects in succinate dehydrogenase in gastrointestinal stromal tumors lacking KIT and PDGFRA mutations. Proc. Natl. Acad. Sci. USA *108*, 314–318.

Khalimonchuk, O., Bird, A., and Winge, D.R. (2007). Evidence for a pro-oxidant intermediate in the assembly of cytochrome oxidase. J. Biol. Chem. *282*, 17442–17449.

Kim, H.J., Jeong, M.Y., Na, U., and Winge, D.R. (2012). Flavinylation and assembly of succinate dehydrogenase are dependent on the c-terminal tail of the flavoprotein subunit. J. Biol. Chem. *287*, 40670–40679.

Longtine, M.S., McKenzie, A., 3rd, Demarini, D.J., Shah, N.G., Wach, A., Brachat, A., Philippsen, P., and Pringle, J.R. (1998). Additional modules for versatile and economical PCR-based gene deletion and modification in *Saccharomyces cerevisiae*. Yeast *14*, 953–961.

Maggert, K.A., Gong, W.J., and Golic, K.G. (2008). Methods for homologous recombination in *Drosophila*. Methods Mol. Biol. *420*, 155–174.

Martinelli, D., Catteruccia, M., Piemonte, F., Pastore, A., Tozzi, G., Dionisi-Vici, C., Pontrelli, G., Corsetti, T., Livadiotti, S., Kheifets, V., Hinman, A., Shrader, W.D., Thoolen, M., Klein, M.B., Bertini, E., and Miller, G. (2012). EPI-743 reverses the progression of the pediatric mitochondrial disease—genetically defined Leigh Syndrome. Mol. Genet. Metab. *107*, 383–388.

McCammon, M.T. (1996). Mutants of *Saccharomyces cerevisiae* with defects in acetate metabolism: isolation and characterization of Acn mutants. Genetics *144*, 57–69.

Munujos, P., Coll-Canti, J., Gonzalez-Sastre, F., and Gella, F.J. (1993). Assay of succinate dehydrogenase activity by a colorimetric-continuous method using iodonitrotetrazolium chloride as electron acceptor. Anal. Biochem. *212*, 506–509.

Ohlenbusch, A., Edvardson, S., Skorpen, J., Bjornstad, A., Saada, A., Elpeleg, O., Gartner, J., and Brockmann, K. (2012). Leukoencephalopathy with accumulated succinate is indicative of SDHAF1 related complex II deficiency. Orphanet J. Rare Dis. *7*, 69.

Robinson, K.M., and Lemire, B.D. (1996). Covalent attachment of FAD to the yeast succinate dehydrogenase flavoprotein requires import into mitochondria, presequence removal, and folding. J. Biol. Chem. *271*, 4055–4060.

Rustin, P., and Rotig, A. (2002). Inborn errors of complex II—unusual human mitochondrial diseases. Biochim. Biophys. Acta *1553*, 117–122.

Rzezniczak, T.Z., Douglas, L.A., Watterson, J.H., and Merritt, T.J. (2011). Paraquat administration in *Drosophila* for use in metabolic studies of oxidative stress. Anal. Biochem. *419*, 345–347.

Schwarze, S.R., Weindruch, R., and Aiken, J.M. (1998). Oxidative stress and aging reduce COX I RNA and cytochrome oxidase activity in Drosophila. Free Radic. Biol. Med. *25*, 740–747.

Selak, M.A., Armour, S.M., MacKenzie, E.D., Boulahbel, H., Watson, D.G., Mansfield, K.D., Pan, Y., Simon, M.C., Thompson, C.B., and Gottlieb, E. (2005). Succinate links TCA cycle dysfunction to oncogenesis by inhibiting HIF-alpha prolyl hydroxylase. Cancer Cell *7*, 77–85.

Shrader, W.D., Amagata, A., Barnes, A., Enns, G.M., Hinman, A., Jankowski, O., Kheifets, V., Komatsuzaki, R., Lee, E., Mollard, P., Murase, K., Sadun, A.A., Thoolen, M., Wesson, K., and Miller, G. (2011). Alpha-tocotrienol quinone modulates oxidative stress response and the biochemistry of aging. Bioorg. Med. Chem. Lett. *21*, 3693–3698.

Sun, F., Huo, X., Zhai, Y., Wang, A., Xu, J., Su, D., Bartlam, M., and Rao, Z. (2005). Crystal structure of mitochondrial respiratory membrane protein complex II. Cell *121*, 1043–1057.

Toyn, J.H., Gunyuzlu, P.L., White, W.H., Thompson, L.A., and Hollis, G.F. (2000). A counterselection for the tryptophan pathway in yeast: 5-fluoroanthranilic acid resistance. Yeast *16*, 553–560.

Wagener, N., Ackermann, M., Funes, S., and Neupert, W. (2011). A pathway of protein translocation in mitochondria mediated by the AAA-ATPase Bcs1. Mol. Cell *44*, 191–202.

Walker, D.W., Hajek, P., Muffat, J., Knoepfle, D., Cornelison, S., Attardi, G., and Benzer, S. (2006). Hypersensitivity to oxygen and shortened lifespan in a *Drosophila* mitochondrial complex II mutant. Proc. Natl. Acad. Sci. USA *103*, 16382–16387.

Wiedemann, N., Urzica, E., Guiard, B., Muller, H., Lohaus, C., Meyer, H.E., Ryan, M.T., Meisinger, C., Muhlenhoff, U., Lill, R., and Pfanner, N. (2006). Essential role of Isd11 in mitochondrial iron-sulfur cluster synthesis on Isu scaffold proteins. EMBO J. *25*, 184–195.

Wittig, I., Braun, H.P., and Schagger, H. (2006). Blue native PAGE. Nat. Protoc. *1*, 418–428.

Wodarz, A., Hinz, U., Engelbert, M., and Knust, E. (1995). Expression of crumbs confers apical character on plasma membrane domains of ectodermal epithelia of *Drosophila*. Cell *82*, 67–76.

Xiao, M., Yang, H., Xu, W., Ma, S., Lin, H., Zhu, H., Liu, L., Liu, Y., Yang, C., Xu, Y., Zhao, S., Ye, D., Xiong, Y., and Guan, K.L. (2012). Inhibition of alpha-KG-dependent histone and DNA demethylases by fumarate and succinate that are accumulated in mutations of FH and SDH tumor suppressors. Genes Dev. *26*, 1326–1338.

Yu, W., Polepalli, J., Wagh, D., Rajadas, J., Malenka, R., and Lu, B. (2012). A critical role for the PAR-1/MARK-tau axis in mediating the toxic effects of Abeta on synapses and dendritic spines. Hum. Mol. Genet. *21*, 1384–1390.

CHAPTER 6

CONCLUSIONS

Mitochondria are dynamic and complex organelles that play a central role in many aspects of cellular biology, including energy production, intermediary metabolism, and apoptosis (Wallace, 2005). Consistent with these broad cellular functions, mitochondrial dysfunction is associated with a wide range of diseases, including cancer, type 2 diabetes, and neurodegenerative disorders such as Alzheimer's disease, Parkinson's disease, Huntington's disease, and amyotrophic lateral sclerosis (Baysal et al., 2000; Chatterjee et al., 2006; Hanahan and Weinberg, 2011; Lin and Beal, 2006; Mootha et al., 2003; Patti et al., 2003; Petersen et al., 2004; Yan et al., 2009). The critical role of mitochondria in normal cellular function and human disease have led to large efforts to define the mitochondrial proteome (Calvo and Mootha, 2010). The most comprehensive proteomic analysis to date identified over 1,000 proteins that localize to mitochondria in mammals (Pagliarini et al., 2008). Remarkably, however, roughly 20% of these proteins have no known function (Pagliarini et al., 2008; Schmidt et al., 2010). These include many proteins that are highly conserved throughout eukarya, which indicates that they perform a fundamentally important function. We have been working to functionally characterize these conserved mitochondrial proteins using yeast and *Drosophila* model systems. Through this approach, we have discovered novel factors critical for

mitochondrial energy metabolism. In Chapter 2, we identify components of the previously unidentified mitochondrial pyruvate carrier (MPC), which links glycolysis to the TCA cycle through the import of pyruvate through the inner mitochondrial membrane (IMM). In a follow up study presented in Chapter 3, we demonstrate that *Drosophila* mutants lacking the MPC display characteristics of diabetes, including hyperglycemia, impaired glucose tolerance, and defects in the insulin signaling pathway (Inzucchi, 2012; Kirk et al., 2008). In Chapters 4 and 5, we identify two novel succinate dehydrogenase complex assembly factors (SDHAFs), thus providing a more comprehensive understanding of the process of SDH assembly and revealing new candidate-causative genes for diseases characterized by SDH deficiency.

The MPC proteins are required for mitochondrial pyruvate uptake in yeast, *Drosophila*, and humans

Over the past ~40 years, a series of biochemical experiments performed on isolated mitochondria have shown that a specific pyruvate carrier was present at the IMM (Schell and Rutter, 2013). Despite this extensive biochemical characterization, the molecular identity of the MPC was never elucidated (Hildyard and Halestrap, 2003; Todisco et al., 2006). In Chapter 2, we show that the MPC is comprised of members of the evolutionarily conserved and related MPC1 and MPC2 protein families (Figure 2.5). MPC1 and MPC2 are part of an ~150 kDa transmembrane protein complex localized to the IMM (Figures 2.1B, 2.1C, 2.6D, and 2.6E). *Drosophila MPC1* (*dMPC1*) mutants display defects in carbohydrate metabolism, including an inability to survive on a sugar-only diet, elevated carbohydrate levels, and reduced ATP (Figures 2.2A and 2.2C–2.2E).

Moreover, *Drosophila* and yeast *MPC1* mutants accumulate pyruvate, whereas TCA cycle intermediates are depleted in *dMPC1* mutants fed the sugar-only diet, indicating the presence of a specific disruption in pyruvate metabolism (Figures 2.2F and 2.3A). Since PDH activity is not significantly affected in mitochondria isolated from yeast *MPC1* mutant cells (Figure 2.3C) we hypothesized that the MPC1 proteins may be involved in mitochondrial pyruvate import. Consistent with this hypothesis, mitochondria isolated from yeast *MPC1* mutants display reduced uptake of radiolabeled pyruvate (Figure 2.3E). Furthermore, through the identification of a point mutant in yeast *MPC1* that promotes resistance to a known inhibitor of the MPC, we demonstrate that MPC1 is either a target of the drug or closely associated with its target (Figures 2.3F and 2.3G) (Halestrap, 1976). This result demonstrates that the MPC1/MPC2 complex exhibits a key defining feature of the MPC described almost 40 years ago (Halestrap, 1976; Halestrap and Denton, 1974). Finally, we show that RNA interference (RNAi)-mediated silencing of *MPC1* or *MPC2* reduces pyruvate oxidation in cultured mammalian cells, demonstrating that the role of the MPC proteins is conserved from yeast to humans (Figures 2.4A and 2.4B). Building on this observation, we showed that patients described in a previous publication with a hereditary disease associated with a defect in mitochondrial pyruvate uptake carry causative mutations in the *MPC1* locus (Figures 2.4C–2.4H) (Brivet et al., 2003). Overall, we conclude that the MPC proteins are required for mitochondrial pyruvate import across Eukarya and thus provide a molecular framework for further studies of this critical link between cellular glycolysis and mitochondrial OxPHOS (Halestrap and Denton, 1974; Schell and Rutter, 2013).

This discovery raises several interesting questions that should be addressed in future work. First, it is unclear whether there are any other unidentified components of the MPC involved in mitochondrial pyruvate import. In a paper copublished with ours, it was shown that expression of MPC1 and MPC2 together, but not individually, is sufficient to promote pyruvate uptake in bacterial cells (Herzig et al., 2012). This result suggests that the MPC is comprised of MPC1 and MPC2 exclusively (Herzig et al., 2012). Members of the Rutter lab, however, have been unable to reproduce this result (Jared Rutter, personal communication). This could be due to the technical difficulty associated with this kind of experiment, or perhaps, it could indicate that components other than MPC1/MPC2 are required to truly reconstitute pyruvate transport in a heterologous system. In future studies, it will be interesting to differentiate between these possibilities. A recent perspective article from Halestrap called into question whether the MPC proteins are truly involved in pyruvate transport, suggesting that the apparent pyruvate uptake defect observed in our study and the paper by Herzig et al. results from a pyruvate metabolic defect in *MPC1* mutants (Halestrap, 2012a). The subsequent demonstration that methyl-pyruvate can bypass pyruvate metabolic defects in cells in which *MPC1* is silenced, however, supports our conclusion (Divakaruni et al., 2013). Since methyl-pyruvate can diffuse freely across the inner mitochondrial membrane before it is cleaved by esterases in the matrix to generate intramitochondrial pyruvate, this result provides further evidence that the MPC complex is required for pyruvate uptake specifically, and not downstream pyruvate metabolic steps (Divakaruni et al., 2013).

Our current model for the structure of the MPC is a hetero-oligomeric complex of MPC1 and MPC2, each of which is relatively small and only contains two to three

transmembrane domains (Figure 2.5) (Divakaruni and Murphy, 2012; Herzig et al., 2012). This is an unusual configuration for a membrane metabolite transporter, which is typically represented by a single protein containing 6 to 12 transmembrane domains (Halestrap, 2012b; Palmieri and Pierri, 2010). Interestingly, this raises the possibility that the relative stoichiometry of the subunits may be a regulatory mechanism to control MPC activity *in vivo*. There is precedent for this type of regulatory mechanism exemplified by the mitochondrial calcium uniporter (MCU), which is a heterotetramer of two small and related proteins—MCU and MCUb (Patron et al., 2013). In this complex, MCUb functions as a negative regulator, inhibiting uniporter activity (Raffaello et al., 2013). Thus, the stoichiometry of MCU and MCUb in a given complex may be used to regulate mitochondrial calcium efflux differently under a variety of conditions (Raffaello et al., 2013). There is some evidence that the MPC might represent a rate-limiting step in pyruvate metabolism suggesting that the regulation of MPC activity may be a mechanism to modulate pyruvate utilization, although this topic is controversial (Halestrap and Armston, 1984; Pande and Parvin, 1978; Shearman and Halestrap, 1984; Titheradge and Coore, 1976). A potential regulatory function of the MPC is particularly interesting in light of the recent discoveries that a PPAR gamma-sparing thiazolidinedione (TZD) derivative and a phosphodiesterase inhibitor Zaprinast both promote metabolic changes in cultured cells and inhibit the MPC (Colca et al., 2013; Divakaruni et al., 2013; Du et al., 2013). These results suggest that the MPC could be responsible for some of the physiological responses elicited by these drugs. In future studies, we will attempt to determine if the MPC can be regulated through the stoichiometry of its subunits similar to the MCU. Building on these analyses, it will also be interesting to determine if MPC

function is affected in disorders like type 2 diabetes (discussed in Chapter 3) and cancer, where alterations in pyruvate metabolism are known to correlate with disease progression (McFate et al., 2008; Schummer et al., 2008).

Drosophila MPC1 mutants display defects in carbohydrate homeostasis and hallmarks of diabetes

In Chapter 3, we describe further studies of the defects in carbohydrate homeostasis seen in *Drosophila MPC1* mutants. We discovered that *dMPC1* mutants display several defining hallmarks of diabetes including sensitivity to dietary sugar, hyperglycemia during fasted and fed states, impaired glucose tolerance, and a reduction in insulin signaling activity in peripheral tissues (Figures 3.1A–3.1D, 3.2A, 3.2B, 3.4A–3.4C, 3.5B, and 3.5C) (Inzucchi, 2012). Since mitochondrial pyruvate metabolism by PDH was previously shown to be critical for glucose-stimulated insulin secretion (GSIS) in mice, we hypothesized that the MPC might be required for DILP secretion in *Drosophila* (Srinivasan et al., 2010). Consistent with this hypothesis, we observed a defect in the secretion of a *Drosophila* insulin-like peptide (DILP) from the insulin producing cells (IPCs) of *dMPC1* mutants (Figures 3.6A and 3.6B). Based on these results, we conclude that the MPC in *Drosophila* facilitates a metabolic state that promotes euglycemia and normal insulin signaling. The exact mechanism underlying this function, however, is unclear and is the subject of the future directions described in Chapter 3. Interestingly, the role of the MPC in the regulation of glucose homeostasis and insulin signaling may be conserved in mammals, as a PPARγ sparing TZD derivative was identified that ameliorates diabetic phenotypes and directly inhibits the MPC in

Drosophila and mammalian cells (Colca et al., 2013; Divakaruni et al., 2013; Rohatgi et al., 2013). It is unclear, however, if MPC inhibition underlies the beneficial effects of these drugs. Therefore, continuing to characterize the diabetic phenotypes of *dMPC1* mutants is likely to provide insight into the role of the MPC in euglycemia and insulin signaling that may translate to humans.

Independent of the diabetic phenotypes, our characterization of *dMPC1* mutants provides insight into the physiological role of the MPC in *Drosophila*. For example, our analysis suggests that *dMPC1* mutants display a developmental delay, but not lethality, which indicates that the MPC is not absolutely required for viability. Conversely, flies carrying transgenes that induce global silencing of PDH by RNAi die during development (Dona Wisidagama, personal communication). Since pyruvate must enter the mitochondrion to be converted to Acetyl-CoA by PDH, we would expect that a complete block in mitochondrial pyruvate should also cause lethality (Gray et al., 2013). Therefore, these results suggest that the MPC is not completely required for mitochondrial pyruvate import in *Drosophila in vivo*. Consistent with this hypothesis, we observe that the flux of glucose-derived carbons to TCA cycle intermediates is reduced, but not absent, in *dMPC1* mutants (data not shown). Thus, it appears that loss of *dMPC1* results in an incomplete block in mitochondrial pyruvate import. This residual transport could potentially be explained by the presence of a plasma membrane monocarboxylate transporter as one has been purported to also localize to mitochondria in mammalian cells (Brooks et al., 1999). It will be interesting to determine if *MPC1* and *MPC2* are essential genes in other species and whether the magnitude of their contribution to mitochondrial pyruvate import varies across evolution.

The identification of novel succinate dehydrogenase complex assembly factors provides a more comprehensive understanding of SDH assembly

The SDH complex occupies a pivotal step in cellular energy metabolism since it directly links the TCA cycle with the ETC (Berg et al., 2002). Despite this fundamental metabolic role, little is known about how the SDH complex is assembled (Rutter et al., 2010). Two proteins, called Sdhaf1 and Sdhaf2 (Sdh6 and Sdh5 in yeast), were shown to be required for SDH assembly (Ghezzi et al., 2009; Hao et al., 2009). Sdhaf2 is required for the covalent flavination of the SdhA subunit, whereas the molecular function of Sdhaf1 was not determined (Ghezzi et al., 2009; Hao et al., 2009). In Chapters 4 and 5, we identify and characterize two novel SDH assembly factors called Sdhaf3 and Sdhaf4 (Sdh7 and Sdh8 in yeast) and also describe the molecular function of Sdhaf1. For clarity, the nomenclature of SDH assembly factors and SDH complex subunits in animals will be used hereafter. Sdhaf1, Sdhaf3, and Sdhaf4 are all mitochondrial matrix proteins that play an evolutionarily conserved role in facilitating SDH function (Ghezzi, et al., 2009) (Figures 4.1B, 4.1D, and 5.5B). Loss of any one of these factors results in an accumulation of succinate and a depletion of fumarate and malate in yeast and flies (Figures 4.1F, 4.2, 4.5B, 4.6A, 5.1D, and 5.10D), as well as reduced steady-state levels of SDH holocomplex (Figures 4.2E, 4.3C, 4.4A, 5.1F, 5.10E, 5.13A, and 5.13C) and SDH activity (Figures 4.2C, 4.3B, 4.6B, 5.1E, 5.10F, and 5.10G). Each of these proteins directly interacts with an SDH subunit to promote SDH assembly. SDHAF4 physically interacts with soluble flavo-SdhA in the matrix prior to its association with SdhB and the rest of the SDH complex at the IMM (Figures 4.11A, 4.11C, 4.11D, 4.12A, and 4.12C),

potentially to prevent reactive oxygen species (ROS) production from FAD auto-oxidation. Consistent with this model, yeast *Sdhaf4* mutant cells produce excess endogenous ROS (Figures 4.13E and 4.14B) and both yeast and *Drosophila Sdhaf4* mutants are sensitive to exogenous oxidative stressors (Figures 4.9F and 4.13D). Moreover, toxicity associated with SdhA overexpression in yeast is worsened by loss of *Sdhaf4* and ameliorated by *Sdhaf4* overexpression (Figures 4.13A, 4.13B, and 4.14A). On the contrary, Sdhaf1 and Sdhaf3 physically interact with the iron sulfur (FeS) cluster-containing SdhB subunit in the mitochondrial matrix (Figures 5.3D, 5.13E, and 5.5A). Like Sdhaf4, Sdhaf1 and Sdhaf3 are critical for ROS homeostasis, as yeast and fly *Sdhaf3* mutants and yeast *Sdhaf1* mutants, are sensitive to oxidative stress (Figures 5.7A–5.7C, 5.8A, 5.8B, 5.8D, 5.10B, 5.10C, 5.12A, and 5.12B). Unlike *Sdhaf4* mutants, however, the toxicity associated with ROS in *Sdhaf1* and *Sdhaf3* mutants is caused specifically by ROS-mediated destabilization of SdhB, and not by the increased activity of a pro-oxidant molecule (Figures 5.7A–5.7C and 5.8A–5.8D). Moreover, Sdhaf1 and Sdhaf3 may facilitate the maturation of FeS clusters in SdhB, as supplementation of exogenous iron can partially rescue yeast *Sdhaf1* or *Sdhaf3* mutant phenotypes (Figure 5.6D). The exact mechanism by which Sdhaf1 and Sdhaf3 promote FeS cluster maturation, however, is unclear and will be the subject of future studies. Taken together, these results provide us with a more complete model for SDH complex assembly (Figure 6.1). First SdhA is flavinated in an Sdhaf2-dependent manner (Figure 6.1A). Flavo-SdhA then binds to Sdhaf4 to prevent SdhA auto-oxidation, thus facilitating the stability of SdhA and/or binding of SdhA to SdhB (Figure 6.1B). Shdaf1 and Sdhaf3 promote the stability of the

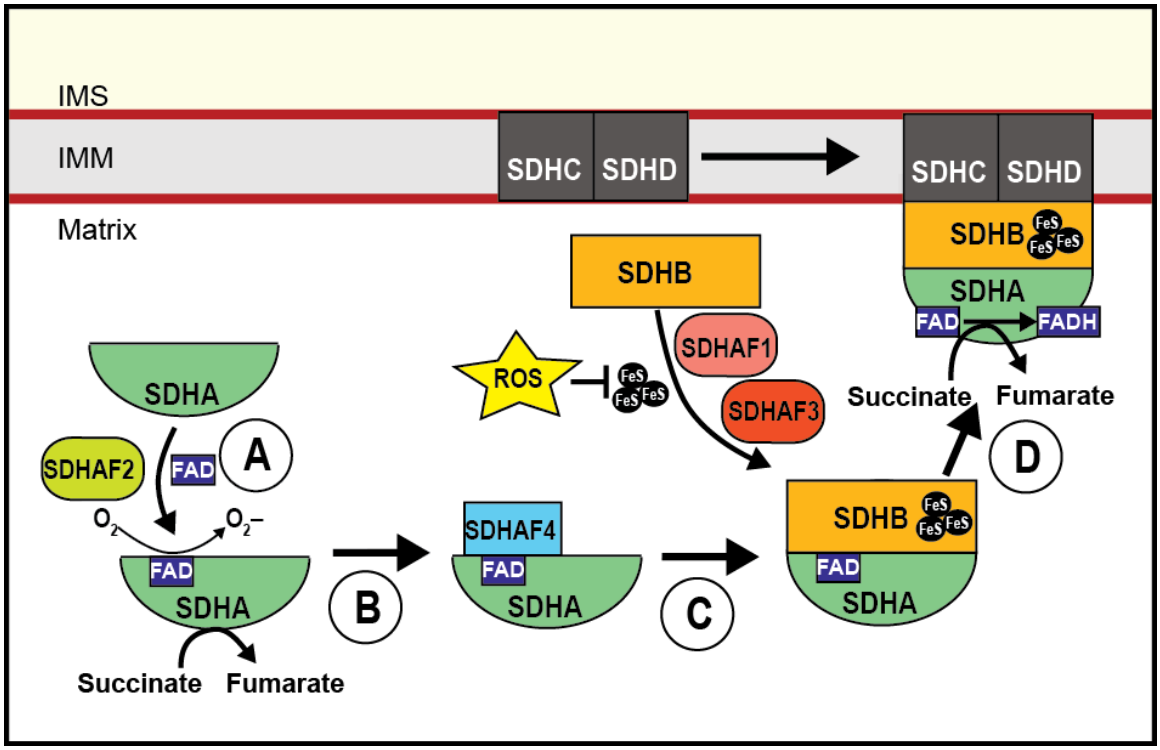

Figure 6.1. Model of SDH assembly.
The proposed steps of SDH complex assembly are depicted in chronological order. (A) SdhA is flavinated in an Sdhaf2-dependant manner. (B) Flavinated SdhA binds to Sdhaf4 to protect against SdhA auto-oxidation. (C) Sdhaf1 and Sdhaf3 promote the maturation of the iron sulfur (FeS) clusters in SdhB by shielding them from the damaging effects of reactive oxygen species (ROS). The actions of Sdhaf3 and Sdhaf1 facilitate the formation of the SdhA/SdhB dimer. (D) The SdhA/SdhB dimer is anchored to the inner mitochondrial membrane (IMM) by SdhC/SdhD. The intermembrane space (IMS) is also shown. (This figure is adapted from Figures 4.13F and 5.13D).

SdhB subunit, potentially by protecting the FeS clusters from the damaging effects of ROS, such that SdhB can bind to SdhA (Figure 6.1C). The combined actions of these assembly factors are required for the proper assembly of functional SDH complexes (Figures 6.1A–6.1D). In addition, the identification of Sdhaf3 and Sdhaf4 yields novel candidate causative genes that may be involved in a group of pathologies characterized by SDH deficiency, which include forms of cancer and neurodegenerative diseases that lack mutations in core SDH subunits (Feichtinger et al., 2010; Horvath et al., 2006; Jain-Ghai et al., 2013; Janeway et al., 2011). In future studies, it will be interesting to sequence DNA isolated from patients with these diseases to determine if mutations are present in the *SDHAF3* or *SDHAF4* loci.

Sdhaf3 and Sdhaf4 are critical for neuronal and muscular function in *Drosophila*

Consistent with the important role of mitochondria in nervous and muscular tissues, *Drosophila Sdhaf3* and *Sdhaf4* mutants display phenotypes associated with neuronal and muscular dysfunction. These include an age-progressive sensitivity to mechanically induced seizures (bang sensitivity) and reduced movement in *dSdhaf4* mutants, which are characteristics commonly associated with neurodegeneration in *Drosophila* (Figures 4.9B, 4.9C, 4.10A, and data not shown) (Feany and Bender, 2000; Fergestad et al., 2006; Liu et al., 2007). Consistent with these behavioral phenotypes, *dSdhaf4* mutants display retinal degeneration (Figure 4.9D). Bang sensitivity in *dSdhaf4* mutants can be rescued by specific expression of *dSdhaf4* in the nervous system, suggesting that *dSdhaf4* promotes neuronal maintenance and/or function cell-

autonomously (Figures 4.9E and 4.10D). In addition, ~30% of *dMPC1* mutants hold their wings in an abnormal position. This defect is associated with muscular degeneration caused by mitochondrial dysfunction (Figure 4.10B) (Clark et al., 2006; Greene et al., 2003; Park et al., 2006; Yang et al., 2006). Interestingly, neuronal and muscular dysfunction are also characteristics of Leigh's syndrome in humans, one form of which was shown be caused by mutations in *SdhA* in humans (Horvath et al., 2006). Overall, loss of *dSdhaf3* leads to phenotypes that are similar to those seen in *dSdhaf4* mutants, but they tend to be less severe. For example, *dSdhaf3* mutants are not sensitive to bang-induced seizures, but they do display an age-progressive reduction in locomotor activity (Figures 5.9F and 5.12H). This phenotype can be rescued by expression of *dSdhaf3* in the muscles or neurons, indicating that it is caused by combined muscular and neuronal dysfunction (Figure 5.12F). Moreover, *dSdhaf3* and *dSdhaf4* mutants are both sensitive to oxidative stress induced by hypoxia, but hypoxia is more toxic to *dSdhaf4* mutants (Figures 4.9F and 5.10C). The weaker phenotypes observed in *dSdhaf3* mutants relative to *dSdhaf4* mutants are consistent with the strength of the SDH defect, as *dSdhaf3* mutants display an ~50% reduction in SDH activity, whereas *dSdhaf4* mutants display an ~85% reduction in SDH activity (Figures 4.6B and 5.10F). These results also indicate that *dSdhaf3* and *dSdhaf4* are not absolutely required for SDH function. Consistent with this idea, reduction of *SdhA* or *SdhB* gene dose in *dSdhaf3* or *dSdhaf4* mutants causes lethality, demonstrating that these subunits are present at functionally significant levels (Figures 4.7C, 4.8F, and 5.11A). At this point, the mechanism underlying the neuronal and muscular defects in *dSdhaf3* and *dSdhaf4* mutants is unclear. *dSdhaf4* mutants do not display a reduction in overall ATP levels, suggesting that ROS may drive the pathology

in these tissues (Figures 4.5B and 4.6A). Future research will be aimed at addressing this question and better characterizing the physiological defects that result from a loss of *dSdhaf3* or *dSdhaf4* function.

References

Baysal, B.E., Ferrell, R.E., Willett-Brozick, J.E., Lawrence, E.C., Myssiorek, D., Bosch, A., van der Mey, A., Taschner, P.E., Rubinstein, W.S., Myers, E.N., et al. (2000). Mutations in SDHD, a mitochondrial complex II gene, in hereditary paraganglioma. Science *287*, 848–851.

Berg, J.M., Tymoczko, J.L., and Stryer, L. (2002). Biochemistry. Volume 5. (New York: W. H. Freeman). Accessed online at http://www.ncbi.nlm.nih.gov/books/NBK21154.

Brivet, M., Garcia-Cazorla, A., Lyonnet, S., Dumez, Y., Nassogne, M.C., Slama, A., Boutron, A., Touati, G., Legrand, A., and Saudubray, J.M. (2003). Impaired mitochondrial pyruvate importation in a patient and a fetus at risk. Mol. Genet. Metab. *78*, 186–192.

Brooks, G.A., Brown, M.A., Butz, C.E., Sicurello, J.P., and Dubouchaud, H. (1999). Cardiac and skeletal muscle mitochondria have a monocarboxylate transporter MCT1. J. Appl. Physiol. *87*, 1713–1718.

Calvo, S.E., and Mootha, V.K. (2010). The mitochondrial proteome and human disease. Ann. Rev. Genomics Hum. Genet. *11*, 25–44.

Chatterjee, A., Mambo, E., and Sidransky, D. (2006). Mitochondrial DNA mutations in human cancer. Oncogene *25*, 4663–4674.

Clark, I.E., Dodson, M.W., Jiang, C., Cao, J.H., Huh, J.R., Seol, J.H., Yoo, S.J., Hay, B.A., and Guo, M. (2006). *Drosophila* pink1 is required for mitochondrial function and interacts genetically with parkin. Nature *441*, 1162–1166.

Colca, J.R., McDonald, W.G., Cavey, G.S., Cole, S.L., Holewa, D.D., Brightwell-Conrad, A.S., Wolfe, C.L., Wheeler, J.S., Coulter, K.R., Kilkuskie, P.M., et al. (2013). Identification of a mitochondrial target of thiazolidinedione insulin sensitizers (mTOT)—relationship to newly identified mitochondrial pyruvate carrier proteins. PloS One *8*, e61551.

Divakaruni, A.S., and Murphy, A.N. (2012). Cell biology. A mitochondrial mystery, solved. Science *337*, 41–43.

Divakaruni, A.S., Wiley, S.E., Rogers, G.W., Andreyev, A.Y., Petrosyan, S., Loviscach, M., Wall, E.A., Yadava, N., Heuck, A.P., Ferrick, D.A., et al. (2013). Thiazolidinediones are acute, specific inhibitors of the mitochondrial pyruvate carrier. Proc. Natl. Acad. Sci. USA *110*, 5422–5427.

Du, J., Cleghorn, W.M., Contreras, L., Lindsay, K., Rountree, A.M., Chertov, A.O., Turner, S.J., Sahaboglu, A., Linton, J., Sadilek, M., et al. (2013). Inhibition of mitochondrial pyruvate transport by zaprinast causes massive accumulation of aspartate at the expense of glutamate in the retina. J. Biol. Chem. *288*, 36129–36140.

Feany, M.B., and Bender, W.W. (2000). A Drosophila model of Parkinson's disease. Nature *404*, 394–398.

Feichtinger, R.G., Zimmermann, F., Mayr, J.A., Neureiter, D., Hauser-Kronberger, C., Schilling, F.H., Jones, N., Sperl, W., and Kofler, B. (2010). Low aerobic mitochondrial energy metabolism in poorly- or undifferentiated neuroblastoma. BMC Cancer *10*, 149.

Fergestad, T., Ganetzky, B., and Palladino, M.J. (2006). Neuropathology in Drosophila membrane excitability mutants. Genetics *172*, 1031–1042.

Ghezzi, D., Goffrini, P., Uziel, G., Horvath, R., Klopstock, T., Lochmuller, H., D'Adamo, P., Gasparini, P., Strom, T.M., Prokisch, H., et al. (2009). SDHAF1, encoding a LYR complex-II specific assembly factor, is mutated in SDH-defective infantile leukoencephalopathy. Nat. Genet. *41*, 654–656.

Gray, L.R., Tompkins, S.C., and Taylor, E.B. (2013). Regulation of pyruvate metabolism and human disease. Cell. Mol. Life Sci. Advanced online publication. PMID: 24363178.

Greene, J.C., Whitworth, A.J., Kuo, I., Andrews, L.A., Feany, M.B., and Pallanck, L.J. (2003). Mitochondrial pathology and apoptotic muscle degeneration in *Drosophila* parkin mutants. Proc. Natl. Acad. Sci. USA *100*, 4078–4083.

Halestrap, A.P. (1976). The mechanism of the inhibition of the mitochondrial pyruvate transportater by alpha-cyanocinnamate derivatives. Biochem. J. *156*, 181–183.

Halestrap, A.P. (2012a). The mitochondrial pyruvate carrier: has it been unearthed at last? Cell Metab. *16*, 141–143.

Halestrap, A.P. (2012b). The monocarboxylate transporter family—structure and functional characterization. IUBMB Life *64*, 1–9.

Halestrap, A.P., and Armston, A.E. (1984). A re-evaluation of the role of mitochondrial pyruvate transport in the hormonal control of rat liver mitochondrial pyruvate metabolism. Biochem. J. *223*, 677–685.

Halestrap, A.P., and Denton, R.M. (1974). Specific inhibition of pyruvate transport in rat liver mitochondria and human erythrocytes by alpha-cyano-4-hydroxycinnamate. Biochem. J. *138*, 313–316.

Hanahan, D., and Weinberg, R.A. (2011). Hallmarks of cancer: the next generation. Cell *144*, 646–674.

Hao, H.X., Khalimonchuk, O., Schraders, M., Dephoure, N., Bayley, J.P., Kunst, H., Devilee, P., Cremers, C.W., Schiffman, J.D., Bentz, B.G., et al. (2009). SDH5, a gene required for flavination of succinate dehydrogenase, is mutated in paraganglioma. Science *325*, 1139–1142.

Herzig, S., Raemy, E., Montessuit, S., Veuthey, J.L., Zamboni, N., Westermann, B., Kunji, E.R., and Martinou, J.C. (2012). Identification and functional expression of the mitochondrial pyruvate carrier. Science *337*, 93–96.

Hildyard, J.C., and Halestrap, A.P. (2003). Identification of the mitochondrial pyruvate carrier in *Saccharomyces cerevisiae*. Biochem. J. *374*, 607–611.

Horvath, R., Abicht, A., Holinski-Feder, E., Laner, A., Gempel, K., Prokisch, H., Lochmuller, H., Klopstock, T., and Jaksch, M. (2006). Leigh syndrome caused by mutations in the flavoprotein (Fp) subunit of succinate dehydrogenase (SDHA). J. Neurol. Neurosurg. Psychiatry *77*, 74–76.

Inzucchi, S.E. (2012). Clinical practice. Diagnosis of diabetes. N. Engl. J. Med. *367*, 542–550.

Jain-Ghai, S., Cameron, J.M., Al Maawali, A., Blaser, S., MacKay, N., Robinson, B., and Raiman, J. (2013). Complex II deficiency—a case report and review of the literature. Am. J. Med. Genet. Part A *161A*, 285–294.

Janeway, K.A., Kim, S.Y., Lodish, M., Nose, V., Rustin, P., Gaal, J., Dahia, P.L., Liegl, B., Ball, E.R., Raygada, M., et al. (2011). Defects in succinate dehydrogenase in gastrointestinal stromal tumors lacking KIT and PDGFRA mutations. Proc. Natl. Acad. Sci. USA *108*, 314–318.

Kirk, J.K., Graves, D.E., Craven, T.E., Lipkin, E.W., Austin, M., and Margolis, K.L. (2008). Restricted-carbohydrate diets in patients with type 2 diabetes: a meta-analysis. J. Am. Diet. Assoc. *108*, 91–100.

Lin, M.T., and Beal, M.F. (2006). Mitochondrial dysfunction and oxidative stress in neurodegenerative diseases. Nature *443*, 787–795.

Liu, W., Gnanasambandam, R., Benjamin, J., Kaur, G., Getman, P.B., Siegel, A.J., Shortridge, R.D., and Singh, S. (2007). Mutations in cytochrome c oxidase subunit VIa cause neurodegeneration and motor dysfunction in *Drosophila*. Genetics *176*, 937–946.

McFate, T., Mohyeldin, A., Lu, H., Thakar, J., Henriques, J., Halim, N.D., Wu, H., Schell, M.J., Tsang, T.M., Teahan, O., et al. (2008). Pyruvate dehydrogenase complex activity controls metabolic and malignant phenotype in cancer cells. J. Biol. Chem. *283*, 22700–22708.

Mootha, V.K., Lindgren, C.M., Eriksson, K.F., Subramanian, A., Sihag, S., Lehar, J., Puigserver, P., Carlsson, E., Ridderstrale, M., Laurila, E., et al. (2003). PGC-1alpha-responsive genes involved in oxidative phosphorylation are coordinately downregulated in human diabetes. Nat. Genet. *34*, 267–273.

Pagliarini, D.J., Calvo, S.E., Chang, B., Sheth, S.A., Vafai, S.B., Ong, S.E., Walford, G.A., Sugiana, C., Boneh, A., Chen, W.K., et al. (2008). A mitochondrial protein compendium elucidates complex I disease biology. Cell *134*, 112–123.

Palmieri, F., and Pierri, C.L. (2010). Structure and function of mitochondrial carriers – role of the transmembrane helix P and G residues in the gating and transport mechanism. FEBS Lett. *584*, 1931–1939.

Pande, S.V., and Parvin, R. (1978). Pyruvate and acetoacetate transport in mitochondria. A reappraisal. J. Biol. Chem. *253*, 1565–1573.

Park, J., Lee, S.B., Lee, S., Kim, Y., Song, S., Kim, S., Bae, E., Kim, J., Shong, M., Kim, J.M., et al. (2006). Mitochondrial dysfunction in *Drosophila* PINK1 mutants is complemented by parkin. Nature *441*, 1157–1161.

Patron, M., Raffaello, A., Granatiero, V., Tosatto, A., Merli, G., De Stefani, D., Wright, L., Pallafacchina, G., Terrin, A., Mammucari, C., et al. (2013). The mitochondrial calcium uniporter (MCU): molecular identity and physiological roles. J. Biol. Chem. *288*, 10750–10758.

Patti, M.E., Butte, A.J., Crunkhorn, S., Cusi, K., Berria, R., Kashyap, S., Miyazaki, Y., Kohane, I., Costello, M., Saccone, R., et al. (2003). Coordinated reduction of genes of oxidative metabolism in humans with insulin resistance and diabetes: potential role of PGC1 and NRF1. Proc. Natl. Acad. Sci. USA *100*, 8466–8471.

Petersen, K.F., Dufour, S., Befroy, D., Garcia, R., and Shulman, G.I. (2004). Impaired mitochondrial activity in the insulin-resistant offspring of patients with type 2 diabetes. N. Engl. J. Med *350*, 664–671.

Raffaello, A., De Stefani, D., Sabbadin, D., Teardo, E., Merli, G., Picard, A., Checchetto, V., Moro, S., Szabo, I., and Rizzuto, R. (2013). The mitochondrial calcium uniporter is a multimer that can include a dominant-negative pore-forming subunit. EMBO J. *32*, 2362–2376.

Rohatgi, N., Aly, H., Marshall, C.A., McDonald, W.G., Kletzien, R.F., Colca, J.R., and McDaniel, M.L. (2013). Novel insulin sensitizer modulates nutrient sensing pathways and maintains beta-cell phenotype in human islets. PloS One *8*, e62012.

Rutter, J., Winge, D.R., and Schiffman, J.D. (2010). Succinate dehydrogenase – Assembly, regulation and role in human disease. Mitochondrion *10*, 393–401.

Schell, J.C., and Rutter, J. (2013). The long and winding road to the mitochondrial pyruvate carrier. Cancer Metab. *1*, 6.

Schmidt, O., Pfanner, N., and Meisinger, C. (2010). Mitochondrial protein import: from proteomics to functional mechanisms. Nat. Rev. Mol. Cell Biol. *11*, 655–667.

Schummer, C.M., Werner, U., Tennagels, N., Schmoll, D., Haschke, G., Juretschke, H.P., Patel, M.S., Gerl, M., Kramer, W., and Herling, A.W. (2008). Dysregulated pyruvate dehydrogenase complex in Zucker diabetic fatty rats. Am. J. Physiol. Endocrinol. Metab. *294*, E88–96.

Shearman, M.S., and Halestrap, A.P. (1984). The concentration of the mitochondrial pyruvate carrier in rat liver and heart mitochondria determined with alpha-cyano-beta-(1-phenylindol-3-yl)acrylate. Biochem. J. *223*, 673–676.

Srinivasan, M., Choi, C.S., Ghoshal, P., Pliss, L., Pandya, J.D., Hill, D., Cline, G., and Patel, M.S. (2010). Beta-cell-specific pyruvate dehydrogenase deficiency impairs glucose-stimulated insulin secretion. Am. J. Physiol. Endocrinol. Metab. *299*, E910–917.

Titheradge, M.A., and Coore, H.G. (1976). Hormonal regulation of liver mitochondrial pyruvate carrier in relation to gluconeogenesis and lipogenesis. FEBS lett. *72*, 73–78.

Todisco, S., Agrimi, G., Castegna, A., and Palmieri, F. (2006). Identification of the mitochondrial NAD+ transporter in *Saccharomyces cerevisiae*. J. Biol. Chem. *281*, 1524–1531.

Wallace, D.C. (2005). A mitochondrial paradigm of metabolic and degenerative diseases, aging, and cancer: a dawn for evolutionary medicine. Annu. Rev. Genet. *39*, 359–407.

Yan, H., Parsons, D.W., Jin, G., McLendon, R., Rasheed, B.A., Yuan, W., Kos, I., Batinic-Haberle, I., Jones, S., Riggins, G.J., et al. (2009). IDH1 and IDH2 mutations in gliomas. N. Engl. J. Med. *360*, 765–773.

Yang, Y., Gehrke, S., Imai, Y., Huang, Z., Ouyang, Y., Wang, J.W., Yang, L., Beal, M.F., Vogel, H., and Lu, B. (2006). Mitochondrial pathology and muscle and dopaminergic neuron degeneration caused by inactivation of *Drosophila* Pink1 is rescued by Parkin. Proc. Natl. Acad. Sci. USA *103*, 10793–10798.